ANTIOXIDANT AND ANTI-INFLAMMATORY PROPERTIES OF BIOTRANSFORMED PROANTHOCYANIDINS IN RELATION TO NONALCOHOLIC FATTY LIVER DISEASE

by

Wasitha Praveen de Wass Thilakarathna

Submitted in partial fulfillment of the requirement
for the degree of Doctor of Philosophy

at

Dalhousie University
Halifax, Nova Scotia
August 2023

Dalhousie University is located in Mi'kma'ki, the ancestral and unceded territory of the Mi'kmaq. We are all Treaty people.

DEDICATION

I would like to dedicate this thesis to,

My loving parents, Priyanthi Silva and Wasantha Thilakarathna

Love of my life, my wife Nilakshi Abeysinghe

and

My two loving sisters, Dinelka and Heshanka Thilakarathna

for your love, support, encouragement, and for believing in me

To all who work tirelessly to broaden the horizons of science…!

Believe in your dreams, because dreams do come true.

TABLE OF CONTENTS

LIST OF TABLES

LIST OF FIGURES

ABSTRACT

Nonalcoholic fatty liver disease (NAFLD) is the most common chronic liver disease worldwide. Despite the number of new NAFLD cases predicted to increase, there are no United States Food and Drug Administration-approved drugs for NAFLD. Bioactive dietary polyphenols such as proanthocyanidins (PAC) are potent in reducing the risk of NAFLD. The majority of dietary PAC are oligomeric PAC (OPAC) and polymeric PAC (PPAC), which are low in bioavailability. The biotransformation of OPAC and PPAC into bioavailable metabolites using probiotics can enhance their physiological benefits. Initially, an ultrasonication-assisted aqueous-ethanol-based PAC extraction method was developed to obtain food-grade PAC suitable for use in the development of synbiotics. The optimum conditions to extract PAC from grape seeds were by using 47% aqueous-ethanol at 60 °C temperature, 10.14:1 solvent to solid ratio, and 53 min of sonication time. The ability of a mixture of *Lactobacillus* and *Bifidobacterium* probiotic bacteria (PB) together with novel PB *Akkermansia muciniphila* to biotransform PPAC was evaluated in the C57BL/6 mice. PB could biotransform PAC into bioavailable metabolites and improve the PPAC biotransformation in the mice. Oral supplementation of isolated PPAC indirectly induced nonalcoholic steatohepatitis (NASH) in the mice by impairing the gut epithelial barrier function and subsequently enabling bacterial lipopolysaccharides translocation into the liver. OPAC and PPAC were biotransformed *in vitro* by using *Saccharomyces cerevisiae* to obtain bioactive metabolites while reducing the toxicity of PPAC. The biotransformed (BT)-OPAC and BT-PPAC significantly reduced the palmitic acid (PA)-induced lipid accumulation in mouse hepatocytes (AML12) by suppressing the *de novo* lipogenesis and promoting the fatty acid *β*-oxidation. Also, BT-PAC ameliorated PA-induced oxidative stress by activating the nuclear factor erythroid 2-related factor 2 antioxidant pathway and upregulating the expressions of antioxidant enzymes. Moreover, BT-PAC significantly reduced PA and LPS-induced inflammation in AML12 cells by suppressing the activation of toll-like receptor 4-mediated inflammatory signaling pathways. Taken together, these results suggest the potential to develop PAC-based synbiotics to mitigate the risk of NAFLD and NASH. However, such synbiotics must be critically evaluated for their safety for human consumption.

LIST OF ABBREVIATIONS USED

DCFDA	2′,7′-Dichlorofluorescein diacetate
HMG-CoA	3-Hydroxy-3-methylglutaryl coenzyme A
DMAC	4-Dimethylaminocinnamaldehyde
ACC	Acetyl-CoA carboxylase
ATGL	Adipose triglyceride lipase
AM	*Akkermansia muciniphila*
ALT	Alanine aminotransferase
AMPK	5′ Adenosine monophosphate-activated protein kinase
ANOVA	Analysis of variance
AP-1	Activator protein-1
ApoB	Apolipoprotein B
AST	Aspartate aminotransferase
ATF6α	Activating transcription factor-6 alpha
BAT	Brown adipose tissue
BSA	Bovine serum albumin
BT-OPAC	Biotransformed oligomeric proanthocyanidins
BT-PPAC	Biotransformed polymeric proanthocyanidins
HRMS	High-resolution mass spectrometry
C/EBP	CCAAT-enhancer-binding protein
CAT	Catalase
CE	Catechin equivalence
CCL2	C-C motif chemokine ligand 2
CD36	Cluster of differentiation 36
CCD	Central composite design
CHOP	CCAAT-enhancer-binding protein-homologous protein
ChREBP	Carbohydrate response element-binding protein
CPT1	Carnitine-palmitoyl-transferase-1
DAMP	Damage-associated molecular patterns

DDA	Data-dependent acquisition
DI	Deionized
DGAT1	Diacylglycerol acyltransferase 1
DNL	*de novo* Lipogenesis
DW	Dry weight
ER	Endoplasmic reticulum
ECM	Extracellular matrix
ERK	Extracellular signal-regulated kinase
FA	Fatty acid
FXR	Farnesoid X receptor
FAS	Fatty acid synthase
FATP	FA transport proteins
FBS	Fetal bovine serum
FFA	Free fatty acids
FFAR2	Free fatty acids receptor 2
F/B	Firmicutes/Bacteroidetes
FW	Fresh weight
FOS	Fructooligosaccharides
GCKR	Glucokinase regulatory protein
GLP-1	Glucagon-like peptide-1
GPx	Glutathione peroxidase
GS	Grape seed
GSP	Grape seed powder
HCC	Hepatocellular carcinoma
HCV	Hepatotropic hepatitis C virus
HDL	High-density lipoprotein
H&E	Hematoxylin and eosin
HFD	High-fat diet
HFHS	High-fat and high-sucrose
HPLC	High-performance liquid chromatography

HSC	Hepatic stellate cells
I/R	Ischemia/reperfusion
IHL	Intrahepatic lipid
IL	Interleukin
INSIG2	Insulin-induced gene-2
ITS	Insulin-transferrin-selenium
IRE1α	Inositol-requiring enzyme-1 alpha
JNK	c-Jun-N-terminal kinase
LBPB	*Lactobacillus* and *Bifidobacterium* probiotic bacteria
LAL	Lysosomal acid lipase
LCFA	Long-chain FA
LNB	Lean and non-obese
LPL	Lipoprotein lipase
LPS	Lipopolysaccharides
MDA Eq	Malondialdehyde equivalence
MAM	Mitochondria-associated ER membranes
MAPK	Mitogen-activated protein kinases
MDM	Monocyte-derived macrophages
MDP	Mean degree of polymerization
MetS	Metabolic syndrome
miR	Micro ribonucleic acids
mRNA	Messenger ribonucleic acid
MTP	Microsomal triglyceride transfer protein
NADPH	Nicotinamide adenine dinucleotide phosphate
NAFLD	Nonalcoholic fatty liver disease
NASH	Nonalcoholic steatohepatitis
NF-κB	Nuclear factor-*kappa*-light-chain-enhancer of activated B cells
Nrf2	Nuclear factor erythroid 2-related factor 2
OTUs	Observed operational taxonomical units
OPAC/ O-PAC	Oligomeric proanthocyanidin

OD_{600}	Optical density at 600 nm
ORO	Oil Red O stain
PAC	Proanthocyanidins
PA	Palmitic acid
PB	Probiotic bacteria
PEPCK	Phosphoenolpyruvate carboxylase
PMS	Phenazine methosulphate
PTEN	Phosphate and tensin homolog
PBS	Phosphate-buffered saline
PI3K	Phosphoinositide 3-kinase
PPAC/ P-PAC	Polymeric proanthocyanidins
PPAR	Peroxisome proliferator-activated receptor
AKT	Protein kinase B
Tregs	Regulatory T-cells
RSM	Response surface method
RT	Room temperature
ROS	Reactive oxygens species
SCFA	Short-chain fatty acids
SHP	Small heterodimer partner
SNP	Single nucleotide polymorphism
s:s	Solvent:solid ratio
SREBP	Sterol regulatory element binding protein
SCD	Stearoyl CoA desaturase
SOD	Superoxide dismutase
T2D	Type-2 diabetes
TGR5	Takeda G protein-coupled receptor 5
TG	Triglyceride
TBARS	Thiobarbituric acid reactive substances
TJ	Tight-junction
TIMP-1	Tissue inhibitor of metalloproteinase-1

TNF-α	Tumour necrosis factor-alpha
TLR4	Toll-like receptor 4
TPC	Total phenolic content
TPAC	Total proanthocyanidins content
TFEB	Transcription factor EB
TGF	Transforming growth factor
UHPLC-ESI-MS	Ultra-high performance liquid chromatography-electrospray ionization-mass spectrometry
UPR	Unfolded protein response
VEGF-B	Vascular endothelial growth factor B
VLDL	Very-low-density lipoprotein
WAT	White adipose tissue
YGM	Yeast growth media
α-SMA	Alpha-smooth muscle actin

ACKNOWLEDGEMENTS

I am blessed enough to be surrounded by many well-wishers, without who's support, completion of my doctoral degree would have been much more difficult. I am grateful to all of you, for being with me in the hours of need.

I must thank my supervisor Dr. H.P. Vasantha Rupasinghe for giving me the opportunity to become a doctoral student and a member of his research team. I am grateful to you, for your guidance, support, and encouragement to complete my doctoral thesis. You were always there for me, and you always had answers and means to overcome the challenges I faced during both my master's and doctoral studies. Thank you for teaching me how to do research and become a critical thinker and showing me the dedication and patience required to become a researcher by example. Thank you, for directing me to contribute to other research projects, I learned a lot from each project. I am forever grateful to you for giving me this wonderful opportunity to come to Canada and build my life in this beautiful country. Sir, you are my idol and I wish one day I can become a successful researcher and a person like you.

I thank my advisory committee, Dr. Graham Dellaire and Dr. Morgan G.I. Langille, for their guidance and support to complete my doctoral studies. Your knowledge and experience were immensely helpful in the conceptualization and the modifications introduced during the conducting of my research. I always appreciate your enthusiasm for my research work and your encouragement to explore new experimental techniques and models. Thank you, Dr. Langille, for helping me to learn about the analysis of 16S rRNA sequencing data and sharing your laboratory resources with me.

I would like to acknowledge the financial assistance I received from the A. David Crowe Graduate Scholarship, Robert P. Longley Graduate Scholarship, Andrew Wilson Scholarship, and Second Century Endowment Graduate Scholarship to complete my doctoral studies. My research project was also funded by the Discovery grant of the Natural Sciences and Engineering Research Council (NSERC) of Canada and the Killam Chair funds received by my supervisor, Dr. H.P. Vasantha Rupasinghe. I heartily appreciate the scholarship donors and the funding agencies for providing financial support to complete my doctoral studies. Thank you, Dr. David Crowe, for being the primary donor of my stipend during the first three years of my doctoral studies and being an admirer of my research work.

I heartily appreciate the support I received from the past and present members of Dr. Rupasinghe's research group and other colleagues. Madumani Amararathna, Dr. Niluni Wijesundara, Dr. Wasundara Fernando, Surangi Dharmawansa, and Tharindu Suraweera thank you for sharing your knowledge and research expertise with me. Thank you, Dr. Wasundara Fernando and Gayani Gamage, for helping me to conduct mouse experiments in the Carleton animal care facility of Dalhousie University. I am grateful to Dr. Jose Merlin, Dr. Sajeev Wagle, and Dr. Fagbohun Oladapo for their contributions to improving my research and for allowing me to collaborate with their research work. Dr. Cijo G. Vazhappilly, thank you for teaching me cell culturing and cell culture-based assays. Kithma de Silva, Cindy Yu, Monica Guillen Poot, Flavia Adais Rochca dos Santos, Janani Radhakrishnan, and Vandana Tannira, thank you for being the best lab mates, I cherish the time spent with you. Dr. Atefeh Nasri, Damith Costa, Dinushi Kaushalya, Harichandana Valisakkagari, and Chandrika Chaturvedi, I heartily appreciate your support during the

time of thesis writing, please keep bringing your research questions I want to get distracted time to time.

I feel extremely fortunate to have many friends who genuinely care about me. Dayan Silva, thank you for being the best friend anyone can ask for. Thank you for taking care of the apartment and all the cooking during the time I was busy with my research work. Buddika Malaweera, thank you for being a brother to me, you were never hesitant to help me. Chamara Jayasinghe and Dushanthi Sampath, thank you for making me a part of your family. Champika Gamage, thank you for all the support and your valuable advice. Ashan Sethiya, Ajeethan Vijerathnam, and Nivethika Vadivelu, I heartily appreciate all the support I received from you to complete my doctoral studies.

I can not thank enough, my family, for their love, support, guidance, and encouragement. I am extremely grateful to my mother, Priyanthi Silva, and father, Wasantha Thilakarathna, for supporting my dreams and wishes. You are the light of my life, I deeply appreciate all your sacrifices to make my life a better one. Thank you, my loving sisters, Dinelka and Heshanka Thilakarathna for taking care of the family during my long absences devoted to studies. I must greatly appreciate the support from my ever-loving wife, Nilakshi Abeysinghe. Thank you for all the love, your sacrifices, and for listening to my worries. I sincerely appreciate your patience during my absence. Thank you, Cooper Puppy for keeping my wife accompanied while I am away. I owe you many belly rubs.

THANK YOU…!!!

CHAPTER 1. INTRODUCTION

1.1. PROANTHOCYANIDINS

1.1.1. Classification and chemistry of proanthocyanidins

Plants and plant-derived foods are significant sources of bioactive compounds with beneficial health effects. A variety of phytochemicals, such as polyphenols, carotenoids, amines and peptides, dietary fibres, terpenes, phytosterols, and vitamins have been extensively evaluated for biological activities and proven to be beneficial against multiple diseases (Samtiya et al., 2021). There are more than 8,000 known natural phenolic compounds, making polyphenols one of the largest groups of phytochemicals (Lund, 2021). Polyphenols can be classified as phenolic acids, flavonoids, stilbenes, and lignans due to their extensive structural diversity (Kumar et al., 2019). Flavonoids are the most abundant dietary polyphenols, and all flavonoids share a basic C6-C3-C6 carbon skeleton of two benzene rings (A- and B-rings) linked together with three carbon atoms arranged into an oxygenated heterocycle (C-ring) (Fig. 1.1a). Flavonoids can be sub-divided into six groups, namely, flavonols, flavanones, isoflavones, flavanols, flavones, and anthocyanins based on the chemistry of heterocyclic rings (Pandey and Rizvi, 2009). The flavanols, also termed flavan-3-ols, are different from most other flavonoids by not having a double bond between C2 and C3, and a carbonyl group at C4 of the C-ring (Tsao, 2010). Proanthocyanidins (PAC), also known as condensed tannins, are oligomeric and polymeric molecules resulting from the condensation of flavan-3-ols (Mannino et al., 2021). The differentiation of oligomeric PAC from polymeric PAC is based on molecular size. Some researchers consider PAC with 2 – 5 monomers as the oligomers and PAC with 6 – 60 monomers as the polymers (Mannino et al., 2021) while others consider PAC with 2 – 10

monomers as the oligomers and PAC larger than 10 monomers as the polymers (Vazquez-Flores et al., 2018). There are three main PAC monomers (flavan-3-ols) based on the number and the location of hydroxyl groups attached to the B-ring. The propelagordins have a single hydroxyl group, while procyanidins and prodelphinidins have two and three hydroxyl groups attached to the B-ring, respectively (Mannino et al., 2021). Therefore, PAC can be categorized as propelagordins, procyanidins, and prodelphinidins based on the monomer composition. The procyanidins are primarily consisted of (epi)catechin subunits and they are the most abundant PAC. The propelagordins and prodelphinidins are mainly consisted of (epi)afzelechin and (epi)gallocatechin subunits, respectively (Ky et al., 2016). PAC monomers also depict structural differences based on stereochemistry. The C2 and C3 of the C-ring are chiral carbons that enable four different molecular configurations, (2*R*, 3*S*), (2*R*, 3*R*), (2*S*, 3*R*), and (2*S*, 3*S*). The most common PAC monomers are 2,3-*trans*-(+)-catechin (2*R*, 3*S*) and 2,3-*cis*-(−)-epicatechin (2*R*, 3*R*) which only differ from each other by having opposite stereochemistry at the C3. Almost all the PAC monomers found in nature have the *R* configuration at the C2 (Fig. 1.1b and c) (He et al., 2008).

The condensation of PAC monomers into oligomers or polymers occurs through the formation of interflavan linkages. The bonding can occur between C4 of the heterocyclic C-ring of one PAC monomer and C6 or C8 of the A-ring of another PAC monomer, creating single B-type linkages (Fig. 1.1e). In A-type linkages, PAC monomers are linked together by two bonds, an ether bond between C2 of the C-ring and O7 of the A-ring, and a C4 – C8 bond. PAC are divided into two groups, A-type and B-type PAC, based on the predominant type of linkages present in the molecular structure (Fig. 1.1d) (Yokota et al., 2013). B-type PAC are more common in the human diet with A-type PAC

found in foods such as cranberries, plums, avocado, peanut, and cinnamon (Gu et al., 2004). PAC are an exceptionally diverse group of phytochemicals and the bioactivities of PAC depend on the chemical structure (Yokota et al., 2013).

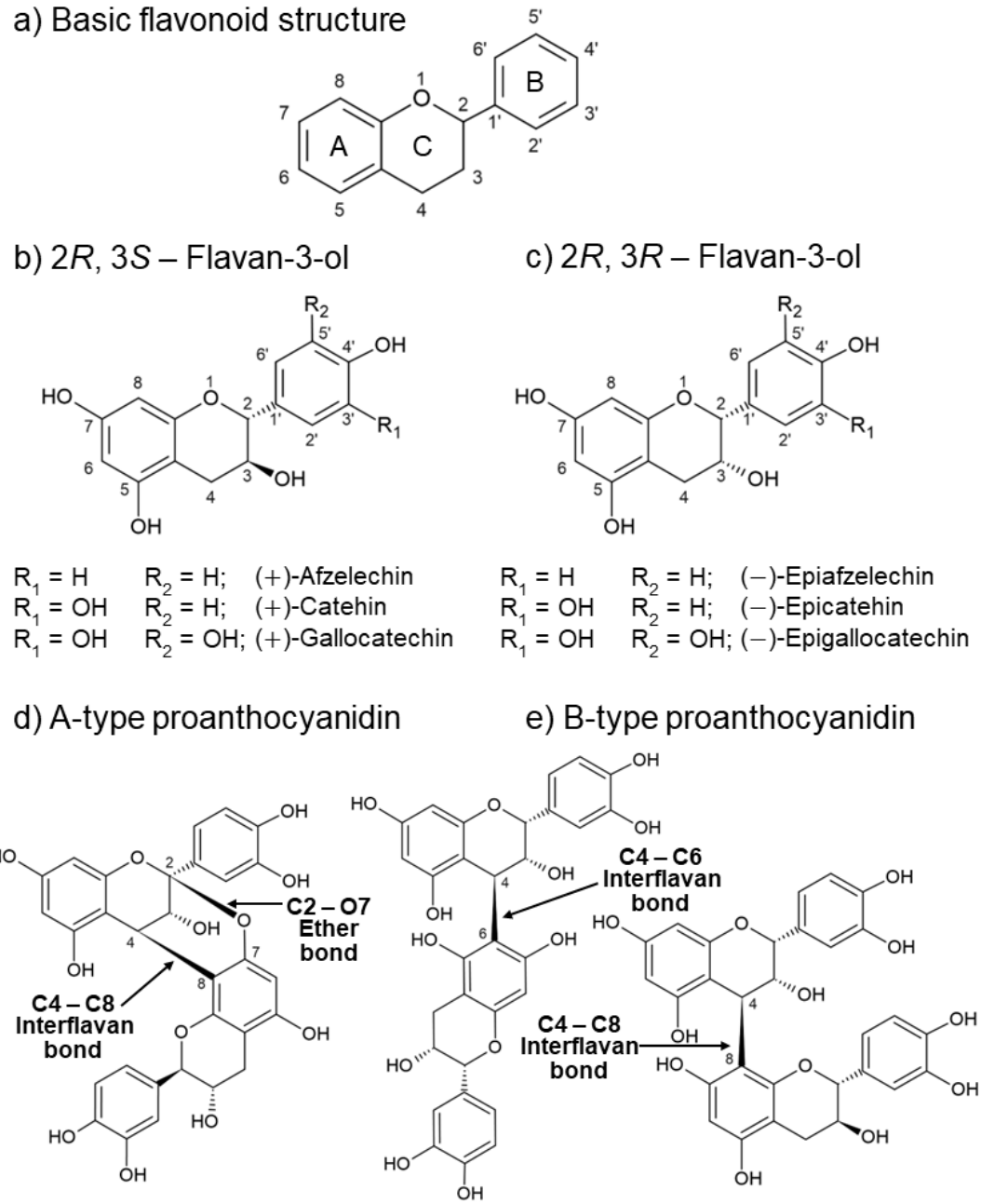

Figure 1.1. Chemistry of proanthocyanidins. The basic carbon structure of flavonoids (a), the stereochemistry of common flavan-3-ol/ PAC monomer molecules (b and c), and the basic molecular arrangement of A- and B-type proanthocyanidins (d and e).

1.1.2. Biosynthesis of PAC

Polyphenols including PAC are plant secondary metabolites important to protect the plants from biotic and abiotic stresses such as drought, temperature, UV light, pathogens, and herbivores. The hydrolyzable and condensed tannins primarily act as insect and herbivores repellents due to their bitter taste and toxicity (Tuladhar et al., 2021). In plants, PAC are biosynthesized by the phenylpropanoid and flavonoid pathways (He et al., 2008). PAC biosynthesis is a complex process regulated by several enzymes (Fig. 1.2). Initially, phenylalanine is converted to cinnamic acid and subsequently into *p*-coumaric acid and *p*-coumaroyl-CoA by the phenylalanine ammonia-lyase, cinnamate 4-hydroxylase, and 4-coumarate-CoA ligase, respectively (Dong and Lin, 2021). The chalcone synthase then synthesizes chalcone by using *p*-coumaroyl-CoA and malonyl-CoA as the substrates. This is the first step of the flavonoid biosynthesis pathway. Then, the isomerization of the chalcone into naringenin (flavanones) is facilitated by the chalcone isomerase (Dong and Lin, 2021). The naringenin can be converted into either eriodictyol by the flavonoid 3′-hydroxylase (F3′H) enzyme or pentahydroxy flavone by the flavonoid 3′,5′-hydroxylase (F3′5′H). The F3′H facilitates hydroxylation of the C3′ of the B-ring of the naringenin while the F3′5′H facilities the hydroxylation at both C3′ and C5′. Therefore, this step determines the type of flavanol monomers (propelagordins, procyanidins, or prodelphinidins) created by the biosynthesis process (Lim and Ha, 2021). Then, the flavanone 3-hydroxylase (F3H) converts the eriodictyol and pentahydroxy flavone into dihydroquercetin and dihydromyricetin, respectively, by hydroxylation of the C3 of the C-ring. Alternatively, the F3H can convert naringenin into dihydrokaempferol, which is then converted into dihydroquercetin and dihydromyricetin by the F3′H and F3′5′H,

respectively. The carbonyl group at C4 of the dihydrokaempferol, dihydroquercetin, and dihydromyricetin is reduced to a hydroxyl group by the dihydroflavonol 4-reductase enzyme to generate leucoanthocyanidins. The leucoanthocyanidins are the precursors of PAC monomers with the 2R, 3S molecular configuration, including (+)-catechin, (+)-afzelechin, and (+)-gallocatechin. Conversion of the leucoanthocyanidins into PAC monomers is catalyzed by the leucoanthocyanidin reductase, which further reduces the C4 of the C-ring. The leucoanthocyanidins can be synthesized into anthocyanidins by the anthocyanidin synthase. Anthocyanidins are the precursors of PAC monomers with the 2R, 3R molecular configuration such as (−)-epicatechin, (−)-epiafzelechin, and (−)-epigallocatechin. Conversion of the anthocyanidins into PAC monomers is catalyzed by the anthocyanidin reductase, which neutralizes the positively charged oxygen of anthocyanidin molecules (Lim and Ha, 2021). The mechanisms of polymerization of the PAC monomers remain inconclusive. Even though, PAC monomers can polymerize non-enzymatically and through reactions catalyzed by the laccases, the resulting PAC oligomers are not commonly found in nature (Yu et al., 2022). A recent study suggests that PAC monomers (flavan-3-ols) can exist as carbocations in plants and these carbocations facilitate the polymerization of PAC monomers (P. Wang et al., 2020). Polymerization can occur through the progressive addition of flavan-3-ol carbocations (extension units) onto a flavan-3-ol molecule (starter unit) through nucleophilic attacks (P. Wang et al., 2020; Yu et al., 2022). The Biosynthesis of PAC is a complex process capable of synthesizing a plethora of structurally diverse PAC molecules.

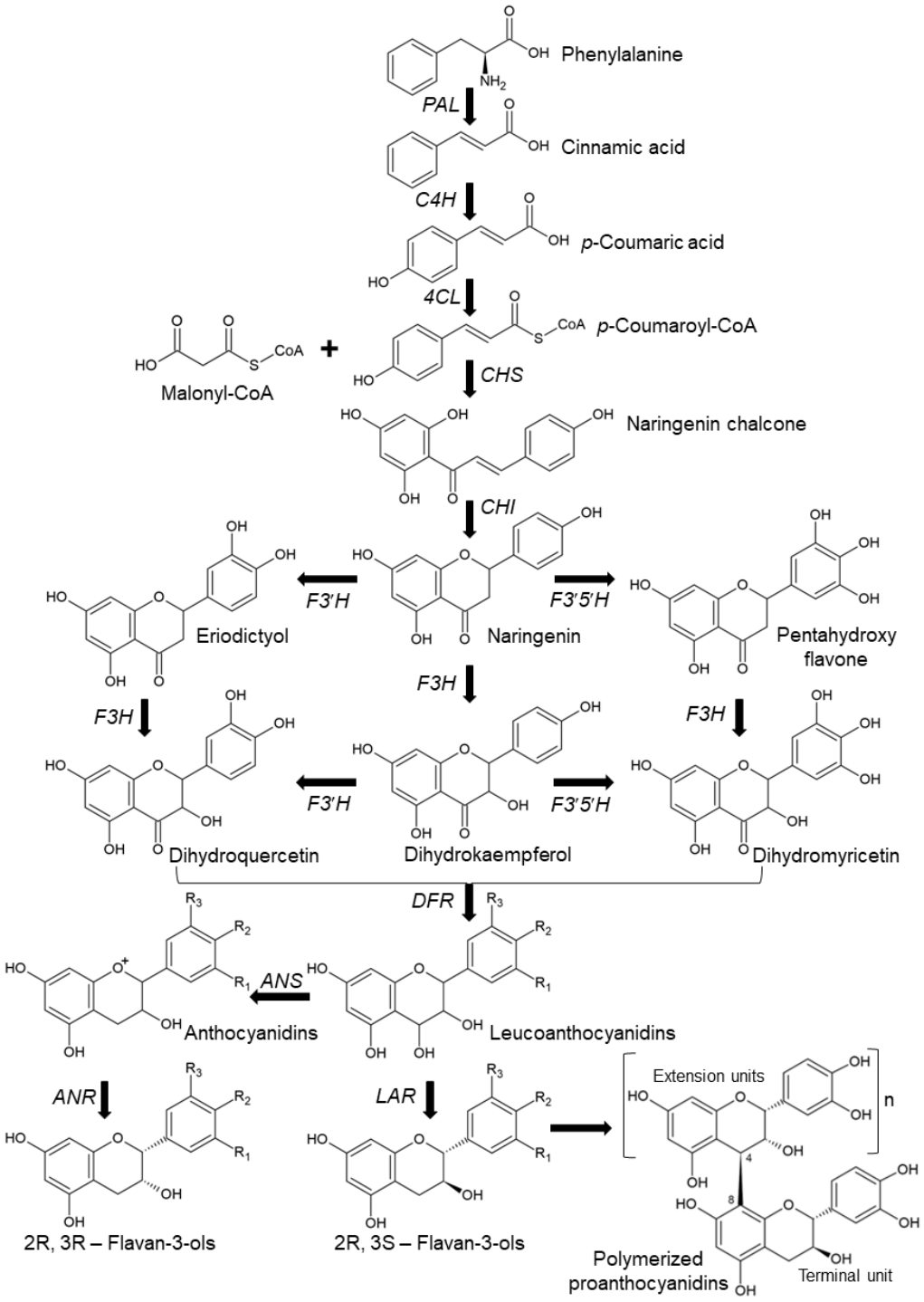

Figure 1.2. General biosynthetic pathway of proanthocyanidins. 4CL, 4-Coumarate-CoA ligase; ANR, anthocyanidin reductase; ANS, anthocyanidin synthase; C4H, cinnamate 4-hydroxylase; CHI, chalcone isomerase; CHS, chalcone synthase; DFR, dihydroflavonol 4-reductase; F3′5′H, flavonoid 3′,5′-hydroxylase; F3′H, flavonoid 3′-hydroxylase; F3H, flavanone 3-hydroxylase; LAR, leucoanthocyanidin reductase; PAL, phenylalanine ammonia-lyase.

1.1.3. Distribution and consumption of PAC

PAC are ubiquitously present in plants and plant-derived foods (Nie and Stürzenbaum, 2019). PAC can be found in all plant tissues, especially in seeds, bark, leaves, flowers, fruits/nuts, and roots (Rauf et al., 2019; Yu et al., 2020). The concentrations and characteristics of PAC can considerably vary between different tissues of the same plant. For instance, in the Shiraz and Cabernet Sauvignon grape varieties, the seeds contain more PAC compared to the grape skin and the PAC in the seeds are less polymerized compared to the skin (Hanlin et al., 2011). Thus, characteristics and concentrations of the PAC in foods can greatly vary based on their origin.

Berries such as chokeberries, cranberries, and lowbush blueberries are excellent sources of PAC with about 6.6, 4.2, and 3.30 mg/g fresh weight (FW) of PAC, respectively. Most of the other commonly consumed berries such as strawberries (1.45 mg/g FW) contain low concentrations of PAC (Gu et al., 2004). The by-products of berry processing can be used for the extraction of PAC. The availability of extractable concentrations of PAC in the by-products of berry processing had been reported in a study producing decoctions. Residues of strawberry, raspberry, blueberry, and blackberry remaining after the decoction process contain about 20 – 34 mg/g (*Ceratonia siliqua* L. oligomeric PAC equivalence) of extractable PAC (Reynoso-Camacho et al., 2021). The red and green grapes contain less PAC compared to many of the berries (0.6 and 0.8 mg/g FW, respectively). PAC and anthocyanins are the major polyphenols found in wines produced by grape fermentation. PAC concentration in wine primarily depends on the grape variety used and the fermentation process. The average concentrations of PAC in red and white wines are around 180 and 10 mg/L, respectively (Sánchez-Moreno et al., 2003). The by-

products of grape processing, especially the seeds are a rich source of PAC. Grape seeds together with stems and skins are the main by-products of the wine fermentation process (Teixeira et al., 2014). Grape seeds contain about 3.5% PAC based on the dry weight (DW) (Gu et al., 2004). During the current study, I found that, although PAC leaches into wine during the fermentation, the remaining post-fermentation by-products retain enough PAC to warrant them as sources for PAC extraction (Thilakarathna and Rupasinghe, 2022). Similar to grapes, apples are one of the most widely consumed fruits in the world. About 2/3 of the polyphenols found in apples are oligomeric and polymeric PAC. The PAC concentration in apples depends on the apple variety. Renetta, Red Delicious, and Granny Smith apple varieties contain higher concentrations of PAC (1 – 2 mg/g FW) compared to the other varieties such as Royal Gala, Braeburn, and Fuji (0.5 – 0.7 mg/g FW) (Vrhovsek et al., 2004). Apple processing for the production of juice, sauce, and pie, generates significant amounts of waste as pressed pomace, core, peels, and seeds. Apple processing by-products, especially apple peels, contain PAC monomers such as catechin and epicatechin (Rupasinghe and Kean, 2008). The PAC concentration in Red Delicious apple skin is estimated to be 7.2 mg/g DW, which accounts for 44.5% of the total phenolics in the apple skin (Mendoza-Wilson et al., 2016).

Cereals, beans, nuts, and spices are also important dietary sources of PAC. The PAC concentrations in sorghum (1.9 mg/g FW) (Gu et al., 2004) and brown rice (1 – 2 mg/g, moisture < 14% *w:w*) (Gunaratne et al., 2013) are considerably high compared to the other cereals such as barley, which contains only 0.3 – 0.7 mg/g FW of PAC (Verardo et al., 2015). Major cereals, corn, wheat, and white rice are not significant sources of PAC (Gu et al., 2004). The low concentrations of PAC in major cereals may be a result of

excessive processing. By-products of cereal milling, such as bran and germ are proven to contain tannins (Smuda et al., 2018). Grain legumes, especially the ones with red or black seed coats are rich sources of dietary PAC. The oligomeric PAC (up to heptamers) concentrations in red and black cowpea are around 1.6 and 2.6 mg/g DW, respectively (Orita et al., 2019). The total PAC concentration in red kidney beans can be high as 5.6 mg/g FW (Gu et al., 2004).

Cocoa is an important dietary source of PAC due to its integration with many food products. Commercially available cocoa powder contains about 19 – 24 mg/g of PAC while baking chocolate contains about 12 – 16 mg/g of PAC. The PAC concentration in dark chocolate (2 – 4 mg/g) is significantly high compared to milk chocolate (0.4 – 0.7 mg/g) (Miller et al., 2006). Also, by-products of cocoa processing can be used for the extraction of bioactive PAC (Cádiz-Gurrea et al., 2017). PAC are also found in commonly consumed nuts. The PAC concentration in hazelnuts and pecans is about 5 mg/g FW. Peanuts (roasted) and cashews are not significant sources of PAC (Gu et al., 2004). However, peanut skin contains about 5 mg/g FW of PAC and is considered a suitable source for PAC extraction (de Camargo et al., 2017). PAC are widely available in commonly consumed foods, and the by-products of food processing can be used for the extraction of PAC.

In the United States (US) the daily intake of PAC by an adult (> 19 years) is estimated to be 95 mg. The majority of the PAC consumed by the US adult population are the oligomeric and polymeric PAC. Polymeric PAC account for 30% of the total consumed PAC while oligomeric PAC (4 – 10 monomers) account for 26%. The monomeric, dimeric, and trimeric PAC account for 22%, 16%, and 5% of the total PAC consumed by the US adult population, respectively (Y. Wang et al., 2011). The majority of the PAC consumed

in the European and Mediterranean countries are polymers larger than decamers (Knaze et al., 2012). In the US, women consume more PAC compared to men when PAC consumption is adjusted to energy intake. Interestingly, PAC intake by alcohol consumers (adjusted for energy intake) is higher compared to the population not consuming alcohol. This can be explained by the positive relationship between PAC intake and wine consumption. In fact, wine together with tea and legumes are the primary food sources of PAC for the US population (Y. Wang et al., 2011). The average PAC consumption considerably varies between countries. In the European Union (EU) countries, the average PAC intake by adults (18 – 64 years) is estimated to be 124 mg/day. The PAC consumption in Spain, Italy, and France is higher when compared to the other EU countries with average PAC consumption estimated to be 178, 161, and 144 mg/day, respectively. The distribution of PAC consumption is considerably skewed in all the EU countries. For instance, the median PAC intake in Germany is only 5 mg/day despite the average intake is high as 143 mg/day. This wide disparity in PAC intake overlaps with the regional variations of food patterns (Vogiatzoglou et al., 2015). Thus, PAC consumption significantly varies among individuals based on demography and food patterns.

1.1.4. Absorption, metabolism, and colonic degradation of PAC

In foods, PAC may exist bound with carbohydrates, proteins, and metal ions. Oligomeric and polymeric PAC can bind with the amylose and linear fragments of amylopectin. Interactions between PAC and these carbohydrate molecules are believed to occur through hydrophobic interactions (Barros et al., 2012). Similarly, PAC can spontaneously bind with food protein through hydrophobic interactions, hydrogen bonds, and van der Waals forces (Tang et al., 2021). The PAC bound to food components must be

uncoupled before absorption. Only the free-PAC solubilized in the aqueous phase can be absorbed into the body (Ou and Gu, 2014). However, digestion of the PAC-carbohydrate/protein complexes can be challenging, as PAC are known to reduce nutrient digestibility. PAC, especially the ones of higher degrees of polymerization, can significantly reduce amylase and protease activity together with the digestibility of calcium and zinc *in vivo* (Zhong et al., 2018).

Findings about the depolymerization of PAC during the gastrointestinal transition are controversial. Several *in vitro* studies have suggested the ability of PAC to undergo depolymerization when subjected to simulated digestion. The PAC trimers and polymers can be depolymerized into monomers under simulated oral digestion (Tao et al., 2020). Similarly, oligomeric PAC (trimers to hexamers) isolated from cocoa can be depolymerized in the simulated gastric juice (pH 2). Depolymerization of the cocoa PAC oligomers is a rapid process that progressively turns 60% – 80% of the PAC oligomers into monomers and dimers within the first 1.5 h of the simulated digestion process. Interestingly, depolymerization of the PAC dimers can be significantly inefficient under the same digestion conditions. Only 15% of the dimers had been depolymerized into monomers after 2.5 h of simulated gastric digestion (Spencer et al., 2000). Thus, depolymerization during the gastrointestinal transition may depend on the degree of polymerization. Moreover, the highly acidic conditions in gastric digestion may be important to uncouple PAC from proteins (Tao et al., 2020) and increase the absorbable free-PAC content. PAC may also degrade under alkaline conditions. Both PAC trimers and tetramers may be unstable under the alkaline conditions of intestinal digestion and undergo depolymerization (Tao et al., 2020). Procyanidin B2 and B5 isolated from cocoa had

undergone depolymerization into epicatechin after *ex vivo* perfusion through the small intestines of rats (Spencer et al., 2001).

Despite *in vitro* experiments indicating the ability of PAC to be depolymerized during the gastrointestinal transition, the *in vivo* studies indicate otherwise. Oligomeric procyanidins of cocoa (up to pentamers) had been stable during gastric digestion in humans (Rios et al., 2002). Similarly, sorghum procyanidins remained intact during the gastrointestinal transition in rats (Gu et al., 2007). The depolymerization of PAC during the gastrointestinal transition may depend on the type of PAC. Sorghum PAC are resistant to depolymerization in simulated digestion while bayberry PAC undergo depolymerization. Unlike sorghum PAC, which are predominantly procyanidins of catechin and epicatechin monomers, bayberry PAC are primarily prodelphinidins made of epigallocatechin gallate monomers (Tao et al., 2020). Thus, further studies are required to study the ability of different types of PAC to undergo depolymerization during the gastrointestinal transition.

The absorbability of PAC drastically declines with the increasing degree of polymerization. Catechin, together with PAC dimers and trimers could permeate through human colorectal adenocarcinoma (Caco-2) cell monolayers *in vitro*. The permeability coefficients ($0.9 – 2.0 \times 10^{-6}$ cm s^{-6}) of the monomer, dimers, and trimers had been similar and comparable to mannitol. Mannitol is a small hydrophilic molecule that permeates through cell monolayers *via* the paracellular route (Deprez et al., 2001). Procyanidin dimers B2 and B5 had been observed to permeate through the small intestines of rats in an *ex vivo* perfusion experiment (Spencer et al., 2001). An *in situ* perfusion study indicated that monomeric PAC are better absorbed than dimeric PAC in the small intestines

of rats. Only 5% – 10 % of the A-type procyanidin dimers are absorbed in the small intestines of rats compared to the monomeric epicatechin. Moreover, procyanidin dimers A1 and A2 can be better absorbed than procyanidin B2. However, A-type PAC trimers and tetramers are not absorbed in the small intestine of rats (Appeldoorn et al., 2009b), demonstrating the decline of PAC absorption efficiency with the increasing polymerization. Permeation of oligomeric PAC, with a mean degree of polymerization of six, through Caco-2 cell monolayers is estimated to be 10 times lower compared to the PAC trimers. Permeation of the small PAC molecules through Caco-2 cell monolayers is believed to occur through passive diffusion *via* the paracellular route (Deprez et al., 2001). Absorption of the PAC oligomers and polymers *in vivo* is notably limited. PAC oligomers or their metabolic conjugates had not been detected in the blood plasma and urine of the rats supplemented with catechin, procyanidin dimer B3, and grape seed PAC. Only the catechin and epicatechin had been absorbed into the rats (Donovan et al., 2002). The absorption of the procyanidin B2 and other PAC oligomers (dimers to decamers) is negligible in humans (Ottaviani et al., 2012).

The absorbed PAC monomers can undergo extensive phase 2 metabolism in the small intestine and liver (Donovan et al., 2001). Methylated, sulphated, and glucuronidated epicatechins had been detected in the blood plasma of humans after the consumption of epicatechin-rich dark chocolate. Epicatechin-3′-*β*-*D*-glucuronide, epicatechin 3′-sulphate, and 3′-*O*-methyl epicatechin sulphates were the major epicatechin metabolites identified in this study (Actis-Goretta et al., 2012). Similar metabolites had been detected in the blood plasma of Wistar rats perfused with catechin. Glucuronidation of the PAC monomers primarily occurs in the intestine while sulfation and methylation mainly occur in the liver

(Donovan et al., 2001). Unlike PAC monomers, phase 2 metabolism of the dimers is limited (Appeldoorn et al., 2009b). Metabolites of catechin and epicatechin have been detected in the bile of both humans (Actis-Goretta et al., 2013) and rats (Donovan et al., 2001). This indicates the elimination of the absorbed PAC monomers with bile in addition to urine.

The majority of the ingested PAC evades absorption in the small intestine and reaches the colon. In a human study, 70% of the ingested green tea flavanols had reached the ileum without being absorbed (Stalmach et al., 2010). The colonic microbiota can degrade these unabsorbed PAC into simple metabolites. Incubation of PAC monomers and dimers with human fecal microbes could degrade procyanidins into simple metabolites such as benzoic acid, 2-phenylacetic acid, 3-phenylpropionic acid, 2-(3′-hydroxyphenyl) and 2-(4′hydroxyphenyl)acetic acids, 3-(3′-hydroxyphenyl)propionic acid, hydoxyphenylvaleric acid, and *γ*-valerolactones (Ou et al., 2014). PAC degradation by microbes is a multi-step process. Fermentation of grape seed PAC (a mixture of monomers to trimers), initially produces 5-(3′,4′-diydroxyphenyl)-*γ*-valerolactone and 4-hydroxy-5-(3′,4′-dihydroxyphenyl)-valeric acid as the intermediate metabolites in the first 10 h of the fermentation process. The concentrations of phenolic acids such as 3-(3,4-dihydroxyphenyl)-propionic, 3,4-dihydroxyphenylacetic, 4-hydroxymandelic and gallic acids also significantly increase during the first 5 – 10 h of fermentation. Subsequently, the intermediate metabolites and phenolic acids undergo dehydroxylation during 10 – 48 h of the fermentation to generate mono- and non-hydroxylated metabolites such as phenyl propionic, phenylacetic, and benzoic acid derivatives together with catechol (Sánchez-Patán et al., 2012). The efficiency of the colonic degradation of PAC considerably varies

between individuals. Fecal microbiota isolated from three individuals demonstrated varying efficiencies in the degradation of PAC *in vitro*. Only one of the three individuals has been able to rapidly degrade both galloylated and non-galloylated PAC. Such variations in PAC degradation may have resulted from the gut microbiota disparity among the three individuals (Sánchez-Patán et al., 2012). The potential of colonic bacteria to degrade PAC declines with increasing polymerization. Human fecal bacteria can degrade about 54% and 57% (*w:w*) of catechin and epicatechin, respectively, within 24 h. Degradation of the procyanidin B2, procyanidin A2, and oligomeric PAC from apples and cranberry had been around only 38%, 28%, 21%, and 20% (*w:w*), respectively (Ou et al., 2014). Another *in vitro* study contradicts these results by demonstrating that dimers and trimers undergo microbial degradation better than PAC monomers when incubated with human fecal microbes (Tao et al., 2020). The same study reports that fecal microbiota prefers to utilize PAC dimers and trimers over monomers (Tao et al., 2020).

The probable pathways of B-type PAC (procyanidin B2,) degradation and common metabolites generated during this degradation process have been identified by the fermentation of epicatechin and procyanidin B2 with human fecal microbiota (Fig. 1.3) (Stoupi et al., 2010). Initially, the microbes can cleave the C-ring of the procyanidin B2 dimer (1) at the C2 position (2) or oxidize and cleave the A-ring (3). Oxidation of the A-ring can occur simultaneously with the cleaving of the C-ring without cleaving the A-ring (4). Fecal microbes can also cleave the C4 – C8 interflavan linkage of procyanidin B2 to form two epicatechin molecules (5). Subsequently, C-rings of the epicatechin molecules are cleaved by the microbes at the C2 position (6 and 7) (Ou et al., 2014; Stoupi et al., 2010). However, degradation of procyanidin B2 through cleaving of the C4 – C8

interflavan bond can be inefficient (Appeldoorn et al., 2009a) and a majority of the procyanidin B2 may be degraded through the pathways that directly inflict cleaving and/or oxidation on the dimer (Ou and Gu, 2014). The human fecal microbiota can convert these initial metabolites into 5-(3′,4′-dihydroxyphenyl)-γ-valerolactone (8) and 5-(3′-hydroxyphenyl)-γ-valerolactone (9) (Stoupi et al., 2010). Subsequently, the microbes convert γ-valerolactones into phenylvaleric acid derivatives through acid hydrolysis (10 – 13). The phenylvaleric acid derivatives then undergo β-oxidation and α-oxidation at the aliphatic chain to form phenylpropionic acid derivatives (14 and 15) and phenylacetic acid derivatives (16 and 17), respectively (Stoupi et al., 2010). Microbial catabolism of PAC is a complex process that requires further experimentation to fully understand the reactions, enzymes, and microbes involved in the degradation process. Also, further studies are required to elucidate the catabolism of PAC oligomers and polymers by the human gut microbiota.

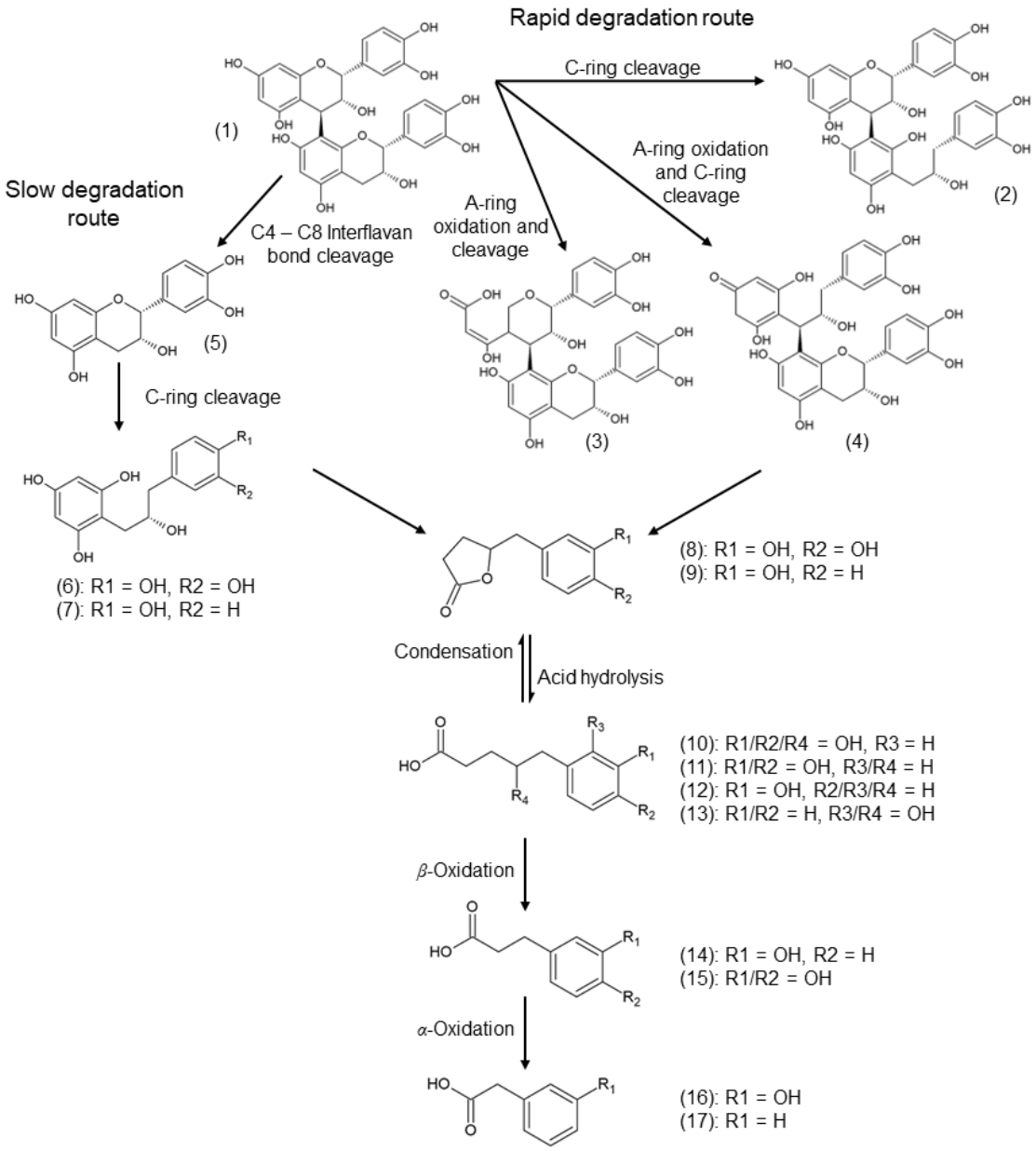

Figure 1.3. Probable pathway of procyanidin B2 catabolism by the human fecal microbiota (Ou et al., 2014; Stoupi et al., 2010). (1), procyanidin B2; (5), epicatechin; (6), 1-(3′,4′-dihydroxy phenyl)-3-(2″,4″,6″-trihydroxy phenyl) propan-2-ol; (7), 1-(hydroxy phenyl)-3-(2″,4″,6″-trihydroxy phenyl) propan-2-ol; (8), 5-(3′,4′-dihydroxy phenyl)-γ-valerolactone; (9), 5-(3′-hydroxy phenyl)-γ-valerolactone; (10), 5-(4-hydroxy)-(3′,4′-dihydroxy) phenyl valeric acid (tentative); (11), 5-(3′,4′-dihydroxy phenyl) valeric acid; (12), 5-(3′-hydroxy phenyl) valeric acid; (13), 5-(3′,4′-dihydroxy phenyl) valeric acid; (14), 3-(3′-hydroxy phenyl) propionic acid; (15), 3-(3′,4′-dihydroxy phenyl) propionic acid; (16), 3′-hydroxy phenyl acetic acid; (17), phenyl acetic acid.

1.2. NONALCOHOLIC FATTY LIVER DISEASE

1.2.1. Prevalence and etiology

Nonalcoholic fatty liver disease (NAFLD) is the primary cause of chronic liver diseases in the world (Tariq et al., 2020). About 30% of the global population is affected by NAFLD (Younossi et al., 2023) and the global prevalence of NAFLD among the adult population is predicted to increase up to 55.7 % by 2040 (Le et al., 2022). The term NAFLD is collectively used to describe hepatic abnormalities characterized by excessive lipid accumulation in the absence of alcohol consumption at levels harmful to the liver. These abnormalities can vary from simple steatosis to nonalcoholic steatohepatitis (NASH), which may progress to fibrosis, cirrhosis, and hepatocellular carcinoma (HCC) (Bedossa, 2017). Steatosis, also known as nonalcoholic fatty liver, is defined as the presence of intrahepatic lipids in excess of 5% of the liver weight or the presence of lipid vacuoles in more than 5% of the hepatocytes (Bedossa, 2017; Nassir et al., 2015). Simple steatosis can progress into NASH in 20% – 30% of NAFLD patients with the occurrence of lobular inflammation and hepatocyte ballooning (Fernando et al., 2019). In hepatocyte ballooning (balloon degeneration), the hepatocytes lose the normal polygonal shape and become rounded with a diameter of 1.5 – 2 times larger than healthy hepatocytes. Moreover, ballooned hepatocytes have a thin cytoplasm with a degraded cytoskeleton and consisted of vacuoles of varying sizes together with Mallory-Denk bodies (Caldwell and Lackner, 2017). Both hepatic steatosis and NASH conditions can progress into liver fibrosis and this progression is more aggressive with the NASH (Singh et al., 2015). Chronic liver damage by steatosis and NASH can lead to fibrosis by the excessive accumulation of extracellular proteins such as collagen in the liver. Continuous accumulation of the extracellular proteins

in the liver can form fibrous scars. These fibrous scars can alter hepatic parenchyma structure, and together with nodules developed by the regenerating hepatocytes can be manifested as hepatic cirrhosis (Bataller and Brenner, 2005). Chronic liver injury and cirrhosis are the primary elicit of hepatocellular carcinoma (HCC). In fact, 80% of the HCC cases onset under the presence of cirrhosis and chronic liver diseases (Suresh et al., 2020).

Obesity is a primary risk factor for NAFLD development (Fig. 1.4). The increased prevalence of NAFLD is directly proportional to the increasing prevalence of obesity (Marjot et al., 2020). A study conducted using US-based population data found that NAFLD prevalence in obese individuals (body mass index, BMI $\geq$ 30 kg/m^2) is high as 48.1% and the prevalence of NAFLD in non-obese individuals is only 18.9%. Maintaining a healthy body weight reduces the risk of NAFLD. However, being obese in an earlier stage of life can significantly increase the risk of NAFLD. Individuals currently not obese, yet had been in early adulthood are more prone to develop NAFLD compared to individuals with no history of obesity (Wang et al., 2023). Moreover, central obesity creates a higher risk of NAFLD compared to general obesity. The fold NAFLD risk increment in the individuals with higher waist circumference, waist-to-hip ratio, and BMI are 1.34, 3.06, and 1.85, respectively (Pang et al., 2015). Obesity is a major risk factor for insulin resistance, type-2 diabetes (T2D), and metabolic syndrome (MetS). These conditions can induce the pathogenesis of NAFLD and commonly coexist in NAFLD patients (Kosmalski et al., 2022). The prevalence of NAFLD in the T2D population is estimated to be 54%, based on the meta-analysis of data from multiple studies (Atan et al., 2017). Both MetS and insulin resistance are closely associated with NAFLD. In fact, NAFLD is reckoned as the hepatic component of MetS and insulin resistance (Bugianesi et al., 2010). The major

physiological abnormalities manifested in MetS include central obesity, hypertriglyceridemia, hyperglycemia, hypertension, and depletion of blood plasma high-density lipoprotein (HDL). The prevalence of NAFLD in MetS patients is estimated to be 73%, based on a study conducted using one hundred MetS patients. The same study estimated the prevalence of NAFLD in the non-MetS population to be only 38% (Goyal et al., 2020).

High-caloric diets together with physical inactivity are the root cause of all primary risk factors of NAFLD (Fig. 1.4). Induction of NAFLD had been demonstrated in multiple high-fat and high-sucrose (HFHS) diet-fed mouse models (Demaria et al., 2023). Intermittent consumption of high-caloric diets can significantly increase the risk of NAFLD. Administration of an HFHS diet weekly had been sufficient to induce NAFLD in C57BL/6J mice. Interestingly, after 12 weeks, the severity of the measured NAFLD parameters in these mice had been comparable with mice daily fed with the HFHS diet. (Demaria et al., 2023). Therefore, food patterns and lifestyle changes can significantly avert the risk of NAFLD. Physical exercises can significantly reduce the NAFLD risk by restricting steatosis through increased hepatic fatty acid (FA) oxidation and reduced *de novo* lipogenesis (DNL). Moreover, physical exercises can reduce the release of damage-associated molecular patterns that can induce mitochondrial and hepatocyte damage (van der Windt et al., 2018). Smoking is another modifiable lifestyle risk factor of NAFLD. The NAFLD risk is considerably high among current, past, and passive smokers (Rezayat et al., 2018). According to a Japanese cohort study, smoking can double the risk of NAFLD. Moreover, the risk of NAFLD can significantly increase with the number of cigarettes smoked daily (Okamoto et al., 2018).

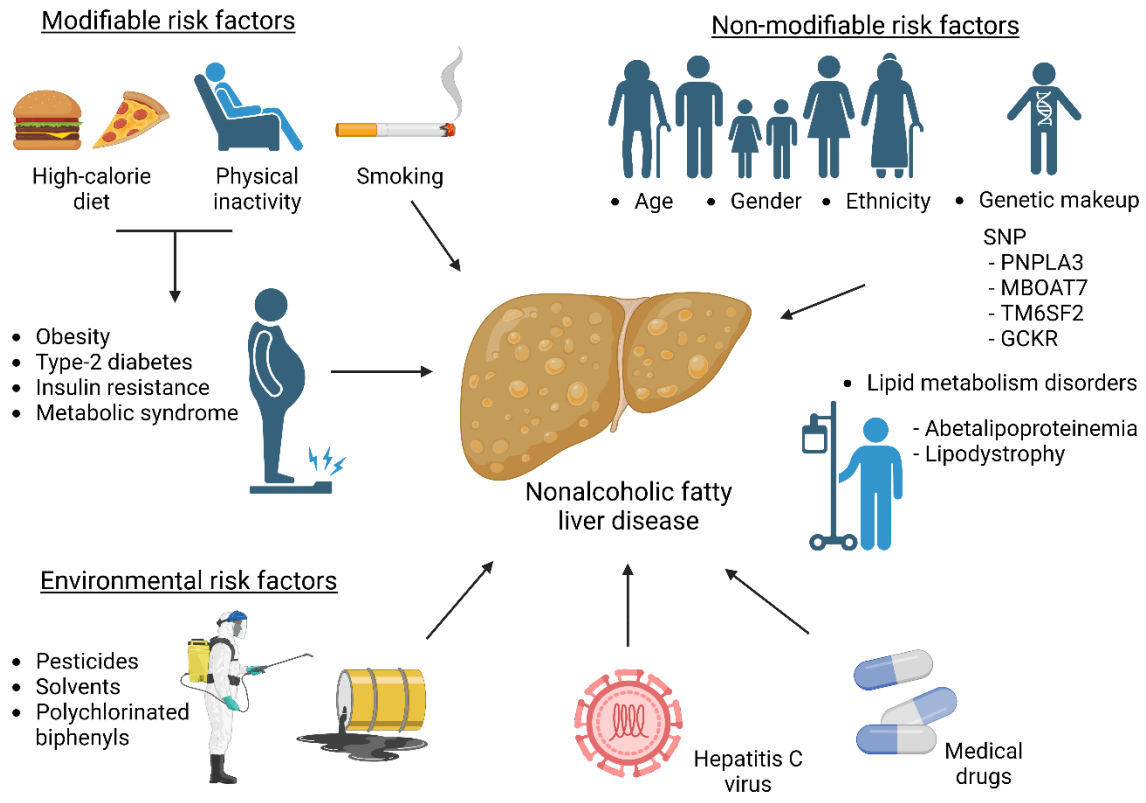

Figure 1.4. Major risk factors of nonalcoholic fatty liver disease. GCKR, glucokinase regulatory protein; MBOAT7, membrane-bound *O*-acetyltransferase domain-containing protein 7; PNPLA3, patatin-like phospholipase domain-containing protein 3; SNP, single nucleotide polymorphism; TM6SF2, transmembrane 6 superfamily member 2 (Created with BioRender.com, a license purchased).

Apart from the risk factors linked with poor lifestyle choices, age, gender, ethnicity, and genetic makeup can predispose some individuals to NAFLD (Fig. 1.4). The risk of NAFLD considerably increases with age. A Chinese cohort study had estimated the NAFLD incident rates (both male and female cumulative) of the 20 – 34, 35 – 49, 50 – 64, and over 65 years of age groups to be 11.7%, 15.9%, 21.5%, and 22.8%, respectively. The highest incidence rate in men is reported for the 35 – 49 years age group. In women, the highest incidence rate is observed in the age group over 65 years (Lin et al., 2022). This late onset of NAFLD in women may be explained by their resistance to dysmetabolism. Many studies suggest that the low incidence rate of NAFLD in women is the result of

estrogen-mediated regulation of metabolism and inflammation. In pre-menopause women, estrogen can ameliorate steatosis by favouring subcutaneous lipid accumulation, inhibiting lipolysis in adipose tissues, reducing the free fatty acids (FFA) uptake, and promoting FA *β*-oxidation. Promotion of the FA *β*-oxidation limits the oxidative reactive oxygen species (ROS) generation that can damage hepatocytes and induce inflammatory responses (Torre, 2020). A recent meta-analysis estimated that NAFLD risk is 19% lower in women compared to men. However, the risk of fibrosis in women is significantly higher (37%) than in men, especially after 50 years of age. This increment in the NAFLD risk in elderly women can be attributed to the wearing protection of estrogen after menopause (Balakrishnan et al., 2021).

Ethnicity is another factor that determines the NAFLD risk in individuals. A US population-based study has revealed that prevalence of the NAFLD is significantly high in the Hispanic population compared to the non-Hispanic white population (22.9% *vs*. 14.4%). The lowest NAFLD prevalence was observed among the black population (13%) (Rich et al., 2018). The variations in food patterns, lifestyle, and socioeconomic status together with genetics may create the NAFLD prevalence heterogeneity between different ethnic populations (Riazi et al., 2022). A cohort study for the identification of genetic variants associated with liver damage markers revealed that Mexican Americans may be more genetically prone to NAFLD compared to the United Kingdom and Japanese cohorts (Sabotta et al., 2022). Genetic mutations by single nucleotide polymorphism (SNP) on several genes can increase the risk of NAFLD (Fig. 1.4). The CC genotype (G > C, rs738409) of the patatin-like phospholipase domain-containing protein 3 (PNPLA3) and the TT genotype (C > T, rs64173) of the membrane-bound *O*-acetyltransferase domain-

containing protein 7 (MBOAT7) genes are associated with increased incidence of the NAFLD (Mu et al., 2022). Also, SNP in transmembrane 6 superfamily member 2 (TM6SF2) (A > G, rs58542926) and glucokinase regulatory protein (GCKR) (C > T, rs1260326) genes can increase the risk of NAFLD pathogenesis (Martin et al., 2021). However, SNP in some genes such as AA genotype (G > A, rs744166) of signal transducer and activator of transcription (STAT) 3 can reduce the risk of NAFLD (Mu et al., 2022).

The genetic mutations favouring the pathogenesis of NAFLD had been identified as a major risk factor for lean and non-obese (LNB) NAFLD. In lean NAFLD, the hepatic abnormalities of NAFLD are present in individuals with healthy body weight, BMI < 25 kg/m^2 for Caucasians and BMI < 23 kg/m^2 for Asians. The term non-obese NAFLD is used when NAFLD is present in non-obese individuals, BMI < 30 kg/m^2 for Caucasians and BMI < 25 kg/m^2 for Asians. The prevalence of LNB-NAFLD is estimated to be 5% of the global population and about 20% of the total NAFLD cases (Kuchay et al., 2021). The secondary risk factors of NAFLD such as lipid metabolism disorders, viral infections, and toxins may play key roles in the pathogenesis of LNB-NAFLD. Rare lipid metabolism disorders such as abetalipoproteinemia, hypobetalipoproteinemia, familial combined hyperlipidemia, glycogen storage disease, Weber-Christian syndrome, and lipodystrophy are associated with the early-life pathogenesis of NAFLD (Kneeman et al., 2012). The hepatotropic hepatitis C virus (HCV) can induce steatosis and NASH by the dysregulation of lipid and glucose metabolism in hepatocytes. The mean prevalence of NAFLD in HCV infection is high as 55%. The HCV core proteins can promote hepatic lipid accumulation by upregulating sterol regulatory element binding protein (SREBP)-1 and -2, peroxisome proliferator-activated receptor (PPAR), promoting DNL, and downregulating microsomal

triglyceride transfer protein (MTP) (Adinolfi et al., 2016). Environmental chemicals such as pesticides, solvents, and polychlorinated biphenyls are associated with the development of NAFLD (Al-Eryani et al., 2015). Medicinal drugs, even the most commonly consumed drugs, including acetaminophen and aspirin, can be hepatotoxic and contribute the NAFLD pathogenesis (Kolaric et al., 2021). NAFLD is a disease with multiple primary and secondary etiologies. Lifestyle and food pattern improvements can significantly reduce the risk of NAFLD. Identification of the demographic, genetic, and other secondary risk factors is crucial to avert the continued to increase risk of NAFLD.

1.2.2. Pathogenesis of steatosis and NASH

The pathogenesis of steatosis occurs by the imbalance between hepatic triglyceride (TG) accumulation and expenditure. The liver is not the primary location of TG storage, yet it is the central organ for lipid metabolism (Kawano and Cohen, 2013). The TG in the liver can derive from the diet, DNL, and non-esterified FA/ FFA (Fig. 1.5). The serum FFA can originate from the adipose tissue lipolysis and FA spillover during chylomicron degradation. In NAFLD patients, the contribution of diet, DNL, and FFA to hepatic TG accumulation is 14.9%, 26.1%, and 59%, respectively (Donnelly et al., 2005). Therefore, diet, DNL, and FFA are therapeutic targets with similar importance for steatosis mitigation. Postprandial lipid metabolism is a finely regulated complex process. Briefly, dietary FA absorbed in the gut is converted to TG in the enterocytes and temporarily stored as cytoplasmic lipid droplets or assembled into chylomicrons (D'Aquila et al., 2016). These chylomicrons enter the bloodstream through the lymphatic system. The adipose tissues and skeletal muscles can uptake the TG in chylomicrons by the activity of the lipoprotein lipase (LPL). The remnants of chylomicrons that remain after unloading the TG content are

cleared by the liver. However, under excessive availability of dietary lipids, the adipose and muscle tissues may fail to uptake all the FA released from chylomicrons, creating a spillover of FFA (Brouwers et al., 2016). Excessive dietary carbohydrate (sugars) intake can create hyperglycemic and hyperinsulinemia conditions that upregulate carbohydrate response element-binding protein (ChREBP) and SREBP-1, respectively. Both ChREBP and SREBP-1 can promote DNL by the upregulation of acetyl-CoA carboxylase (ACC) and fatty acid synthase (FAS) enzymes (Heeren and Scheja, 2021). ACC is the rate-limiting enzyme of FA synthesis. The liver attempts to prevent excessive lipid accumulation by increasing TG secretion in very-low-density lipoprotein (VLDL) and promoting FA oxidation in mitochondria (Brouwers et al., 2016).

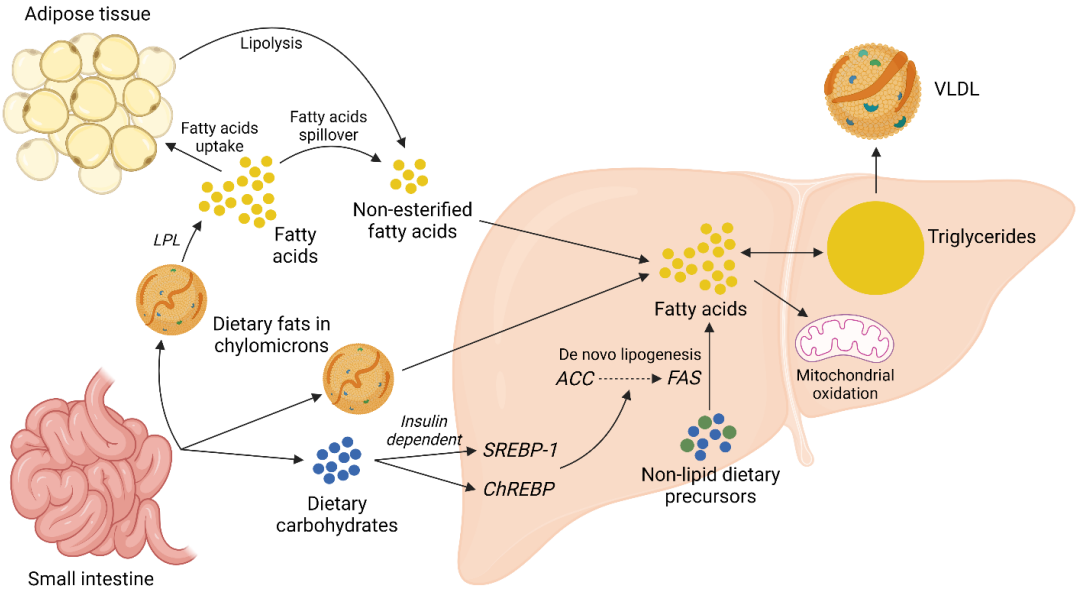

Figure 1.5. Hepatic lipid metabolism. ACC, acetyl-CoA carboxylase; ChREBP, carbohydrate response element-binding protein; FAS, fatty acid synthase; LPL, lipoprotein lipase; SREBP-1, sterol regulatory element binding protein-1; VLDL, very-low-density lipoprotein (Created with BioRender.com, a license purchased).

1.2.2.1. Overexpression of FA transporters

During the pathogenesis of steatosis, substantial alterations in the hepatic lipid metabolism can arise to favour excessive lipid accumulation. There are multiple membrane proteins in the hepatocytes to facilitate FFA uptake from the bloodstream. FA transport proteins (FATP), cluster of differentiation 36 (CD36)/ fatty acid translocase, and caveolin-1 are the major proteins involved in the transmembrane influx of FA (Li et al., 2022). Hepatic expression of the FATP can significantly increase during the pathogenesis of NAFLD. Overexpression of the FATP1, FATP2, and FATP3 had been confirmed at the hepatic mRNA level in a high-fat diet (HFD)-fed mouse model (Ran et al., 2023). CD36 is another well-known FFA transporter overexpressed in NAFLD. Increased expression of the CD36 had been observed at hepatic mRNA and protein levels in both steatosis and NASH patients. Interestingly, overexpression of the CD36 can be driven by multiple risk factors of NAFLD, including, insulin resistance, hyperinsulinemia, and HCV infection (Miquilena-Colina et al., 2011). The role of CD36 in NAFLD pathogenesis is not merely limited to FFA uptake. CD36 can activate insulin-dependent DNL through the SREBP-1-mediated activation of the adenosine triphosphate (ATP) citrate lyase (ACLY), ACC, and FAS lipogenic enzymes. CD36 promotes the activation of SREBP-1 by binding with the insulin-induced gene-2 (INSIG2). The unavailability of INSIG2 to bind with SREBP cleavage-activating protein (SCAP) facilitates the translocation of SREBP-1 from the endoplasmic reticulum (ER) to Golgi for processing and subsequent activation (Zeng et al., 2022a). The ability of CD36 to disrupt FA β-oxidation can further promote hepatic lipid accumulation. Palmitoylation of the CD36 restricts the FA β-oxidation in HepG2 cells *in vitro*. Inhibition of CD36 palmitoylation can re-establish the FA β-oxidation by activating

the 5′ adenosine monophosphate-activated protein kinase (AMPK) pathway (Zhao et al., 2018). Also, inhibition of palmitoylation promotes the translocation of CD36 onto the mitochondrial membrane. On the mitochondrial membrane, CD36 acts as a bridge to transfer long-chain FA (LCFA) to long-chain acyl-CoA synthase 1 (ACSL1) to produce acyl-CoA to undergo *β*-oxidation (Zeng et al., 2022b). The overexpression of CD36 is associated with the progression of hepatic steatosis to NASH by the induction of hepatic inflammation. There is a positive correlation between CD36 expression and hepatocyte apoptosis in obese NASH patients. Hepatocyte apoptosis can trigger inflammation and fibrosis of the liver tissue (Bechmann et al., 2010). Moreover, palmitoylated CD36 may induce hepatic inflammation through the c-Jun-N-terminal kinase (JNK) and nuclear factor-*kappa*-light-chain-enhancer of activated B cells (NF-*κ*B) signalling (Zhao et al., 2018). The ability of CD36 to identify pathogen-associated molecular patterns (PAMP) and damage-associated molecular patterns (DAMP) can promote hepatic inflammation by the activation of mitogen-activated protein kinases (MAPK) and NF-*κ*B inflammatory cascades (Y. Chen et al., 2022). The cellular FA uptake can also occur through the special invaginations of the cell membrane known as caveolae lipid rafts. Caveolin-1 is a FA binding protein of the caveolae lipid rafts (Meshulam et al., 2006). A significant hepatic upregulation of the expression of caveolin-1 had been observed in mice with NAFLD (Qiu et al., 2013). Moreover, caveolin-1 may regulate cellular FA uptake by controlling the availability of CD36 in the cell membrane (Ring et al., 2006). Similar to CD36, caveolin-1 may also have multiple roles in the progression of NAFLD. Caveolin-1 is overexpressed in hepatocellular carcinoma (HCC) patients with a history of NAFLD. Overexpression of caveolin-1 can increase the proliferation and ensure the survival of the hepatoma cells *in*

vitro (Takeda et al., 2018). However, a recent study contradicts these findings and suggests a beneficial role of caveolin-1 in the mitigation of NAFLD. In this study, a significant reduction of the hepatic caveolin-1 levels had been observed in mice fed with an HFD. Restoration of the depleted caveolin-1 levels by using caveolin-1 scaffolding domain peptides mitigated the hepatic lipid accumulation and promoted autophagy in the mice (Xue et al., 2020). The transmembrane FA transporters play a key role in NAFLD pathogenesis by acting as gateways for excessive FFA influx and regulation of hepatic lipid metabolism and inflammation.

1.2.2.2. Disruption of FA oxidation

The hepatocytes attempt to regulate the excessive influx of FFA by oxidation in mitochondria and excretion in VLDL (Brouwers et al., 2016). The oxidation of FA is dependent on the transport of FA into the mitochondrial matrix to undergo β-oxidation. Initially, the LCFA are converted into acyl-CoA and esterified with the L-carnitine to produce acetyl-carnitine. Esterification of the acyl-CoA with L-carnitine is facilitated by the carnitine-palmitoyl-transferase-1 (CPT1) or carnitine-acyl-transferase-1 (CAT1) located on the outer membrane of the mitochondria. The acyl-carnitine can enter the intermembrane space of the mitochondria. The carnitine-acylcarnitine translocase (CACT) enzyme on the inner mitochondrial membrane transports acyl-carnitine into the mitochondrial matrix in exchange for free L-carnitine. In the mitochondrial matrix, CPT2 de-esterifies acyl-carnitine into acyl-CoA and L-carnitine (Savic et al., 2020). The oxidation of dietary FA in NAFLD patients is considerably low compared to healthy subjects. A breath-test study using ^{13}C labelled palmitic acid estimated that FA oxidation in NAFLD patients is 27% lower than in healthy subjects (Naguib et al., 2020). This

reduction in FA oxidation is attributed to the disruption of FA β-oxidation under NAFLD conditions. The reduction of L-carnitine and acyl-carnitine levels in mice with hepatic lipid accumulation signifies the importance of FA β-oxidation for hepatic lipid homeostasis (Xia et al., 2011). Similar to the L-carnitine, the hepatic levels of CPT1 considerably decline in NAFLD, suggesting impaired mitochondrial FA β-oxidation (Tokoro et al., 2020). However, disruption of FA oxidation may not occur in early NAFLD but once the disease progress to NASH. In early NAFLD, the mitochondria may adapt to the excessive influx of FA by increasing FA oxidation. A study comparing liver biopsies revealed that hepatic mitochondrial respiration in obese individuals with or without steatosis is 4.3 – 5.0 times higher compared to healthy lean individuals. Mitochondrial respiration declines by 31% – 40% when steatosis progresses into NASH (Koliaki et al., 2015). PPAR-α is a master regulator of mitochondrial FA β-oxidation. Activation of the PPAR-α can promote the FA β-oxidation in hepatocytes (Fig. 1.6). PPAR-α is activated by multiple stimulators such as postprandial insulinemia, FA ligands derived by lipogenesis and TG hydrolysis, glucagon secreted during fasting, and AMPK-mediated energy generation (Pawlak et al., 2015). Apart from the hepatic glucose and lipid metabolism, the PPAR-α plays a key role to prevent hepatic inflammation through multiple mechanisms. The FA β-oxidation promoted by PPAR-α prevents the excessive accumulation of hepatic lipids ready to undergo lipid peroxidation and subsequent ROS generation. Reduction of ROS generation (oxidative stress) can ameliorate hepatic inflammation and fibrosis induced by hepatocyte damage (Pawlak et al., 2015). Moreover, PPAR-α can directly inhibit proinflammatory transcription factors such as NF-κB, activator protein (AP)-1, and STAT to mitigate hepatic inflammation (Bougarne et al., 2018). Analysis of the liver biopsies revealed a negative

association between the PPAR-α expression and the severity of NASH (Francque et al., 2015). Thus, activation of PPAR-α is believed to be a viable therapeutic target for the mitigation of NAFLD. Reactivation of PPAR-α by using fenofibrate (a PPAR-α agonist) could significantly reduce liver damage markers and improve lipid metabolism in NAFLD patients. Moreover, PPAR-α activation prevented the loss of lysosomal acid lipase (LAL) activity under NAFLD conditions *in vitro*. LAL prevents hepatic lipid accumulation by the hydrolysis of TG and cholesterol esters to FFA (Gomaraschi et al., 2019). Disruption of FA oxidation is a major contributor to the pathogenesis of NAFLD. PPAR-α plays a critical role to maintain hepatic lipid homeostasis by regulating the FA β-oxidation.

1.2.2.3 TG secretion in VLDL

The hepatic excretion of TG with VLDL can be considerably increased in NAFLD patients (Fujita et al., 2009). The assembling of VLDL for TG excretion is a two-step process that occurs in the ER. Initially, TG is transferred onto apolipoprotein B (ApoB) by the MTP to form small and dense VLDL precursors. These VLDL precursors undergo maturation by fusion with the protein-free TG droplets in the ER (Shelness and Sellers, 2001). Mutations of the ApoB and MTP such as in familial hypobetalipoproteinemia (Tanoli et al., 2004) and abetalipoproteinemia (Berriot-Varoqueaux et al., 2000) respectively, can increase the risk of NAFLD by impaired TG secretion as VLDL. In NAFLD patients, the increased TG secretion in VLDL is evident by the increased blood serum VLDL concentrations and upregulated expression of ApoB100 and MTP. However, the expression of ApoB and MTP are significantly low in the NASH patients compared to the patients with simple hepatic steatosis, suggesting possible impairment of TG secretion as VLDL with the progression of steatosis into NASH (Fujita et al., 2009). A study on the

VLDL secretion rate in nondiabetic obese subjects revealed that the rate of VLDL secretion depends on the intrahepatic lipid (IHL) content. The VLDL secretion rate increases up to 5% of IHL accumulation, plateaus between 5% – 10%, and declines thereafter (Lytle et al., 2019).

1.2.2.4. Adipose tissue dysfunction

The obesity-related adipose tissue dysfunction is associated with the pathogenesis of steatosis and progression to NASH (Fig. 1.6). Human adipose tissues can be categorized as visceral and subcutaneous based on the anatomical location and as white adipose tissue (WAT) and brown adipose tissue (BAT) based on the colour (Parker, 2018). Both subcutaneous and visceral fat contribute to the development of NAFLD. However, a recent study suggests that the amount of visceral fat is more closely associated with the severity of NAFLD compared to the subcutaneous fat content (Mahmoud et al., 2023). Moreover, the density of visceral fat has a higher association with the prevalence of NAFLD compared to the amount (area) of visceral fat (Igarashi et al., 2022). The WAT is primarily specialized for energy (TG) storage while BAT is for thermogenesis. The unique expression of uncoupling protein 1 in the BAT uncouples the mitochondrial respiration to facilitate the release of energy as heat (Parker, 2018). Even though BAT can spend dietary FA as heat, this dietary FA clearance is trivial compared to the heart, liver, skeletal muscles, and WAT. Only about 0.3% of dietary FA are cleared by BAT in cold-acclimated men (Blondin et al., 2017). Insulin resistance and inflammation in WAT can significantly increase the risk of NAFLD pathogenesis. Insulin resistance in the adipose tissue can impair glucose uptake (Leguisamo et al., 2012), increasing the circulating glucose that can induce hepatic TG accumulation through upregulating DNL (Smith et al., 2020). This impairment of glucose

uptake in insulin resistance is associated with the reduced expression of insulin-regulated glucose transporter type 4 (GLUT4) (Leguisamo et al., 2012). Under insulin resistance, the diminished anti-lipolytic activity of insulin causes excessive release of FFA into the bloodstream which can induce hepatic TG accumulation (Friedman et al., 2018). The vascular endothelial growth factor B (VEGF-B) can contribute to NAFLD pathogenesis by promoting lipolysis in the WAT. The expression of VEGF-B significantly increases in the WAT under obesity and NAFLD. Also, the expression of VEGF-B positively correlates with the expression of genes upregulating lipolysis in WAT, and FA uptake, DNL, and inflammatory progression of the steatosis in liver (Falkevall et al., 2023).

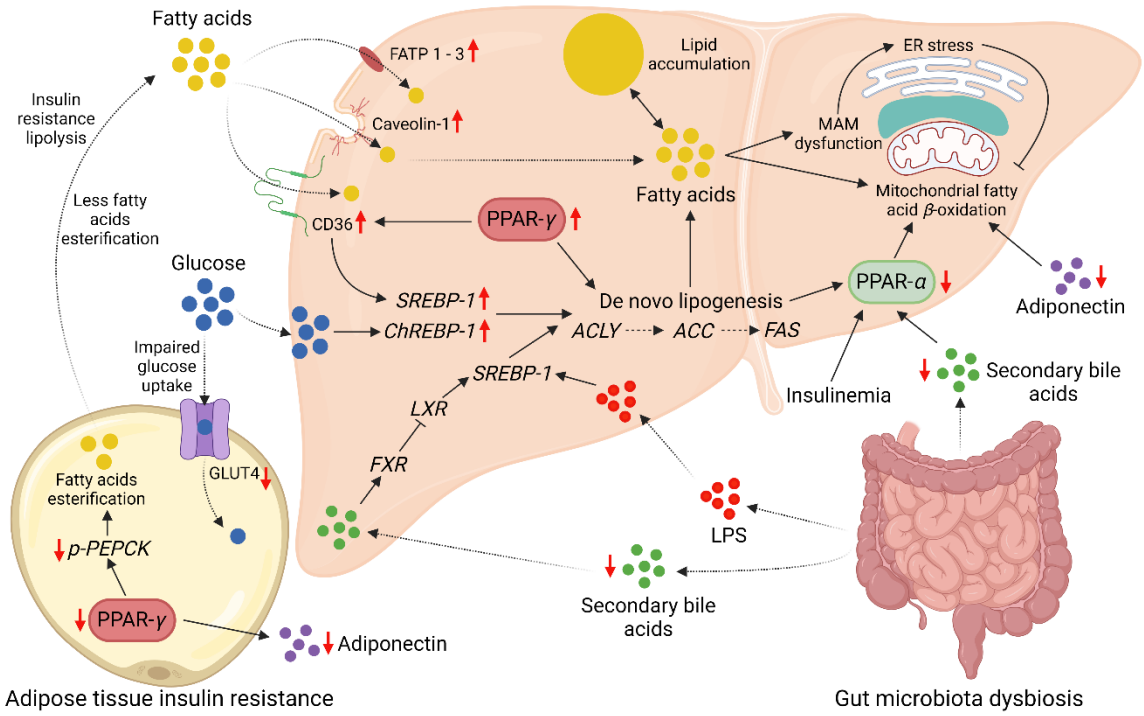

Figure 1.6. Mechanisms of steatosis pathogenesis. The red arrows indicate the increased or decreased expression/production under hepatic steatosis. ACC, acetyl-CoA carboxylase; ACLY, adenosine triphosphate citrate lyase; CD 36, cluster of differentiation 36; ChREBP, carbohydrate response element-binding protein; ER, endoplasmic reticulum; FAS, fatty acid synthase; FATP, fatty acids transport protein; FXR, farnesoid X receptor; GLUT4, glucose transporter type 4; LPS, lipopolysaccharides; LXR, liver X receptor; MAM,

mitochondria-associated ER membrane; PPAR, peroxisome proliferator-activated receptor; *p*-PEPCK, phosphorylated phosphoenolpyruvate carboxylase; SREBP-1, sterol regulatory element binding protein-1 (Created with BioRender.com, a license purchased).

The PPAR-γ is a central regulator of FA metabolism in the adipocytes (Fig. 1.6). Activation of the PPAR-γ increases the transport of FFA into the adipocytes by upregulating the expression of CD36, adipocyte protein 2, and LPL enzyme. PPAR-γ facilitates the conversion of influx FFA into TG for storage by upregulating the expression of the phosphoenolpyruvate carboxykinase (PEPCK) enzyme. PEPCK enzyme is responsible to supply the glycerol backbone required for the esterification of FFA into TG. Also, in adipose tissue, PPAR-γ increases the secretion of adiponectin that can ameliorate NAFLD by promoting hepatic insulin sensitivity and β-oxidation, restricting hepatic gluconeogenesis, and suppressing the production of proinflammatory cytokine tumour necrosis factor (TNF)-α (Skat-Rørdam et al., 2019). The adipocyte expression of PPAR-γ may deplete under the conditions favouring NAFLD pathogenesis. A significant reduction of the expression (at mRNA level) and DNA binding ability of the PPAR-γ in epidermal WAT had been observed in C57BL/6J mice fed with an HFD (Illesca et al., 2019). Thus, activation of the PPAR-γ in adipose tissues can be beneficial to mitigate the risk of NAFLD. In contrast to the adipose tissue, expression of the PPAR-γ is upregulated in the liver under NAFLD. A study evaluating the obese-steatosis and obese-NASH patients revealed that hepatic expression of PPAR-γ can increase largely by 112% and 188%, respectively, at the mRNA level (Pettinelli and Videla, 2011). Activation of the PPAR-γ in the liver promotes lipid accumulation similar to in the adipocytes (Skat-Rørdam et al., 2019). Targeted deletion of the PPAR-γ in hepatic tissue could significantly reduce NAFLD pathogenesis in HFD-fed mice by downregulating the expressions of FA

transporters (CD36, liver-type FA-binding protein, and MTP) and DNL promoters (stearoyl-CoA desaturase 1, SREBP-1, and ACC). However, the deletion of PPAR-γ downregulated the expression of β-oxidation promoters PPAR-α and acetyl-CoA oxidase in the mice livers (Morán-Salvador et al., 2011). Functions of the PPAR-γ in NAFLD pathogenesis are tissue-specific, with underexpression in adipose tissue and overexpression in the hepatic tissue favouring the pathogenesis and progression of the disease.

1.2.3. Two-hit and multiple-hit hypotheses of NAFLD progression

Traditionally, the progression of simple steatosis into NASH and fibrosis is described by the two-hit hypothesis. Overnutrition, obesity, insulin resistance, or metabolic syndrome can act as the first-hit to induce hepatic lipid accumulation and lipid peroxidation. Second-hit continues the hepatic assault by introducing hepatocyte injury and inflammation. The second-hit is driven by hepatocellular oxidative stress, mitochondrial dysfunction, Fas ligand activation, and proinflammatory cytokines production. The endotoxins of gut microbiota can assist the second-hit by promoting hepatic inflammation through innate immune responses (Giorgio et al., 2013). However, recent studies suggest that the pathogenesis and progression of NAFLD are driven by multiple parallel hits. The multiple-hits hypothesis describes the possibility of simultaneous occurrence of several hepatic assaults in the subjects genetically predisposed to NAFLD (Buzzetti et al., 2016). Insulin resistance, hepatic ER and oxidative stresses, mitochondrial dysfunction, adipose tissue lipotoxicity, gut microbiota dysbiosis, and genetic predisposition are the major hits recognized in the multiple-hits hypothesis (Buzzetti et al., 2016; Tilg et al., 2021).

1.2.3.1. ER stress in NAFLD progression

The ER stress assists the progression of steatosis to NASH through multiple mechanisms (Fig. 1.7) associated with the unfolded protein response (UPR) (Lebeaupin et al., 2018). Several studies have illustrated the positive correlation between hepatic lipid accumulation and ER stress both *in vitro* (Rennert et al., 2020) and *in vivo* (Wang et al., 2006). The mitochondria-associated ER membranes (MAM) bridge the ER and mitochondria in hepatocytes both functionally and structurally. Many of the enzymes required for the biosynthesis of TG and cellular lipid metabolism are located in the ER membrane and mitochondria. The MAM are also rich in these enzymes and essential for phospholipid, steroid, glucose, and FA metabolism. The synthesis of phosphatidylcholine, phosphatidyl ethanolamine, and cholesterol occurs in the MAM. Moreover, MAM facilitate the flux of lipid metabolites and calcium between the ER and mitochondria (J. Wang et al., 2020). Lipotoxicity in hepatocytes can disrupt MAM both functionally and structurally. A significant reduction in the calcium flux from ER to mitochondria together with shrinkage of the MAM contact area had been observed in the HepG2 cells overloaded with palmitic acid. This disruption of MAM is assumed to be mediated by the increased distance between the ER and mitochondria through the downregulation of the expression of the MAM structural component mitofusin-2 (Shinjo et al., 2017). Disruption of the MAM leads to ER and oxidative stresses, promoting the progression of NAFLD (J. Wang et al., 2020). Apart from palmitic acid, free cholesterol, lysophosphatidylcholine, and sphingolipids such as ceramides are known activators of hepatic ER stress (Song and Malhi, 2019). The ER stress is manifested by the accumulation of unfolded protein in the ER lumen. The UPR attempts to resolve ER stress by activating three ER transmembrane

stress sensors (Fig. 1.7), namely, protein kinase R-like ER kinase (PERK), inositol-requiring enzyme-1α (IRE1α), and activating transcription factor-6α (ATF6α) (Lebeaupin et al., 2018). These three stress sensors are capable of activating the intrinsic apoptotic pathway through CCAAT-enhancer-binding protein (C/EBP)-homologous protein (CHOP) signalling (Hu et al., 2019). IRE1α activation assists NAFLD progression by inducing inflammatory responses through the nucleotide-binding domain, leucine-rich-containing family, pyrin domain-containing-3 (NLRP3) inflammasomes, and NF-κB and JNK signalling (Lebeaupin et al., 2018). Also, activation of IRE1α in the liver resident macrophages, the Kupffer cells, can induce hepatic ischemia/reperfusion (I/R) injury. Inhibition of IRE1α in mice induced for I/R injury had depicted significant reductions in the hepatic infiltration of $Ly6G^+$ neutrophils, and serum levels of interleukin (IL)-1β and TNF-α proinflammatory cytokines together with C-C motif chemokine ligand 2 (CCL2) and C-X-C motif chemokine ligand 10 (CXCL10) proinflammatory chemokines (Cai et al., 2022). Thus, ER stress is a primary driver of the progression of hepatic steatosis to NASH. Moreover, ER stress may assist to sustain hepatic lipid accumulation by impairing the mitochondrial β-oxidation (DeZwaan-McCabe et al., 2017).

1.2.3.2 Oxidative stress in NAFLD progression

Cellular ER stress can induce oxidative stress through mitochondrial dysfunction-mediated ROS generation (Kim et al., 2018). Also, increased FA oxidation in the mitochondria and peroxisomes, and activation of the nicotinamide adenine dinucleotide phosphate oxidase (NOX) enzyme can induce cellular oxidative stress during NAFLD by promoting the production of ROS (Z. Chen et al., 2020). Cellular oxidative stress is a primary modulator of the NAFLD pathogenesis and progression (Fig. 1.7). A recent study

has proposed that increased cellular oxidative stress can promote cellular lipid accumulation by upregulating DNL via SREBP-1 activation (Podszun et al., 2020). The ability of ROS to damage cellular protein, lipids, and nucleic acids promotes hepatic apoptosis through both structural and functional damage to the hepatocytes (Cichoż-Lach and Michalak, 2014). Liver resident macrophages, the Kupffer cells engulf the apoptotic bodies produced by the hepatocytes undergoing apoptosis. Engulfment of the apoptotic bodies activates the Kupffer cells to produce TNF-related apoptosis-inducing ligand (TRAIL), Fas, and TNF-α cell death ligands capable of further promoting hepatic apoptosis (Malhi et al., 2010). Hepatic oxidative stress and inflammation are interdependent, and occur simultaneously to exacerbate the hepatic damage (Li et al., 2016). Increased hepatic oxidative stress promotes hepatic inflammation by the production of proinflammatory cytokines, IL-1β and IL-18, through MAPK and NF-κB signalling (Nan et al., 2021). Activation of the MAPK and NF-κB inflammatory signalling had also been observed in HepG2 cells overloaded with glucose. Hyperglycemia in HepG2 cells could promote TNF-α and IL-6 production through ROS-induced MAPK and NF-κB signalling (Panahi et al., 2018). Proinflammatory cytokines such as TNF-α (J. Zhang et al., 2022) and DAMP can activate the inflammatory responses of the Kupffer cells (Cha et al., 2018). DAMP further intensifies hepatic inflammation by the recruiting of monocyte-derived macrophages (MDM), also termed as infiltrating macrophages. Both Kupffer cells and MDM expand the hepatic inflammatory assault by the production of proinflammatory cytokine and chemokines (Cha et al., 2018). Once activated, the Kupffer cells may promote hepatic oxidative stress through ROS production (Maeda et al., 2022), thus, initiating a harmful cycle of oxidative stress and inflammation. Moreover, ROS can activate hepatic stellate

cells (HSC) into a myofibroblast-like phenotype and stimulates HSC for the production of extracellular matrix (ECM). Excessive ECM production by the HSC leads to the progression of NAFLD into liver fibrosis and cirrhosis (Gandhi, 2012). Hepatic oxidative stress accelerates the progression of steatosis to NASH and subsequent development of hepatic fibrosis and cirrhosis.

1.2.3.3. Adipose tissue dysfunction for NAFLD progression

Adipose tissue dysfunction may contribute to hepatic inflammation by increasing the levels of proinflammatory cytokines such as TNF-α and IL-6 in the circulation (Fig. 1.7). These cytokines primarily originate from the macrophages that infiltrate the adipose tissue in response to adipocyte apoptosis (Alkhouri et al., 2010). Adipose tissue dysfunction is positively associated with obesity. Significant increments in the circulating TNF-α and CCL2 levels had been observed in obese individuals. The circulating TNF-α and CCL2 increments are similar between the obese subjects presented with and without NAFLD (Fuchs et al., 2021), suggesting the sustained adipose tissue-mediated inflammation during the pathogenesis and progression of NAFLD. Also, adiponectin and leptin secreted by the adipose tissue assist NAFLD pathogenesis and progression when deviating from normal physiological levels. Other adipokines such as resistin, visfatin, chemerin, retinol-binding protein 4 (RBP-4), and irisin are assumed to be important for regulating hepatic lipid metabolism and inflammation (Boutari et al., 2018). In NAFLD patients, the serum adiponectin concentration is considerably low, and this hypoadiponectinemia condition may promote the progression of steatosis to NASH (Polyzos et al., 2011). Adiponectin can prevent hepatic injury by restricting monocyte adhesion to endothelial cells and reducing expressions of TNF-α and aldehyde oxidase-1

enzyme. Aldehyde oxidase-1 enzyme induces hepatic oxidative stress and liver injury together with fibrosis (Polyzos et al., 2009). In contrast to adiponectin, the serum concentration of leptin is significantly high in NAFLD patients. A study based on the US population data revealed that serum leptin concentration is considerably elevated in NAFLD patients and the leptin concentration is positively associated with the severity of NAFLD (Rotundo et al., 2018). The ability of leptin to promote hepatic inflammation by upregulating the expressions of CCL2 and IL-6, and induce hepatic fibrosis by the activation of HSC had been demonstrated in a cholestasis mouse model (Petrescu et al., 2022). Adipokine dyshomeostasis contributes to the progression of NAFLD by advancing hepatic inflammation and fibrosis.

1.2.3.4. Gut microbiota dysbiosis in NAFLD pathogenesis and progression

The gut microbiota plays a pivotal role to regulate body energy metabolism and immune response. Dysbiosis of the gut microbiota is associated with obesity-related diseases including NAFLD (Sankararaman et al., 2023). Studies analyzing fecal material had revealed that Firmicutes/Bacteroidetes (F/B) ratio is significantly higher in NAFLD patients compared to healthy individuals (Lee et al., 2021; Yoon et al., 2023). However, the F/B ratio might be inadequate for the estimation of NAFLD severity as the correlation between the F/B ratio and steatosis is only moderately strong ($r = 0.43$) and no correlation is found between F/B ratio and fibrosis (Jasirwan et al., 2021). The gut microbiota diversity is significantly low in NAFLD patients and the abundance of bacteria phyla, Proteobacteria and Fusobacteria is significantly high in NAFLD patients (Shen et al., 2017). In fact, one study suggests that the increased abundance of Proteobacteria is the most important alteration in the gut microbiota to favour NAFLD pathogenesis through the gut-liver axis.

Proteobacteria are gram-negative bacteria with lipopolysaccharides (LPS) in the outer membrane that are capable of inducing hepatic steatosis and inflammation (Vasques-Monteiro et al., 2021). The composition of the gut microbiota alters with the progression of NAFLD. The abundance of the *Lachnospiraceae* family and its descendant *Blautia* genus are significantly higher in NASH patients whereas the abundance of the *Enterobacteriaceae* family and its descendant Shigella genus are higher in fibrosis patients (Shen et al., 2017). Depletion of the *Blautia* genus bacteria using antibiotics had restricted NASH development in mice fed with a choline-low HFHS diet mimicking the Western diet. The re-establishment of the *Blautia* genus bacteria significantly intensified the hepatic inflammation and fibrosis in these mice (Yang et al., 2023). These pathogenic effects are believed to be mediated by the production of 2-oleoylglycerol in the gut through interaction between *Blautia* genus bacteria and the Western diet. 2-Oleoylglycerol produced in the gut can reach the liver through the portal vein and activate the macrophages. The activated macrophages produce transforming growth factor (TGF)-β1 which activates the HSC and upregulates the expression of ECM genes to promote hepatic fibrosis (Yang et al., 2023). Gut microbiota dysbiosis had also been observed in lean NAFLD patients. However, unlike in obesity-mediated NAFLD the F/B ratio is significantly lower in lean NAFLD patients compared to healthy individuals (Wang et al., 2016).

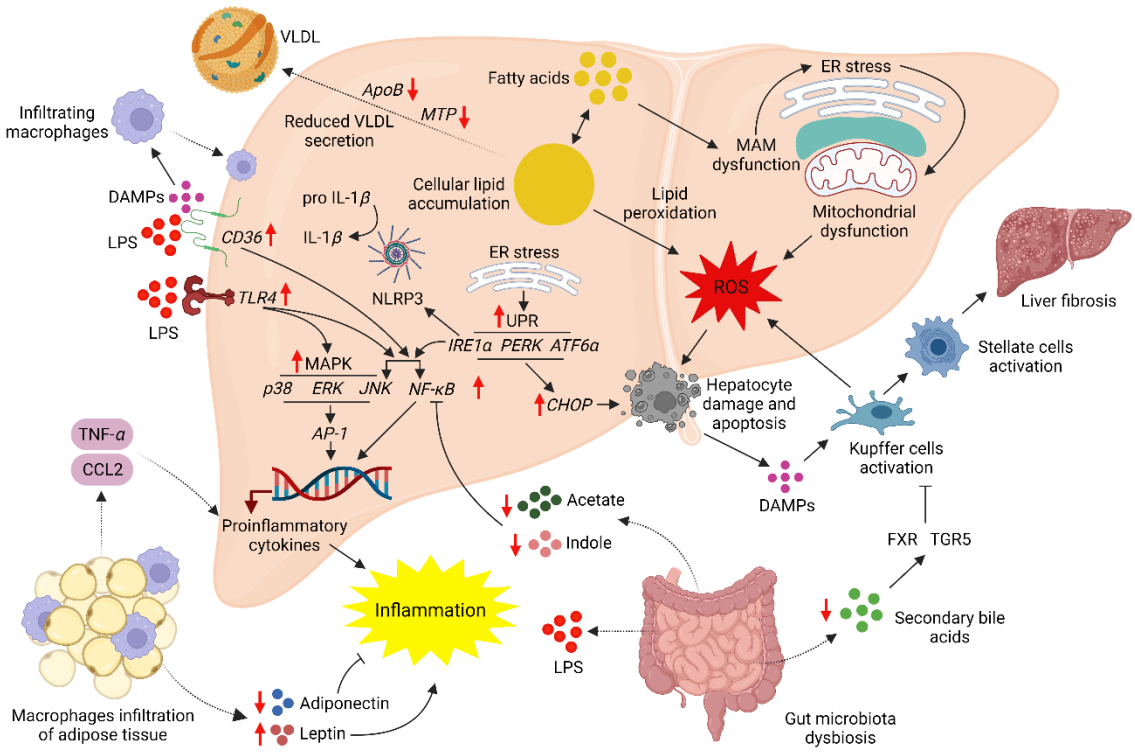

Figure 1.7. Mechanisms of steatosis progression to nonalcoholic steatohepatitis. The red arrows indicate the increased or decreased expression/production under nonalcoholic steatohepatitis. ApoB, apolipoprotein B; ATF6*α*, activating transcription factor-6*α* ;CCL2, C-C motif chemokine ligand 2; CD 36, cluster of differentiation 36; CHOP, CCAAT-enhancer-binding protein-homologous protein; DAMPs, damage-associated molecular patterns; ER, endoplasmic reticulum; ERK, extracellular signal-regulated kinase; FXR, farnesoid X receptor; IL, interleukin; IRE1α, inositol-requiring enzyme-1α; JNK, c-Jun-N-terminal kinase; LPS, lipopolysaccharides; MAM, mitochondria-associated ER membrane; MAPK, mitogen-activated protein kinases; MTP, microsomal triglyceride transfer protein; NF-κB, nuclear factor-kappa-light-chain-enhancer of activated B cells; NLRP3, nucleotide-binding domain, leucine-rich-containing family, pyrin domain-containing-3 inflammasomes; PERK, protein kinase R-like ER kinase; ROS, reactive oxygen species; TGR5, Takeda G protein-coupled receptor 5; TLR4, toll-like receptor 4; TNF-*α*, tumor necrosis factor-*α*; UPR, unfolded protein response; VLDL, very-low density lipoprotein (Created with BioRender.com, license purchased).

Bile acid metabolism by the gut microbiota is important to maintain glucose and lipid homeostases. The gut microbiota converts the conjugated primary bile acids (cholic and chenodeoxycholic acids) into secondary bile acids (deoxycholic and lithocholic acids) through multiple reactions involving deconjugation, oxidation, 7-dehydroxylation,

esterification, and desulfation (Chen et al., 2019). Bile acids act as detergents to facilitate the absorption of dietary lipids, steroids, and lipid-soluble vitamins. Also, the bile acids can function as signalling molecules to maintain bile acid and body energy homeostases by stimulating the nuclear farnesoid X receptor (FXR) and membrane Takeda G protein-coupled receptor 5 (TGR5) receptors (Chiang and Ferrell, 2020). Activation of the FXR receptor restricts the hepatic lipid accumulation through multiple mechanisms (Fig. 1.7). FXR can inhibit the TG synthesis by downregulating the expressions of lipogenic FAS and stearoyl CoA desaturase (SCD)-1 enzymes (Schmitt et al., 2015) *via* SREBP-1c inhibition (Watanabe et al., 2004). FXR activates the small heterodimer partner (SHP), which downregulates the SREBP-1c expression by inhibiting the liver X receptor (LXR) (Watanabe et al., 2004). Also, FXR activation may ameliorate hepatic lipid accumulation by promoting FA β-oxidation via upregulation of the PPAR-α expression (Torra et al., 2003). However, a recent study demonstrated that FXR can inhibit hepatic lipogenesis through a SHP and SREBP-1c independent mechanism and the activation of intestinal cell FXR is sufficient to ameliorate hepatic lipid accumulation by reducing the dietary lipid absorption (Clifford et al., 2021). Moreover, FXR activation in immune cells can manifest anti-inflammatory and antifibrogenic activities. FXR stimulation inhibits the activation of circulating immune cells together with the Kupffer cells and the subsequent activation of the HSC (Fiorucci et al., 2022). Similar to the FXR, activation of the TGR5 is important to maintain energy and immune homeostases (Guo et al., 2016). Overexpression of the TGR5 in enteroendocrine L cells induces secretion of glucagon-like peptide (GLP)-1 and improves glucose tolerance in obese mice (Thomas et al., 2009). GLP-1 can promote insulin secretion and pancreatic islet survival and proliferation. Moreover, in mice TGR5-

mediated GLP-1 secretion promotes the energy expenditure by the BAT and muscle tissues (Thomas et al., 2009), thus, reducing the risk of obesity-related NAFLD. The importance of TGR5 for the suppression of hepatic inflammation had been demonstrated in an LPS-mediated inflammation mouse model. Deletion of the TGR5 in mice significantly increased hepatic inflammation and necrosis. Anti-inflammatory effects of the TGR5 are mediated through the inhibition of NF-κB-based inflammatory response in the mice macrophages, Kupffer cells, and hepatocytes (Y.-D. Wang et al., 2011). Even though anti-inflammatory effects are important to prevent liver fibrosis by inhibiting the activation of HSC, a recent study had revealed the unbeneficial potential of TGR5 to promote liver fibrosis. 12α-Hydroxylated bile acids, taurodeoxycholate and glycoldeoxycholate, could activate the HSC and induce fibrogenesis in mice by the activation of TGR5-mediated MAPK, extracellular signal-regulated kinase (ERK) 1/2 and p38 (Xie et al., 2021). However, many researchers believe that activation of the FXR and TGR5 present therapeutic targets to ameliorate the NAFLD. Gut microbiota dysbiosis in the NAFLD is associated with the reduce conversion of primary bile acids into secondary bile acids and low activity of bile acid receptors, FXR, TGR5, pregnane X receptor, and vitamin D receptor (Chen et al., 2019). Thus, gut microbiota dysbiosis promotes the pathogenesis and progression of NAFLD by disrupting the bile acid metabolism.

The metabolic products and cellular components of the gut microbiota can be both beneficial and detrimental in the NAFLD (Fig. 1.7). The gut microbiota is capable of producing short-chain FA (SCFA) such as acetate, propionate, and butyrate by fermenting the resistant starches (Aoki et al., 2021). In a high-fat/fructose/cholesterol-fed mouse model, supplementation with the resistant starch inulin significantly reduced hepatic

steatosis and fibrosis. These hepato-protective effects are attributable to the production of acetate by the gut microbiota-mediated fermentation of the inulin. The acetate stimulates the FFA receptor 2 (FFAR2), which may reduce the NAFLD pathogenesis and progression by reducing insulin resistance, NF-κB and TNF-α mediated inflammation, and expression of collagen promoters (Aoki et al., 2021). In NASH and NAFLD-cirrhosis patients, the SCFA concentrations in blood plasma are significantly diminished. Moreover, the negative association between the blood plasma concentrations of SCFA and proinflammatory cytokine TNF-α in these patients (Xiong et al., 2022) suggests the importance of SCFA to reduce NAFLD-related inflammation. However, another study contradicts these findings by reporting elevated levels of fecal SCFA and SCFA-producing gut bacteria in NASH patients (Rau et al., 2018). Moreover, elevated fecal acetate and propionate levels may be associated with increased inflammation in NASH patients as observed by the diminished anti-inflammatory regulatory T-cells (Tregs) and the increased ratio of proinflammatory T helper 17 cells (Th17)/Tregs in the blood (Rau et al., 2018). Thus, further studies are required to understand the functions of gut microbiota-derived SCFA in NAFLD pathogenesis and progression. Indole and indole derivatives produced by the gut microbiota-mediated metabolism of tryptophan had depicted multiple hepatoprotective effects (Li et al., 2021). Oral administration of the indole significantly reduced the hepatic inflammation in LPS-injected mice by restricting the NF-κB signalling and the expressions of its downstream targets, notably IL-1β, IL-6, IL-10, TNF-α, nitric oxide synthase 2 (NOS2), and NOX1 (Beaumont et al., 2018). Similar anti-inflammatory activity together with a reduction in hepatic macrophage infiltration had been observed for indole-3-acetate in mice induced for the NAFLD by an HFD. Also, indole-3-acetate could improve the

blood glucose and lipid profiles and ameliorate the hepatic TG and cholesterol content by downregulating the expression of lipogenic SREBP-1, SCD-1, ACC1, and PPAR-γ. Moreover, the potential of indole-3-acetate to mitigate HFD-induced oxidative stress is important to prevent the pathogenesis and progression of NAFLD (Ji et al., 2019). In NAFLD, hepato-protective effects of the indole and indole derivatives may be diminished by the disruption of tryptophan metabolism due to gut microbiota dysbiosis (Chen and Vitetta, 2020).

Gut microbiota dysbiosis in the NASH can lead to an increased abundance of ethanol-producing bacteria and a higher concentration of endogenous ethanol in the peripheral blood. The gut microbiota of obese individuals and NASH patients are similar. However, the abundance of ethanol-producing *Escherichia* bacteria and blood ethanol concentrations are higher in NASH patients compared to obese individuals (Zhu et al., 2013). Endogenous ethanol can induce hepatic steatosis and injury in mice by prompting mitochondria dysfunction-mediated oxidative stress (X. Chen et al., 2020). Thus, trivial changes in the gut microbiota composition might be sufficient for the progression of NAFLD. Gut microbiota dysbiosis in the NAFLD leads to the disruption of gut epithelial barrier function. Gut bacteria-derived metabolites such as endogenous ethanol and ethanol metabolites are capable of disrupting the gut barrier by degrading tight-junction (TJ) protein, allowing gut bacteria and bacterial endotoxins (LPS) to translocate into the liver (Park et al., 2022). Overgrowth of the LPS-producing bacteria such as *Enterobacter cloacae* B29, *Escherichia coli* PY102, and *Klebsiella pneumoniae* A7 in NAFLD patients (Fei et al., 2020) may further intensify the endotoxin-mediated liver assault. Significantly higher concentrations of LPS had been detected in the blood serum and livers of NASH

patients compared to healthy individuals. However, hepatic LPS levels between the simple steatosis patients and healthy subjects had been statistically similar (Carpino et al., 2020), suggesting the importance of bacterial endotoxins for the progression of the NALFD. Activation of the NF-κB inflammatory signalling is the most prominent mechanism in LPS-mediated hepatic inflammation. The LPS initially binds with LPS-binding protein (LBP) and subsequently forms a complex with myeloid differentiation factor 2 (MD2) and pattern-recognition receptor cluster of differentiation 14 (CD14) to activate the toll-like receptor 4 (TLR4) (Tong et al., 2020). TLR4 is expressed in both parenchymal hepatocytes and nonparenchymal liver cells including Kupffer cells, HSC, biliary cells, and endothelial cells. Kupffer cells and HSC are the most stimulated by the LPS to induce inflammatory responses (Fisher et al., 2013). The activated TLR4 initiates the NF-κB signalling that induces the production of many proinflammatory cytokines, including IL-1α, IL-1β, IL-6, IL-12, TNF-α, and granulocyte-macrophage colony-stimulating factor (GM-CSF) (Hamesch et al., 2015). TLR4 is also capable of activating the MAPK (p38, ERK, and JNK) and interferon regulatory factor 3 (IRF3) signalling to induce hepatic inflammation through the increased production of proinflammatory cytokines (Tong et al., 2020). The proinflammatory cytokines secreted by the Kupffer cells and infiltrated macrophages can activate the HSC. Activated Kupffer cells can secrete transforming growth factor β (TGFβ) that stimulates the HSC to produce ECM constituents, the collagens and fibronectin. Excessive synthesis of the ECM leads to hepatic fibrosis (Gandhi, 2020). Although many of the LPS-mediated effects support the NAFLD progression into NASH and fibrosis, LPS may also play a role in the induction of hepatic steatosis. LPS could induce hepatic steatosis in a disaccharide-rich diet-fed rat model by upregulating the expressions of lipogenic

SREBP-1c and FAS (Fukunishi et al., 2014). Moreover, in an HFD-fed germ-free mouse model monoassociation of the germ-free mice with LPS-producing bacteria had been required to induce hepatic steatosis and inflammation (Fei et al., 2020). However, LPS had been able to ameliorate lipid accumulation in the HSC through lipophagy while sensitizing the HSC to TGFβ-mediated fibrosis response (Chen et al., 2017). Thus, LPS may be playing disease-stage-specific roles in NAFLD. The increased LPS production together with the impaired gut epithelial barrier function under the gut microbiota dysbiosis are critical triggers for NAFLD pathogenesis and progression. Gut microbiota dysbiosis is strongly associated with dietary habits such as consumption of fructose-rich diets. Excessive consumption of fructose may induce hepatic inflammation and fibrosis by increasing the translocation of gut microbiota-derived LPS into liver. Fructose can impair gut epithelial barrier function to increase LPS translocation by downregulating the expression of TJ and adherent junction proteins (Cho et al., 2021). NAFLD pathogenesis and progression are contributed by multiple risk factors. Many of the primary risk factors are associated with modifiable lifestyle patterns. Despite the existence of several potential therapeutic targets to mitigate the risk of NAFLD an approved medicine is not currently available to treat the disease (Mundi et al., 2020). Therefore, novel approaches combined with improved lifestyle patterns are necessary to reduce the global burden of NAFLD.

1.3. PROBIOTIC MICROBES-MEDIATED MECHANISMS FOR NAFLD RISK REDUCTION

The administration of probiotic microbes is proven to be beneficial in many diseases (Milner et al., 2021; Zommiti et al., 2020). Probiotics can reduce the risk of NAFLD pathogenesis and progression by indirect and direct mechanisms (Table 1.1). The

ability of probiotics to mitigate insulin resistance and T2D is indirectly beneficial for the prevention of NAFLD. A mixture of *Lactobacillus* (*L*.) and *Bifidobacterium* (*B*.) probiotic bacteria had been able to ameliorate HFD and streptozotocin-induced diabetes in C57BL/6J mice by improving glucose tolerance and reducing insulin resistance. These beneficial effects are believed to be mediated by the ability of probiotic bacteria to modulate gut microbiota and increase the availability of GLP-1 and peptide tyrosine-tyrosine through SCFA production (Gu et al., 2022). Smoking is a non-traditional risk factor of NAFLD that can promote the progression of steatosis to NASH. In cigarette smokers, nicotine accumulated in the intestine can facilitate the formation of ceramides by phosphorylation of sphingomyelin phosphodiesterase 3 (SMPD3) *via* AMPKα signalling (B. Chen et al., 2022). Ceramides are known activators of hepatic ER stress (Song and Malhi, 2019). Gut bacterium *Bacteroides xylanisolvens* is capable of restricting the ceramides formation by degrading nicotine, thus, reducing the risk of NASH. Therefore, *Bacteroides xylanisolvens* can be a promising novel probiotic bacteria to reduce the risk of NASH in cigarette smokers (B. Chen et al., 2022).

Many studies have illustrated the potential of probiotic bacteria to reduce the risk of NAFLD by ameliorating overweight and obesity. A study on obese NAFLD patients revealed that supplementation with a mixture of *Lactobacillus* and *Bifidobacterium* probiotic bacteria can significantly reduce the IHL and triglyceride levels together with the body weight and total fat content (Ahn et al., 2019). Similarly, mixtures of probiotic bacteria can improve the blood lipid profile and reduce the blood concentrations of liver damage markers, alanine aminotransferase (ALT), aspartate aminotransferase (AST), and γ-glutamyl transferase (GGT) (Cai et al., 2020), demonstrating the ability of probiotic

bacteria to regulate lipid metabolism and hepatic injury. Probiotic bacteria such as *L. plantarum* Q16 (isolated from yogurt) are capable of preventing hepatic steatosis by the regulation of lipid metabolism. *L. plantarum* Q16 had been able to reduce hepatic steatosis in an HFD-fed mouse model by restricting DNL through downregulation of the expressions of SREBP-1 targets, SCD-1, ACC, and FAS (Tang et al., 2022). Moreover, *L. plantarum* Q16 is capable of upregulating the expression of FA β-oxidation promoters, CPT-1α and PPAR-α. The potential of *L. plantarum* Q16 to increase the expression of adipose triglyceride lipase (ATGL) and reduce the expression of diacylglycerol acyltransferase 1 (DGAT1) in the liver is further beneficial for NAFLD mitigation by inhibiting the hepatic TG synthesis. ATGL regulates the TG hydrolysis and is important to maintain PPAR-α mediated FA β-oxidation in the mitochondria (Tang et al., 2022). DGAT1 can promote hepatic steatosis by esterification of exogenous FA (Villanueva et al., 2009).

The adipose tissue dysfunction during obesity is a major contributor to the NAFLD pathogenesis and progression to NASH (Wang et al., 2021). The probiotic bacteria *Bacillus coagulans* T4 had been able to ameliorate adipose tissue dysfunction in obese mice (Hashemnia et al., 2023). Supplementation with the *Bacillus coagulans* T4 had significantly reduced the infiltration of macrophages into the adipose tissue and polarization into the proinflammatory M1 phenotype. Moreover, the mRNA expression of endotoxin receptors, TLR2 and TLR4 together with the proinflammatory cytokines IL-6 and TNF-α had been significantly diminished by the probiotic bacteria supplementation. This inflammation reduction may be attributable to the ability of *Bacillus coagulans* T4 to reduce endotoxemia by promoting gut epithelial barrier function (Hashemnia et al., 2023). The adipokines secreted by the adipocytes are important to maintain hepatic lipid and

immune homeostasis (Boutari et al., 2018). *Lactobacillus* probiotic bacteria are capable of restoring the blood serum adipokine levels in obese mice by increasing the adiponectin level and decreasing the leptin level (M. Wang et al., 2020). The adiponectin deficiency and leptin overexpression can promote hepatic steatosis by restricting the FA β-oxidation, and facilitate the steatosis progression to NASH by advancing hepatic inflammation (Petrescu et al., 2022; Skat-Rørdam et al., 2019).

The hepatic ER stress and oxidative stress can initiate the progression of steatosis to NASH by introducing hepatic inflammation and injury. The ability of probiotic bacteria to mitigate ER stress response (the UPR) had been demonstrated in HepG2 cells induced for steatosis by exposure to oleic acid. Treatment of the HepG2 cells with the cell-free extracts of *L. acidophilus* NX2-6 significantly reduced the UPR by downregulating the expressions of glucose-regulated protein 58 kD (GRP58), ATF6, IRE1α, X-box binding protein 1 (XBP1), and CHOP (Tang et al., 2020). The potential of probiotic-derived cell-free extract to prevent mitochondria dysfunction (Tang et al., 2020) may have contributed to mitigating ER stress. Prevention of mitochondrial dysfunction together with lipid peroxidation and ROS generation had significantly diminished the oxidative stress in the HepG2 cells (Tang et al., 2020). A mixture of 20 strains of lactic acid-producing probiotic bacteria had been able to mitigate the hepatic inflammation and subsequent NAFLD progression to fibrosis and HCC in a phosphate and tensin homolog (PTEN) gene knockout mouse model (Arai et al., 2022). Hepatocyte-specific deletion of the tumour suppressor gene PTEN mimics NAFLD conditions by inducing hepatomegaly, TG accumulation, inflammation, and hepatic injury (Horie et al., 2004). Supplementation with the probiotic bacteria significantly reduced the hepatic oxidative stress by restoring the cellular levels of

glutathione in the PTEN knockout mice. Also, in the same mouse model, probiotics significantly reduced the expression of proinflammatory cytokines and averted hepatic injury by reducing hepatocyte apoptosis. Moreover, probiotic bacteria hindered the induction of hepatic fibrosis by downregulating the expressions of tissue inhibitors of metalloproteinase-1 (TIMP-1) and α-smooth muscle actin (α-SMA) (Arai et al., 2022). In hepatic fibrosis, TIMP-1 inhibits the matrix metalloproteases (MMP) which can prevent fibrosis by the degradation of ECM (Thiele et al., 2017). Increased expression of the α-SMA in HSC may induce the secretion of ECM component collagen-1 through mechanical signals such as cellular contraction tension (Rockey et al., 2019).

The gut microbiota dysbiosis can support the pathogenesis and progression of NAFLD through multiple mechanisms (Jasirwan et al., 2019). Many studies reporting the benefits of probiotics for NAFLD risk reduction had revealed the potential of probiotics to mitigate gut microbiota dysbiosis. In fact, the anti-inflammatory activity of probiotics in NAFLD is primarily attributable to the prevention of dysbiosis-mediated endotoxemia and gut-epithelial barrier dysfunction (Khan et al., 2021). During the NAFLD, loss of gut-epithelial barrier function allows the translocation of bacteria and bacterial endotoxins to the liver (Park et al., 2022) that induces inflammation by activating the TLR4 inflammatory signalling cascade (Hamesch et al., 2015). In an HFD-fed mouse model, supplementation with *L. acidophilus* probiotic bacteria relieved the gut microbiota dysbiosis by increasing the bacteria richness and diversity (Kang et al., 2022). Also, *L. acidophilus* could reduce the F/B ratio (Kang et al., 2022), which is commonly increased in NAFLD patients (Yoon et al., 2023), and reduce the LPS contributing gram-negative bacteria (Kang et al., 2022). The same study demonstrated the ability of *L. acidophilus* to prevent LPS translocation by

protecting the gut-epithelial barrier function through increased expression of the intestinal epithelial protein, intectin, and the TJ protein, occludin. Reduction of the LPS translocation significantly ameliorated the hepatic inflammation by inhibiting TLR4/NF-κB-mediated inflammation pathway (Kang et al., 2022). The potential of probiotic bacteria to regulate gut microbiota-derived metabolites is beneficial for NAFLD risk reduction. Supplementation with the *L. acidophilus* significantly reduced the hepatic steatosis and injury by upregulating the bile acid receptor FXR/fibroblast growth factor 15 (FGF15) signalling, suggesting the potential of probiotic bacteria to mitigate NAFLD through the regulation of bile acids metabolism (Luo et al., 2021). Encapsulated *L. acidophilus*, *B. longum*, and *Enterococcus faecalis* probiotic bacteria can ameliorate gut microbiota dysbiosis in obese mice and restore the abundance of SCFA-producing bacteria such as *Olsenella* and *Allobaculum* (Kong et al., 2019). SCFA can reduce NAFLD pathogenesis and progression by inhibiting insulin resistance together with hepatic inflammation and fibrosis (Aoki et al., 2021). Thus, traditional and novel probiotic bacteria are capable of reducing the NAFLD risk through multiple mechanisms.

Table 1.1. Probiotic microbes-mediated functions and mechanisms to reduce the NAFLD risk.

Probiotics	Experimental model	Biological functions and mechanisms	Reference
1) A mixture of *L. acidophilus*, *L. rhamnosus*, *L. paracasei*, *P. pentosaceus*, *B. lactis*, and *B. breve*.	Obese NAFLD patients were supplemented with the probiotic bacteria mixture (1×10^9 cfu/day) for 12-weeks.	- Reduce body weight and total fat content. - Reduce intrahepatic fat and triglyceride contents.	(Ahn et al., 2019)
2) A mixture of *Lactobacillus*, *Bifidobacterium*, and *Enterococcus* probiotic bacteria.	NAFLD patients were supplemented with the probiotic bacteria (1 g twice per day) concomitantly with a low-calorie diet and exercise therapy for three months.	- Improve blood lipid profile by reducing the total cholesterol, triglyceride, and LDL levels. - Reduce the concentration of liver damage markers, ALT, AST, and GGT in the blood.	(Cai et al., 2020)

Probiotics	Experimental model	Biological functions and mechanisms	Reference
3) *L. plantarum Q16*	Mice induced for NAFLD by feeding a high-fat diet were supplemented with the probiotic bacteria (1×10^9 cfu/day) for 8-weeks.	- Reduce hepatic lipogenesis by downregulating the expressions of SREBP-1, SCD-1, ACC, and FAS. - Promote hepatic FA oxidation by upregulating the expressions of CPT-1α and PPAR-α. - Promote hepatic triglyceride hydrolysis and reduce triglyceride synthesis by up and downregulation of the expressions of ATGL and DGAT1, respectively. - Improve gut microbiota composition.	(Tang et al., 2022)
4) *Bacillus coagulans* T4	C57BL/6J mice were fed a high-fat diet for 10-weeks to induce obesity. Then, the mice were supplemented with the probiotic bacteria (1×10^9 cfu/day) for 8-weeks while	- Reduce body weight gain and adiposity, and improve glucose tolerance. - Reduce infiltration of macrophages into the white adipose tissue and polarization into proinflammatory M1 phenotype. - Downregulate the expressions of LPS-sensitive TLR2	(Hashemnia et al., 2023)

Probiotics	Experimental model	Biological functions and mechanisms	Reference
	feeding with a high-fat diet.	- and TLR4 in adipose tissue. - Downregulate the expression of proinflammatory cytokines TNF-α and IL-6 while upregulating anti-inflammatory IL-10. - Ameliorate gut microbiota dysbiosis, improve acetate and propionate SCFA production, and improve gut epithelial barrier function.	
5) *L. casei*, *L. fermentum*, *L. acidophilus*, *L. rhamnosus*, and *L. paracesei*.	C57BL/6J mice induced for obesity by feeding with a high-fat diet were administered with the different strains of probiotic bacteria separately.	- Improve blood lipid profile by reducing the levels of total cholesterol, triglycerides, and LDL while increasing the level of HDL. - Increase blood serum level of adiponectin and reduce the level of leptin.	(M. Wang et al., 2020)
6) *L. acidophilus* cell-free extract	HepG2 cells were treated with the cell-free extract of	- Mitigate cellular lipid accumulation by downregulating the expressions of SREBP-1c and FAS.	(Tang et al., 2020)

Probiotics	Experimental model	Biological functions and mechanisms	Reference
	probiotic bacteria for 24 h. Then, the cells were exposed to oleic acid (0.9 mM) for 24 h to induce lipid accumulation.	- Promote FA oxidation by upregulating the expression of CPT-1. - Avert cellular ER stress response (unfolded protein response) by downregulating the expressions of GRP58, ATF6, IRE1α, XBP-1, and CHOP. - Ameliorate cellular oxidative stress by preventing mitochondria dysfunction, and reducing lipid peroxidation and ROS generation. - Reduce cellular inflammation by downregulating the NF-κB-mediated IL-1β and IL-6 production.	
7) A mixture of 20 strains of lactic acid bacteria.	C57BL/6 mice of hepatocyte-specific phosphate and tensin homolog (PTEN) gene knockout were supplemented	- Ameliorate hepatic oxidative stress and restore glutathione levels. - Mitigate lobular inflammation and suppress the expression of LPS receptor TLR4 and proinflammatory	(Arai et al., 2022)

Probiotics	Experimental model	Biological functions and mechanisms	Reference
	with the probiotic bacteria for 8-weeks and 40-weeks (fibrosis model). Probiotics were administered with drinking water (4 g/L, 1×10^9 cfu/g).	cytokines IL-1β, TNF-α, and chemokine CCL2. - Alleviate hepatic injury by preventing hepatocyte apoptosis. - Reduce the induction of fibrosis by downregulating the expressions of TIMP-1 and α-SMA. - May prevent NAFLD progression to hepatocellular carcinoma.	
8) *L. acidophilus*	C57BL/6J mice were fed a high-fat diet for 11-weeks. Then supplemented with the probiotic bacteria (5×10^9 cfu/day) and the high-fat diet concomitantly for another week.	- Reduce body weight, body fat content, and insulin resistance. - Alleviate gut microbiota dysbiosis by increasing bacteria richness and diversity. Reduce the Firmicutes/Bacteroidetes ratio and the abundance of endotoxins carrying gram-negative bacteria. - Protect the gut-epithelial barrier function and reduce the	(Kang et al., 2022)

Probiotics	Experimental model	Biological functions and mechanisms	Reference
		TL4/NF-κB-mediated hepatic inflammation by preventing LPS translocation.	
9) *L. acidophilus* tablet	Sprague Dawley rats were fed a high-fat diet for 6-weeks. Then, the rats were supplemented with the probiotic tablet (312 mg/kg of body weight/day, 1×10^7 cfu/g of tablet) and high-fat diet concomitantly for 8-weeks.	- Mitigate hepatic steatosis and injury by the activation of the bile acid receptor FXR/FGF15 signalling pathway. - Ameliorate gut microbiota dysbiosis by increasing bacteria diversity and reducing the abundance of pathogenic bacteria.	(Luo et al., 2021)

ACC, acetyl-CoA carboxylase; ALT, alanine aminotransferase; AST, aspartate aminotransferase; ATF6, activating transcription factor-6; ATGL, adipose triglyceride lipase; *B*., *Bifidobacterium*; cfu, colony-forming units; CHOP, CCAAT-enhancer-binding protein-homologous protein; CPT-1α, carnitine-palmitoyl-transferase-1 α; DGAT1, diacylglycerol acyltransferase 1; FAS, fatty acid synthase; FGF15, fibroblast growth factor 15; FXR, farnesoid X receptor; GGT, γ-glutamyl transferase; GRP58, glucose regulated protein 58 kD; HDL; high-density lipoprotein; IL, interleukin; IRE1α, inositol-requiring enzyme-1α; *L*., *Lactobacillus*; LDL, low-density lipoprotein; LPS, lipopolysaccharides; NAFLD, nonalcoholic fatty liver disease; NASH, nonalcoholic steatohepatitis; NF-κB, nuclear factor-kappa-light-chain-enhancer of activated B cells; *P*., *Pediococcus*; PPAR-α, peroxisome proliferator-activated receptor-α; SCD-1, stearoyl-CoA desaturase 1; SREBP-1, sterol regulatory element binding protein-1; TIMP-1, tissue inhibitor of metalloproteinase-1; TLR, toll-like receptors; TNF-α, tumor necrosis factor-α; XBP-1, X-box binding protein 1; α-SMA, α-smooth muscle actin.

1.4. PAC-MEDIATED MECHANISMS FOR NAFLD RISK REDUCTION

Supplementation with PAC is beneficial to reduce the risk of NAFLD and alleviate the symptoms in NAFLD patients (Table 1.2). Oral administration of the PAC can mitigate hyperlipidemia in NAFLD patients together with hepatic injury (Mojiri-Forushani et al., 2022). Many of the PAC-mediated benefits in NAFLD are associated with the potential of PAC to regulate hepatic energy metabolism. PAC can mitigate insulin resistance in HepG2 cells by activating the phosphoinositide 3-kinase (PI3K)/protein kinase B (AKT) pathway. Activation of the PI3K/AKT signalling by PAC is suggested to be achieved by the upregulation of microRNA (miR)-29a, miR-122, and miR-423 (Wang et al., 2022). In oleic acid-overloaded HepG2 cells, PAC can reduce the expressions of lipogenic SREBP-1 and ACC enzyme together with the cholesterol synthesis enzyme 3-hydroxy-3-methylglutaryl coenzyme A (HMG-CoA) reductase. PAC mediates these metabolic functions by the activation of AMPK energy metabolism pathways (Zhang et al., 2017). The ability of PAC to mitigate NAFLD pathogenesis had been demonstrated in diet-induced obesity and NAFLD murine models. PAC supplementation can significantly reduce hepatic steatosis by reducing the DNL and lipid storage, and promoting FA β-oxidation. PAC can significantly reduce the expressions of DNL-promoting mediators such as SREBP-1c, ChREBP, and ACC (Feldman et al., 2023). The potential of PAC to mitigate hepatic lipid accumulation is demonstrated by the downregulated expressions of the PPAR-γ (Sun et al., 2022) and the lipid droplets associated proteins, fat-specific protein 27 (FSP27), perilipins, and adipophilin (Yogalakshmi et al., 2013). Also, PAC can increase the FA β-oxidation by upregulating the expressions of PPAR-α, CPT-1, and PPAR-γ coactivator-1α (PGC-1α) (Feldman et al., 2023). Moreover, PAC may reduce lipid accumulation in the hepatocytes

by activating the transcription factor EB (TFEB). TFEB is a master regulator of lysosomal biogenesis. Activation of the TFEB induces lipid degradation through the lysosomal pathway (Su et al., 2018).

PAC supplementation can be beneficial to prevent the progression of simple steatosis to NASH. ER stress and oxidative stress act as the primary drivers of NAFLD progression. Supplementation with the PAC can significantly reduce HFD-mediated hepatic assault by alleviating ER stress (Sun et al., 2022). In obese rats, PAC supplementation mitigated the UPR by downregulating the mRNA expressions of ATF6 and CHOP. Moreover, PAC ameliorated liver injury by reducing hepatocyte apoptosis through the upregulation of antiapoptotic B-cell lymphoma 2 (BCL-2) expression. These beneficial effects are believed to be mediated by the activation of the Wnt-3a/β-catenin signalling pathway (Sun et al., 2022). Cellular ER stress can promote oxidative stress through mitochondria dysfunction (Kim et al., 2018). PAC are natural antioxidants that can relieve hepatic oxidative stress by scavenging the ROS and superoxide anion radicals (Su et al., 2018). Also, the potential of PAC to increase the genetic expression and activity of the antioxidant enzymes, glutathione peroxidase (GPx), catalase (CAT), and superoxide dismutase (SOD) is beneficial to mitigate the hepatic oxidative stress in the NAFLD (Feldman et al., 2023; Su et al., 2018). The sustained hepatic injury induces the production of proinflammatory cytokines. Multiple studies had demonstrated the ability of PAC to reduce the production of proinflammatory cytokines such as IL-1β, IL-6, and TNF-α (Sun et al., 2022).

The potential of PAC to ameliorate adipose tissue inflammation is beneficial to reduce the risk of NAFLD. In mice fed with an HFD, PAC could significantly reduce the

production of the proinflammatory cytokines in the white adipose tissue and prevent adipokine dyshomeostasis. PAC could increase the blood serum level of adiponectin and decrease the level of leptin (Y. Zhang et al., 2022). Adiponectin is known to mitigate hepatic inflammation, oxidative stress, and fibrosis (Polyzos et al., 2009). Similarly, reduction of the leptin level can mitigate hepatic inflammation and HSC-mediated hepatic fibrosis (Petrescu et al., 2022). The potential of PAC to mitigate NAFLD progression to hepatic fibrosis had been demonstrated in rats induced for liver damage by CCl_4 administration (Amer et al., 2022). The ability of PAC to downregulate the expressions of collagen-1, α-SMA, and TIMP-1 in the HSC is beneficial to prevent hepatic fibrosis by inhibiting excessive ECM secretion. PAC may reduce the excessive ECM secretion from the HSC by inhibiting the PI3K/AKT, MAPK, and NF-κB signalling cascades (Jiang et al., 2017).

Gut microbiota dysbiosis plays a critical role in the pathogenesis and progression of NAFLD (Sankararaman et al., 2023). PAC can mitigate HFD-induced gut microbiota dysbiosis by reducing the abundance of *Firmicutes* and increasing the abundance of *Bacteroidetes*. Also, PAC increases the production of SCFA such as propionic and butyric acids by increasing the abundance of SCFA-producing bacteria (Xiao et al., 2020). SCFA are beneficial to reduce hepatic inflammation and fibrosis (Aoki et al., 2021). Furthermore, PAC administration can activate the FXR signalling cascade by modulating gut microbiota-mediated bile acids metabolism (Wu et al., 2022). Activation of the FXR signalling inhibits the hepatic DNL by downregulating the expression of SREBP-1c (Watanabe et al., 2004). Moreover, PAC protects the gut-epithelial barrier function during HFD-induced dysbiosis by upregulating the expressions of TJ proteins, zonula occludens-1 (ZO-1) and occludin.

Therefore, PAC reduces the translocation of gut microbiota-derived LPS into the bloodstream (Y. Zhang et al., 2022) and the subsequent activation of the LPS-mediated hepatic inflammatory response (Hamesch et al., 2015). The potential of PAC to modulate lipid metabolism, ER stress, oxidative stress, inflammatory response, and gut microbiota is beneficial to mitigate the risk of NAFLD pathogenesis and progression.

Table 1.2. Proanthocyanidin-mediated functions and mechanisms to reduce the NAFLD risk.

Experimental model	Biological functions and mechanisms	Reference
1) Supplementation of NAFLD patients with PAC-rich grape seed extract (200 mg twice per day) for 2-months.	- Ameliorate hyperlipidemia by reducing triglyceride, LDL, and cholesterol levels, and increasing HDL levels. - Reduce the fasting blood sugar level. - Mitigate hepatic injury (as depicted by the low ALT and AST levels).	(Mojiri-Forushani et al., 2022)
2) C57BL/6 mice were supplemented with the cranberry PAC (200 mg/kg bw/day) and an HFHS diet concomitantly for 12-weeks.	- Reduce hepatic lipogenesis by downregulating the expression of SERBP-1c, ChREBP, and FAS. - Promote hepatic FA oxidation by upregulating the expressions of CPT-1, PPAR-α, and PGC-1α. - Mitigate hepatic inflammation by suppressing NF-κB mediated production of proinflammatory TNF-α and COX-2. - Alleviate oxidative stress by upregulating the expressions of GPx, SOD, and Nrf2.	(Feldman et al., 2023)

Experimental model	Biological functions and mechanisms	Reference
3) Wistar rats induced for NAFLD by feeding with an HFHF-diet for 30 days were supplemented with grape seed PAC (100 mg/kg bw/day) for another 15-days concomitantly with the HFHF diet.	- Reduce hepatic steatosis by downregulating the expressions of lipogenic SREBP-1c and the lipid droplet proteins, FSP27, perilipins, and adipophilin. - Promote FA oxidation by upregulating the expression of PPAR-α. - Reduce cholesterol synthesis by downregulating the expression of the HMG-CoA reductase enzyme.	(Yogalakshmi et al., 2013)
4) Sprague Dawley rats were fed with an HFD for 8-weeks to induce obesity. The mice were supplemented with grape seed PAC (500 mg/kg bw/day) and HFD concomitantly for 4-weeks.	- Mitigate hepatic steatosis by downregulating the expression of PPAR-γ. - Alleviate ER stress response (the UPR) by downregulating the expressions of ATF6 and CHOP at the mRNA level. - Reduces apoptosis-mediated hepatic injury by upregulating the expression of antiapoptotic BCL-2. - Alleviate hepatic inflammation by downregulating the expressions of IL-1β and TNF-α.	(Sun et al., 2022)

Experimental model	Biological functions and mechanisms	Reference
5) HepG2 and L02 liver cells were exposed to a mixture of oleic and palmitic acids (0.2 mM for 24 h) and treated with procyanidin B2 (2.5 – 10 µg/mL for 24 h). C57BL/6 mice were fed with an HFD for 10-weeks to induce obesity. Then, mice were administered with procyanidin B2 (50 and 150 mg/kg bw/day) and fed with the HFD concomitantly for 10-weeks.	- Promote hepatic lipid degradation by activating the TFEB-mediated lysosomal pathway. - Mitigate hepatic oxidative stress by scavenging ROS and superoxide anion redials, protecting the mitochondria membrane potential, preventing glutathione depletion, and increasing the activity of GPx, SOD, and CAT antioxidant enzymes. - May reduce hepatic steatosis by restoring hepatic TFEB expression and subsequent lipid degradation by the lysosomal pathway. - Mitigate hepatic steatosis by reducing the expressions of PPAR-γ, C/EBPα, and SREBP-1c. - Alleviate hepatic oxidative stress by increasing the activity of GPx, SOD, and CAT. - Mitigate hepatic inflammation by reducing the production of proinflammatory cytokines, IL-6 and TNF-α.	(Su et al., 2018)

Experimental model	Biological functions and mechanisms	Reference
6) An LPS-injected mouse model to evaluate intestinal inflammation. C57BL/6 mice were supplemented with grape seed PAC (250 mg/kg bw/day) for 20 days.	- Improve the gut microbiota by increasing bacteria richness and diversity. - Increase the mRNA expressions of the bile acid receptor FXR and its targets FGF15 and SHP by modulating the gut microbiota-mediated bile acid metabolism.	(Wu et al., 2022)
7) C57BL/6 mice were fed with an HFD containing procyanidin B2 (0.2% *w:w*) for 8-weeks.	- Increase the activity of hepatic antioxidant enzymes CAT and SOD. - Improve gut microbiota by reducing the abundance of *Firmicutes* and increasing the abundance of *Bacteroidetes.* - Promote the production of SCFA, propionic and butyric acids by the gut microbiota.	(Xiao et al., 2020)
8) C56BL/6J mice were fed with an HFD and administered with PAC isolated from bayberry leaves (100 mg/kg bw/day) for 8-weeks.	- Mitigate hepatic lipid accumulation by downregulating the expressions of lipogenic SREBP-1c, ACC, and FAS. - Increase FA oxidation by upregulating the expressions of PPAR-α and CPT-1.	(Y. Zhang et al., 2022)

Experimental model	Biological functions and mechanisms	Reference
	- Increase the blood serum concentration of adiponectin and reduce the concentration of leptin. - Protect gut-epithelial barrier function in the ileum and colon by upregulating the expressions of tight junction proteins, ZO-1 and occludin. - Reduce the level of circulating LPS and the production of proinflammatory cytokines, IL-6 and TNF-α, in the liver and white adipose tissue.	

ACC, acetyl-CoA carboxylase; ALT, alanine aminotransferase; AST, aspartate aminotransferase; ATF6, activating transcription factor-6; BCL-2, B-cell lymphoma 2; bw, body weight; C/EBPα, CCAAT-enhancer-binding protein α; CAT, catalase; CHOP, C/EBP-homologous protein; ChREBP, carbohydrate response element-binding protein; COX-2, cycloogenase-2; CPT-1, carnitine-palmitoyl-transferase-1; ER, endoplasmic reticulum; FA, fatty acids; FAS, fatty acid synthase; FGF15, fibroblast growth factor 15; FSP27, fat specific protein 27; FXR, farnesoid X receptor; GPx, glutathione peroxidase; HDL, high-density lipoprotein; HFD, high-fat diet; HFHF, high-fat and high-sucrose; HFHS, high-fat and high-sucrose; HMG-CoA, 3-hydroxy-3-methylglutaryl coenzyme A; IL, interleukin; LDL, low-density lipoprotein; LPS, lipopolysaccharides; NAFLD, nonalcoholic fatty liver disease; Nrf2, nuclear factor erythroid 2-related factor 2; PAC, proanthocyanidins; PGC-1α, PPAR-γ coactivator-1α; PPAR- Peroxisome proliferator-activated receptor; ROS, reactive oxygen species; SCFA, short-chain fatty acids; SHP, small heterodimer partner; SOD, superoxide dismutase; SREBP-1c, sterol regulatory element binding protein-1c; TFEB, transcription factor EB; TNF-α, tumor necrosis factor-α; UPR, unfolded protein response; ZO-1, zonula occludens-1.

1.5. PAC-BASED SYNBIOTICS FOR NAFLD RISK REDUCTION

Traditionally, a mixture of probiotics and prebiotics with health benefits was considered a synbiotic. Recently, with emerging new knowledge, synbiotics were re-defined as "a mixture of live microorganism(s) and substrate(s) selectively utilized by host microorganisms that confers a health benefit on the host" (Swanson et al., 2020). Thus, the new definition allows the use of nonconventional microorganisms and substrates to develop synbiotics, given that the health benefits and safety for use in intended hosts are established. Synbiotics can be categorized into two groups, synergistic synbiotics, and complementary synbiotics. The synergistic synbiotics are comprised of a substrate that can be selectively utilized by microorganisms in the synbiotic mixture. The beneficial health effects of the synergistic synbiotics are more prominent compared to the administration of the substrate and the microorganisms separately. The complementary synbiotics are mixtures of already known probiotics and prebiotics that can modulate indigenous microbiota to deliver health benefits (Swanson et al., 2020).

Most of the studies testing the efficacy of synbiotics against NAFLD had utilized carbohydrates such as inulin and fructooligosaccharides (FOS) as the synbiotic substrates. The ability of inulin and FOS-based synbiotics to ameliorate hepatic injury (Bakhshimoghaddam et al., 2018), steatosis, inflammation, and fibrosis (Eslamparast et al., 2014; Mofidi et al., 2017) had been demonstrated in the NAFLD patients. The recent findings on synbiotics have revealed the potential to utilize polyphenols as synbiotic substrates for NAFLD risk reduction. Administration of a quercetin-based synbiotic of *Akkermansia muciniphila* had shown beneficial effects in an HFD-fed NAFLD rat model. Administration of this synbiotic significantly reduced hepatic steatosis by downregulating

the expressions of lipogenic DGAT2 and C/EBPα and upregulating the expression of FA oxidation promoter PPAR-α. Moreover, this synbiotic may mitigate hepatic inflammation by suppressing the expression of proinflammatory cytokine IL-6. These beneficial effects are attributable to the potential of quercetin-based synbiotic to modulate gut microbiota and bile acid metabolism (Juárez-Fernández et al., 2021).

Studies directly evaluating the potential of PAC-based synbiotics to mitigate the risk of NAFLD are limited. A synbiotic based on the PAC-rich grapes seed powder (GSP) and lactic acid bacteria isolated from kefir could significantly reduce the NAFLD risk in an HFD-induced obesity mouse model (Cho et al., 2018; Kwon et al., 2019). Supplementation with this GSP synbiotic significantly reduced the body weight gain together with the weights of liver and adipose tissues in the mice while ameliorating insulin resistance, glucose intolerance, and plasma lipid profile (Cho et al., 2018; Kwon et al., 2019). Even though, the administration of the GSP and probiotic bacteria separately could depict similar activities in the mice, the superiority of synbiotic administration had been demonstrated by the significantly lower level of liver damage marker AST in the blood plasma of mice (Kwon et al., 2019). Analysis of the hepatic gene expressions revealed that GSP synbiotic can modulate cellular signalling to mitigate the NAFLD risk. Most notably, the GSP synbiotic had downregulated the expressions of INSIG2, SCD-1, and SCD-3 genes that can regulate hepatic lipogenesis. Also, the GSP synbiotic may ameliorate NAFLD progression by downregulating the expressions of genes related to NF-κB and LPS inflammatory signalling, and resolving the hepatic oxidative stress (Kwon et al., 2019). This reduction of hepatic inflammation may be attributable to the potential of GSP synbiotic to prevent endotoxemia by protecting the gut epithelial barrier function.

Furthermore, the ability of GSP synbiotic to modulate adipose tissue lipogenesis and inflammatory response together with the SCFA (propionic acid) production in the mice gut can be beneficial to mitigate the risk of NAFLD (Cho et al., 2018). Moreover, beneficial effects of the GSP synbiotic correlated with the increased richness of the mice gut microbiota and the abundance of *Akkermansia muciniphila*, and *Nocardia coeliaca* bacteria (Seo et al., 2020). Interestingly, administration of the GSP alone demonstrated similar activities at comparable levels except for the plasma AST concentration (Cho et al., 2018; Kwon et al., 2019). Another synbiotic approach using flavan-3-ol-rich green tea powder and *L. plantarum* had reported beneficial effects against NAFLD in HFD-fed mice. This synbiotic approach significantly mitigated insulin resistance, liver damage marker ALT, and hepatic TG level (Axling et al., 2012). The expressions of lipogenic enzymes SREBP-1c and PPAR-γ had also been significantly downregulated in the mice. Moreover, the synbiotic supplementation had improved adipose tissue function as depicted by the suppressed adiposity and blood plasma concentration of leptin. Administration of the green tea powder alone depicted similar beneficial activities at comparable levels. However, the synbiotic administration performed better by suppressing the cholesterol synthesis and hepatic inflammation as depicted by the downregulated mRNA expressions of the HMG-CoA reductase enzyme and proinflammatory cytokine TNF-α, respectively (Axling et al., 2012). Development of the PAC-based synbiotics may present novel opportunities to reduce the NAFLD risk. Supplementation with epigallocatechin gallate and *L. fermentum* can significantly increase the expression of nuclear factor erythroid 2-related factor 2 (Nrf2) in hepatocytes (Sharma et al., 2019). Activation of the Nrf2 signalling in NAFLD can prevent hepatic injury by resolving the oxidative stress (Zhou et al., 2022). PAC-based

synbiotics may mitigate the risk of NAFLD by reducing the hepatic lipogenesis, inflammation, and oxidative stress while regulating the adipose tissue function, protecting the gut epithelial barrier function, and modulating the gut microbiota. However, further studies are required to boost the PAC-probiotics synergistic activities beneficial for the NAFLD risk reduction.

Development of the PAC-based synbiotics can be beneficial to further improve the protective effects of PAC against NAFLD. The majority of dietary PAC are oligomers and polymers (Gu et al., 2004) and their bioavailability is considerably low (Tao et al., 2019). Most of the ingested PAC reach the colon and undergo biotransformation into valerolactone-derivatives and simple phenolic acids by the colonic microbiota (Tao et al., 2019). The beneficial effects of PAC on hepatic lipid metabolism and inflammatory markers significantly depend on the biotransformation into simple metabolites by the gut microbiota. In HFD-fed mice, PAC-mediated improvements to the inflammatory markers correlated with the concentration of procyanidin A2 metabolites produced by the gut microbiota (Yang et al., 2021). Thus, biotransformation of the oligomeric and polymeric PAC into absorbable metabolites may promote their potential to mitigate the risk of NAFLD. Therefore, formulation of the synbiotics by combining PAC and probiotic bacteria to biotransform PAC into bioavailable and bioactive metabolites is a viable strategy to increase the bioactivity of PAC against NAFLD. The potential of probiotic bacteria *L. rhamnosus* to biotransform cranberry PAC, and the antiproliferative effect of resulting metabolites in the HepG2 liver cancer cells had been demonstrated *in vitro* (Rupasinghe et al., 2019). Moreover, PAC-based synbiotics may promote the bioactivities of probiotic bacteria against NAFLD as PAC is capable of modulating the growth and

metabolism of probiotic bacteria. Cranberry PAC can increase the growth of probiotic bacteria *L. plantarum*. Also, treatment with the PAC can modulate the metabolism of *L. plantarum* to utilize FOS, a substrate not generally utilized by the *L. plantarum* bacteria (Özcan et al., 2021). Considering the huge potential to develop PAC-based synbiotics for NAFLD risk reduction, I initially developed an aqueous ethanol-based extraction process to extract PAC suitable for food and nutraceutical applications. Then, I investigated the potential of probiotic bacteria to biotransform polymeric PAC into bioavailable metabolites in a C57BL/6 mouse model. Also, I evaluated the safety of polymeric PAC and probiotic bacteria supplementation in the mice. Even though, PAC is generally recognized as safe for human consumption (Sano, 2017), PAC can depict antinutritional effects (Zhong et al., 2018) and digestive tract complications that compromise the gut epithelial barrier function in animals (Li et al., 2020; Mbatha et al., 2002). Moreover, probiotic bacteria of *Lactobacillus* and *Enterococcus* can become opportunistic pathogens (Krawczyk et al., 2021; Rossi et al., 2019). Therefore, I further investigated the potential to biotransform PAC using *Saccharomyces cerevisiae in vitro* so that the adverse health effect of the polymeric PAC can be evaded. The potential of the PAC biotransformed with the *S. cerevisiae* to mitigate steatosis and steatosis progression to NASH was evaluated using palmitic acid and LPS-induced AML12 normal mouse hepatocyte cell models. Palmitic acid-induced cellular lipotoxicity is governed by multiple mechanisms. Palmitic acid favours cellular lipid accumulation by upregulating the expression of FA transporters such as CD36 and DNL promoters, SREBP-1, SCD-1, and PPAR-γ. Moreover, palmitic acid can promote ER stress through calcium ion imbalance which may continue cellular assault by increasing the activity of cytochrome P450 2E1 oxidative enzyme and inducing

apoptosis (Nissar et al., 2015). The current study is a novel investigation of the potential to develop PAC-based synbiotics capable of NAFLD risk reduction. This study also presents insights into the safety of PAC-based synbiotics consumption and a novel approach for the synbiotics-based NAFLD risk mitigation.

1.6. PROBLEM STATEMENT

NAFLD is the most common liver disease worldwide, currently affecting around 30% of the world population and is predicted to impact more than 50% of the global adult population by 2040. Despite the high prevalence of NAFLD and the continued increase in new NAFLD cases, a drug approved by the United States Food and Drug Administration (FDA) is not available to mitigate the risk of NAFLD pathogenesis and progression. Current NAFLD management strategies primarily involve modifications to the dietary and behavioural patterns that promote low-calorie diets and physical activity. Recent findings had indicated the potential of bioactive phytochemicals, especially polyphenols to mitigate the risk of NAFLD. PAC is the most abundant dietary polyphenol and the ability of the PAC to reduce the risk of NAFLD had been demonstrated in a few studies (Table 1.2). The majority of dietary PAC are oligomers and polymers with a limited bioavailability. Thus, the bioactivities of the PAC oligomers and polymers depend on the biotransformation into bioavailable metabolites by the gut microbiota. However, the ability of gut microbiota to biotransform PAC oligomers and polymers is low, and the biotransformation efficiency greatly varies between individuals. Therefore, the combination of the PAC oligomers and polymers with probiotic microbes may be a viable strategy to biotransform PAC into bioactive and bioavailable metabolites. Since supplementation with probiotics is also beneficial for the mitigation of NAFLD (Table 1.1), such synbiotic formulations may

promote the bioactivities of PAC and probiotic bacteria synergistically against NAFLD. However, current knowledge on the probiotics capable of PAC biotransformation and the bioactivities of the resulting metabolites against the NAFLD is limited. Also, it is important to experiment with novel synbiotic approaches such as biotransformation of PAC before the administration, to improve the bioactivities of the PAC and probiotics synergistically. Moreover, studies evaluating the safety of PAC-based synbiotics are extremely scarce. It is important to identify sources of PAC that are of low economical significance and abundantly available to extract the PAC required for the formulation of synbiotics. Also, efficient PAC extraction methods that use non-toxic extraction solvents must be explored to obtain food and nutraceutical-grade PAC for the development of synbiotics. The current doctoral thesis research is dedicated to filling these fundamental knowledge gaps and is expected to be the foundation for novel approaches to NAFLD management by the administration of PAC-based synbiotics.

1.7. RESEARCH HYPOTHESIS

Probiotic microbes can biotransform grape seed (GS)-PAC oligomers and polymers into bioavailable and bioactive metabolites capable of reducing the risk of NAFLD and NASH in experimental models. Supplementation with the GS-PAC and probiotics is safe and does not confer negative health effects in experimental mice.

1.7.1. Overall objective

To investigate the potential of developing a PAC-based synbiotic by combining GS-PAC and probiotic microbes to mitigate the risk of NAFLD pathogenesis and progression to NASH using *in vitro* and *in vivo* experimental models.

1.7.2. Specific objectives

Chapter 2: Development of an aqueous-ethanol-based GS-PAC extraction method.

- To develop and optimize an aqueous-ethanol-based extraction process for food-grade GS-PAC.
- To evaluate the bioactivity of extracted GS-PAC against NAFLD *in vitro*.
- To identify by-products of wine production as a source for PAC extraction.

Chapter 3: Probiotic bacteria can biotransform polymeric GS-PAC into simple and bioavailable metabolites in C57BL/6 mice.

- To evaluate the potential of common probiotic bacteria to biotransform polymeric GS-PAC into bioavailable metabolites in C57BL/6 mice.
- To evaluate the effects of probiotic bacteria and polymeric GS-PAC supplementation on the natural gut microbiota of C57BL/6 mice.
- To evaluate the effects of probiotic bacteria and polymeric GS-PAC supplementation on the liver health of C57BL/6 mice.

Chapter 4: *Saccharomyces cerevisiae* can biotransform oligomeric and polymeric GS-PAC into bioavailable metabolites capable of reducing the risk of NAFLD.

- To evaluate the potential of *S. cerevisiae* to biotransform oligomeric and polymeric GS-PAC into bioavailable metabolites.
- To investigate the ability of PAC metabolites generated by *S. cerevisiae* to ameliorate NAFLD pathogenesis and progression to NASH *in vitro*.

CHAPTER 2. OPTIMIZATION OF THE EXTRACTION OF PROANTHOCYANIDINS FROM GRAPE SEEDS USING ULTRASONICATION-ASSISTED AQUEOUS ETHANOL AND EVALUATION OF ANTI-STEATOSIS ACTIVITY *IN VITRO*

The data presented in this chapter have been published in a peer-reviewed article.

Thilakarathna, W.P.D.W., Rupasinghe H.P.V., 2022. Optimization of the extraction of proanthocyanidins from grape seeds using ultrasonication-assisted aqueous ethanol and evaluation of anti-steatosis activity *in vitro*. Molecules 27 (4), 1363. https://doi.org/10.3390/molecules27041363

Author contributions: W.P.D.W. Thilakarathna performed all the experiments, analyzed the data, and drafted the manuscript. H.P. Vasantha Rupasinghe, the principal investigator, acquired the funds and resources, supervised the project, and reviewed the manuscript. Both authors have made intellectual contributions to the manuscript. Both authors have read and approved the final manuscript.

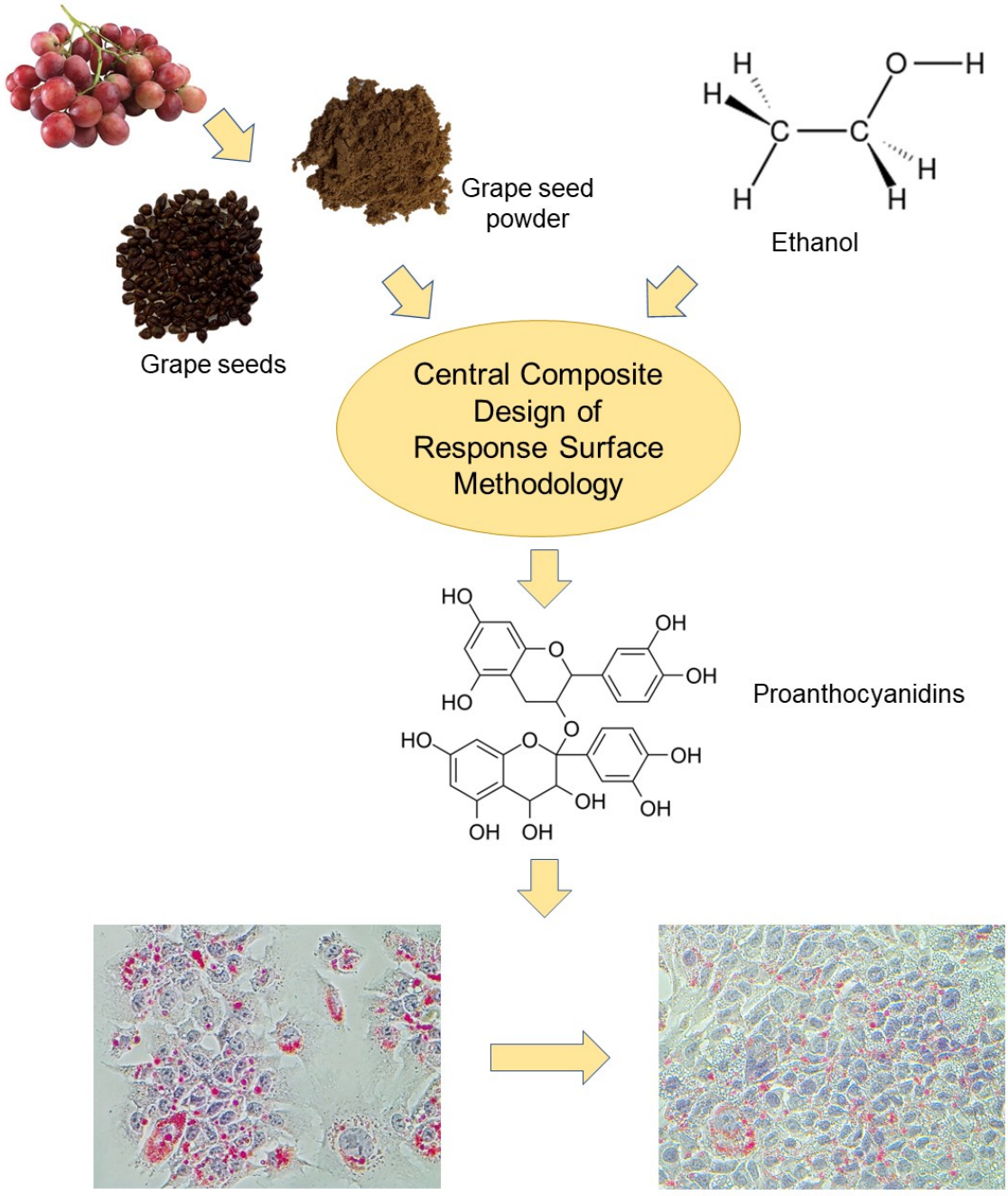

Chapter 2. Graphical abstract

2.1. ABSTRACT

Conventional extraction methods of proanthocyanidins (PAC) are based on toxic organic solvents, which can raise concerns about the use of extracts in supplemented food and nutraceuticals. Thus, a PAC extraction method was developed for grape seeds (GS) and grape seed powder using food-grade ethanol by optimizing the extraction conditions to generate the maximum yield of PAC. Extraction parameters, % ethanol, solvent:solid (s:s) ratio, sonication time, and temperature were optimized by the central composite design of the response surface method. The yields of PAC under different extraction conditions were quantified by the methyl-cellulose precipitable tannin assay. The final optimum conditions were 47% ethanol, 10:1 s:s ratio (*v:w*), 53 min sonication time, and 60 °C extraction temperature. High-performance liquid chromatography analysis revealed the presence of catechin, procyanidin B2, oligomeric and polymeric PAC in the grape seed-proanthocyanidin extracts (GS-PAC). GS-PAC significantly reduced reactive oxygen species and lipid accumulation in the palmitic acid-induced mouse hepatocytes (AML12) model of steatosis. About 50% of the PAC of the GS was found to be retained in the by-product of wine fermentation. Therefore, the developed ethanol-based extraction method is suitable to produce PAC-rich functional ingredients from grape by-products to be used in supplemented food and nutraceuticals.

Keywords: steatosis; flavonoids; grapes; by-products; green extraction; condensed tannins; ultrasonication

2.2. INTRODUCTION

Proanthocyanidins (PAC), also known as condensed tannins, are the oligomers or polymers of flavan-3-ol molecules linked together through interflavan linkages. Oligomeric and polymeric PAC predominantly consist of catechin and epicatechin monomers (Symma and Hensel, 2021). Monomers of gallocatechin, epigallocatechin, afzelechin, and epiafzelechin are also present in the molecular structure of some PAC (Ou and Gu, 2014). PAC are ubiquitously found in plant-based food, including berries, nuts, cereals, beans, and their products (Smeriglio et al., 2017). PAC can be used as a food additive to impart astringency, microbial stability, foamability, oxidative stability, and heat stability to food products (Rauf et al., 2019).

The interest in PAC has considerably increased over time with the discovery of the potential beneficial physiological function of PAC (Rodríguez-Pérez et al., 2019; Unusan, 2020). PAC are excellent antioxidant and anti-inflammatory molecules (Cádiz-Gurrea et al., 2017) capable of influencing cell-signalling pathways (Lee et al., 2017). The potential of PAC to alleviate chronic metabolic diseases has been shown by a number of studies. Supplementation of PAC has reduced obesity and obesity-associated complications by improving the blood lipid profile (Zhou et al., 2017), intestinal microflora (Morissette et al., 2020), and interfering adipogenesis (Zhang et al., 2017). However, the potential of PAC ingestion to reduce body weight is still controversial (Liu et al., 2020). The ability of PAC to improve vascular endothelial function and improve blood lipid profile by reducing triglyceride and low-density lipoprotein cholesterol levels is beneficial in reducing the risk of hypertension and cardiovascular diseases (Nunes et al., 2016). PAC also depict anticancer properties, especially in colorectal cancers (Ravindranathan et al., 2018). PAC

can promote cancer cell death (Kaplum et al., 2018) and inhibit angiogenesis and cancer metastasis (Yang et al., 2017; Zhang et al., 2018). However, the bioavailability of oligomeric and polymeric PAC depends on their bioconversion by the colonic microbiota. The microbial metabolites of PAC are proven to possess anticancer properties (Thilakarathna and Rupasinghe, 2019). The interdependency of PAC and bioconverting microbes can open a new field of study to develop PAC-based synbiotics with health benefits (Thilakarathna et al., 2018).

Grape seeds (GS) are an excellent source of PAC (around 35 mg/g dry seeds) (Gu et al., 2004) and a widely available, underutilized by-product of grape juice and wine processing (Smeriglio et al., 2017). Grape seed-proanthocyanidin (GS-PAC) is a heterogeneous mixture of 5 – 30% monomers, 17 – 63% oligomers, and 11 – 39% polymers (Ma and Zhang, 2017). A number of PAC isolation methods of GS, such as single and multiple solvent extractions aided by ultrasound, microwave, enzymatic, and mechanical treatment as well as liquid/liquid phase separation, have been reported (Cao et al., 2018; Chen et al., 2016, 2020; Fernández et al., 2015). Ultrasonication can be coupled with many conventional PAC extraction methods to enhance extraction efficiency (Ranjha et al., 2021). When plant materials are used as the source of bioactive, ultrasonication can be applied to destroy the cell walls to enable better interaction of extraction solvents with phytochemicals. Moreover, the application of ultrasonication has been proven to increase extraction efficiency at low temperatures (Annegowda et al., 2012), which is significantly important to prevent the thermal degradation of phytochemicals (Altemimi et al., 2017). Many of the recently reported liquid/liquid-based proanthocyanidin extraction methods use aqueous organic solutions (e.g., acetone, methanol, and ethanol) as the extraction solvent

(Dang et al., 2014; Ran et al., 2019; Zhao et al., 2021). These aqueous two-phase extraction (ATPE) methods can use ionic liquids (salt solutions) to increase the efficiency of proanthocyanidin extraction (Ran et al., 2019). Despite the high extraction efficiencies and low impact on the environment, the scalability of ATPE methods to a commercial level remains controversial due to the complexity of phase separation procedures, solvent recovery, and operational costs (Torres-Acosta et al., 2019). Subcritical water (Yan et al., 2020) and supercritical CO2 extraction (Da Porto et al., 2014) methods are also among the tested PAC extraction methods. Ethyl acetate, acetone, hexane, methanol, ethanol, and water are the most commonly used solvents to extract PAC (Kim et al., 2010; Liu, 2012). However, ethanol is preferred over other solvents for the extraction of plant bioactives due to its lesser toxicity (Liu, 2012) and better extraction efficiency than water (Kim et al., 2010). Therefore, extraction methods based on aqueous ethanol are advantageous to extract PAC for applications in foods and nutraceuticals.

The objective of this study was to develop and optimize a PAC extraction method using food-grade ethanol as the extraction solvent to recover PAC from GS and grape seed powder (GSP). Aqueous ethanol has been used in both conventional (Lincheva et al., 2017) and advanced PAC extraction methods, including supercritical fluid extractions (Da Porto et al., 2014). Extraction conditions such as temperature, together with the % ethanol, can significantly affect the recovery of PAC (Beaver et al., 2020). Therefore, the PAC extraction method for GS and GSP was optimized by central composite design (CCD) of response surface method (RSM) for three initial extraction parameters: % ethanol, extraction time, and solvent:solid (s:s) ratio. GS and GSP were originated from commercial grape varieties of *Vitis vinifera*, *V. labrusca*, and hybrids of native American varieties with

V. *vinifera*. GS and GSP from a mixture of grape varieties were used with the intention of generalizing the new PAC extraction method for GS and GSP from different grape varieties. Ultrasonication and heat were later introduced to increase the efficiency of the extraction process. The extracted GS-PAC were characterized by high-performance liquid chromatography (HPLC), and retention of biological activity was tested in a palmitic acid-induced steatosis cell model. We further analyzed the PAC content of different grape varieties before and after fermentation in wine processing to determine the suitability of wine by-products as a source of PAC extraction. Identification of suitable PAC extraction sources and the development of food-compatible extraction methods can benefit the development of functional foods and nutraceuticals enriched with PAC.

2.3. MATERIAL AND METHODS

2.3.1. Materials and chemicals

The GS and GSP used in this study were provided by the Royal Grapeseed, Milton, NY, USA. Both the GS and GSP came from a mixture of commercial grape varieties; *V*. *vinifera*, *V*. *labrusca*, and hybrids of native American species with *V*. *vinifera*. Grape mash before and after fermentation in wine processing was provided by the Jost Vineyards, Malagash, NS, Canada. Grape mashes from five different grape varieties, Triomphe d'Alsace, Leon Millot, Lucie Kuhlmann, Marquette, and Baco Noir, were tested in this study. Anhydrous ethanol (P016EAAN) for PAC extraction was purchased from Commercial Alcohols, Brampton, ON, Canada. Acetone (A18) for the conventional extraction of PAC and isopropanol (BP2618) were purchased from Thermo Fisher Scientific, Fair Lawn, NJ, USA. Dulbecco's Modified Eagle Medium/Nutrient Mixture F-12 (DMEM:F-12) cell culture medium (30-2006TM) was purchased from American Type

Culture Collection (ATCC®), Manassas, VA, USA. Phenol-red-free DMEM:F-12 culture medium (GibcoTM 21041025) was purchased from Fisher Scientific, Saint-Laurent, QC, Canada. Bovine serum albumin (BSA), catechin (C1251), 2′,7′-dichlorofluorescein diacetate (DCFDA, D6883), dexamethasone, dimethyl sulfoxide (DMSO), fetal bovine serum (FBS), insulin-transferrin-selenium (ITS) liquid media supplement (I3146), methylcellulose cP 1500 (MC, M0387), Oil Red O stain (ORO, O0625), paraformaldehyde, palmitic acid (P5585), penicillin-streptomycin, phenazine methosulphate (PMS), phosphate-buffered saline (PBS), and procyanidin B2 (42157) were purchased from MilliporeSigma, Oakville, ON, Canada. Oligomeric PAC from grape seeds (1298219) was purchased from USP, Rockville, MD, USA, to use as a standard for HPLC analysis. CellTiter 96® aqueous MTS reagent powder (G1111) was purchased from Promega Corporation, Madison, WI, USA.

2.3.2. Cell line and culture conditions

AML12 normal mouse liver cells were used in experiments for evaluating the biological activity of extracted GS-PAC by means of their potential to reduce cellular ROS generation and lipid accumulation. AML12 cells (CRL-2254TM) were purchased from ATCC®, Manassas, VA, USA. DMEM:F-12 cell culture medium was supplemented with FBS (10%), dexamethasone (40 ng/mL), penicillin (50 U/mL)-streptomycin (50 µg/mL), and ITS liquid media supplement (10 µg/mL, 5.5 µg/mL, and 5 ng/mL, respectively) to prepare the complete growth medium. AML12 cells were cultured at 37 °C in a humidified incubator with a 5% CO2 atmosphere. The cells were supplied with fresh, complete growth media every 2 to 3 days and sub-cultured at 80% confluence.

2.3.3. Experimental design

The CCD of RSM was used to determine the optimal conditions of PAC extraction using aqueous ethanol as the extraction solvent. The CCD consisted of 20 runs of combinations of three optimization parameters at the low-axial, low, center, high, and high-axial levels. Initially, % ethanol in water, s:s ratio (*v:w*), and extraction time (h) were optimized (Table 2.1). The initial optimization approach resulted in a significantly long extraction time and required a large volume of extraction solvent. To reduce the extraction time and extraction solvent volume, ultrasonication combined with heating was introduced into the extraction process. A second optimization was performed using a CCD of 20 runs with three optimization parameters; temperature (°C), s:s ratio (*v:w*), and sonication time (min), similar to the initial optimization approach (Table 2.1). The CCD was generated and analyzed using Minitab 18 (version 18.1) statistical software to determine the optimal conditions for the recovery of PAC from GS and GSP using aqueous ethanol as the extraction solvent.

2.3.4. Extraction of PAC by aqueous ethanol

Prior to the extraction process, GS were cleaned by removing any debris and damaged seeds. GS or GSP (1.0 g) were weighed into 50 mL plastic tubes. Anhydrous ethanol was mixed with deionized (DI) water to prepare the ethanol-based extraction solvent at different levels (0, 20.24, 50, 79.76, and 100 %), agreeing with the CCD. GS and GSP were mixed with the ethanol extraction solvent (10, 16.07, 25, 33.92, or 40 mL) in 50 mL plastic tubes. The extraction process was performed for different periods (24, 62.86, 120, 177.14, or 216 h) while slowly shaking (50 rpm) the tubes at 20 °C. The optimum conditions for the extraction process were statistically determined by the CCD of RSM.

A second PAC extraction was performed to reduce the extraction time and extraction solvent volume by introducing ultrasonication and heating into the extraction process. Only GS were used in this extraction process, as a large difference was not observed between GS and GSP for the PAC yields and optimum conditions of the tested parameters. Based on the first optimization approach, the ethanol level was set at 47% during this second optimization. Similar to the first extraction, GS (1.0 g) was weighed into 50 mL plastic tubes and mixed with different volumes of 47% ethanol in DI water (4, 5.62, 8, 10.38, or 12 mL). The extraction process was performed at different temperatures (20, 28.1, 40, 51.9, or 60 °C) while ultrasonicating for 10, 20.12, 35, 49.88, or 60 min. The optimum conditions for the extraction process were established by the CCD of RSM statistical method. The accuracy of the predicted optimized parameters was tested by performing the extraction process at the optimum values generated by the CCD analysis. The optimum conditions predicted by the CCD analysis were 47% ethanol, 10:1 s:s ratio (*v:w*), 53 min of sonication time, and an extraction temperature of 60 °C. The accuracy of the predicted optimum values was evaluated by the MC precipitable tannin assay in three individual experiments.

2.3.5. Conventional extraction of PAC

Conventional extraction of PAC was conducted as described by Rupasinghe et al. (2019) (Rupasinghe et al., 2019) with modifications to compare with the ethanol-based extraction method. Briefly, the extraction solvent was prepared by mixing acetone and formic acid with DI water (70:0.1:29.9 *v:v:v*). The original extraction s:s ratio was increased from 6:1 to 12:1 in order to match the optimum value of the aqueous ethanol-based extraction method. The extraction temperature was also increased to 60 °C. GS or

GSP (1.0 g) mixed with the acetone-based extraction solvent (12 mL) were sonicated for 30 min × 3, with 10 min intervals in between to prevent the temperature from rising. This extraction process was individually performed three times.

2.3.6. Quantification of PAC in extracts

PAC content in extracts was quantified by MC precipitable tannin assay modified to high throughput 96-well format (Mercurio et al., 2007). All extracted samples were initially filtered through coarse porous (20 – 25 µm) filter papers. The filtrates (only 1 mL) were filtered again using 0.22 µm nylon filters. Standard catechin solutions (1 – 100 µg/mL) were prepared in 50% aqueous ethanol. MC solution of 0.04% was prepared to quantify the PAC in filtered extracts. Initially, 0.4 g of MC was slowly dissolved in 300 mL of DI water at 80 °C while magnetic stirring to prevent clumping. After completely dissolving MC, 650 mL of ice-cold water (0 – 5 °C) was mixed with the hot MC solution. We continued stirring ice-cold water into the MC solution for 40 min and ultrasonicated it for 15 min. The final MC solution was marked up to 1 L in a volumetric flask.

To measure the PAC quantity, 100 µL of filtered extract or catechin standard was mixed with 300 µL of MC solution, 200 µL of saturated $(NH4)_2SO_4$ solution, and 400 µL of DI water in 1.5 mL Eppendorf tubes. The controls were prepared for each extracted sample and catechin standard by replacing the MC solution with an extra 300 µL of DI water. Eppendorf tubes were centrifuged at 10,000 × g for 5 min, and the supernatants were pipetted (200 µL/ well) into a UV-transparent 96-well plate (Corning Incorporated, Kennebunk, ME, USA) in triplicate. The absorbance of the wells was measured at 280 nm (Infinite® M200 PRO, Tecan Trading AG, Mannedorf, Switzerland), and the absorbance differences between extracts/catechin standards and respective controls were calculated. A

catechin standard curve was created by plotting the absorbance difference against catechin concentration. PAC quantity in extracted samples was calculated using the catechin standard curve, and the results were expressed in mg catechin equivalence/g sample.

2.3.7. Purification of crude GS-PAC to generate a sugar-free fraction

Crude GS-PAC was purified by flash chromatography to generate a sugar-free PAC extract. The sugar-free fraction of GS-PAC was used for HPLC analysis and AML12 cell-based experiments to evaluate biological activity. Initially, crude PAC was extracted from GS under the optimized conditions (50 g in 500 mL of 47% ethanol in water). Part of the PAC extract (300 mL) was loaded into a glass flash chromatography column (6.5 × 45 cm, Sati International Scientific Inc., Dorval, QC, Canada) packed with 400 g of Sorbent beads (Sorbent SP207-05 Sepabeads resin brominated styrenic adsorbent, Sorbent Technologies, Atlanta, GA, USA) and eluted with DI water until Brix value reached below 0.1% (no sugars present in the elute). Then, PAC was eluted by using 80% acetone in water and concentrated by rotary evaporation at 35 °C until the PAC concentrate was free of acetone. The crude GS-PAC extract (200 mL) was also concentrated by rotary evaporation until the PAC concentrate was free of ethanol. Concentrated PAC samples were freeze-dried for 24 h and stored at −80 °C.

2.3.8. HPLC analysis of PAC extracted by the ethanol-based optimized method

The composition of the sugar-free GS-PAC extract was determined by HPLC analysis. Catechin (25 µg/mL), procyanidin B2 (25 µg/mL), and oligomeric PAC from grape seeds (50 µg/mL) were dissolved in 80% ethanol in water to prepare the standards for HPLC analysis. Sugar-free GS-PAC extract (200 µg/mL) was also dissolved in 80% ethanol in water to inject into HPLC. All samples were syringe-filtered through 0.22 µm

filters before injecting them into the HPLC. The HPLC system used for this analysis consisted of a Waters 2695 separation module coupled with a Waters 2996 photodiode array (PDA) detector (Waters, Milford, MA, USA) and equipped with an Xselect® HSS C18, 5 µm column (4.6 × 150 mm, Waters, Milford, MA, USA). The HPLC separation was performed by using 0.1% formic acid in water (solvent A) and acetonitrile (solvent B) as the mobile phases at a flow rate of 0.7 mL/min. The HPLC run method was comprised of linear and isocratic gradients of mobile phases, where the proportion of acetonitrile (% solvent B) was altered over time; 5 – 15% from 0 – 45 min (linear), 15 – 80% from 45 – 50 min (linear), 80% from 50 – 53 min (isocratic), and 5% from 53 – 70 min (isocratic recalibration). HPLC sample injection volume was 10 µL, and PDA detection was set to 280 nm wavelength.

2.3.9. Evaluation of the biological activity of extracted GS-PAC

The biological activity of extracted GS-PAC was evaluated by using the palmitic acid-induced steatosis model of AML12 mouse liver cells. Palmitic acid was solubilized in 20% BSA in PBS as described by Zeng et al. (2020) (Zeng et al., 2020) to produce a stock solution of 10 mM. AML12 cells were treated with different concentrations of palmitic acid (10 – 750 µM) for 24 h, and the development of ROS and the cellular accumulation of lipids were measured by DCFDA assay and ORO staining of cells, respectively. Cell viability of AML12 cells under different concentrations of palmitic acid was determined by MTS cell viability assay. A concentration of 200 µM of palmitic acid was selected for further experiments considering low toxicity to AML12 cells (> 90% cell viability) and potential to promote ROS generation (142% compared to negative control) and cellular lipid accumulation.

2.3.9.1. Determination of toxicity of GS-PAC in AML12 cells

The toxicities of crude GS-PAC and purified sugar-free GS-PAC extracted by the optimized extraction method were evaluated by the MTS cell viability assay. AML12 cells were seeded in 96-well plates at a density of 10,000 cells/well and incubated overnight under normal culture conditions. Then, cells were treated with different concentrations of crude and sugar-free GS-PAC (1 – 1000 µg/mL) for 24 h. After treatment with PAC, 20 µL of MTS/PMS solution (MTS, 333 µg/mL and PMS, 25 µM of final concentration) was added into wells and incubated for 3 h at normal culture conditions. After incubation, absorbance for each well was measured at 490 nm using a microplate reader (Infinite® M200 PRO, Tecan Trading AG, Mannedorf, Switzerland). The absorbance values between the PAC treatments and control were compared and expressed in percentages as an indirect measurement of cell viability.

2.3.9.2. Evaluation of extracted GS-PAC to alleviate palmitic acid-induced ROS generation

The potential of GS-PAC obtained by optimized extraction method in mitigation of palmitic acid-induced ROS generation in AML12 cells was studied by DCFDA assay. A 100 mM stock solution of DCFDA was prepared by dissolving it in DMSO. AML12 cells were seeded in black 96-well plates for fluorescence-based assay at a density of 10,000 cells/well and incubated overnight under normal culture conditions. Then, cells were pre-treated with 10, 25, and 50 µg/mL concentrations of crude and sugar-free GS-PAC for 24 h. After treatment with PAC, cellular ROS generation was induced by exposing cells to 200 µM palmitic acid diluted in complete DMEM:F-12 culture medium for 24 h. A 5 µM working solution of DCFDA was prepared by diluting the stock solution in a complete

DMEM:F-12 culture medium. AML 12 cells exposed to palmitic acid were gently washed with PBS, and 200 µL of DCFDA working solution was added to each well. After incubation for 30 min under normal culture conditions, cells were gently washed with PBS three times, and 200 µL of phenol red-free DMEM:F-12 culture medium was added to each well. The fluorescence of each well was measured at 485 nm (excitation)/ 535 nm (emission) using a microplate reader (Infinite® M200 PRO, Tecan Trading AG, Mannedorf, Switzer-land).

2.3.9.3. Evaluation of extracted GS-PAC to alleviate palmitic acid-induced steatosis *in vitro*

The ability of crude and sugar-free GS-PAC obtained by the optimized extraction method to alleviate palmitic acid-induced steatosis in AML12 cells was studied by the ORO staining of cellular lipids. AML12 cells were seeded in 6-well plates at a density of 2.5×10^5 cells/well and incubated overnight under normal culture conditions. Then, cells were treated with 10, 25, and 50 µg/mL concentrations of crude and sugar-free GS-PAC for 24 h and exposed to 200 µM palmitic acid diluted in complete DMEM:F-12 culture medium to induce cellular lipid accumulation. A stock solution of ORO stain was prepared by dissolving 60 mg of ORO powder in 20 mL of isopropanol. The stock solution was mixed with DI water (3:2 *v:v*) and syringe-filtered through 0.22 µM filters to create the ORO stain working solution. AML12 cells exposed to palmitic acid were gently washed with PBS twice and fixed by incubating with 4% paraformaldehyde solution for 45 min at room temperature (RT). After fixation, cells were gently washed twice with DI water and permeabilized by incubating with 60% isopropanol in DI water for 5 min at RT. Cellular lipid was stained with ORO by incubating cells with ORO working solution for 15 min at

RT. After staining, cells were gently washed with DI water three times and incubated with hematoxylin nuclear stain for 1 min at RT. Excess hematoxylin was removed by gently washing the cells with DI water (3 times), and microscopic images (at × 100) of stained cells were observed while cells were immersed in DI water. Palmitic acid-induced lipid accumulation in cells was indirectly measured by quantifying ORO stain retention in cells. To quantify cellular retention of ORO stain in AML12 cells, first, the plate wells were washed three times with 60% isopropanol in DI water. Then, the ORO stain in the cells was extracted by using 1 mL of 100% isopropanol and slowly rocking the 6-well plate for 5 min. The ORO stain concentrations in isopropanol extracts were expressed as absorbance values at 492 nm.

2.3.10. Extraction of PAC from grape mashes before and after fermentation

PAC retention in grape mashes after fermentation for wine production was measured to determine the suitability of wine by-products as a source of PAC extraction. The mashes before fermentation consisted of grape skin, flesh, stems, and seeds. After the fermentation process, only grape seeds and skin were available as the by-products. Five different grape varieties, Triomphe d'Alsace, Leon Millot, Lucie Kuhlmann, Marquette, and Baco Noir, were tested in this study for the retention of PAC after fermentation. Grape mashes before and after fermentation of wine processing were freeze-dried for 48 h. Freeze-dried samples were ground into a fine powder, and PAC was extracted by the optimized PAC extraction method. Briefly, 1 g of powdered grape mash was mixed with 10 mL of 47% aqueous ethanol and ultrasonicated for 53 min at 60 °C. Extracted PAC quantity was measured by the MC precipitable tannin assay.

2.3.11. Statistical analysis

Statistical analysis was conducted as previously described by Chen et al. (2020) (Chen et al., 2020). Optimum conditions for extracting the maximum yield of PAC from GS and GSP were determined by CCD of RSM with 20 runs. Normal distribution and constant variance of the error terms were established by normal probability plots and residual versus fits plots. The independence was assumed by the randomization of run order. A second-order polynomial model was used to describe the variation of the response variable (PAC yield) by the independent variables (extraction parameters), and the regression coefficients were calculated.

$$Y = \beta_0 + \beta_1X_1 + \beta_2X_2 + \beta_3X_3 + \beta_1^2X_1^2 + \beta_2^2X_2^2 + \beta_3^2X_3^2 + \beta_1\beta_2X_1X_2 + \beta_1\beta_3X_1X_3 + \beta_2\beta_3X_2X_3$$

Y is the PAC yield and β_0 is the constant; β_1, β_2, and β_3 are the regression coefficients of linear effect terms; β_1^2, β_2^2, and β_3^2 are the quadratic effect terms and $\beta_1\beta_2$, $\beta_1\beta_3$, and $\beta_2\beta_3$ are the interaction effect terms; X_1, X_2, and X_3 are the three extraction parameters tested.

The adequacy of the model was confirmed by the non-significant lack of fit ($p > 0.05$). The significance of each term (extraction parameter) was tested by analysis of variance (ANOVA), and contour plots were constructed. The optimum condition of each parameter to extract the maximum content of PAC was determined by the response optimizer. The mean PAC content of different PAC extracts was compared by the one-way ANOVA at 0.05 significance level. The differences in mean % cell viabilities, cellular ROS generation, cellular lipid accumulation, and PAC quantities in the grape mash before and after fermentation were also tested by the one-way ANOVA at a 0.05 significance level. The CCD generation and all statistical analyses were performed by Minitab® statistical software (version 18.1).

2.4. RESULTS

2.4.1. Response surface models

A CCD of response surface modelling with 20 runs was used to optimize the PAC extraction from GS and GSP using aqueous ethanol as the extraction solvent. Initially, three extraction parameters: % ethanol, extraction time (h), and s:s ratio (*v:w*) were optimized. PAC yields extractable under combinations of low-axial, low, center, high, and high-axial levels of these parameters were determined by the MC precipitable tannin assay (Table 2.2). The experimental PAC yields were fitted to a second-order polynomial response surface model, and the significance of the model components was tested by analysis of variance (ANOVA) (Table 2.3). The response surface models were excellent in describing the variation of PAC yields with the three extraction parameters. Both GS and GSP models were non-significant ($p > 0.05$) for lack-of-fit (0.299 and 0.736, respectively). The adjusted R^2 for GS and GSP models were 97.38% and 99.89%, respectively.

A second optimization was performed by introducing heat and ultrasonication to reduce the extraction time and volume of 47% aqueous ethanol. Only the GS was selected for the second optimization as optimum conditions and predicted yields were almost similar for GS and GSP. Similar to the first optimization approach, PAC yields extractable under different combinations of extraction parameters; temperature (°C), s:s ratio (*v:w*), and sonication time (min) were determined (Table 2.4). A second-order polynomial model well described the variation of PAC yields by the extraction parameters. The lack-of-fit (0.182) of the model was not significant, and the adjusted R^2 was 99.08% (Table 2.5).

2.4.2. Optimization of the aqueous ethanol-based PAC extraction conditions

2.4.2.1. First extraction approach

Contour plots (Fig. 2.1 and Fig. 2.2) were created to study the influence of selected extraction parameters on the PAC yield. In both GS and GSP extraction optimizations, extraction parameters showed a significant influence on the extractable PAC yield. Higher quantities of PAC were extractable from GS (> 14.6 mg catechin equivalence/g fresh weight [mg CE/g FW]) and GSP (> 12.8 mg CE/g FW) when the % ethanol was around 50%. Interestingly, PAC yield significantly dropped at higher % ethanol (Fig. 2.1a, b, d, and e). The PAC extraction time was slightly shorter for GSP compared to the GS (Fig. 2.1a and d). The PAC yield continued to increase with the s:s ratio, suggesting the need to use higher volumes of aqueous ethanol in future extraction attempts (Fig. 2.1b, c, e, and f). The extraction conditions were optimized by creating optimization plots with a focus to maximize the PAC yield (Fig. 2.2). Optimization of the extraction process for GS predicted a maximum PAC yield of 16.1 mg CE/g FW (Fig. 2.2a). Optimum extraction conditions were 47% of ethanol, 150 h of extraction time, and an s:s ratio of 40 (*v:w*). Optimum extraction conditions for GSP were closely similar to the GS. A maximum PAC yield of 15.3 mg CE/g FW was predicted for GSP when the extraction conditions were tuned to 47% of ethanol, 142.6 h of extraction time, and an s:s ratio of 40:1 (*v:w*) (Fig. 2.2b). The contour plots and the optimization plots suggest an s:s ratio over 40:1 (*v:w*) to achieve the maximum yield of PAC. Thus, further incrementation of the s:s ratio may increase the extractable PAC yield, and the real optimum s:s ratio may be higher than 40:1 (*v:w*).

2.4.2.2. Second extraction approach

The initial extraction process was considered inefficient and resource intense. The extraction process required a large volume of aqueous ethanol (40 mL/g FW), and the extraction time was six days long. Therefore, a second extraction approach was attempted to reduce the extraction time and s:s ratio by introducing heat and ultrasonication to the extraction process. Previously optimized % ethanol (47%) was used for the extraction process. Only GS was used in this optimization attempt, considering the similarity of predicted yields and optimum conditions for GS and GSP in the initial extraction processes. The tested extraction parameters, temperature, s:s ratio, and ultrasonication time significantly influenced the PAC yield of GS (Fig. 2.3a). The predicted PAC yield (26.6 mg CE/g FW) was considerably higher compared to the first extraction approach. The PAC yield continued to increase with the increasing temperature, suggesting the possibility of using higher temperatures to increase the PAC yield (Fig. 2.3, ai and aii). The s:s ratio and the extraction time were considerably lower compared to the first extraction approach. Optimization plots were created to identify the optimum extraction conditions to obtain the highest yield of PAC (Fig. 2.3b). Optimum conditions to extract PAC from GS were a temperature of 60 °C, an s:s ratio of 10.14:1 (*v:w*), and an ultrasonication time of 53 min. The predictable PAC yield was 26.6 mg CE/g FW. The optimum temperature of 60 °C is the highest temperature tested in this extraction process. Considering the optimization plots and contour plots, more PAC could be extracted at temperatures higher than 60 °C. However, temperatures over 60 °C were not tested, considering the negative effect of high temperatures on the stability of PAC.

2.4.3. Evaluation of the predicted PAC yield and comparison with acetone-based extraction method

Optimum conditions of the extraction parameters were tested to compare the PAC yield predicted in the second extraction approach. Under the optimum extraction conditions, 25.3 ± 1.26 mg CE/g FW of PAC, compared to the predicted value of 26.6 mg CE/g FW, was extracted from GS. The extracted PAC yield was not considerably different from that of the predicted PAC yield. The extracted PAC yield was significantly higher compared to the aqueous acetone-based extraction method. The PAC yield from the acetone-based extraction of GS was 9.15 ± 0.20 mg CE/g FW.

2.4.4. HPLC analysis of the sugar-free fraction of extracted PAC

The sugar-free fraction of the GS-PAC extracted by the optimized method was analyzed by HPLC to determine the monomeric, oligomeric, and polymeric composition. The HPLC chromatogram of sugar-free GS-PAC was compared with catechin (monomeric PAC), procyanidin B2 (dimeric PAC), and a GS-PAC oligomeric standard (Fig. 2.4). The sugar-free fraction of GS-PAC was comprised of peaks for catechin (20 min), procyanidin B2 (26 min), and oligomeric PAC (33–43 min). Several peaks from 48–68 min were detected that might be attributed to polymeric PAC. The optimized aqueous ethanol-based PAC extraction method is suitable for extracting GS-PAC ranging from monomers to polymers.

2.4.5. Biological activity of GS-PAC extracted by the optimized method in palmitic acid-induced steatosis model of AML12 cells

Initially, non-toxic concentrations of crude and sugar-free GS-PAC extracts were determined by the MTS cell viability assay (Fig. 2.5). The crude GS-PAC extract showed

a considerable reduction in cell viability (<75%) at concentrations over 50 µg/mL. The sugar-free GS-PAC extract depicted higher toxicity in AML12 cells compared to the crude extract. Concentrations over 25 µg/mL of sugar-free GS-PAC extract reduced the % cell viability below 50%. Based on these results, 10, 25, and 50 µg/mL concentrations of crude and sugar-free GS-PAC extracts were selected to determine biological activity.

Palmitic acid-induced AML12 cells were used to assess the extracts for the reduction of cellular reactive oxygen species (ROS) generation and cellular lipid accumulation, which mimic steatosis. The ROS generation in AML12 cells was measured by the DCFDA cellular ROS detection assay (Fig. 2.6). Exposure to palmitic acid (200 µM) alone (the experimental model) significantly increased the cellular ROS generation in AML12 cells. Both crude and sugar-free GS-PAC extracts significantly reduced the palmitic acid-induced ROS generation by 10% – 20%. In crude GS-PAC-treated AML12 cells, the reduction of ROS generation was dose-dependent. Interestingly, 25 and 50 µg/mL concentrations were equally effective in the reduction of cellular ROS generation. The 10 and 25 µg/mL concentrations of sugar-free GS-PAC were similarly effective in reducing cellular ROS generation (by 20%). The highest ROS suppression was observed for 50 µg/mL concentration of the sugar-free GS-PAC extract. However, this additional ROS reduction may be attributed to the loss of viable cells, as 50 µg/mL of sugar-free GS-PAC was toxic to AML12 cells.

Cellular lipid accumulation in AML12 cells was visualized and measured by ORO staining of the cells (Fig. 2.7). Both crude and sugar-free GS-PAC significantly reduced the palmitic acid-induced lipid accumulation in cells. The reductions of lipid accumulation by different concentrations of crude GS-PAC extract were similar. The highest reduction

of cellular lipid accumulation was observed for 10 µg/mL concentration of sugar-free GS-PAC extract. Interestingly, the 10 µg/mL concentration of sugar-free GS-PAC extract significantly reduced the cellular lipid accumulation greater than the 25 and 50 µg/mL concentrations did. Moreover, cellular lipid reduction by the 10 µg/mL concentration of sugar-free GS-PAC extract was statistically similar to that of the 25 and 50 µg/mL concentrations of crude GS-PAC extract. Both GS-PAC extracts depicted promising abilities to suppress palmitic acid-induced steatosis in AML12 cells as measured by cellular ROS reduction and cellular lipid accumulation.

2.4.6. PAC retention in grape mashes after fermentation

The PAC contents in grape mash from five common grape varieties (Triomphe d'Alsace, Leon Millot, Lucie Kuhlmann, Marquette, and Baco Noir) were quantified before and after fermentation for wine production (Fig. 2.8). Initial PAC content (before fermentation) was high in the Leon Millot (20.9 mg CE/g dry weight [DW]) and Lucie Kuhlmann (20.7 mg CE/g DW) grape varieties compared to the other three grape varieties; Triomphe d'Alsace, Marquette, and Baco Noir. All the tested grape varieties, except for the Triomphe d'Alsace, showed a significant reduction in PAC content after the fermentation process. The Lucie Kuhlmann grape variety depicted the highest reduction in PAC content after the fermentation (20.7 to 10.6 mg CE/g DW). The PAC contents of the Leon Millet (20.9 to 14.1 mg CE/g DW) and Marquette (10.6 to 4.45 mg CE/g DW) grape varieties were also considerably lowered by the fermentation process. The Leon Millet (even after a significant PAC drop) and the Baco Noir grape varieties retained the highest quantities of PAC after the fermentation process (14.1 and 13.2 mg CE/g DW, respectively). Thus, grape by-products of wine production are a suitable source for PAC

extraction, and it is important to consider the grape variety when using grape by-products for PAC extraction.

2.5. DISCUSSION

The interest in utilizing PAC as functional food ingredients and nutraceuticals has continued to grow over time. The conventional PAC extraction methods require organic solvents such as ethyl acetate and acetone, which may leave harmful solvent residues along with extracted PAC as well creating environmental impacts. Therefore, extraction methods solely based on water (e.g., subcritical water extraction) or aqueous food-grade ethanol are favourable in extracting PAC for food and nutraceutical applications (Liu, 2012). However, extraction of PAC with only water requires higher extraction temperatures (Kim et al., 2010; Ku et al., 2011), which causes the degradation of PAC (Huh et al., 2004; Kitao et al., 2001). The antioxidant activity of GS-PAC declines at temperatures over 50 °C (Huh et al., 2004; Kitao et al., 2001). Moreover, the stability and yield of PAC by grape pomace are considerably reduced at temperatures over 60 °C (Khanal et al., 2010). Large quantities of GS have been generated annually as underutilized by-products of grape processing. GS accounts for around 13% of the grape's weight and is rich in phenolic compounds (around 7%), including PAC (Smeriglio et al., 2017). Thus, GS is a viable source for PAC extraction on a large scale. The development of an aqueous ethanol-based PAC extraction method for GS will be beneficial to producing cost-effective, supplemented food and nutraceuticals enriched with PAC.

The optimum % ethanol predicted by the optimization plots for both GS and GSP was 47%. The extraction of PAC from GS is possible with water as the sole extraction solvent. The presence of ethanol can increase the rate of PAC extraction within the first six

days of the extraction process (Henandez-Jimenez et al., 2012). Moreover, the yield of PAC increases with the % ethanol (0% – 15%), even though the extraction rates become identical after the sixth day of the extraction process (Henandez-Jimenez et al., 2012). The optimum % ethanol seems to rely on the plant source used to extract PAC. A much higher % ethanol (93.7%) is recommended as the optimum condition to recover PAC from Chinese wild rice (Chu et al., 2019). The extraction times required for GS and GSP were closely similar (150 h *Vs*. 143 h). Also, the predictable PAC yields were not different between GS and GSP (16.1 mg CE/g FW Vs. 15.3 mg CE/g FW). Therefore, the grinding of grape seeds to create GSP is not required to increase the PAC extraction efficiency with aqueous ethanol. The optimum s:s ratio could not be determined for GS and GSP in the first optimization approach, as the aqueous ethanol requirement was over the maximum s:s ratio (40:1 *v:w*) used. This is obvious from the previous PAC extraction optimization studies. A s:s ratio of 50:1 is recommended as the optimum condition for maximizing the yield of PAC from Chinese wild rice when aqueous ethanol is used with ultrasound-assisted extraction (Chu et al., 2019). Similarly, a s:s ratio of 58:1 (*v:w*) is reported for grape seeds extracted with methanol: acetone: water: acetic acid (30:42:7.5:0.5, *v:v:v:v*) in an ultrasonication-assisted solvent extraction process (Andjelkovi et al., 2014).

A second optimization approach was designed to increase PAC extraction efficiency and reduce the aqueous ethanol requirement. Heat and ultrasonication were introduced into the extraction process. Only GS was used, considering the similarity of predicted yields and optimum conditions between GS and GSP. The percentage of ethanol was fixed at 47% based on the knowledge from the first optimization approach. The introduction of heat and ultrasonication significantly reduced the extraction time

(sonication time of 53 min) and aqueous ethanol requirement (10.14:1 *v:w*) while considerably increasing the PAC yield (16.1 mg CE/g FW Vs. 26.6 predicted mg CE/g FW). The optimum temperature for this ultrasonication-assisted extraction process could not be determined as the optimum condition was above the maximum extraction temperature (60 °C) used. However, higher extraction temperatures were not tested in this study as the stability and biological activity of PAC starts to drop above 50 – 60 °C (Huh et al., 2004; Khanal et al., 2010; Kitao et al., 2001). The PAC yield may continue to increase with temperatures even higher than 100 °C. In a previous study, the PAC yield from GS continued to increase with temperature and maximized at 120 °C in a 70% aqueous acetone-based accelerated high-pressure extraction process (Bozan and Altinay, 2014). The introduction of ultrasonication into the extraction process can significantly reduce the extraction time. Ultrasonication can disrupt the plant cell wall and improve the permeation of extraction solvent and target compounds through cell membranes (Kalli et al., 2018).

The extraction solvent has a significant impact on the extractable yield of PAC (Ngo et al., 2017). The optimized aqueous ethanol-based ultrasonication-assisted PAC extraction method generated a significantly high PAC yield compared to the aqueous acetone-based extraction method (25.3 mg CE/g FW *Vs*. 9.1 mg CE/g FW). Several previous studies contradict this comparison and declare the superiority of acetone-based extractions over aqueous ethanol (Bozan and Altinay, 2014; Downey and Hanlin, 2010; Ngo et al., 2017). However, a study on the extraction of bioactive compounds from macadamia skin waste suggests that aqueous ethanol (50%) can extract more PAC compared to aqueous acetone (50%) (Dailey and Vuong, 2015). The extractable PAC yield greatly varies depending on the extraction conditions. A higher yield of PAC may be

possible to obtain from the acetone-based extraction method if the s:s ratio or extraction temperature is further increased. However, under the tested extraction conditions, the aqueous ethanol-based extraction method is superior to the acetone-based method. Therefore, the developed ethanol-based extraction method can be recommended for efficient scale-up recovery of PAC from GS by the industry.

The HPLC analysis of sugar-free GS-PAC established the ability of the optimized method to extract PAC, ranging from monomers to polymers. Sica et al. (2018) has observed a similar chromatogram for a GS extract by using a very sophisticated ultra-high performance liquid chromatography-charged aerosol detector (UHPLC-CAD) instrument (Sica et al., 2018). A broad oligomeric PAC peak was detected by the CAD detector (similar to the peak between 33 – 43 min in Fig. 2.4), and further analysis revealed this peak represents polymerized tannins with six or more monomeric catechin units (Sica et al., 2018). A number of other studies have reported similar chromatograms in approaches to characterize PAC-rich GS extracts (Kuhnert et al., 2015; Muñoz-Labrador et al., 2019; Suo et al., 2019). However, many of these chromatograms do not report a second broad PAC peak similar to the peak observed between 60 – 68 min (Fig. 2.4) in this study. The second broad peak can be a mixture of highly polymerized PAC, and further studies can be recommended for its resolution.

Since the aqueous ethanol-based PAC extraction method was developed with the intention of generating PAC suitable for applications in food and nutraceuticals, it is important to establish the retaining of the biological activity of PAC after the extraction process. A cell model of steatosis using palmitic acid-induced AML12 cells was used to test the biological activity of extracted crude and sugar-free GS-PAC. Initial cell viability

assays revealed the dose-dependent toxicity of extracted GS-PAC on AML12 cells. The toxicity of PAC in cells has previously been established by several studies, especially for cancer cells (Chen et al., 2017b, 2017a; Wang et al., 2019). PAC can induce cellular ROS generation and cause apoptosis in a dose-dependent manner. A considerable loss of cell viability (< 80%) was observed in cells treated with low concentrations of PAC (> 20 μg/mL) from multiple plant sources (Chen et al., 2017b, 2017a). Higher cytotoxicity was observed for the purified, sugar-free GS-PAC extract compared to the crude GS-PAC extract. The high toxicity of the sugar-free GS-PAC extract can be attributed to the high PAC concentration in the purified extract after flash chromatography.

GS-PAC extracted by the optimized method was able to ameliorate steatosis markers in AML12 cells incubated with palmitic acid. Cellular ROS generation was measured in the AML12 cells as steatosis is associated with increased generation of ROS in hepatocytes (Reiniers et al., 2014). PAC can reduce cellular ROS generation through multiple mechanisms. PAC is a natural antioxidant; therefore, it can neutralize cellular ROS by direct scavenging. PAC can also modulate multiple cell-signalling pathways to alleviate cellular ROS generation. Activation of nuclear factor erythroid 2-related factor 2 (Nrf2) (Suraweera et al., 2020), suppression of mitogen-activated protein kinase (MAPK), nuclear factor-kappa-light-chain-enhancer of activated B cells (NF-κB), and phosphoinositide 3-kinase (PI3K)/Akt pathways have been identified as PAC-mediated interventions to reduce cellular oxidative stress (Yang et al., 2018). Procyanidin B2 was found in the GS-PAC extracted by the optimized method. Procyanidin B2 helps to maintain cellular redox homeostasis by protecting mitochondrial membrane potential and improving the activity of cellular antioxidant enzymes superoxide dismutase (SOD), glutathione

peroxidase (GPx), and catalase (CAT) in hepatocytes (Su et al., 2018). Similar to ROS generation, lipid accumulation was also measured as a marker of steatosis in AML12 cells. Extracted GS-PAC was able to significantly reduce palmitic acid-induced lipid accumulation in AML12 cells. This reduction of cellular lipid accumulation can be explained by the effects of PAC on cell signalling pathways regulating lipid degradation and lipogenesis. Procyanidin B2 can promote lysosomal-mediated lipid degradation by upregulating the expression of Lamp1, Mcoln, and Uvrag genes through modulating transcription factor EB (TFEB). Also, PAC B2 restricts lipogenesis by the downregulation of peroxisome proliferator-activated receptor γ (PPARγ), C/EBPα, and sterol regulatory element-binding protein-1 (SREBP-1) genes (Su et al., 2018). A similar result has been reported by Yogalakshmi et al. (2013) when GS-PAC was supplemented to mice fed with a high-fat-high-fructose diet to induce steatosis (Yogalakshmi et al., 2013). Therefore, interventions of GS-PAC can alleviate steatosis by inhibiting fatty acid synthesis in mice (Yogalakshmi et al., 2013).

We tested the suitability of grape by-products from wine production for the extraction of PAC using the optimized method. The PAC content of grape mashes from five grape varieties was quantified before and after the fermentation process. All the tested grape varieties except for Triomphe d'Alsace depicted a significant reduction in the PAC content after fermentation. The loss of PAC from the initial grape mash during fermentation is evident by the presence of PAC in wine (Fujimaki et al., 2018; Jordão et al., 2010). It is the polymeric fraction of PAC (degree of polymerization > 12 – 15) abundant in both red and white wines (Jordão et al., 2010). Thus, the reduction of PAC from grape mashes after fermentation may result from the loss of polymeric PAC. The

grape mash consists of grape skins, flesh, stems, and seeds. About half of the monomeric and oligomeric PAC in GS leaches into the wine during fermentation. However, GS does not contribute to the polymeric PAC in wine. The polymeric PAC in wine mainly originates from the grape skins and stems (Sun et al., 1999). Moreover, red wine contains more PAC compared to white wine (Jordão et al., 2010). Therefore, the selection of grape by-products from white wine production can be useful for extracting a higher yield of PAC. However, it is also important to consider the grape variety, as PAC content before and after fermentation greatly varies depending on the grape variety.

2.6. CONCLUSIONS

The development of an aqueous ethanol-based PAC extraction method is beneficial for the supplemented food and nutraceutical industries. The optimum ethanol concentration for the extraction of PAC from GS and GSP is 47%. PAC yields and optimum extraction conditions are similar for GS and GSP. Therefore, grinding grape seeds into powder is not necessary for increasing the yield and extraction efficiency with aqueous ethanol. The extraction of PAC from GS and GSP using aqueous ethanol at room temperature is highly inefficient and requires a large volume of ethanol. The introduction of ultrasonication and heating into the extraction process can significantly reduce the extraction time and aqueous ethanol requirement while increasing the PAC yield. The optimized conditions to extract PAC from GS are 47% aqueous ethanol, 60 °C temperature, 10.14:1 s:s ratio, and 53 min of sonication time. The developed aqueous ethanol-based extraction method can generate a higher yield of PAC from GS compared to the conventional acetone-based extraction method. HPLC analysis of sugar-free GS-PAC revealed that the optimized method could extract catechin, procyanidin B2, oligomeric, and polymeric PAC from GS. Both crude

and sugar-free GS-PAC extracted by the optimized method depict toxicity in AML12 mouse hepatocytes at low concentrations (> 25 μg/mL). Also, extracted GS-PAC could ameliorate palmitic acid-induced steatosis in AML12 cells by reducing cellular ROS generation and lipid accumulation. The PAC content of grapes greatly varies depending on the variety. A significant reduction of PAC occurs in the grape mash during fermentation for wine production. However, grape by-products, even after fermentation, retain enough PAC to consider them as a source of PAC. The developed extraction method can be recommended for extracting PAC from GS and grape by-products from wine production without losing biological activity to use in supplemented food and nutraceutical products.

2.7. ACKNOWLEDGEMENTS

This research received funds from the Discovery grant of the Natural Sciences and Engineering Research Council (NSERC) of Canada (RGPIN2016 05369) to H.P.V. Rupasinghe. The authors are grateful for the A. David Crowe Graduate Scholarship to W.P.D.W. Thilakarathna.

Table 2.1. Optimization parameters and their levels used in the central composite designs of the surface response method.

Optimization Parameter	Level				
	Low-axial (−1.68)	**Low (−1)**	**Center (0)**	**High (+1)**	**High-axial (+1.68)**
1st Optimization approach					
% Ethanol in water	0	20.24	50	79.76	100
Extraction time (h)	24	62.86	120	177.14	216
Solvent:solid ratio (*v:w*)	10	16.07	25	33.92	40
2nd Optimization approach					
Temperature (°C)	20	28.1	40	51.9	60
Solvent:solid ratio (*v:w*)	4	5.62	8	10.38	12
Sonication time (min)	10	20.12	35	49.88	60

Table 2.2. Central composite design (CCD) used in the first optimization approach and the proanthocyanidin yields under different combinations of extraction conditions.

Run Order	Ethanol (%)	Extraction Time (h)	Solvent:Solid Ratio (*v:w*)	Proanthocyanidin Yield (mg CE/g FW)	
				Grape Seeds	Grape Seed Powder
1	20.24 (−1)	62.86 (−1)	33.92 (+1)	13.17	11.19
2	79.76 (+1)	177.14 (+1)	16.07 (−1)	12.63	9.37
3	79.76 (+1)	62.86 (−1)	16.07 (−1)	10.58	9.97
4	50 (0)	120 (0)	25 (0)	14.84	13.60
5	100 (+1.68)	120 (0)	25 (0)	8.30	4.66
6	50 (0)	120 (0)	25 (0)	14.30	13.92
7	0 (−1.68)	120 (0)	25 (0)	6.81	1.58
8	79.76 (+1)	177.14 (+1)	33.92 (+1)	13.11	11.51
9	20.24 (−1)	177.14 (+1)	16.07 (−1)	9.99	4.84
10	50 (0)	120 (0)	25 (0)	14.65	13.69
11	20.24 (−1)	62.86 (−1)	16.07 (−1)	9.40	7.43
12	50 (0)	120 (0)	25 (0)	14.61	13.94
13	20.24 (−1)	177.14 (+1)	33.92 (+1)	12.56	10.22
14	79.76 (+1)	62.86 (−1)	33.92 (+1)	11.13	10.31
15	50 (0)	120 (0)	25 (0)	14.12	13.70
16	50 (0)	24 (−1.68)	25 (0)	12.41	13.36
17	50 (0)	120 (0)	25 (0)	15.10	13.78
18	50 (0)	216 (+1.68)	25 (0)	15.19	11.95
19	50 (0)	120 (0)	40 (+1.68)	16.40	15.20
20	50 (0)	120 (0)	10.00 (−1.68)	12.13	10.28

Low-axial (−1.68), low (−1), center (0), high (+1), and high-axial (+1.68) levels of the three extraction parameters are indicated in brackets. mg CE/g FW, mg catechin equivalence/g fresh weight.

Table 2.3. Analysis of variance (ANOVA) *p*-values and regression coefficients for the second-order response surface model in terms of the first optimization approach.

Source of Variance/ Terms	Grape Seeds		Grape Seed Powder	
	***p*-Value**	**Regression Coefficient**	***p*-Value**	**Regression Coefficient**
Constant	0.000	14.607	0.000	13.7654
% Ethanol	0.010	0.354	0.000	0.9276
Extraction time	0.000	0.636	0.000	−0.3902
Solvent ratio	0.000	1.066	0.000	1.4569
% Ethanol × % Ethanol	0.000	−2.521	0.000	−3.7419
Extraction time × Extraction time	0.016	−0.312	0.000	−0.3704
Solvent ratio × Solvent ratio	0.201	−0.148	0.000	−0.342
% Ethanol × Extraction time	0.006	0.507	0.000	0.5214
% Ethanol × Solvent ratio	0.001	−0.663	0.000	−0.8329
Extraction time × Solvent ratio	0.301	−0.158	0.000	0.4285
Lack-of-fit	0.299		0.736	

Solvent ratio, solvent:solid ratio (*v:w*).

Table 2.4. Central composite design (CCD) used in the second optimization approach to reduce extraction time and solvent volume and to increase the proanthocyanidin yields from grape seeds.

Run Order	Temperature (°C)	Solvent:Solid Ratio (*v:w*)	Sonication Time (min)	Proanthocyanidin Yield (mg CE/g FW)
1	28.1 (−1)	5.62 (−1)	49.88 (+1)	8.39
2	51.9 (+1)	10.38 (+1)	20.12 (−1)	18.00
3	51.9 (+1)	5.62 (−1)	20.12 (−1)	12.45
4	40 (0)	8 (0)	35 (0)	19.68
5	60 (+1.68)	8 (0)	35 (0)	21.82
6	40 (0)	8 (0)	35 (0)	19.06
7	20 (−1.68)	8 (0)	35 (0)	7.77
8	51.9 (+1)	10.38 (+1)	49.88 (+1)	25.80
9	28.1 (−1)	10.38 (+1)	20.12 (−1)	13.61
10	40 (0)	8 (0)	35 (0)	18.98
11	28.1 (−1)	5.62 (−1)	20.12 (−1)	6.48
12	40 (0)	8 (0)	35 (0)	19.85
13	28.1 (−1)	10.38 (+1)	49.88 (+1)	12.32
14	51.9 (+1)	5.62 (−1)	49.88 (+1)	20.00
15	40 (0)	8 (0)	35 (0)	19.80
16	40 (0)	4 (−1.68)	35 (0)	11.35
17	40 (0)	8 (0)	35 (0)	19.80
18	40 (0)	12 (+1.68)	35 (0)	20.36
19	40 (0)	8 (0)	60 (+1.68)	17.58
20	40 (0)	8 (0)	10 (−1.68)	10.25

Low-axial (−1.68), low (-1), center (0), high (+1), and high-axial (+1.68) levels of the three extraction parameters are indicated in brackets. mg CE/g FW, mg catechin equivalence/g fresh weight.

Table 2.5. Analysis of variance (ANOVA) *p*-values and regression coefficients for the second-order response surface model in terms of the second optimization approach.

Source of Variance	***p*-Value**	**Regression Coefficient**
Constant	0.000	19.528
Temperature	0.000	4.325
Solvent ratio	0.000	2.75
Sonication time	0.000	2.072
Temperature × Temperature	0.000	−1.661
Solvent ratio × Solvent ratio	0.000	−1.287
Sonication time × Sonication time	0.000	−1.971
Temperature × Solvent ratio	0.840	0.038
Temperature × Sonication time	0.000	1.842
Solvent ratio × Sonication time	0.070	−0.37
Lack-of-fit	0.182	

Solvent ratio, solvent:solid ratio (*v:w*).

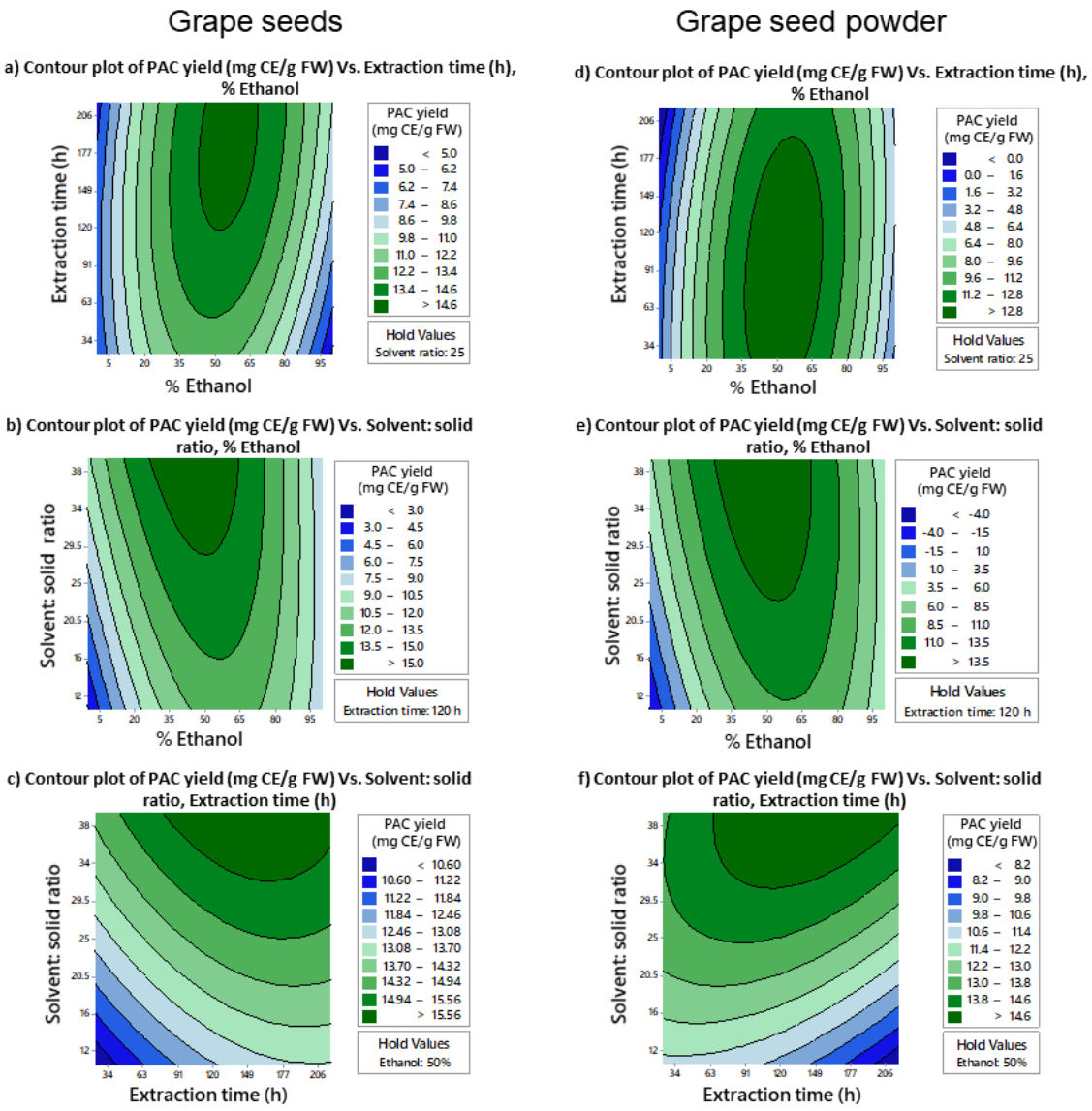

Figure 2.1. Contour plots of PAC yield variation (mg CE/g FW) under different extraction conditions and combinations of optimized parameters in the first optimization approach; % ethanol, solvent:solid ratio (*v:w*), and extraction time (h). Contour plots (a) and (d) describe the variation of PAC yields from grape seeds and grape seed powder, respectively, when % ethanol and extraction time are changed while holding the solvent:solid ratio at 25 (*v:w*). Contour plots (b) and (e) describe the variation of PAC yields under different combinations of % ethanol and solvent:solid ratio for grape seeds and grape seed powder, respectively, while holding extraction time at 120 h. Similarly, contour plots (c) and (f) describe the variation of PAC yields under different extraction times and solvent:solid ratios for grape seeds and grape seed powder, respectively, when % ethanol is held at 50%. mg CE/g FW, mg catechin equivalence/g fresh weight; PAC, proanthocyanidins; *v:w*, volume:weight.

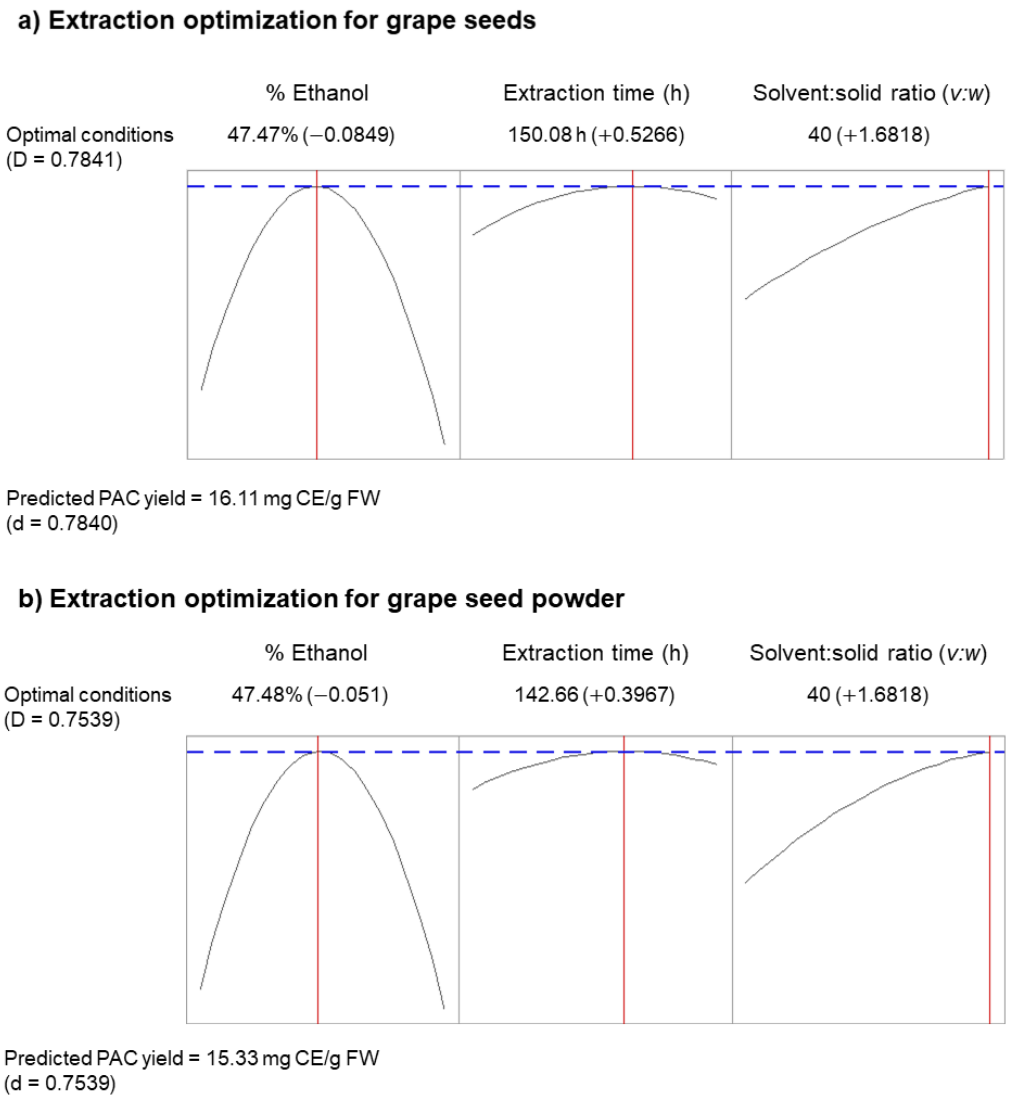

Figure 2.2. Optimization plots to predict maximum PAC yields and determine the optimum conditions to extract PAC from grape seeds (a) and grape seed powder (b). The optimization plots for grape seeds (a) predicted 47.47% ethanol and 150.08 h of extraction time as optimum conditions to extract PAC from grape seeds. The optimum solvent:solid ratio lies beyond the highest solvent:solid ratio (40 *v:w*) used in the experiment. At extraction conditions of 47.47% ethanol, 150.08 h of extraction time, and solvent:solid ratio of 40 (*v:w*), the predicted PAC yield for grape seeds is 16.11 mg CE/g FW. Similarly, the optimization plots for grape seed powder (b) predicted 47.48% ethanol and 142.66 h of extraction time as optimum conditions to extract PAC from grape seed powder. The optimum solvent:solid ratio lies beyond the highest solvent:solid ratio (40 *v:w*) used in the experiment. At extraction conditions of 47.48% ethanol, 142.66 h of extraction time, and solvent:solid ratio of 40 (*v:w*) the predicted PAC yield for grape seed powder is 15.33 mg CE/g FW. mg CE/g FW, mg catechin equivalence/g fresh weight; PAC, proanthocyanidins; *v:w*, volume:weight.

a) Contour plots

i) Contour plot of PAC yield (mg CE/g FW) Vs. Sonication time (min), Temperature (°C)

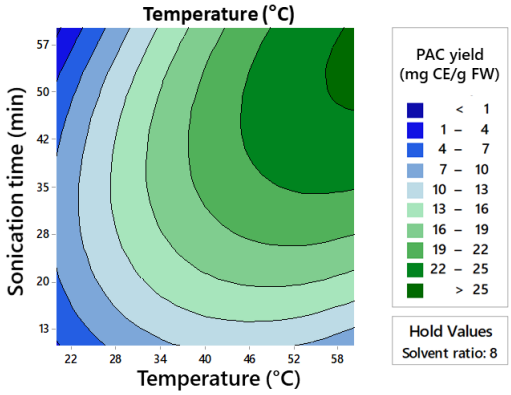

ii) Contour plot of PAC yield (mg CE/g FW) Vs. Solvent: solid ratio, Temperature (°C)

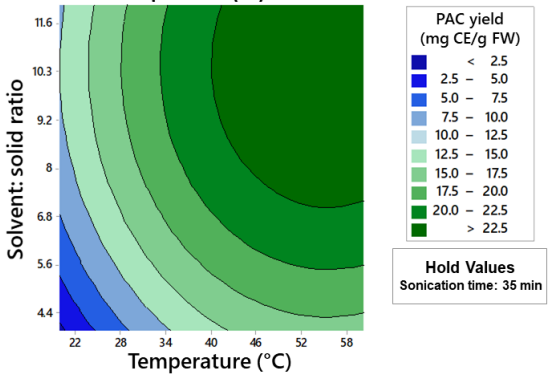

iii) Contour plot of PAC yield (mg CE/g FW) Vs. Sonication time (min), Solvent: solid ratio

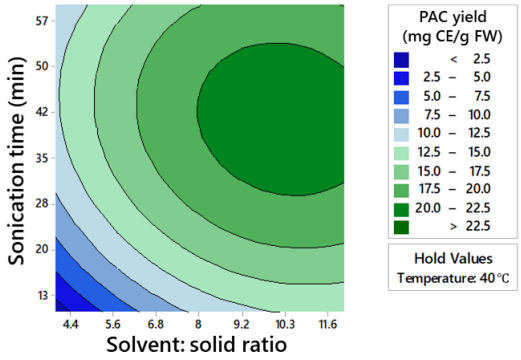

b) Extraction optimization plot

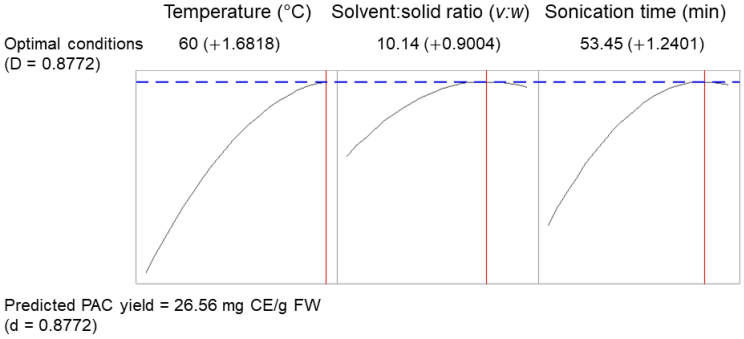

Figure 2.3. Contour plots (a) of PAC yield variation (mg CE/g FW) under different extraction conditions and combinations of optimized parameters in the second optimization approach: extraction temperature (°C), sonication time (min), and solvent:solid ratio (*v:w*); and optimization plots (b) to determine optimum PAC extraction conditions. Contour plot (ai) depicts the variation of PAC yield from grape seeds under different extraction temperatures and sonication time while holding solvent:solid ratio at 8 (*v:w*). Contour plot (aii) depicts the variation of PAC yields from grape seeds under different extraction temperatures and solvent:solid ratios while holding the sonication time at 35 min. Similarly, contour plot (aiii) describes the variation of PAC yields under different solvent:solid ratios and sonication times when extraction temperature is held at 40 °C. The optimization plots (b) predicted the optimum PAC extraction conditions to be 10.14:1 (*v:w*) solvent:solid ratio and 53.45 min sonication time. The optimum extraction temperature lies beyond the highest temperature (60 °C) tested in the study. At extraction conditions of 10.14:1 (*v:w*) solvent:solid ratio, 53.45 min sonication time, and extraction temperature of 60 °C, the predicted PAC yield from grape seeds was 26.56 mg CE/g FW. Ethanol at 47% was used to extract PAC as determined by first optimization approach. mg CE/g FW, mg catechin equivalence/g fresh weight; PAC, proanthocyanidins; *v:w*, volume:weight.

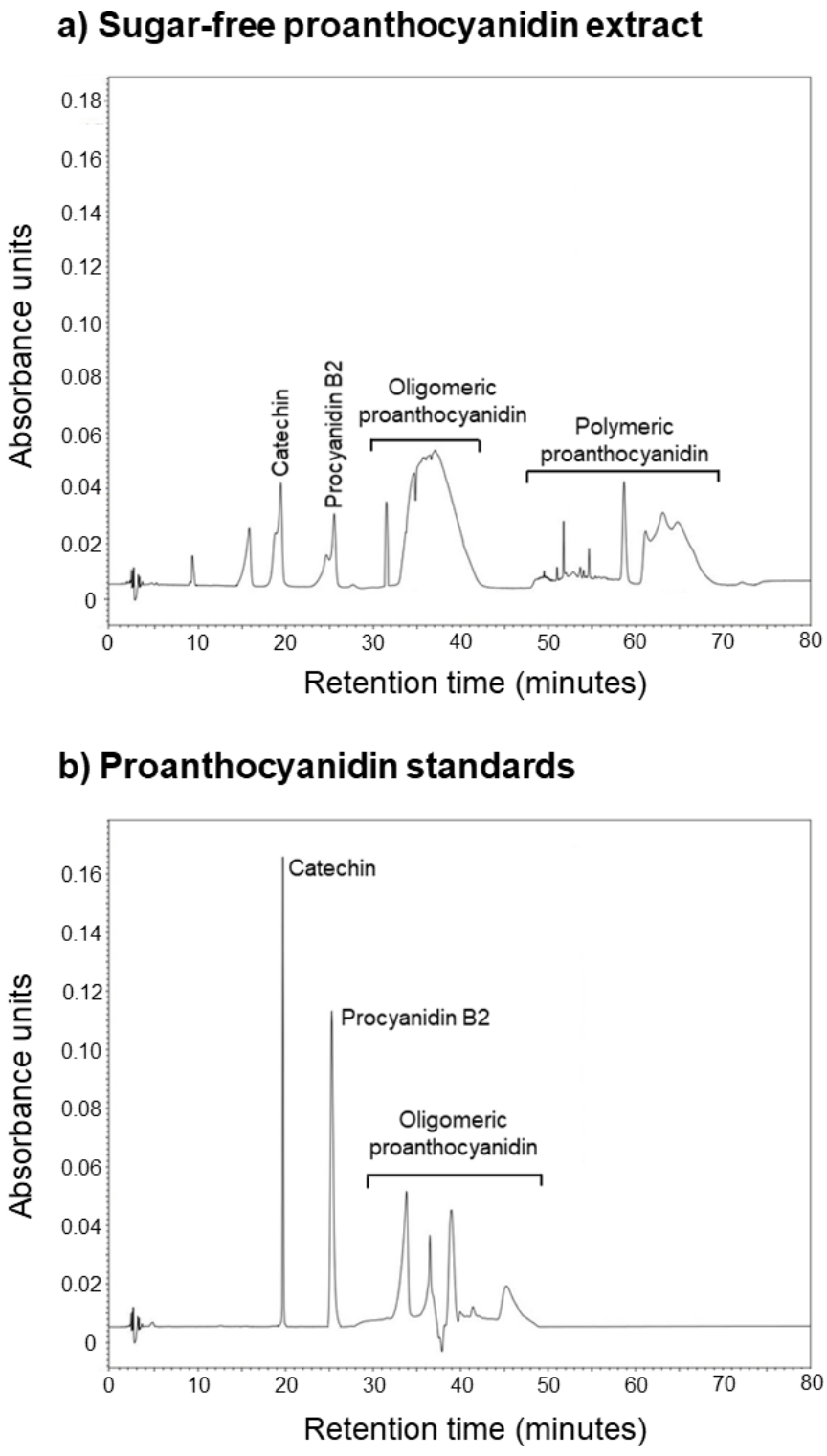

Figure 2.4. HPLC chromatogram of the sugar-free fraction of grape seed PAC (a); and chromatogram of catechin, procyanidin B2, and oligomeric grape seed PAC standard (b). PAC, proanthocyanidins.

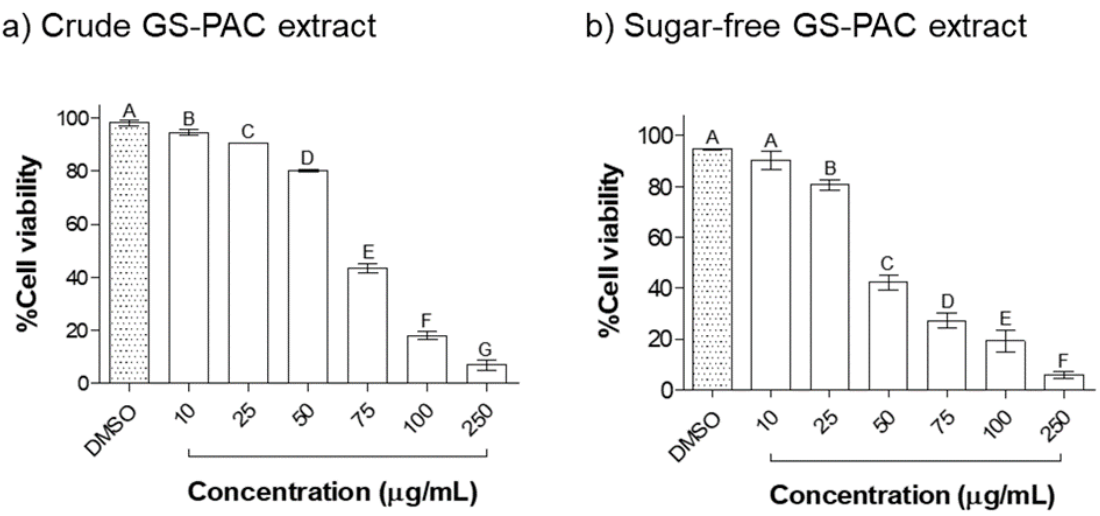

Figure 2.5. Toxicity of crude grape seed PAC (a) and sugar-free grape seed PAC (b) extracts on AML12 mouse liver cells. AML12 cells were treated with different concentrations (10 – 250 µg/mL) of crude and sugar-free extracts of grape seed PAC for 24 h. Cell viability was measured by MTS assay and expressed as % cell viabilities in comparison to the negative control. Results were given as mean ± SD of three independent experiments and means that do not share a similar letter are significantly different ($p \leq 0.01$). DMSO, dimethyl sulfoxide; PAC, proanthocyanidins.

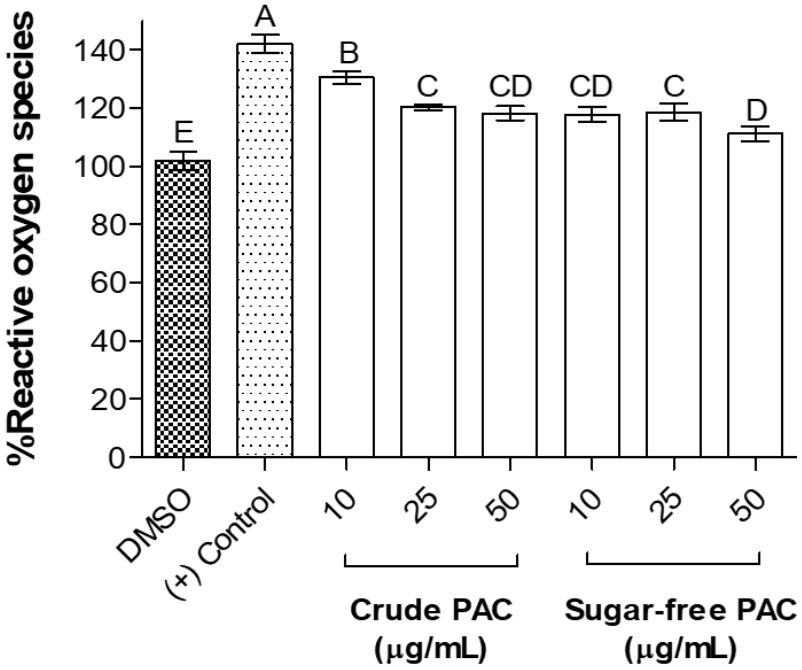

Figure 2.6. Potential of crude and sugar-free grape seed PAC extracts to ameliorate palmitic acid-induced ROS in AML12 mouse liver cells. AML12 cells were pretreated with 10, 25, and 50 μg/mL concentrations of crude and sugar-free grape seed PAC extracts for 24 h and exposed to palmitic acid (200 μM) for 24 h to induce ROS production. Cellular ROS production was measured by DCFDA cellular ROS detection assay and expressed as % ROS compared to negative control. Results were given as the mean ± SD of three independent experiments and means that do not share a similar letter are significantly different ($p \leq 0.01$). DMSO, dimethyl sulfoxide; PAC, proanthocyanidins.

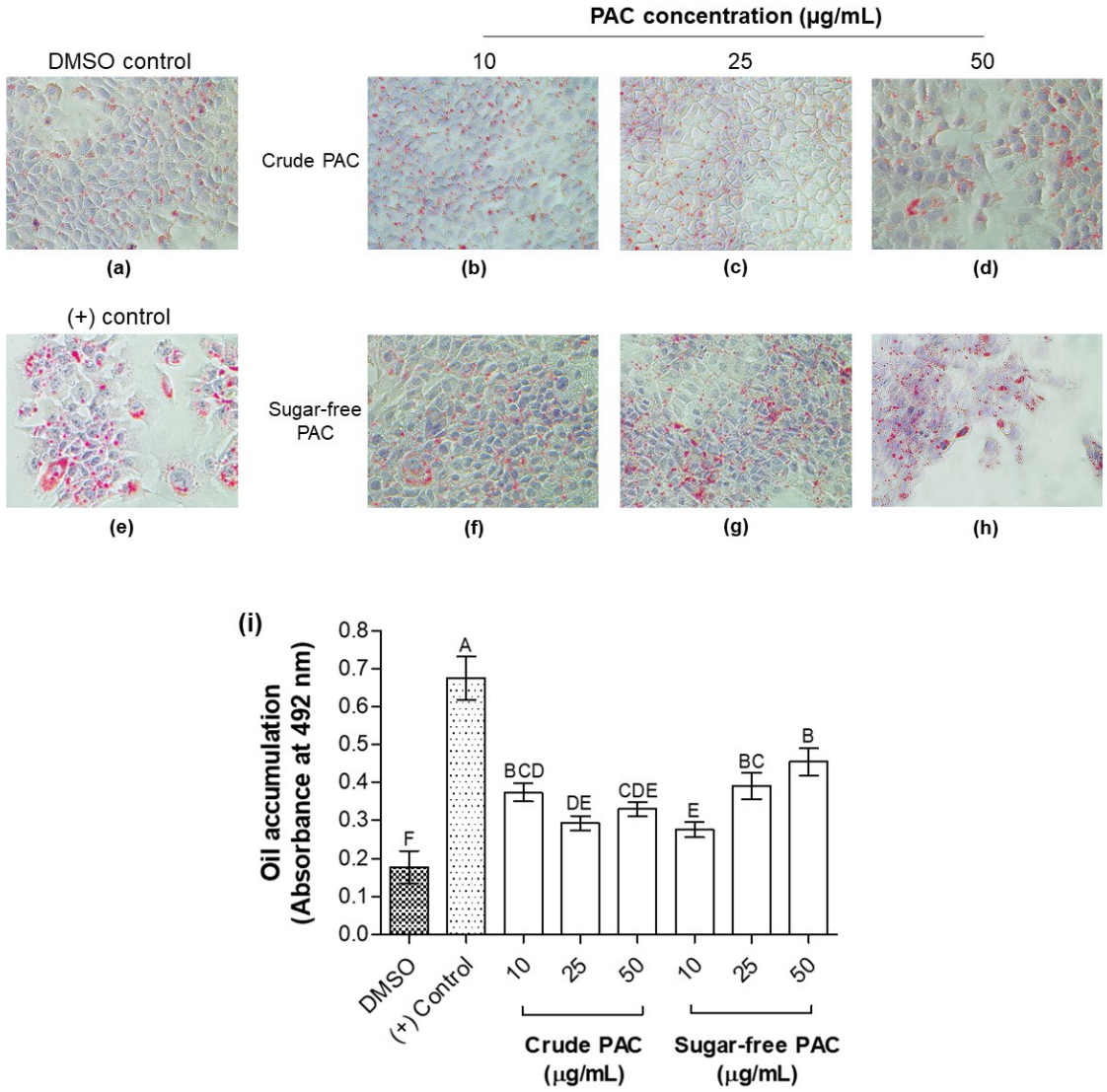

Figure 2.7. The potential of crude and sugar-free grape seed PAC extracts to reduce palmitic acid-induced steatosis in AML 12 cells. AML12 cells were pretreated with 10, 25, and 50 µg/mL concentrations of crude grape seed PAC (b – d) and sugar-free grape seed PAC (f – h) extracts for 24 h and exposed to palmitic acid (200 µM) for 24 h to induce cellular lipid accumulation. Cells were stained with Oil Red O stain and visualized under a microscope (×100) to compare cellular lipid accumulation with vehicle (DMSO) control (a) and positive control (e). After microscopic visualization, Oil Red O stain retained in cells was extracted using 100% isopropanol. Oil Red O stain concentrations in isopropanol extracts were compared by measuring the absorbance at 492 nm as an indirect measurement of cellular lipid accumulation (i). Results were given as mean ± standard deviation of three independent experiments and means that do not share a similar letter are significantly different ($p \leq 0.01$). DMSO, dimethyl sulfoxide; PAC, proanthocyanidins.

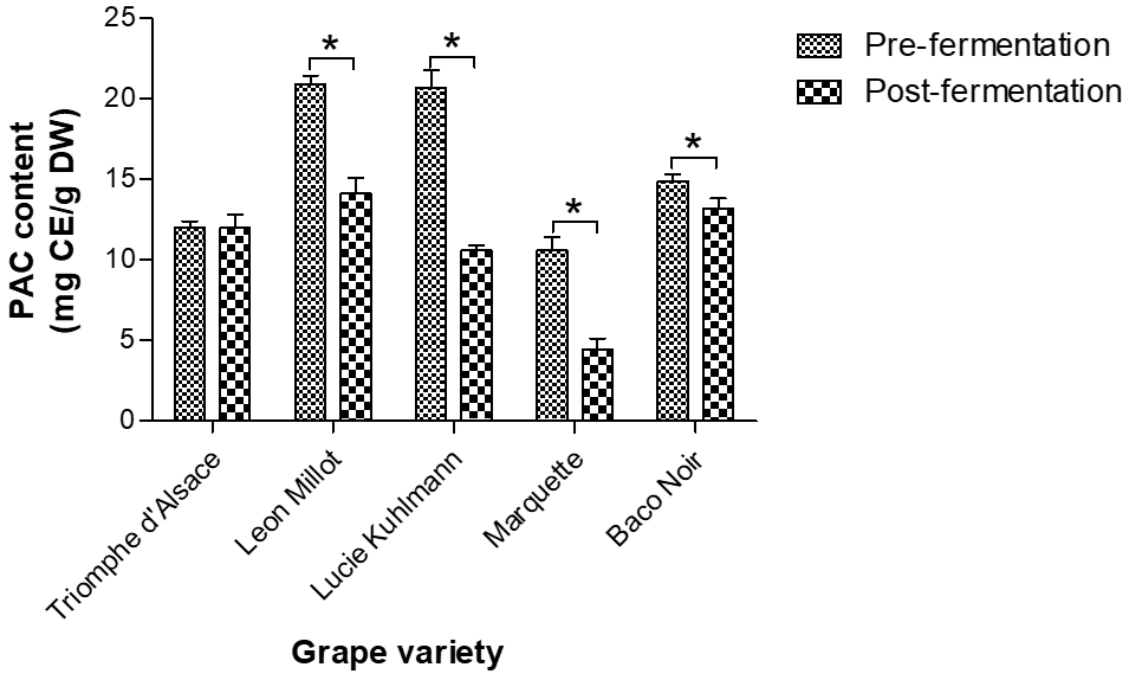

Figure 2.8. The PAC content of grape mashes from five different grape varieties before and after wine fermentation. PAC was extracted from grape mashes pre- and post-fermentation by the optimized method of PAC extraction (47% aqueous ethanol, 60 °C temperature, 10:1 solvent:solid ratio, and 53.45 min sonication time). PAC content of the extracts was measured by the methylcellulose precipitable tannin assay. *Means are significantly different at $p < 0.01$ level. mg CE/g DW, mg catechin equivalence/g dry weight; PAC, proanthocyanidins.

2.7. REFERENCES

Altemimi, A., Lakhssassi, N., Baharlouei, A., Watson, D.G., Lightfoot, D.A., 2017. Phytochemicals: Extraction, isolation, and identification of bioactive compounds from plant extracts. Plants (Basel) 6, 42. https://doi.org/10.3390/plants6040042

Andjelkovi, M.Z., Milenkovi, A.S., Radovanovi, B.C., Radovanovi, A.N., 2014. Optimization of ultrasound-assisted extraction of phenols from seeds of grape pomace. Acta Chimica Slovenica 61, 858–865.

Annegowda, H.V., Bhat, R., Min-Tze, L., Karim, A.A., Mansor, S.M., 2012. Influence of sonication treatments and extraction solvents on the phenolics and antioxidants in star fruits. Journal of Food Science & Technology 49, 510–514. https://doi.org/10.1007/s13197-011-0435-8

Beaver, J.W., Medina-Plaza, C., Miller, K., Dokoozlian, N., Ponangi, R., Blair, T., Block, D., Oberholster, A., 2020. Effects of the temperature and ethanol on the kinetics of proanthocyanidin adsorption in model wine systems. Journal of Agricultural & Food Chemistry 68, 2891–2899. https://doi.org/10.1021/acs.jafc.9b02605

Bozan, B., Altinay, R.C., 2014. Accelerated solvent extraction of flavan-3-ol derivatives from grape seeds. Food Science & Technology Research 20, 409–414. https://doi.org/10.3136/fstr.20.409

Cádiz-Gurrea, M.D.L.L., Borrás-Linares, I., Lozano-Sánchez, J., Joven, J., Fernández-Arroyo, S., Segura-Carretero, A., 2017. Cocoa and grape seed byproducts as a source of antioxidant and anti-inflammatory proanthocyanidins. International Journal of Molecular Sciences 18, 376. https://doi.org/10.3390/ijms18020376

Cao, J., Chen, L., Li, M., Cao, F., Zhao, L., Su, E., 2018. Efficient extraction of proanthocyanidin from Ginkgo biloba leaves employing rationally designed deep eutectic solvent-water mixture and evaluation of the antioxidant activity. Journal of Pharmaceutical and Biomedical Analysis 158, 317–326. https://doi.org/10.1016/j.jpba.2018.06.007

Chen, F., Du, X., Zu, Y., Yang, L., Wang, F., 2016. Microwave-assisted method for distillation and dual extraction in obtaining essential oil, proanthocyanidins and polysaccharides by one-pot process from *Cinnamomi* Cortex. Separation and Purification Technology 164, 1–11. https://doi.org/10.1016/j.seppur.2016.03.018

Chen, J., Thilakarathna, W.P.D.W., Astatkie, T., Rupasinghe, H.P.V., 2020. Optimization of catechin and proanthocyanidin recovery from grape seeds using microwave-assisted extraction. Biomolecules 10, 243. https://doi.org/10.3390/biom10020243

Chen, X.-X., Lam, K.H., Chen, Q.-X., Leung, G.P.-H., Tang, S.C.W., Sze, S.C.-W., Xiao, J.-B., Feng, F., Wang, Y., Zhang, K.Y.-B., Zhang, Z.-J., 2017a. Ficus virens proanthocyanidins induced apoptosis in breast cancer cells concomitantly ameliorated 5-fluorouracil induced intestinal mucositis in rats. Food and Chemical Toxicology 110, 49–61. https://doi.org/10.1016/j.fct.2017.10.017

Chen, X.-X., Leung, G.P.-H., Zhang, Z.-J., Xiao, J.-B., Lao, L.-X., Feng, F., Mak, J.C.-W., Wang, Y., Sze, S.C.-W., Zhang, K.Y.-B., 2017b. Proanthocyanidins from *Uncaria rhynchophylla* induced apoptosis in MDA-MB-231 breast cancer cells while enhancing cytotoxic effects of 5-fluorouracil. Food and Chemical Toxicology 107, 248–260. https://doi.org/10.1016/j.fct.2017.07.012

Chu, M.-J., Du, Y.-M., Liu, X.-M., Yan, N., Wang, F.-Z., Zhang, Z.-F., 2019. Extraction of proanthocyanidins from chinese wild rice (*Zizania latifolia*) and analyses of structural composition and potential bioactivities of different fractions. Molecules 24, 9. https://doi.org/10.3390/molecules24091681

Da Porto, C., Natolino, A., Decorti, D., 2014. Extraction of proanthocyanidins from grape marc by supercritical fluid extraction using CO_2 as solvent and ethanol–water mixture as co-solvent. The Journal of Supercritical Fluids 87, 59–64. https://doi.org/10.1016/j.supflu.2013.12.013

Dailey, A., Vuong, Q.V., 2015. Effect of extraction solvents on recovery of bioactive compounds and antioxidant properties from macadamia (*Macadamia tetraphylla*) skin waste. Cogent Food & Agriculture 1, 1115646. https://doi.org/10.1080/23311932.2015.1115646

Dang, Y.-Y., Zhang, H., Xiu, Z.-L., 2014. Microwave-assisted aqueous two-phase extraction of phenolics from grape (*Vitis vinifera*) seed. Journal of Chemical Technology & Biotechnology 89, 1576–1581. https://doi.org/10.1002/jctb.4241

Downey, M.O., Hanlin, R.L., 2010. Comparison of ethanol and acetone mixtures for extraction of condensed tannin from grape skin. American Journal of Enology & Viticulture 31. https://doi.org/10.21548/31-2-1412

Fernández, K., Vega, M., Aspé, E., 2015. An enzymatic extraction of proanthocyanidins from País grape seeds and skins. Food Chemistry 168, 7–13. https://doi.org/10.1016/j.foodchem.2014.07.021

Fujimaki, T., Mori, S., Horikawa, M., Fukui, Y., 2018. Isolation of proanthocyanidins from red wine, and their inhibitory effects on melanin synthesis in vitro. Food Chemistry 248, 61–69. https://doi.org/10.1016/j.foodchem.2017.12.024

Gu, L., Kelm, M.A., Hammerstone, J.F., Beecher, G., Holden, J., Haytowitz, D., Gebhardt, S., Prior, R.L., 2004. Concentrations of proanthocyanidins in common foods and estimations of normal consumption. The Journal of Nutrition 134, 613–617. https://doi.org/10.1093/jn/134.3.613

Henandez-Jimenez, A., Kennedy, J., Bautista-Ortín, A., Gomez-Plaza, E., 2012. Effect of ethanol on grape seed proanthocyanidin extraction. American Journal of Enology and Viticulture 63, 57–61. https://doi.org/10.5344/ajev.2011.11053

Huh, Y.S., Hong, T.H., Hong, W.H., 2004. Effective extraction of oligomeric proanthocyanidin (OPC) from wild grape seeds. Biotechnology and Bioprocess Engineering 9, 471–475. https://doi.org/10.1007/BF02933488

Jordão, A.M., Gonçalves, F.J., Correia, A.C., Cantão, J., Rivero-Pérez, M.D., SanJosé, M.L.G., 2010. Proanthocyanidin content, antioxidant capacity and scavenger activity of Portuguese sparkling wines (Bairrada Appellation of Origin). Journal of the Science of Food and Agriculture 90, 2144–2152. https://doi.org/10.1002/jsfa.4064

Kalli, E., Lappa, I., Bouchagier, P., Tarantilis, P.A., Skotti, E., 2018. Novel application and industrial exploitation of winery by-products. Bioresources and Bioprocessing 5, 46. https://doi.org/10.1186/s40643-018-0232-6

Kaplum, V., Ramos, A.C., Consolaro, M.E.L., Fernandez, M.A., Ueda-Nakamura, T., Dias-Filho, B.P., Silva, S. de O., de Mello, J.C.P., Nakamura, C.V., 2018. Proanthocyanidin polymer-rich fraction of *Stryphnodendron adstringens* promotes *in vitro* and *in vivo* cancer cell death via oxidative stress. Frontiers in Pharmacology 9, 694. https://doi.org/10.3389/fphar.2018.00694

Khanal, R.C., Howard, L.R., Prior, R.L., 2010. Effect of heating on the stability of grape and blueberry pomace procyanidins and total anthocyanins. Food Research International 43, 1464–1469. https://doi.org/10.1016/j.foodres.2010.04.018

Kim, N.-Y., Jang, M.-K., Lee, D.-G., Yu, K.H., Jang, H., Kim, M., Kim, S.G., Yoo, B.H., Lee, S.-H., 2010. Comparison of methods for proanthocyanidin extraction from pine (*Pinus densiflora*) needles and biological activities of the extracts. Nutrition Research and Practice 4, 16–22. https://doi.org/10.4162/nrp.2010.4.1.16

Kitao, S., Teramoto, M., Matoba, T., 2001. Effect of heat and pH on the radical-scavenging activity of proanthocyanidin-rich extract from grape seeds and production of konjac enriched with proanthocyanidin. Nippon Shokuhin Kagaku Kogaku Kaishi 48, 591–597. https://doi.org/10.3136/nskkk.48.591

Ku, C.S., Mun, S.P., Jang, J., 2011. Effects of water extraction temperatures on the yield, molecular weight, and antioxidant activity of proanthocyanidins extracted from *Pinus radiata* bark. Forest Products Journal 61, 321–325. https://doi.org/10.13073/0015-7473-61.4.321

Kuhnert, S., Lehmann, L., Winterhalter, P., 2015. Rapid characterisation of grape seed extracts by a novel HPLC method on a diol stationary phase. Journal of Functional Foods 15, 225–232. https://doi.org/10.1016/j.jff.2015.03.031

L. Suraweera, T., Rupasinghe, H.P.V., Dellaire, G., Xu, Z., 2020. Regulation of Nrf2/ARE pathway by dietary flavonoids: a friend or foe for cancer management? Antioxidants 9, 973. https://doi.org/10.3390/antiox9100973

Lee, J.-W., Kim, Y.I., Kim, Y., Choi, M., Min, S., Joo, Y.H., Yim, S.-V., Chung, N., 2017. Grape seed proanthocyanidin inhibits inflammatory responses in hepatic stellate cells by modulating the MAPK, Akt and NF-κB signaling pathways. International Journal of Molecular Medicine 40, 226–234. https://doi.org/10.3892/ijmm.2017.2997

Lincheva, V.B., Petkova, N.T., Ivanov, I.G., 2017. Optimization of biologically active substances extraction process from *Potentilla reptans* L. aerial parts. Journal of Applied Pharmaceutical Science 7, 174–179. https://doi.org/10.7324/JAPS.2017.70224

Liu, M., Yun, P., Hu, Y., Yang, J., Khadka, R.B., Peng, X., 2020. Effects of grape seed proanthocyanidin extract on obesity. The European Journal of Obesity 1–13. https://doi.org/10.1159/000502235

Liu, S., 2012. Extraction and Characterization of Proanthocyanidins from Grape Seeds. TOFSJ 6, 5–11. https://doi.org/10.2174/1874256401206010005

Ma, Z.F., Zhang, H., 2017. phytochemical constituents, health benefits, and industrial applications of grape seeds: A mini-review. Antioxidants 6, 71. https://doi.org/10.3390/antiox6030071

Mercurio, M.D., Dambergs, R.G., Herderich, M.J., Smith, P.A., 2007. High throughput analysis of red wine and grape phenolics-adaptation and validation of methyl cellulose precipitable tannin assay and modified Somers color assay to a rapid 96 well plate format. Journal of Agricultural and Food Chemistry 55, 4651–4657. https://doi.org/10.1021/jf063674n

Morissette, A., Kropp, C., Songpadith, J.-P., Junges Moreira, R., Costa, J., Mariné Casadó, R., Pilon, G., Varin, T.V., Dudonné, S., Boutekrabt, L., St-Pierre, P., Levy, E., Roy, D., Desjardins, Y., Raymond, F., Houde, V.P., Marette, A., 2020. Blueberry proanthocyanidins and anthocyanins improve metabolic health through a gut microbiota-dependent mechanism in diet-induced obese mice. American Journal of Physiology-Endocrinology and Metabolism. https://doi.org/10.1152/ajpendo.00560.2019

Muñoz-Labrador, A., Prodanov, M., Villamiel, M., 2019. Effects of high intensity ultrasound on disaggregation of a macromolecular procyanidin-rich fraction from *Vitis vinifera* L. seed extract and evaluation of its antioxidant activity. Ultrasonics Sonochemistry 50, 74–81. https://doi.org/10.1016/j.ultsonch.2018.08.030

Ngo, T.V., Scarlett, C.J., Bowyer, M.C., Ngo, P.D., Vuong, Q.V., 2017. Impact of Different Extraction Solvents on Bioactive Compounds and Antioxidant Capacity from the Root of *Salacia chinensis* L.. Journal of Food Quality 2017, 9305047. https://doi.org/10.1155/2017/9305047

Nunes, M.A., Pimentel, F., Costa, A.S.G., Alves, R.C., Oliveira, M.B.P.P., 2016. Cardioprotective properties of grape seed proanthocyanidins: An update. Trends in Food Science & Technology 57, 31–39. https://doi.org/10.1016/j.tifs.2016.08.017

Ou, K., Gu, L., 2014. Absorption and metabolism of proanthocyanidins. Journal of Functional Foods 7, 43–53. https://doi.org/10.1016/j.jff.2013.08.004

Ran, L., Yang, C., Xu, M., Yi, Z., Ren, D., Yi, L., 2019. Enhanced aqueous two-phase extraction of proanthocyanidins from grape seeds by using ionic liquids as adjuvants. Separation and Purification Technology 226, 154–161. https://doi.org/10.1016/j.seppur.2019.05.089

Ranjha, M.M.A.N., Irfan, S., Lorenzo, J.M., Shafique, B., Kanwal, R., Pateiro, M., Arshad, R.N., Wang, L., Nayik, G.A., Roobab, U., Aadil, R.M., 2021. Sonication, a potential technique for extraction of phytoconstituents: A Systematic Review. Processes 9, 1406. https://doi.org/10.3390/pr9081406

Rauf, A., Imran, M., Abu-Izneid, T., Iahtisham-Ul-Haq, Patel, S., Pan, X., Naz, S., Sanches Silva, A., Saeed, F., Rasul Suleria, H.A., 2019. Proanthocyanidins: A comprehensive review. Biomedicine & Pharmacotherapy 116, 108999. https://doi.org/10.1016/j.biopha.2019.108999

Ravindranathan, P., Pasham, D., Balaji, U., Cardenas, J., Gu, J., Toden, S., Goel, A., 2018. Mechanistic insights into anticancer properties of oligomeric proanthocyanidins from grape seeds in colorectal cancer. Carcinogenesis 39, 767–777. https://doi.org/10.1093/carcin/bgy034

Reiniers, M.J., van Golen, R.F., van Gulik, T.M., Heger, M., 2014. Reactive oxygen and nitrogen species in steatotic hepatocytes: A molecular perspective on the pathophysiology of ischemia-reperfusion injury in the fatty liver. Antioxidant & Redox Signaling 21, 1119–1142. https://doi.org/10.1089/ars.2013.5486

Rodríguez-Pérez, C., García-Villanova, B., Guerra-Hernández, E., Verardo, V., 2019. Grape seeds proanthocyanidins: An overview of in vivo bioactivity in animal models. Nutrients 11, 2435. https://doi.org/10.3390/nu11102435

Rupasinghe, H.P.V., Parmar, I., Neir, S.V., 2019. Biotransformation of cranberry proanthocyanidins to probiotic metabolites by lactobacillus rhamnosus enhances their anticancer activity in HepG2 cells *in vitro*. Oxidative Medicine & Cell Longevity 2019, 4750795. https://doi.org/10.1155/2019/4750795

Sica, V.P., Mahony, C., Baker, T.R., 2018. Multi-detector characterization of grape seed extract to enable in silico safety assessment. Frontiers in Chemistry 6, 334. https://doi.org/10.3389/fchem.2018.00334

Smeriglio, A., Barreca, D., Bellocco, E., Trombetta, D., 2017. Proanthocyanidins and hydrolysable tannins: occurrence, dietary intake and pharmacological effects. British Journal of Pharmacology 174, 1244–1262. https://doi.org/10.1111/bph.13630

Su, H., Li, Y., Hu, D., Xie, L., Ke, H., Zheng, X., Chen, W., 2018. Procyanidin B2 ameliorates free fatty acids-induced hepatic steatosis through regulating TFEB-mediated lysosomal pathway and redox state. Free Radical Biology and Medicine 126, 269–286. https://doi.org/10.1016/j.freeradbiomed.2018.08.024

Sun, B.S., Pinto, T., Leandro, M.C., Ricardo-Da-Silva, J.M., Spranger, M.I., 1999. Transfer of catechins and proanthocyanidins from solid parts of the grape cluster into wine. American Journal of Enology Viticulture. 50, 179–184. https:// 10.5344/ajev.1999.50.2.179

Suo, H., Tian, R., Li, J., Zhang, S., Cui, Y., Li, L., Sun, B., 2019. Compositional characterization study on high-molecular-mass polymeric polyphenols in red wines by chemical degradation. Food Research International 123, 440–449. https://doi.org/10.1016/j.foodres.2019.04.056

Symma, N., Hensel, A., 2021. Advanced analysis of oligomeric proanthocyanidins: latest approaches in liquid chromatography and mass spectrometry based analysis. Phytochemistry Review. https://doi.org/10.1007/s11101-021-09764-2

Thilakarathna, W.P.D.W., Rupasinghe, H.P.V., 2019. Microbial metabolites of proanthocyanidins reduce chemical carcinogen-induced DNA damage in human lung epithelial and fetal hepatic cells *in vitro*. Food and Chemical Toxicology 125, 479–493. https://doi.org/10.1016/j.fct.2019.02.010

Thilakarathna, W.P.D.W., Langille, M.G.I., Rupasinghe, H.P.V., 2018. Polyphenol-based prebiotics and synbiotics: potential for cancer chemoprevention. Current Opinion in Food Science 20, 51–57. https://doi.org/10.1016/j.cofs.2018.02.011

Torres-Acosta, M.A., Mayolo-Deloisa, K., González-Valdez, J., Rito-Palomares, M., 2019. Aqueous two-phase systems at large scale: Challenges and opportunities. Biotechnology Journal 14, 1800117. https://doi.org/10.1002/biot.201800117

Unusan, N., 2020. Proanthocyanidins in grape seeds: An updated review of their health benefits and potential uses in the food industry. Journal of Functional Foods 67, 103861. https://doi.org/10.1016/j.jff.2020.103861

Wang, L., Huang, W., Zhan, J., 2019. Grape seed proanthocyanidins induce autophagy and modulate survivin in HepG2 cells and inhibit xenograft tumor growth *in vivo*. Nutrients 11, 2983. https://doi.org/10.3390/nu11122983

Yan, Z., Zhang, H., Dzah, C.S., Zhang, J., Diao, C., Ma, H., Duan, Y., 2020. Subcritical water extraction, identification, antioxidant and antiproliferative activity of polyphenols from lotus seedpod. Separation and Purification Technology 236, 116217. https://doi.org/10.1016/j.seppur.2019.116217

Yang, L., Xian, D., Xiong, X., Lai, R., Song, J., Zhong, J., 2018. Proanthocyanidins against oxidative stress: From molecular mechanisms to clinical applications. BioMed Research International. https://doi.org/10.1155/2018/8584136

Yang, N., Gao, J., Cheng, X., Hou, C., Yang, Y., Qiu, Y., Xu, M., Zhang, Y., Huang, S., 2017. Grape seed proanthocyanidins inhibit the proliferation, migration and invasion of tongue squamous cell carcinoma cells through suppressing the protein kinase B/nuclear factor-κB signaling pathway. International Journal of Molecular Medicine 40, 1881–1888. https://doi.org/10.3892/ijmm.2017.3162

Yogalakshmi, B., Sreeja, S., Geetha, R., Radika, M.K., Anuradha, C.V., 2013. Grape seed proanthocyanidin rescues rats from steatosis: A comparative and combination study with metformin. journal of lipids 2013, 153897. https://doi.org/10.1155/2013/153897

Zeng, X., Zhu, M., Liu, X., Chen, X., Yuan, Y., Li, L., Liu, J., Lu, Y., Cheng, J., Chen, Y., 2020. Oleic acid ameliorates palmitic acid induced hepatocellular lipotoxicity by inhibition of ER stress and pyroptosis. Nutrition & Metabolism 17, 11. https://doi.org/10.1186/s12986-020-0434-8

Zhang, J., Huang, Y., Shao, H., Bi, Q., Chen, J., Ye, Z., 2017. Grape seed procyanidin B2 inhibits adipogenesis of 3T3-L1 cells by targeting peroxisome proliferator-activated receptor γ with miR-483-5p involved mechanism. Biomedicine & Pharmacotherapy 86, 292–296. https://doi.org/10.1016/j.biopha.2016.12.019

Zhang, Y., Chen, S., Wei, C., Rankin, G.O., Rojanasakul, Y., Ren, N., Ye, X., Chen, Y.C., 2018. Dietary compound proanthocyanidins from Chinese bayberry (*Myrica rubra* Sieb. et Zucc.) leaves inhibit angiogenesis and regulate cell cycle of cisplatin-resistant ovarian cancer cells via targeting Akt pathway. Journal of Functional Foods 40, 573–581. https://doi.org/10.1016/j.jff.2017.11.045

Zhao, M., Bai, J., Bu, X., Tang, Y., Han, W., Li, D., Wang, L., Yang, Y., Xu, Y., 2021. Microwave-assisted aqueous two-phase extraction of phenolic compounds from *Ribes nigrum* L. and its antibacterial effect on foodborne pathogens. Food Control 119, 107449. https://doi.org/10.1016/j.foodcont.2020.107449

Zhou, X., Chen, S., Ye, X., 2017. The anti-obesity properties of the proanthocyanidin extract from the leaves of Chinese bayberry (*Myrica rubra* Sieb.et Zucc.). Food & Function Journal, 8, 3259–3270. https://doi.org/10.1039/C7FO00816C

CHAPTER 3. BIOTRANSFORMATION OF POLYMERIC PROANTHOCYANIDINS BY USING PROBIOTIC BACTERIA IN C57BL/6 MICE.

The data presented in this chapter have been published in a peer-reviewed article.

Thilakarathna, W.P.D.W., Langille, M.G.I., Rupasinghe H.P.V., 2023. Hepatotoxicity of polymeric proanthocyanidins is caused by translocation of bacterial lipopolysaccharides through impaired gut epithelium. Toxicology Letters 379 (2023), 35 – 47. https://doi.org/10.1016/j.toxlet.2023.03.005

Author contributions: W.P.D.W. Thilakarathna performed all the experiments, analyzed the data, and drafted the manuscript. H.P. Vasantha Rupasinghe, the principal investigator, acquired the funds and resources, supervised the project, and reviewed the manuscript. All authors have made intellectual contributions to the manuscript. All authors have read and approved the final manuscript.

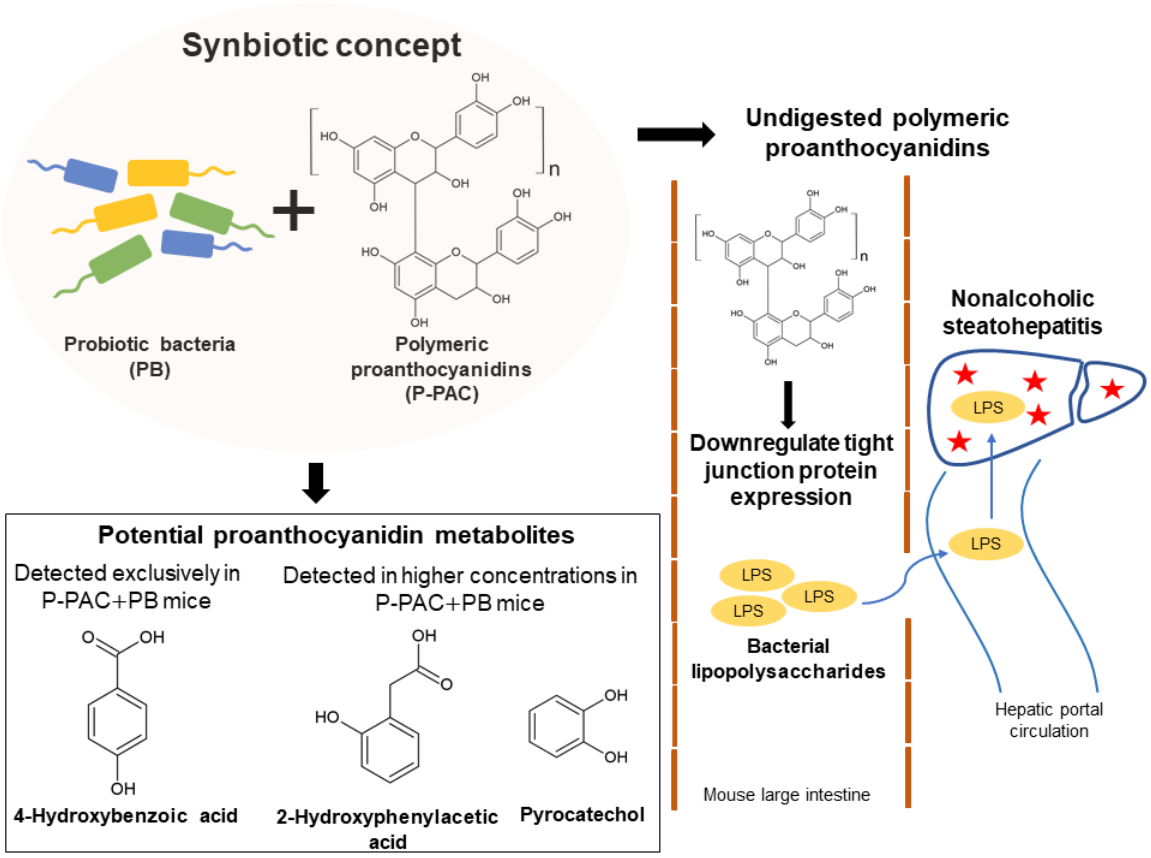

Chapter 3. Graphical abstract

3.1. ABSTRACT

Polymeric proanthocyanidins (P-PAC) induced hepatotoxicity in C57BL/6 mice. Mice were supplemented with P-PAC alone or with a mixture of probiotic bacteria (PB), *Lactobacillus*, *Bifidobacterium,* and *Akkermansia muciniphila* for 14 consecutive days. The liver tissues of sacrificed mice were analyzed by mass spectrometry to identify and quantify the P-PAC metabolites. Potential P-PAC metabolites, 2-hydroxyphenylacetic acid and pyrocatechol were detected in higher concentrations and 4-hydroxybenzoic acid was detected exclusively in the mice supplemented with P-PAC and PB. Supplementation with P-PAC alone or with PB caused no shift in the α-diversity of mice gut microbiota. P-PAC induced nonalcoholic steatohepatitis in mice through increasing liver exposure to intestinal bacterial lipopolysaccharides by reducing expression of gut epithelial tight junction proteins, claudin-3 and occludin. Lipopolysaccharide concentrations in the livers of mice supplemented with P-PAC were significantly high compared to the control mice. Furthermore, P-PAC downregulated the expressions of claudin-3 and claudin-4 tight junction proteins in cultured Caco-2 cell monolayers. PB biotransformed P-PAC into bioavailable metabolites and potentially reduced the toxicity of P-PAC. The toxicity of P-PAC and their synbiotics need to be critically evaluated for the safety of human consumption.

Keywords: Flavonoids, nonalcoholic steatohepatitis, condensed tannins, probiotic bacteria, liver, toxicity mechanisms

3.2. INTRODUCTION

Proanthocyanidins (PAC) are the oligomers or polymers of flavan-3-ols, especially catechin and epicatechin. A significant proportion of dietary polyphenols are made by PAC (Gu et al., 2004). PAC are ubiquitously present in plant foods including, cereals, nuts, fruits, vegetables, and their products (Tao et al., 2019). PAC depicts excellent antioxidant, immunomodulatory, anticancer, cardioprotective, antidiabetic, and neuroprotective activities that can substantially improve human health (Rauf et al., 2019). Low absorption of PAC molecules larger than tetramers by the small intestine limits the health benefits of PAC (Ou and Gu, 2014). The majority of PAC in commonly consumed food is polymeric and comprised of over 10 monomer units (Gu et al., 2004). Thus, the bioavailability of oligomeric PAC (O-PAC) and polymeric PAC (P-PAC) depends on their degradation by the colonic microbiota. PAC that is not absorbed in the small intestine can be bioconverted into simple and easily absorbable metabolites by colonic microbiota (Sallam et al., 2021). PAC are predominantly bioconverted into phenolic acids and phenyl-valerolactones (Ou and Gu, 2014) that may possess beneficial physiological functions (Thilakarathna and Rupasinghe, 2019). However, microbial metabolites of O-PAC and P-PAC remain largely unknown.

The health benefits of O-PAC and P-PAC consumption depend on the biotransformation governed by gut microbiota (Cires et al., 2017). The gut microbiota must consist of bacterial species potent in biotransforming PAC into beneficial metabolites to obtain the health benefits of O-PAC and P-PAC. However, the composition of gut microbiota greatly varies among individuals depending on genetics, diet, and medication (Wen and Duffy, 2017). Therefore, the diversity of PAC metabolites can vary among

individuals. This hurdle can be overcome by using the concept of synbiotics, a mixture of probiotic bacteria and PAC. For instance, *Lactobacillus rhamnosus*, a commonly used probiotic bacteria can depolymerize cranberry PAC into monomeric catechin and epicatechin while generating 4-hydroxyphenylacetic and 3-(4-hydroxyphenyl)propionic acids *in vitro* (Rupasinghe et al., 2019). However, there is a knowledge gap on the biotransformation of PAC using probiotic bacteria *in vivo* and the physiological effects of PAC-based synbiotics.

The aim of this study was to investigate the ability of probiotic bacteria to biotransform P-PAC into bioavailable metabolites and evaluate the physiological effects using a C57BL/6 mouse model. P-PAC required for this study was extracted from grape seed powder (GSP). Grape seeds are an underutilized by-product of wine and grape juice processing, and an excellent source of PAC (Thilakarathna and Rupasinghe, 2022). Mice were supplemented with grape seed P-PAC with and without probiotic bacteria to identify P-PAC metabolite. A mixture of common probiotic bacteria consisting of *Lactobacillus* and *Bifidobacterium* probiotic bacteria (LBPB), and a novel probiotic *Akkermansia muciniphila* (AM) was used to biotransform the P-PAC *in vivo*. The effects of P-PAC and probiotic bacteria supplementation on the natural mouse gut microbiota were investigated. Also, the toxicity of this supplementation on mouse liver was investigated in detail.

3.3. MATERIALS AND METHODS

3.3.1. Extraction of PAC from GSP and fractionation by flash chromatography

O-PAC (3.41 mean degree of polymerization, MDP) and P-PAC (15.1 MDP) were isolated from GSP by an acetone-based extraction and flash chromatography (Rupasinghe et al., 2019). GSP used in this study was provided by the Royal Grapeseed, Milton, NY, USA. The GSP was from a mixture of commercial grape varieties; *Vitis (V). vinifera*, *V. labrusca*, and hybrids of native American species with *V. vinifera*. Initially, lipids and waxes were removed from GSP by using hexane. Crude PAC was extracted from GSP by using extraction solvent, acetone and formic acid in deionized (DI) water (70%, 0.1%, and 29.9% *v:v:v,* respectively). The crude PAC was purified and fractionated by using a flash chromatography column loaded with brominated styrenic adsorbent beads. The column was washed with DI water to remove sugars and simple phenolic acids, 80% aqueous ethanol to elute O-PAC, and 70% aqueous acetone to elute P-PAC. The ethanol and acetone fractions were collected separately, and rotary evaporated at 37 ^{o}C until ethanol and acetone were completely removed. The final PAC-rich GSP extracts were freeze-dried to remove water and chemical solvent residues (Rupasinghe et al., 2019).

3.3.2. Quantification and characterization of PAC in purified GSP extracts

PAC concentrations of the purified GSP extracts were quantified by the methylcellulose precipitable tannins assay modified to high throughput 96-well format (Mercurio et al., 2007). PAC concentrations in GSP extracts were calculated using the catechin standard curve and the results were expressed in mg catechin equivalence (CE)/g dry sample.

Extracted PAC was characterized by the degradation of PAC molecules into monomers through phloroglucinolysis, a method described by Kennedy and Jones (2001) (Kennedy and Jones, 2001) and improved for ultra-high performance liquid chromatography (UHPLC)-electrospray ionization (ESI)-mass spectrometry (MS) (Arapitsas et al., 2021). Briefly, 100 µL of the PAC extracts dissolved in 50% aqueous methanol (5 mg/mL) was reacted with 100 µL of the phloroglucinol working solution (0.1 g/mL phloroglucinol and 0.02 g/mL ascorbic acid in 0.2 N HCl acidified methanol) at 50 °C. After 20 min, phloroglucinolysis reaction was stopped by adding 1 mL of 40 mM aqueous sodium acetate. Control samples were made to quantify the free PAC monomers in PAC extracts before phloroglucinolysis. Prepared samples were analyzed for PAC monomers, (epi)catechin, (epi)gallocatechin, (epi)catechin gallate, (epi)gallocatechin gallate, and their phloroglucinol adducts by UHPLC-ESI-MS (Supplementary Fig. S3.1) (Rupasinghe et al., 2019) and MDP of PAC extracts were calculated (Arapitsas et al., 2021). The galloylation of PAC in extracts was determined by calculating the total percentage (%) of galloylated PAC monomers and phloroglucinol adducts.

3.3.3. Mouse study to evaluate biotransformation of P-PAC by probiotic bacteria

The experiment protocol (19-009) was approved by the University Committee on Laboratory Animals of Dalhousie University, Halifax, NS, Canada. Initially, 15 male C57BL/6 mice (49 – 56 days old) were acclimatized to standard housing conditions, with a 12 h dark/12 h light cycle for one week. Mice were individually caged with access to water and chow *ad libitum*. Mice were randomly assigned into three groups (Fig. 3.1): mice supplemented with P-PAC (P-PAC group), mice supplemented with both P-PAC and probiotic bacteria (P-PAC+PB group), and mice receiving only chow diet (control group).

The probiotic bacteria used in this study was a lyophilized mixture of commonly used LBPB comprised of *Lactobacillus* (*L*). *acidophilus* (LA-1), *L. rhamnosus* (LR-32), *L. salivarius* (LS-33), *L. plantarum* (LP-115), *L. casei* (LC-11), *L. lactis* (LL-23), *Bifidobacterium* (*B*). *breve* (BB-03), *B. infantis* (Bi-26), *B. longum* (BL-05), *B. bifidum* (Bb-06), and *B. lactis* (BL-04). A novel emerging probiotic bacterium, *Akkermansia muciniphila* (AM), was also included in the probiotic mixture. The LBPB mixture (11-strain probiotic powder) was donated by Custom Probiotics Inc., Glendale, CA, USA. AM (BAA-835) was purchased from ATCC®, Manassas, VA, USA. Each mice group consisted of five mice. Feces were collected from the P-PAC+PB mice group to evaluate the initial gut microbiota composition. Mice were transferred individually into sterile cages and the feces were collected quickly after defecation. Feces samples were stored at −80 °C until analyzed by 16S rRNA sequencing methodology. A mice group supplemented only with probiotic bacteria was not included in the study for comparison, considering the 3R principle (Replacement, Reduction, and Refinement) of animal ethics.

The P-PAC+PB group was supplemented with probiotic bacteria continuously for seven days (Fig. 3.1). The PAC and control groups were fed with normal chow during this time. Then, P-PAC+PB group was fed the normal chow diet for 3 days. This 3-day interval is important to evaluate the ability of probiotic bacteria to colonize the mouse gut. Feces samples were collected from P-PAC+PB group on the day-7 and day-10 to analyze the gut microbiota. P-PAC and control groups were also fed the normal chow diet during these three days. After the supplementation interval, P-PAC+PB group was supplemented with both P-PAC and probiotic bacteria for 14 consecutive days. P-PAC group was supplemented with P-PAC and the control group was fed with normal chow diet for 14

days. The dosage of P-PAC used in this study was 200 mg/kg body weight/day. The dosage of probiotic bacteria; LBPB and AM used in this study was 1×10^9 and 1×10^8 colony-forming units/day, respectively. At the end of the mouse study, feces were collected from the mice of all three groups to analyze the differences in gut microbiota between three mice groups. Mice were anesthetized by isoflurane and blood was collected by cardiac puncture. Mice were euthanized by cervical dislocation to harvest livers and large intestines. Harvested livers and large intestines were snapped freeze using liquid nitrogen and stored at −80 ºC until the analysis for P-PAC metabolites by high-resolution mass spectrometry (HRMS) and UHPLC-ESI-MS.

3.3.4. Identification of probiotics-derived P-PAC metabolites

Mouse blood and liver tissues were tested for the availability of PAC metabolites. PAC metabolites in blood and liver tissues were extracted into acetonitrile-acetone solution (80/20 *v:v*) (Fernando et al., 2020) and concentrated by nitrogen evaporation on ice. Concentrated samples were reconstituted with methanol and analyzed by HRMS to identify P-PAC metabolites. Analysis for P-PAC metabolites was conducted by non-targeted scanning mode and data were analyzed by Skyline software version 21.2.0.396 (MacCoss Lab, Department of Genome Sciences, University of Washington, Seattle, WA, USA) to detect the presence of expected PAC metabolites (Supplementary Table S3.1). The HRMS analysis was unable to detect expected PAC metabolites in mouse blood serum. However, analysis of liver tissues suggested the presence of 2- or 4-hydroxyphenylacetic acid, 4-hydroxybenzoic acid, *ρ*-coumaric acid, dihydroferulic acid, dihydroferulic acid-4-*O*-*β*-D-glucuronide, fumaric acid, pyrocatechol, pyrogallol, and syringic acid. Liver tissue samples were further analyzed by UHPLC-ESI-MS to confirm the presence of these metabolites in

mice livers by comparing retention times with analytical standards (Rupasinghe et al., 2019). Concentrations of the detected PAC metabolites were calculated by using the calibration curves of analytical standards.

3.3.5. Analysis of the composition of mouse gut microbiota

Effects of P-PAC and probiotics supplementation on the mouse gut microbiota was studied by the 16S rRNA sequencing technology. Bacterial DNA was extracted and purified from the feces samples collected during the mouse study by using QIAmp 96 PowerFecal QIAcube HT (51531, QIAGEN, Toronto, ON, Canada) commercial microbial DNA extraction kit according to the instructions given by the manufacturer. The V4 – V5 region of the extracted microbial DNA was amplified by polymerase chain reaction by using 16S rRNA gene V4 – V5 fusion primers (515FB – 926R) and high-fidelity Phusion polymerase enzyme. Amplified V4 – V5 region was sequenced by Illumina MiSeq to produce 300 base pair paired-end reads. Raw DNA sequencing data were analyzed by Qiime 2 (version 2020.8) microbiome bioinformatics software (Caporaso et al., 2010). Rarefaction curves for α-diversity matrices, Shannon index, observed operational taxonomical units (OTUs), Faith's phylogenetic diversity (PD), and Pielou's evenness were generated. The relative taxonomical abundances across samples were determined, and the diversity metrics together with AM relative frequency were calculated by the Qiime 2 software (Comeau et al., 2017).

2.3.6. Alanine aminotransferase and aspartate aminotransferase activities in mouse blood serum

The alanine aminotransferase (ALT) and aspartate aminotransferase (AST) activities in mouse blood serum were measured as markers of liver damage by using ALT

Colorimetric Activity (700260) and AST Colorimetric Activity (701640) Assay kits by Cayman Chemical (Ann Arbor, MI, USA). ALT and AST activities of the mouse blood serum were measured by performing the assays as per the instructions given by the manufacturer.

3.3.7. Hematoxylin and eosin (H&E) staining of the mouse liver tissues

To analyze the effects of P-PAC and probiotics supplementation on mouse liver, morphology of liver tissues was studied by H&E staining. Briefly, liver tissue sections were fixed in 4% formalin (over 24 h), dehydrated using aqueous ethanol (a series of 70 – 100 %), cleared by xylene, and embedded in paraffin. Tissues embedded in paraffin were cut into sections of 5 µm thickness by using the microtome and affixed to immunostaining slides by drying in an oven at 60 °C for 20 min. Tissue sections were de-waxed by submerging in xylene and a series of aqueous ethanol (100 – 75 %) and stained by Harris Hematoxylin solution and eosin dye. Stained liver tissue sections were visualized by bright-field microcopy at 200× and 400×.

3.3.8. Thiobarbituric acid reactive substances (TBARS) assay for mouse feed and liver tissues

The presence of oxidized lipids in the diet is associated with liver inflammation and nonalcoholic fatty liver disease (NAFLD) (Hoebinger et al., 2022). Therefore, mouse diets were tested for the presence of secondary products of lipid oxidation by TBARS assay. Mouse liver tissues were also tested for secondary products of lipid oxidation as a marker of oxidative stress common in NAFLD (Chen et al., 2020). The mouse diets and liver tissue samples were finely ground and reacted with thiobarbituric acid under acidic conditions in the presence of butylated hydroxytoluene and absorbance was measured at 535 nm

wavelength. Concentrations of the secondary products of lipid oxidation were calculated by using the standard concentration curve of 1,1,3,3-tetraethoxypropane and results were given in μmole malondialdehyde equivalence (MDA Eq)/g dry sample for mouse diets and μmole MDA Eq/g fresh sample for mice livers (Huber and Rupasinghe, 2009).

3.3.9. Cell lines and culture conditions

AML12 (CRL-2254^{TM}) and Caco-2 (HTB-37^{TM}) cell lines were purchased from the ATCC®, Manassas, VA, USA. AML12 cells were cultured in DMEM:F12 medium supplemented with 10% fetal bovine serum (FBS), 5 mL of 100× ITS liquid media supplement, dexamethasone (40 ng/mL), and penicillin (100 U/mL)-streptomycin (100 μg/mL). Caco-2 cells were cultured in MEME medium supplemented with 20% FBS, L-glutamine (4 mM), and penicillin (100 U/mL)-streptomycin (100 μg/mL). Cell cultures were maintained at 37 °C in a humidified incubator with 5% CO_2 atmosphere and cells were sub-cultured at 80% confluency.

3.3.10. Potential of PAC to induce steatosis in AML12 cells

The potential of O-PAC and P-PAC to promote steatosis in AML12 cells was evaluated by Oil Red O (ORO) staining of the cellular lipids. A stock palmitic acid solution (10 mM) was prepared by dissolving palmitic acid in 20% bovine serum albumin in a phosphate-buffered saline solution (*w:v*) (Zeng et al., 2020). The complete cell culture medium was supplemented with palmitic acid (50 μM) to create a lipid-rich environment for cells. AML12 cells were seeded in a 6-well plate at a density of 1×10^5 cells/well and allowed to reach full confluency. Cells were treated with 25 μg/mL concentration of O-PAC and P-PAC for 24 h. Cells were also treated with 10 and 25 μg/mL concentrations of catechin and O-PAC standard from grape seeds (1298219, USP, Rockville, MD, USA)

respectively for comparison. Non-cytotoxic concentrations of these PAC fractions were determined by the MTS assay (Fig. 3.2a) (Thilakarathna and Rupasinghe, 2022). After PAC treatments, cells were stained with ORO stain to visualize and quantify cellular lipids (Thilakarathna and Rupasinghe, 2022).

3.3.11. Presence of inflammation markers in mouse liver and effects of PAC on the expression of tight junction (TJ) proteins

The presence of inflammation markers, interleukin (IL)-1β, IL-6, and tumor necrosis factor (TNF)-α in mice liver tissues was measured by western blotting. Effects of P-PAC supplementation on the levels of TJ proteins in mice's large intestine tissues and effects of O-PAC and P-PAC on the levels of TJ proteins in Caco-2 cell monolayers were studied by measuring the expressions of claudin-3, claudin-4 and occludin proteins. Caco-2 cells were seeded in T-25 flasks at a density of 5×10^5 cells/flask and allowed to reach full confluency over 8 days to create a Caco-2 cell monolayer. These Caco-2 cell monolayers were treated with O-PAC (25 and 50 µg/mL) and P-PAC (50 and 75 µg/mL) separately for 48 h. Cell monolayers were also treated with catechin (10 µg/mL for 48 h) for comparison. Non-cytotoxic concentrations of different PAC fractions were determined by the MTS assay (Fig. 3.2b) (Thilakarathna and Rupasinghe, 2022). The integrity of Caco-2 cell monolayers at the selected levels of PAC treatments was established by staining for E-cadherin TJ protein using E-cadherin primary antibody (86770, Cell Signaling Technology Inc., Danvers, MA, USA) as per the manufacturer's instructions (Fig. 3.2c). After 48 h treatment with PAC, cells were harvested and proteins were extracted by the radio-immunoprecipitation assay (RIPA) buffer. Mice liver and large intestine tissues were finely ground and proteins were extracted by the RIPA buffer. Western blot analysis of the

extracted protein samples was conducted (Thilakarathna and Rupasinghe, 2019). β-Actin levels in protein samples were measured as the housekeeping protein to normalize the levels of measured proteins. IL-1β (12426S), IL-6 (12912S), TNF-α (3707S), β-actin (12620S), and anti-rabbit secondary antibodies (7074S) were purchased from Cell Signaling Technology Inc., Danvers, MA, USA. Claudin-3 (ab15102), claudin-4 (ab15104), and occludin (ab216327) antibodies were purchased from Abcam, Cambridge, MA, USA.

3.3.12. Bacterial lipopolysaccharides (LPS) in mouse liver tissues

Analysis of the effects of P-PAC on the expression of TJ proteins in mouse large intestine tissues and Caco-2 cell monolayers revealed the ability of P-PAC to reduce the expression of TJ proteins. Therefore, the ability of bacterial LPS to reach mouse liver through impaired large intestine epithelium (and induce steatosis and inflammation) was tested by an HPLC-MS method (Pais de Barros et al., 2015) for LPS quantification. LPS in liver tissue samples were extracted into methanol and concentrated by nitrogen evaporation. Samples were reconstituted with 50% aqueous methanol and reacted with 8 M aqueous HCl solution at 90 °C for 4 h in the presence of NaCl to separate 3-hydroxymyrisitic (3-HM) fatty acid from LPS structure by hydrolysis (Pais de Barros et al., 2015). LPS concentrations in mouse liver tissues were indirectly measured by quantifying 3-HM fatty acid using the UHPLC-ESI-MS (Fernando et al., 2020).

3.3.13. Statistical analysis

Experimental data were analyzed by using the Minitab® statistical software (version 19.2020.1). Results of PAC extraction, PAC quantification, serum ALT/AST activities, TBARS assay for mouse diets and liver tissues, MTS cell viability assay for AML12 and

Caco-2 cells, the ability of PAC to induce steatosis in AML12 cells, and western blot analysis for inflammatory cytokines and TJ proteins were expressed as the mean ± standard deviation of three individual experiments. The results of LPS quantification in mice livers were expressed as the mean ± standard deviation of two individual experiments. The means were compared by one-way analysis of variance (ANOVA) at 95% confidence level with Tukey's multiple mean comparison (95% confidence level).

3.4. RESULTS

3.4.1. Extraction, quantification, and characterization of PAC

The amounts of O-PAC and P-PAC extracted and purified from the GSP were 2.29 ± 0.19 % and 0.96 ± 0.01 % of the dry GSP, respectively. The PAC quantities in purified O-PAC and P-PAC fractions were 54.4 ± 4.81 and 14.4 ± 2.35 mg CE/g dry samples, respectively, as measured by the methylcellulose precipitable tannins assay. The MDP of O-PAC was 3.41 ± 0.29 and the MDP of P-PAC was 15.1 ± 0.15. Galloylation of O-PAC and P-PAC was 6.17 ± 0.08 % and 18.5 ± 0.85 %, respectively. Thus, the P-PAC extract was highly polymerized and galloylated compared to the O-PAC extract.

3.4.2. Biotransformation of P-PAC by probiotic bacteria

Analysis of the liver tissues of mice by HRMS identified nine potential PAC metabolites, 2- or 4-hydroxyphenylacetic acid, 4-hydroxybenzoic acid, *ρ*-coumaric acid, dihydroferulic acid, dihydroferulic acid-4-*O*-*β*-D-glucuronide, fumaric acid, pyrocatechol, pyrogallol, and syringic acid (Supplementary Fig. S3.2). The UHPLC-ESI-MS analysis using pure metabolite standards (Supplementary Fig. S3.3) confirmed the presence of 2-hydroxyphenylacetic, 4-hydroxybenzoic, *ρ*-coumaric, fumaric, pyrocatechol, and syringic acids in the mice liver tissues (Table 3.1). 4-Hydroxybenzoic acid was detected only in the

mice livers of P-PAC+PB group. Pyrocatechol and 2-hydroxyphenylacetic acid were detected in both P-PAC and P-PAC+PB groups with higher concentrations observed in the P-PAC+PB group. Fumaric, *ρ*-coumaric, and syringic acids were common in the liver tissues of all three mouse groups. However, concentrations of these metabolites were higher in the P-PAC+PB group (Table 3.1). Probiotic bacteria generate potential PAC metabolites and promote PAC biotransformation efficiency in mice.

3.4.3. Effects of P-PAC and probiotics supplementation on mouse gut microbiota

The *α*-diversity of microbiota among the three mouse groups was similar ($p > 0.05$) according to the Shannon, Pielou's evenness, observed OTUs, and Faith's PD indices (Fig. 3.3a). Also, *Firmicutes* to *Bacteroidetes* (F/B) ratios were not significantly different ($p > 0.05$) among the mouse groups. P-PAC and probiotic bacteria supplementation did not significantly alter the composition of natural mouse gut microbiota. Furthermore, the relative frequency (%) of the AM in mouse gut microbiota did not significantly change ($p > 0.05$) during the P-PAC and probiotic bacteria supplementation (Fig. 3.3a).

3.4.4. Effects of P-PAC and probiotics supplementation on mouse liver health

Abnormal small white spots, which resemble NAFLD, were observed in the livers of mice of P-PAC and P-PAC+PB groups. Also, the external color of these livers was lighter compared to the livers of the control group mice (Fig. 3.4a – c). The H&E staining of the liver tissue sections revealed that hepatocytes of the P-PAC and P-PAC+PB groups were enlarged, which resembled hepatocyte ballooning (Fig. 3.4d – f). Moreover, hepatic lobular inflammation due to the infiltration of monocytes into the liver tissues was evident in these two mice groups. The liver damage biomarkers, ALT and AST enzyme activities, in the blood serum of P-PAC+PB group mice were significantly higher ($p < 0.05$) compared

to the P-PAC and control group mice (Fig. 3.4g and h). Interestingly, no significant difference was observed in the blood serum ALT and AST activities between the P-PAC and control groups, despite the presence of hepatocyte ballooning in the P-PAC group.

3.4.5. Oxidative stress in the livers of mice as a marker of NAFLD

Concentrations of the oxidized lipid products in mice livers from the P-PAC and P-PAC+PB groups were significantly higher compared to the control group (Fig. 3.5a). Therefore, hepatic oxidative stress should be significantly higher in the P-PAC and P-PAC+PB groups compared to the control group. These results support the H&E observations for the prevalence of NAFLD in P-PAC and P-PAC+PB group mice.

3.4.6. Presence of inflammation markers in mice livers

The hepatic expression of IL-1β, IL-6, and TNF-α proinflammatory cytokines in the P-PAC+PB group was significantly higher compared to the control group (Fig. 3.5c). Interestingly, only IL-6 expression was significantly high in the P-PAC group compared to the control group. These results confirmed the prevalence of hepatic inflammation in the P-PAC and P-PAC+PB mice groups.

3.4.7. Presence of oxidized lipids in mouse diets

The concentration of oxidized lipids in the control chow diet was not significantly different ($p > 0.05$) from the diet containing both P-PAC and probiotics (P-PAC+PB diet). Interestingly, oxidized lipids concentration in the diet containing only P-PAC (P-PAC diet) was significantly low compared to the control chow diet and P-PAC+PB diet (Fig. 3.5b). Therefore, liver inflammation and NAFLD induction in the mice of P-PAC and P-PAC+PB groups did not result from the presence of high concentrations of oxidized lipid products in mouse diets.

3.4.8. Potential of different PAC fractions to induce steatosis in AML12 cells

The potential of different fractions of PAC to promote steatosis in AML12 cells was tested by cellular retention of ORO stain. Visual observation of AML12 cells under the microscope (Fig. 3.3b.I) depicted no signs of steatosis promotion by catechin, O-PAC standard, O-PAC, and P-PAC in the AML12 cells. These results were confirmed by measuring the ORO stain retention in AML12 cells (Fig. 3.3b.II). Different fractions of PAC did not promote lipid accumulation in AML12 cells.

3.4.9. P-PAC-induced intestinal epithelial TJ dysfunction causes hepatotoxicity by enabling LPS translocation

Bacterial LPS levels in the mice livers were measured by quantifying 3-HM concentrations after hydrolysis of LPS (Fig. 3.6a). 3-HM concentrations in the livers of mice of P-PAC and P-PAC+PB groups were significantly higher compared to the control group.

The potential of P-PAC to reduce the levels of TJ proteins in mice's large intestines (and by that increase translocation of LPS) was studied by the western blotting technique for TJ proteins, claudin-3, and occludin. Claudin-3 and occludin levels were significantly low in the large intestines of mice from the P-PAC+PB group compared to the control group mice (Fig. 3.6b). In P-PAC group, only the occludin level was significantly lower compared to the control group mice. Supplementation of mice with P-PAC significantly reduced the expression of TJ proteins in mice's large intestines. Since current knowledge on the ability of P-PAC to reduce the expression of TJ proteins in mouse large intestine is limited, we attempted to reproduce these results in Caco-2 cell monolayers. The levels of claudin-3 and claudin-4 TJ proteins were significantly low in the Caco-2 monolayers

treated with P-PAC (at both 50 and 75 µg/mL levels) compared to the control (Fig. 3.6c). Catechin and O-PAC did not significantly reduce the levels of claudin-3 and claudin-4 TJ proteins compared to the control. Interestingly, O-PAC at 50 µg/mL level significantly increased the level of claudin-3 in Caco-2 cell monolayers. The level of occludin TJ protein was not significantly influenced ($p > 0.05$) in Caco-2 cell monolayers by exposure to catechin, O-PAC, and P-PAC. Different fractions of PAC can selectively influence the expression of TJ proteins in Caco-2 cell monolayers.

3.5. DISCUSSION

The importance of dietary PAC to improve human health and alleviate diseases is evident in many studies (Rauf et al., 2019). However, the physiological effects of PAC largely depend on the bioconversion of P-PAC molecules into metabolites by the colonic microbiota (Ou and Gu, 2014). The ability of probiotic bacteria to biotransform PAC can be used as a concept of synbiotic food development (Thilakarathna et al., 2018). Therefore, we investigated the potential of common LBPB and novel AM probiotic bacteria to generate unique microbial metabolites through dietary supplementation of P-PAC using C57BL/6 mice.

Potential P-PAC metabolites such as 2-hydrophenylacetic, 4-hydroxybenzoic, *ρ*-coumaric, fumaric, syringic acids, and pyrocatechol were confirmed to present in mice livers. In addition, HRMS suggested the presence of potential P-PAC metabolites 4-hydroxyphenylacetic acid, dihydroferulic acid, dihydroferulic acid-4-*O*-*β*-D-glucuronide, and pyrogallol in mice livers. Many of these metabolites have been identified as potential PAC metabolites by previous studies (Thilakarathna et al., 2018). In the current study, 4-hydroxybenzoic acid was detected exclusively in the P-PAC+PB group. Also, the liver

concentrations of pyrocatechol and 2-hyroxyphenylacetic acid were higher in the P-PAC+PB group. Probiotic bacteria may enhance the biotransformation of P-PAC and generate unique metabolites in mice.

A significant difference was not observed in the α-diversity of mouse gut microbiome after the supplementation with P-PAC and probiotic bacteria. Similar results are reported for a high-fat diet-fed C57BL/6 mouse model supplemented with PAC-rich grape seed extract (Liu et al., 2017) and a female pig model supplemented with commercial grape seed extract (Choy et al., 2014). However, contradictory results are presented for a female Wistar rat model gavaged with grape seed PAC (Casanova-Martí et al., 2018). A significant increment of AM population was not observed during the supplementation regime, hinting at the inability of AM to colonize the mouse gut. Though the promotion of AM growth in mice by PAC has been reported (Zhang et al., 2018) P-PAC did not support the colonization of AM in the present study.

H&E staining of the mice's liver tissue sections revealed the presence of hepatocyte ballooning and hepatic lobular inflammation in the P-PAC and P-PAC+PB group mice. The presence of hepatocyte ballooning together with hepatic lobular inflammation confirms the progression of NAFLD to NASH (De and Duseja, 2020) in mice from the two groups. We further confirmed the prevalence of hepatic injury by evaluating the ALT and AST enzyme activities in mouse blood serum, hepatic oxidative stress, and inflammation markers in mouse liver. The activities of ALT and AST enzymes were significantly high in the P-PAC+PB group compared to the control group. However, the ALT and AST enzyme activities were not significantly high in the P-PAC group compared to the control group despite the obvious presence of NASH. Measuring serum ALT activity levels can

be falsely negative in determining the prevalence of hepatic conditions from steatosis to liver fibrosis (Wong et al., 2009). Therefore, in future studies, the intensity and mechanisms of hepatic injury can be further studied by evaluating cytokine-mediated (Roy et al., 2010) and mitochondrial dysfunction-mediated hepatocyte apoptosis (Roy et al., 2009).

Hepatic oxidative stress is another biomarker of steatosis and NASH (Sumida et al., 2013). Hepatic oxidative stress in the mice from the P-PAC and P-PAC+PB groups was significantly higher compared to the mice of the control group. Increased expression of hepatic proinflammatory cytokines, IL-1β, IL-6, and TNF-α is associated with the development and progression of NAFLD (Duan et al., 2022). The prevalence of hepatic inflammation in P-PAC and P-PAC+PB groups was evident by increased expressions of proinflammatory cytokines. These results confirm the prevalence of NASH in mice from the P-PAC and P-PAC+PB groups. The immune responses of the liver are finely regulated by different types of circulatory and resident immune cells. The number of resident Kupffer cells (KC) significantly declines during the progression of steatosis to NASH. This loss of KC is replenished by recruiting $Ly6C^{+}$ monocytes that differentiate into monocyte-derived KC (Huby and Gautier, 2022). Accumulation of KC in the liver had been previously observed in copper-induced hepatotoxicity in rats (Roy et al., 2011). The circulating monocytes recruited into liver tissue can also differentiate into other macrophages known as lipid-associated macrophages (Huby and Gautier, 2022). Hepatic inflammation is positively associated with intestinal inflammation. In chemically-induced ulcerative colitis, the translocation of bacteria can upregulate the hepatic inflammation (Trivedi and Jena, 2013). Therefore, it is important to study the variations of immune cell populations in the

intestine, blood plasma, and liver tissues in the future studies evaluating the P-PAC-mediated hepatotoxicity.

Secondary products of lipid oxidation in diet can induce hepatic lipid accumulation and inflammation (Hoebinger et al., 2022). The diets formulated for P-PAC and P-PAC+PB mice groups did not contain higher concentrations of oxidized lipid products compared to the chow diet of the control group. In fact, the development of oxidized lipid products in the diet for the P-PAC mice group was significantly lower compared to the other two diets. This can be explained by the potential of PAC to reduce lipid oxidation and stabilize foods by acting as a natural antioxidant agent (Su et al., 2015). Since mouse diets did not contribute to the development of NASH in mice, we evaluated the potential of different fractions of PAC to induce lipid accumulation in AML12 cells. Catechin, O-PAC standard, O-PAC, and P-PAC did not promote lipid accumulation in AML12 cells. Several *in vivo* (Yogalakshmi et al., 2013) and clinical studies (Khoshbaten et al., 2010) have presented the potential of PAC to alleviate NAFLD and NASH. However, the degree of polymerization of PAC used in these studies is not well elucidated.

PAC is generally recognized as safe for human consumption (Sano, 2017) and the toxic effects of PAC in humans or other animals are limited. However, a few studies have observed the impact of PAC on the development of digestive tract complications, lesions in the digestive tract of sheep (Hervás et al., 2003), and loss of epithelial cells in the duodenum of Boer goats (Mbatha et al., 2002). In a recent study, grass carps (*Ctenopharyngodon idella*) supplemented with PAC (for 70 days) and challenged with *Aeromonas hydrophila* (for 14 days) developed lesions in the intestine and lost intestinal immune function compared to the control (Li et al., 2020). Moreover, flavonoids can alter

the expression of TJ proteins in epithelial cells. Quercetin and hesperidin aglycone can reduce the claudin-2 expression in Madin-Darby canine kidney (MDCK) II cell monolayers (Nakashima et al., 2020). The effects of PAC on gut epithelium may be driven by the antinutritional effects of PAC. PAC can significantly reduce the bioavailability of dietary iron by chelation (Yun et al., 2011). An adequate supply of dietary iron is necessary to maintain gut epithelial barrier function (Li et al., 2016). Therefore, the potential of P-PAC to induce NASH in mice through hepatic exposure to LPS by impairing gut epithelial barrier function was studied. LPS concentrations in the livers of mice from P-PAC and P-PAC+PB groups were significantly high compared to the control group mice. LPS can impair lipid metabolism in C57Bl/6Ncrj mice and promote hepatic lipid accumulation by altering the expression of key regulatory receptors and enzymes (Ohhira et al., 2007). LPS is proven to induce hepatic inflammation *in vivo* (Khan et al., 2021) by activation of the nuclear factor (NF)-κB inflammatory response cascade (Hamesch et al., 2015). Thus, NASH conditions observed in the P-PAC and P-PAC+PB groups may have resulted from the exposure of mice livers to LPS. Further studies are recommended to measure LPS concentrations in mice blood plasma to establish a correlation with hepatic LPS concentrations.

Loss of gut epithelial barrier function can increase the permeation of endotoxins into the liver through hepatic portal circulation and induce inflammation and liver damage (Fig. 3.7) (Ferro et al., 2020; Kessoku et al., 2021). We observed a significant reduction in the levels of TJ proteins, claudin-3 and occludin, in large intestines of mice from the P-PAC and P-PAC+PB groups. Reduction of TJ protein expression suggests impaired gut epithelial barrier function (Chelakkot et al., 2018) and increased paracellular permeability

for LPS (Hollander and Kaunitz, 2020). Furthermore, P-PAC significantly reduced the expressions of claudin-3 and claudin-4 in Caco-2 cell monolayers, reassuring the potential of P-PAC to reduce the expression of TJ proteins and impair gut epithelial barrier function. It is important to note that the reduction of TJ protein expressions occurred at non-cytotoxic concentrations for Caco-2 cells (as measured by MTS assay) and without losing cells from the Caco-2 cell monolayer (as visualized by E-cadherin staining). Interestingly, O-PAC could significantly increase claudin-3 expression. Several studies contradict the observed results by showing the ability of PAC to promote gut epithelial barrier function both *in vitro* and *in vivo* (Nallathambi et al., 2020; Sheng et al., 2020). However, many of these studies have not reported the MDP and % galloylation of PAC extracts or have used PAC extracts with low degrees of polymerization compared to P-PAC extract used in the current study. These results reveal the importance of determining the nature of PAC extracts before recommending them for human consumption to avoid harmful health effects.

The mouse liver damage and inflammation were prominent in the P-PAC+PB mice group compared to the P-PAC mice group, as shown by ALT/AST activities and levels of liver inflammatory cytokines. The safety of many probiotic bacteria and their potential health benefits are well established. However, probiotic bacteria can possess pathogenic traits that can negatively influence human health (Pradhan et al., 2020). Well-studied probiotic bacteria of *Lactobacillus* (Rossi et al., 2019) and *Enterococcus* (Krawczyk et al., 2021) can act as opportunistic pathogens. Intestinal barrier function is critical to prevent the translocation of these opportunistic bacteria and cause bacteremia (Krawczyk et al., 2021). Thus, impaired gut epithelial barrier function caused by supplementation of P-PAC may have prompted the translocation of LBPB and AM probiotic bacteria and increased

the severity of hepatic injury and inflammation in the P-PAC+PB mice group. Therefore, it is critical to evaluate the safety of supplementation strategies that combine bioactive extracts and probiotics (synbiotics) to achieve better health benefits.

3.6. CONCLUSIONS

Probiotic bacteria such as LBPB and AM can biotransform P-PAC to metabolites (i.e. 4-hydroxybenzoic) in C57BL/6 mice, suggesting their function beyond the natural gut microbiota of mice. Supplementation with P-PAC alone or together with LBPB and AM probiotic bacteria did not influence the α-diversity, F/B ratio, and relative frequency (%) of AM in the natural gut microbiota of C57BL/6 mice. Importantly, supplementation with P-PAC induced NASH in C57BL/6 mice. P-PAC supplementation can significantly reduce the levels of TJ proteins, claudin-3, and occludin in C57BL/6 mice's large intestines. P-PAC can significantly reduce the levels of claudin-3 and claudin-4 TJ proteins in cultured Caco-2 cell monolayers. Interestingly, O-PAC can significantly increase claudin-3 level indicating differential functions depending on the degree of polymerization of PAC. We demonstrated that the reduction of TJ protein expression by P-PAC may impair the gut epithelial barrier function of mice and increase liver exposure to bacterial LPS. Increased bacterial LPS concentrations in mice livers caused NASH as indicated by hepatocyte ballooning and monocyte-infiltrated hepatic lobular inflammation. In conclusion, probiotic bacteria improve P-PAC biotransformation *in vivo* indicating the potential to develop PAC-based synbiotics with health benefits. However, it is critical to evaluate the safety of such PAC-derived synbiotics.

3.7. ACKNOWLEDGEMENT

This research received funds from the Discovery grant of the Natural Sciences and Engineering Research Council (NSERC) of Canada (RGPIN2016 05369) to H.P.V. Rupasinghe. The authors are grateful for the A. David Crowe Graduate Scholarship to W.P.D.W. Thilakarathna and Killam Chair funds of H.P.V. Rupasinghe.

Table 3.1. Concentrations of potential polymeric proanthocyanidin metabolites in the liver tissues of mice.

Proanthocyanidin metabolite	Concentrations of proanthocyanidin metabolite (μg/g fresh liver tissue)		
	Control group	P-PAC group	P-PAC+PB group
1) 4-Hydroxybenzoic acid	0	0	0.61
2) Pyrocatechol	0	0.22	0.62
3) 2-Hydroxyphenylacetic acid	0	0.23	0.56
4) *ρ*-Coumaric acid	0.52	0.65	1.77
5) Fumaric acid	0.51	0.86	1.82
6) Syringic acid	0.14	0.26	0.47

Control group: mice group (n=5) received only the control chow diet; P-PAC group: mice group (n=5) supplemented with polymeric proanthocyanidins (200 mg/kg body weight/day); P-PAC+PB group: mice group (n=5) supplemented with both polymeric proanthocyanidins (200 mg/kg body weight/day) and probiotic bacteria (1×10^9 colony forming units/mouse/day of *Lactobacillus* and *Bifidobacterium* probiotics and 1×10^8 colony forming units/mouse/day of *Akkermansia muciniphila*).

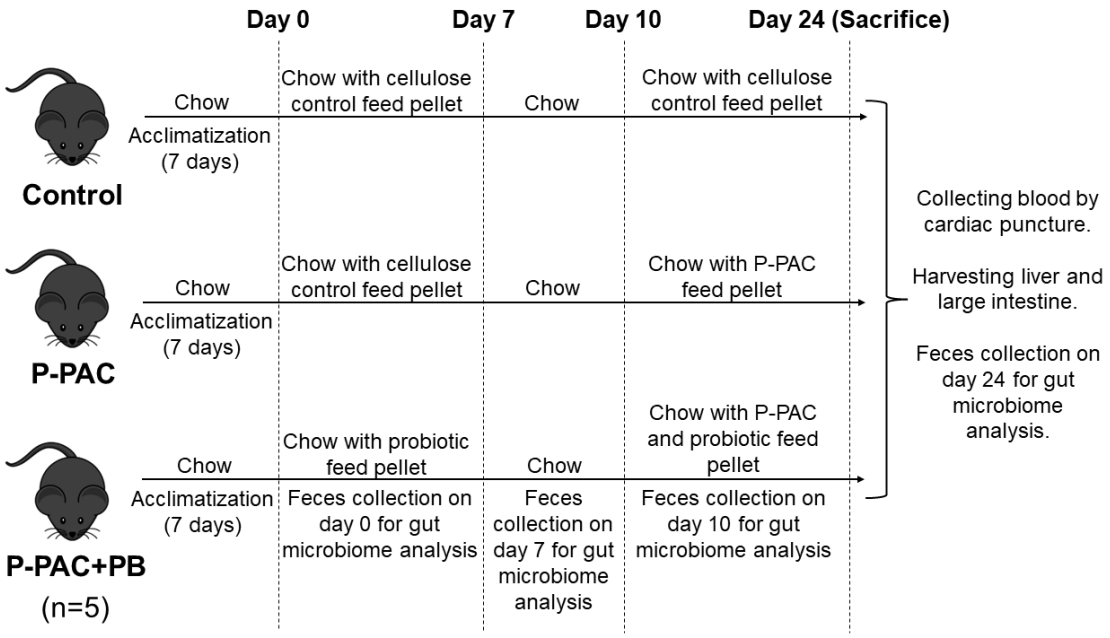

Figure 3.1. Dietary supplementation regime followed during the C57BL/6 mice study. Three groups of male C57BL/6 mice (n=5) were fed with a chow diet (control group), chow diet mixed with polymeric proanthocyanidins (P-PAC), or chow diet mixed with both P-PAC and probiotic bacteria (P-PAC+PB group). Mice feces were collected during the supplementation to study the variations in mice gut microbiota composition. At the end of the study, mouse blood and tissues were collected and tested for the presence of metabolites of proanthocyanidins.

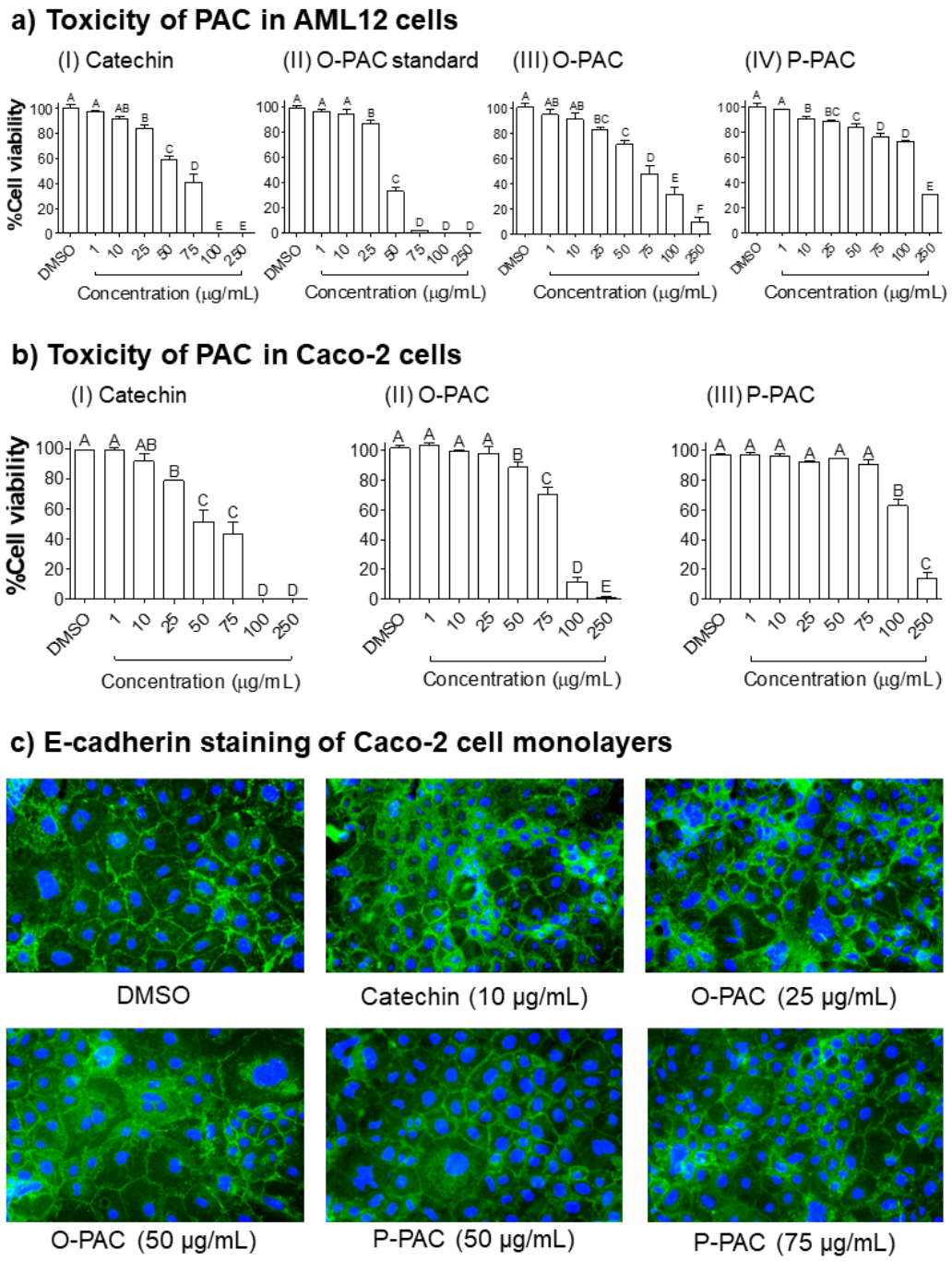

Figure 3.2. Cytotoxicity of different proanthocyanidins (PAC) in AML12 cells (a) and Caco-2 cells (b) as measured by the MTS assay and effect of different PAC on the integrity of Caco-2 cell monolayers (c) as visualized by staining of E-cadherin protein. MTS assay results were presented as mean ± standard deviation of three independent experiments. Means that do not share a similar letter are significantly different at 95% confidence level. DMSO, dimethyl sulfoxide; O-PAC, oligomeric PAC; P-PAC, polymeric PAC.

a) Variations of mouse gut microbiota

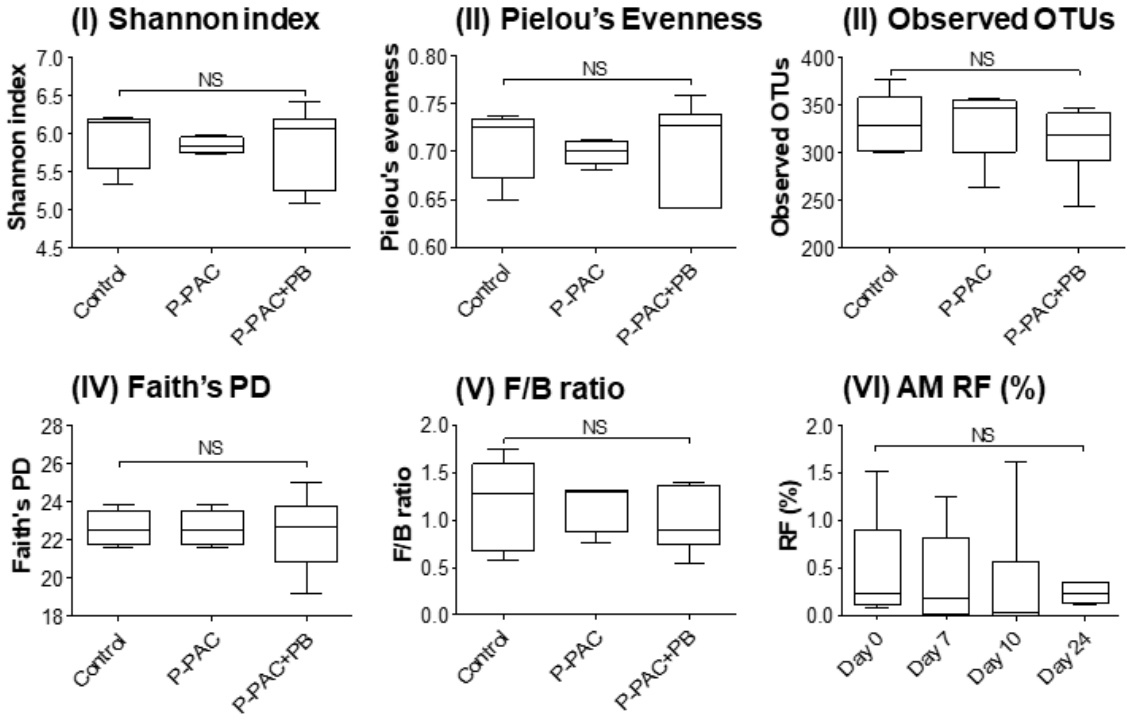

b) Potential of PAC to promote steatosis

(I)

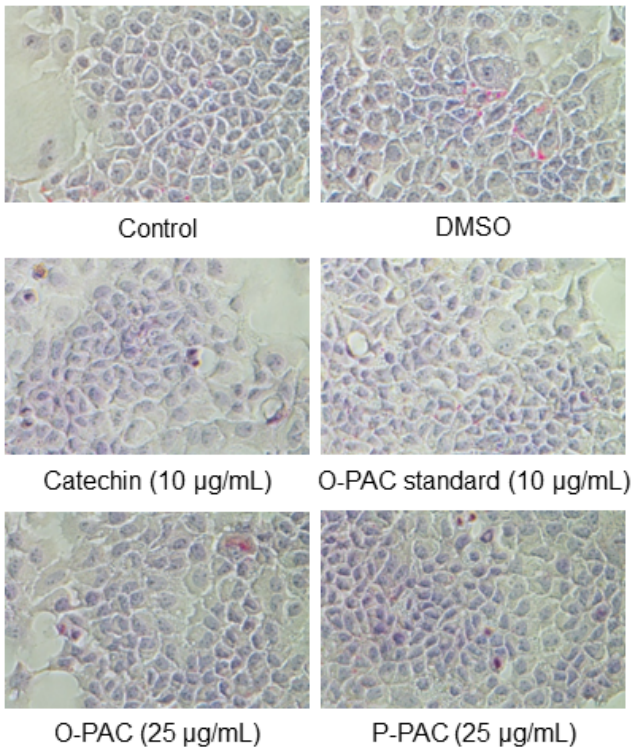

(II)

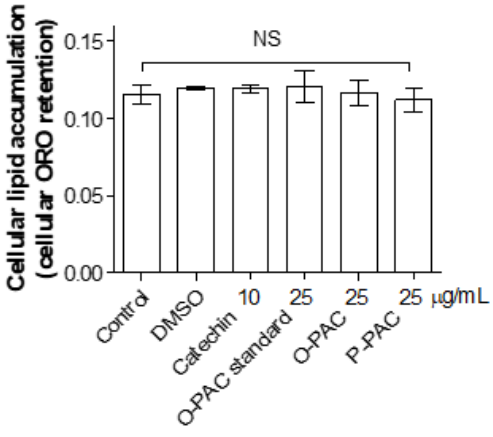

Figure 3.3. Effects of polymeric proanthocyanidins (P-PAC) and probiotic bacteria supplementation on the composition of gut microbiota of C57BL/6 mice (a) and potential of different fractions of proanthocyanidin (PAC) to promote lipid accumulation/induce steatosis in AML12 normal mouse hepatocytes (b). The composition of the mouse gut microbiota was evaluated by the 16S rRNA sequencing technology. Lipid accumulation in AML12 cells was visualized and quantified by Oil Red O (ORO) stain retention assay and results were expressed as mean ± standard deviation of three independent studies. NS, not statistically significant at 95% confidence level. AM RF (%), Akkermansia muciniphila relative frequency (%); DMSO, dimethyl sulfoxide vehicle control; F/B ratio, Firmicutes/Bacteroidetes ratio; Faith's PD, Faith's phylogenetic diversity; observed OTUs, observed operational taxonomy units; O-PAC, oligomeric PAC; P-PAC, polymeric PAC or mice supplemented with P-PAC; P-PAC+PB, mice supplemented with both P-PAC and probiotic bacteria.

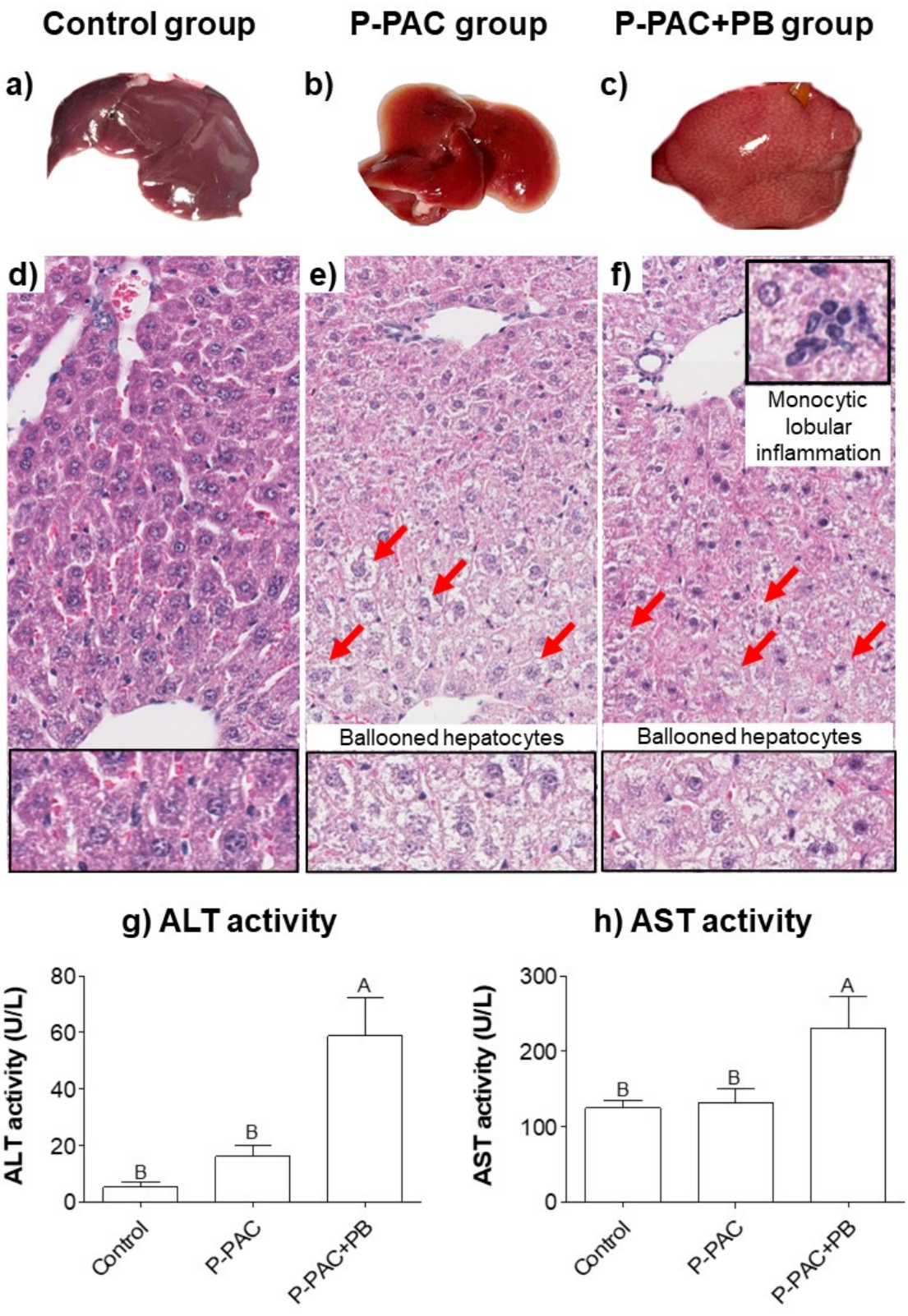
Control group
P-PAC group
P-PAC+PB group
a)
b)
c)
d)
e)
f)
Monocytic lobular inflammation
Ballooned hepatocytes
Ballooned hepatocytes
g) ALT activity
ALT activity (U/L)
80
60
40
20
0
A
B
B
Control
P-PAC
P-PAC+PB
h) AST activity
AST activity (U/L)
300
200
100
0
A
B
B
Control
P-PAC
P-PAC+PB

Figure 3.4. Assessment of hepatotoxicity of polymeric proanthocyanidins and probiotic bacteria supplementation in mice. External appearance of mice livers (a – c) together with histology of liver tissue sections (d – f) and activities of alanine aminotransaminase (ALT, g) and aspartate aminotransaminase (AST, h) enzymes in mice blood serum were evaluated as the biomarkers of liver damage. Measurement of ALT and AST activities were conducted in three independent studies and results were expressed as mean ± standard deviation. Means that do not share a similar letter are significantly different at 95% confidence level. P-PAC group, mice group supplemented with polymeric proanthocyanidin; P-PAC+PB group, mice group supplemented with both polymeric proanthocyanidins and probiotic bacteria.

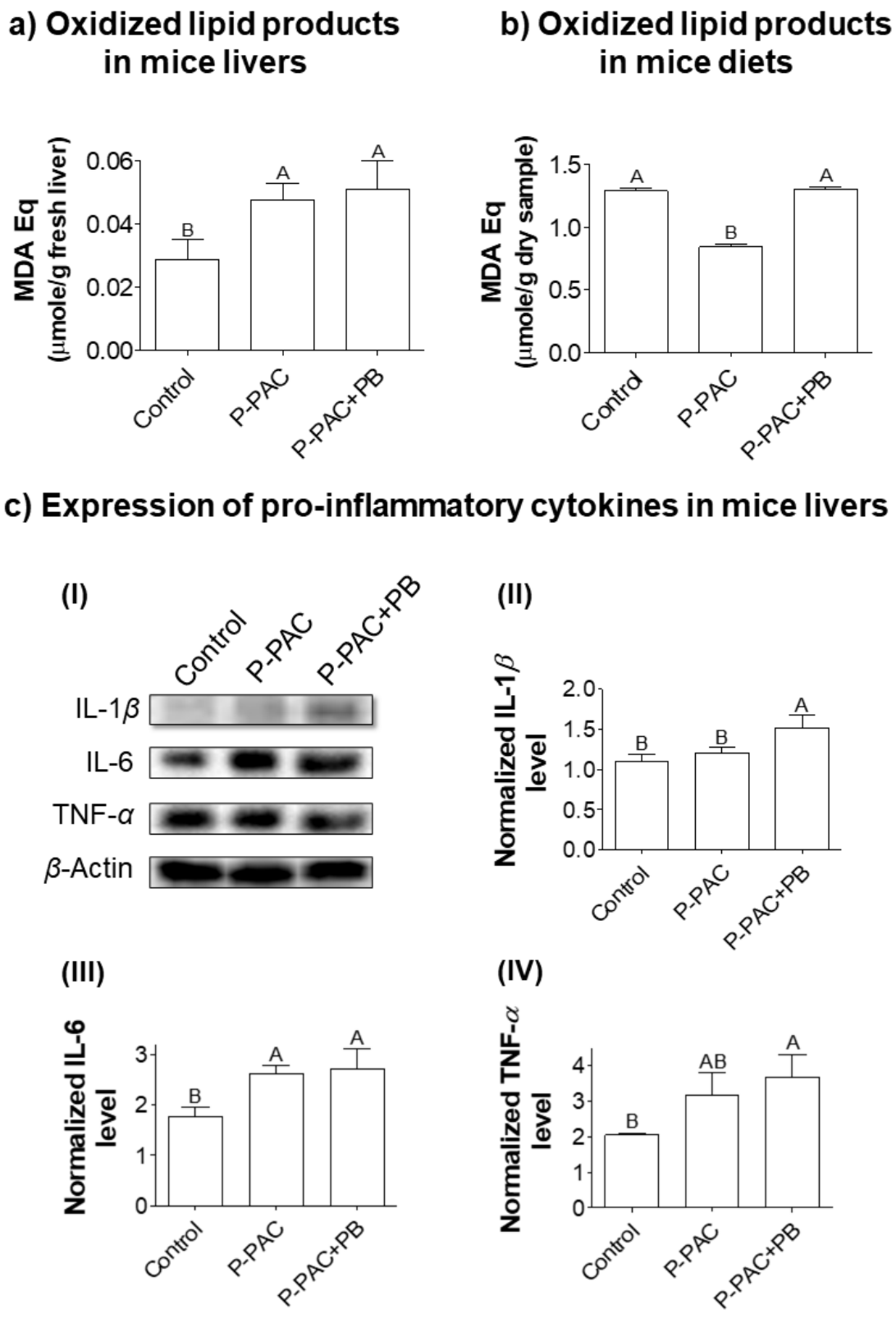
a) Oxidized lipid products in mice livers
MDA Eq (μmole/g fresh liver)
0.06
0.04
0.02
0.00
B
A
A
Control
P-PAC
P-PAC+PB
b) Oxidized lipid products in mice diets
MDA Eq (μmole/g dry sample)
1.5
1.0
0.5
0.0
A
B
A
Contrd
P-PAC
P-PAC+PB
c) Expression of pro-inflammatory cytokines in mice livers
(I)
Control
P-PAC
P-PAC+PB
IL-1β
IL-6
TNF-α
β-Actin
(II)
Normalized IL-1β level
2.0
1.5
1.0
0.5
0.0
B
B
A
Control
P-PAC
P-PAC+PB
(III)
Normalized IL-6 level
3
2
1
0
B
A
A
Control
P-PAC
P-PAC+PB
(IV)
Normalized TNF-α level
4
3
2
1
0
B
AB
A
Control
P-PAC
P-PAC+PB

Figure 3.5. Indicators of lipid oxidation in mouse liver (a) and mouse diets (b), and expression of proinflammatory cytokines in mouse liver (c). Concentrations of secondary products of lipid oxidation in mice livers and mouse diets were measured by the thiobarbituric acid reactive substances assay. Hepatic inflammation in mice was studied by measuring the expression of proinflammatory cytokines by western blot analysis. All experiments were conducted in three independent studies and results were expressed as mean ± standard deviation. Means that do not share a similar letter are significantly different at 95% confidence level. IL-1β, interleukin-1β; IL-6, interleukin-6; MDA Eq, malondialdehyde equivalence; P-PAC, mice group supplemented with polymeric proanthocyanidins; P-PAC+PB, mice group supplemented with both polymeric proanthocyanidins and probiotic bacteria; TNF-α, tumor necrosis factor-α.

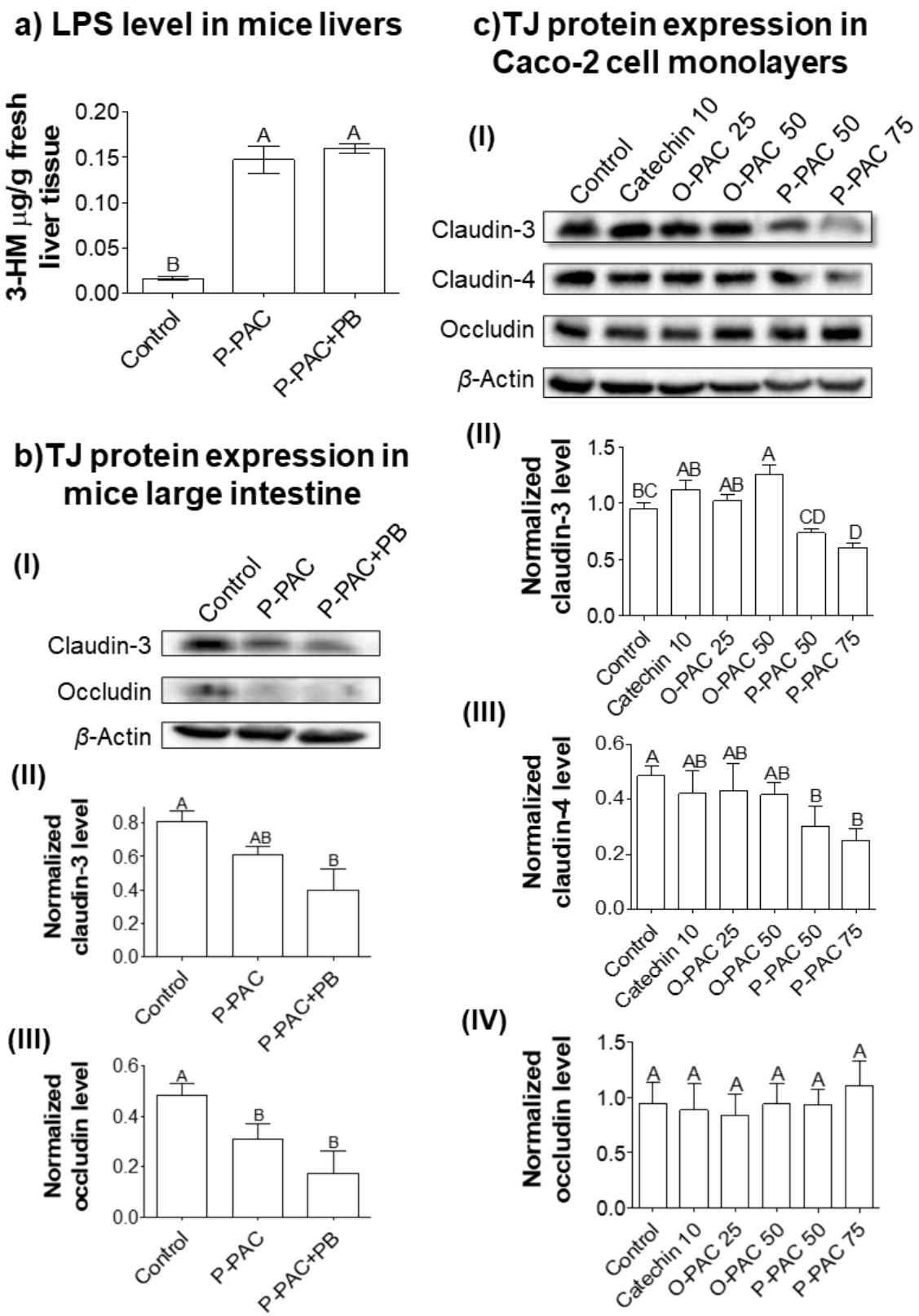
a) LPS level in mice livers
3-HM μg/g fresh liver tissue
0.20
0.15
0.10
0.05
0.00
A
A
B
Control
P-PAC
P-PAC+PB
b)TJ protein expression in mice large intestine
(I)
Control
P-PAC
P-PAC+PB
Claudin-3
Occludin
β-Actin
(II)
Normalized claudin-3 level
0.8
0.6
0.4
0.2
0.0
A
AB
B
Control
P-PAC
P-PAC+PB
(III)
Normalized occludin level
0.6
0.4
0.2
0.0
A
B
B
Control
P-PAC
P-PAC+PB
c)TJ protein expression in Caco-2 cell monolayers
(I)
Control
Catechin 10
O-PAC 25
O-PAC 50
P-PAC 50
P-PAC 75
Claudin-3
Claudin-4
Occludin
β-Actin
(II)
Normalized claudin-3 level
1.5
1.0
0.5
0.0
BC
AB
AB
A
CD
D
Control
Catechin 10
O-PAC 25
O-PAC 50
P-PAC 50
P-PAC 75
(III)
Normalized claudin-4 level
0.6
0.4
0.2
0.0
A
AB
AB
AB
B
B
Control
Catechin 10
O-PAC 25
O-PAC 50
P-PAC 50
P-PAC 75
(IV)
Normalized occludin level
1.5
1.0
0.5
0.0
A
A
A
A
A
A
Control
Catechin 10
O-PAC 25
O-PAC 50
P-PAC 50
P-PAC 75

Figure 3.6. Bacterial lipopolysaccharide concentrations in mice livers (a) and effects of proanthocyanidins on the tight junction protein levels in mice's large intestine (b) and Caco-2 cell monolayers (c). Exposure of mice livers to bacterial lipopolysaccharides was indirectly quantified by measuring the levels of 3-hydroxymyrisitic acid in mice livers. Effects of proanthocyanidins on the levels of tight junction proteins in mice's large intestines and Caco-2 cell monolayers were studied by western blot analysis. Measurement of LPS levels was conducted in two independent studies and western blot analysis for the expression of tight junction proteins was conducted in three independent studies. Results were expressed as mean ± standard deviation. Means that do not share a similar letter are significantly different at 95% confidence level. 3-HM, 3-hydroxymyrisitic acid; LPS, bacterial lipopolysaccharides; O-PAC, oligomeric proanthocyanidins; P-PAC, polymeric proanthocyanidins/ mice group supplemented with polymeric proanthocyanidins; P-PAC+PB, mice group supplemented with both polymeric proanthocyanidins and probiotic bacteria; TJ protein, tight junction protein.

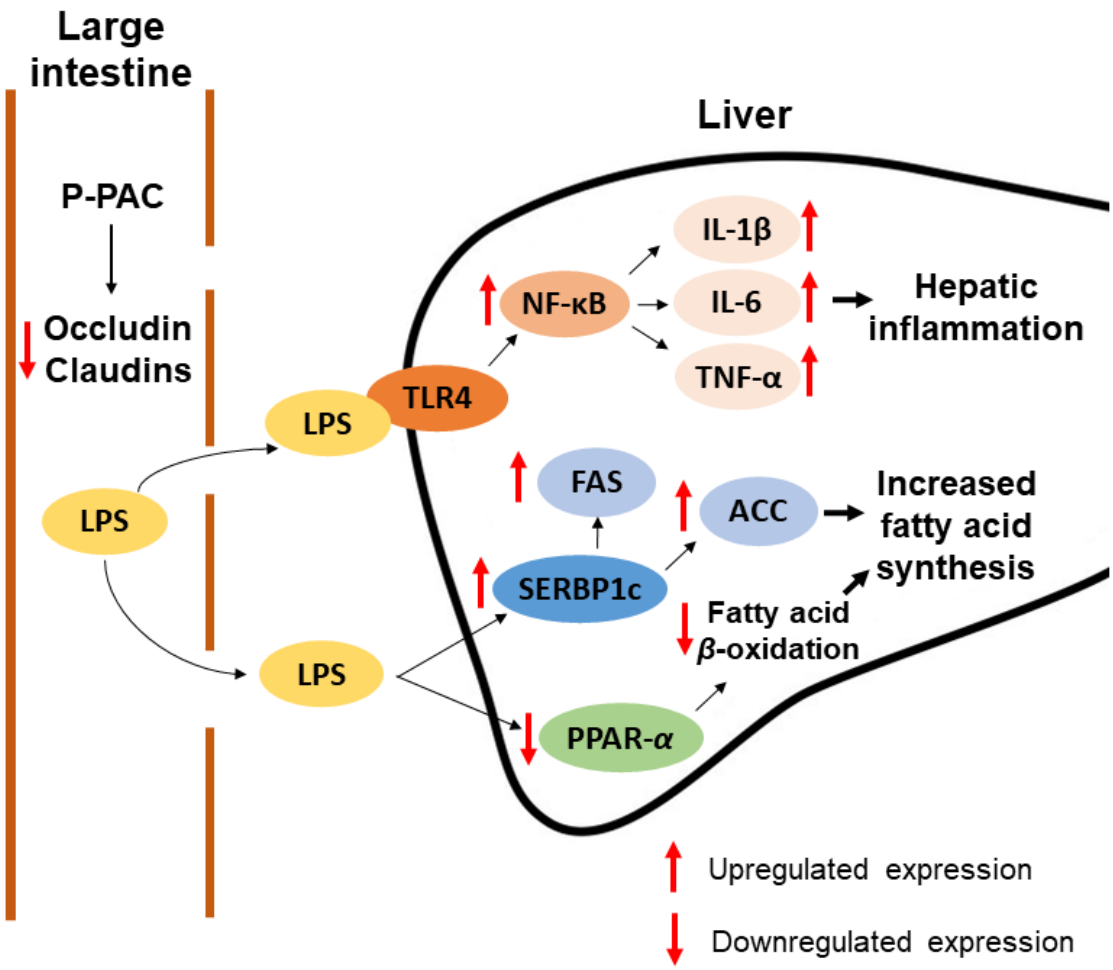

Figure 3.7. Potential mechanism of polymeric proanthocyanidins (P-PAC)-mediated nonalcoholic steatohepatitis induction in C57BL/6 mice. P-PAC downregulates the expression of tight junction proteins, claudins, and occludin in the mouse large intestine epithelium disrupting the gut epithelial barrier function. Bacterial lipopolysaccharides (LPS) can increasingly permeate through disrupted large intestine epithelium to the liver by hepatic portal circulation. At the liver, LPS can bind with toll-like receptor 4 (TLR4) and upregulate nuclear factor-kappa-light-chain-enhancer of activated B cells (NF-κB)-mediated inflammatory cytokines, interleukin (IL)-1β, IL-6, and tumor necrosis factor-alpha (TNF-α) production to induce hepatic inflammation. LPS can promote hepatic fatty acid synthesis by upregulating fatty acid synthase (FAS) and acetyl-CoA carboxylase (ACC) enzymes through upregulating the expression of sterol regulatory elemental binding protein-1c (SREBP1c) transcription factor. LPS can also promote hepatic fatty acid synthesis by reducing the β-oxidation of fatty acids through downregulation of peroxisome proliferator-activated receptor (PPAR)-α.

3.8. SUPPLEMENTARY TABLE

Supplementary table S3.1. Proanthocyanidin metabolites expected to detect by high-resolution mass spectrometry, their molecular formulas and electrospray ionization negative mode mass to charge ratios.

Compound name	Molecular Formula	ESI Negative m/z
Pyrocatechol	$C_6H_6O_2$	109.1
Fumaric acid	$C_4H_4O_4$	115.07
Succinic acid	$C_4H_6O_4$	117.088
p-Hydroxybenzaldehyde	$C_7H_6O_2$	121.123
Pyrogallol	$C_6H_6O_3$	125.11
3-Hydroxybenzoic acid	$C_7H_6O_3$	137.024
4-Hydroxybenzoic acid	$C_7H_6O_3$	137.024
Cinnamic acid	$C_9H_8O_2$	147
trans-Cinnamic acid	$C_9H_8O_2$	147
Hydrocinnamic acid (3-phenyl propionic acid)	$C_9H_{10}O_2$	149.177
3-Hydroxyphenylacetic acid	$C_8H_8O_3$	151.04
4-Hydroxyphenylacetic acid	$C_8H_8O_3$	151.04
Vanillin	$C_8H_8O_3$	151.149
Protocatechuic acid	$C_7H_6O_4$	153.012
p-Coumaric acid	$C_9H_8O_3$	163.16
m-Coumaric acid	$C_9H_8O_3$	163.16
o-Coumaric acid	$C_9H_8O_3$	163.16
m-Dihydrocoumaric acid	$C_9H_{10}O_3$	165.17
o-Dihydrocoumaric acid	$C_9H_{10}O_3$	165.17
p-Dihydrocoumaric acid	$C_9H_{10}O_3$	165.17
3,4-Dihydroxyphenylacetic acid	$C_8H_8O_4$	167.15
Vanillic acid	$C_8H_8O_4$	167.15
2,5-Dihydroxyphenylacetic acid (homogentisic acid)	$C_8H_8O_4$	167.15
Gallic acid	$C_7H_6O_5$	169.12
4-Methoxycinnamic acid	$C_{10}H_{10}O_3$	176.9
5-Phenylvaleric acid	$C_{11}H_{14}O_2$	177.092
Hippuric acid	$C_9H_9NO_3$	178.051
Caffeic acid	$C_9H_8O_4$	179.035
3-(4-methoxyphenyl)propionic acid	$C_{10}H_{12}O_3$	179.2
Homovanillic acid	$C_9H_{10}O_4$	181.051
Dihydrocaffeic acid	$C_9H_{10}O_4$	181.1

Compound name	Molecular Formula	ESI Negative m/z
Methyl 3,4,5-trihydroxybenzoate	$C_8H_8O_5$	183.14
3-*O*-Methylgallic acid	$C_8H_8O_5$	183.14
Quinic acid	$C_7H_{12}O_6$	191.17
Methyl hippuric	$C_{10}H_{11}NO_3$	192.202
3-Hydroxyphenylvaleric acid	$C_{11}H_{14}O_3$	193.087
Isoferulic acid	$C_{10}H_{10}O_4$	193.186
Ferulic acid	$C_{10}H_{10}O_4$	193.186
4-Hydroxyhippuric acid	$C_9H_9NO_4$	194.046
Dihydroferulic acid	$C_{10}H_{12}O_4$	195.1
Dihydroisoferulic acid	$C_{10}H_{12}O_4$	195.1
Syringic acid	$C_9H_{10}O_5$	197.174
Methylferulic acid	$C_{11}H_{12}O_4$	207.2
5-(3,4-Dihydroxyphenyl)-gamma valerolactone	$C_{11}H_{12}O_4$	207.21
Methyldihydroferulic acid	$C_{11}H_{14}O_4$	209
Purpurogallin	$C_{11}H_8O_5$	219.17
5-(3,4,5-Trihydroxyphenyl)-gamma valerolactone	$C_{11}H_{12}O_5$	223.21
3,5-Dimethoxy-4-hydroxycinnamic acid (sinapic acid)	$C_{11}H_{12}O_5$	223.212
p-Coumaric acid-4′-*O*-sulfate	$C_9H_8O_6S$	242.9
m-Coumaric acid-3′-*O*-sulfate	$C_9H_8O_6S$	242.9
Dihydro-*m*-coumaric-3′-*O*-sulfate	$C_9H_9O_6S$	244.9
Dihydro-*p*-coumaric-4′-*O*-sulfate	$C_9H_9O_6S$	244.9
Feruloylglycine	$C_{12}H_{13}NO_5$	250.23
Caffeic-3′-*O*-sulfate	$C_9H_8O_7S$	259.22
Caffeic-4′-*O*-sulfate	$C_9H_8O_7S$	259.22
Dihydrocaffeic acid-3-*O*-sulfate	$C_9H_{10}O_7S$	261.24
Dihydrocaffeic-4′-*O*-sulfate	$C_9H_{10}O_7S$	261.24
O-methyl gallic acid-*O*-sulfate	$C_8H_8O_8S$	263.21
Ferulic acid-4-*O*-sulfate	$C_{10}H_{10}O_7S$	273.25
Isoferulic-3′-*O*-sulfate	$C_{10}H_{10}O_7S$	273.25
Dihydroferulic-4′-*O*-sulfate	$C_{10}H_{12}O_7S$	275.26
Dihydroisoferulic-3′-*O*-sulfate	$C_{10}H_{12}O_7S$	275.26
(+)-Catechin	$C_{15}H_{14}O_6$	289.27
(+)-Catechin	$C_{15}H_{14}O_6$	289.27
Ellagic acid	$C_{14}H_6O_8$	301.19
(Epi)gallocatechin	$C_{15}H_{14}O_7$	305.27

Compound name	Molecular Formula	ESI Negative m/z
(Epi)gallocatechin	$C_{15}H_{14}O_7$	305.27
3-Caffeoylquinic-1,5-lactone	$C_{16}H_{16}O_8$	335.29
4-Caffeoylquinic-1,5-lactone	$C_{16}H_{16}O_8$	335.29
m-Coumaric-3′-*O*-glucuronide	$C_{15}H_{16}O_9$	339
Dihydro-*m*-coumaric-3′-*O*-glucuronide	$C_{15}H_{18}O_9$	341
Dihydro-*p*-coumaric-4′-*O*-glucuronide	$C_{15}H_{18}O_9$	341
3-Feruloylquinic-1,5-lactone	$C_{17}H_{18}O_8$	349.3
4-Feruloylquinic-1,5-lactone	$C_{17}H_{18}O_8$	349.3
3-Caffeoylquinic acid	$C_{16}H_{18}O_9$	353.31
4-Caffeoylquinic acid	$C_{16}H_{18}O_9$	353.31
5-Caffeoylquinic acid	$C_{16}H_{18}O_9$	353.31
Caffeic-3′-*O*-glucuronide	$C_{15}H_{16}O_{10}$	355.28
Caffeic-4′-*O*-glucuronide	$C_{15}H_{16}O_{10}$	355.28
Dihydrocaffeic-3′-*O*-glucuronide	$C_{15}H_{18}O_{10}$	357.3
Dihydrocaffeic-4′-*O*-glucuronide	$C_{15}H_{18}O_{10}$	357.3
3-Feruloylquinic acid	$C_{17}H_{20}O_9$	367.3
4-Feruloylquinic acid	$C_{17}H_{20}O_9$	367.3
5-Ferulloylquinic acid	$C_{17}H_{20}O_9$	367.3
Ferulic-4′-*O*-glucuronide	$C_{16}H_{18}O_{10}$	369.31
Isoferulic-3′-*O*-glucuronide	$C_{16}H_{18}O_{10}$	369.31
(Epi)catechin-*O*-sulfate	$C_{15}H_{14}O_9S$	369.33
Dihydroferulic-4′-*O*-glucuronide	$C_{16}H_{20}O_{10}$	371.32
Dihydroisoferulic-3′-*O*-glucuronide	$C_{16}H_{20}O_{10}$	371.32
4′-*O*-methyl-(epi)catechin-*O*-sulfate	$C_{16}H_{16}O_9S$	383.4
3′-*O*-methyl-(epi)catechin-*O*-sulfate	$C_{16}H_{16}O_9S$	383.4
4′-*O*-methyl-(epi)gallocatechin-*O*-sulfate	$C_{16}H_{15}O_{10}S$	399
5-Caffeoylquinic-3′-*O*-sulfate	$C_{16}H_{17}O_{12}S$	432.9
5-Caffeoylquinic-4′-*O*-sulfate	$C_{16}H_{17}O_{12}S$	432.9
Epicatechin gallate	$C_{22}H_{18}O_{10}$	441.37
5-Feruloylquinic-4′-*O*-sulfate	$C_{17}H_{19}O_{12}S$	446.9
Phloretin-2′-*O*-glucuronide	$C_{21}H_{22}O_{11}$	449.4
(Epi)gallocatechins gallate	$C_{22}H_{18}O_{11}$	457.37
(Epi)gallocatechins gallate	$C_{22}H_{18}O_{11}$	457.37
(Epi)catechin-*O*-glucuronide	$C_{21}H_{22}O_{12}$	465.4
Hesperetin-7-*O*-glucuronide	$C_{22}H_{22}O_{12}$	477.4
(Epi)gallocatechin-*O*-glucuronide	$C_{21}H_{22}O_{13}$	481.4
4′-*O*-Methyl-(epi)gallocatechin-*O*-glucuronide	$C_{22}H_{24}O_{13}$	495.12

Compound name	Molecular Formula	ESI Negative m/z
Phloretin-*O*-glucuronide-*O*-sulfate	$C_{21}H_{21}O_{14}S$	529
5-Feruloylquinic-4′-*O*-glucuronide	$C_{23}H_{28}O_{15}$	543.1
(Epi)catechin-*O*-glucuronide-*O*-sulfate	$C_{21}H_{21}O_{15}S$	545
Hesperetin-*O*-glucuronide-*O*-sulfate	$C_{22}H_{21}O_{15}S$	557
Procyanidin B1 dimer	$C_{30}H_{26}O_{12}$	577.5
Procyanidin B1 dimer	$C_{30}H_{26}O_{12}$	577.5
Procyanidin B2 dimer	$C_{30}H_{26}O_{12}$	577.5
Procyanidin B3 dimer	$C_{30}H_{26}O_{12}$	577.5
Procyanidin C1 trimer	$C_{45}H_{38}O_{18}$	865.8
Procyanidin C1 trimer	$C_{45}H_{38}O_{18}$	865.8

ESI negative, electrospray ionization negative mode; m/z, mass to charge ratio.

3.9. SUPPLEMENTARY FIGURES

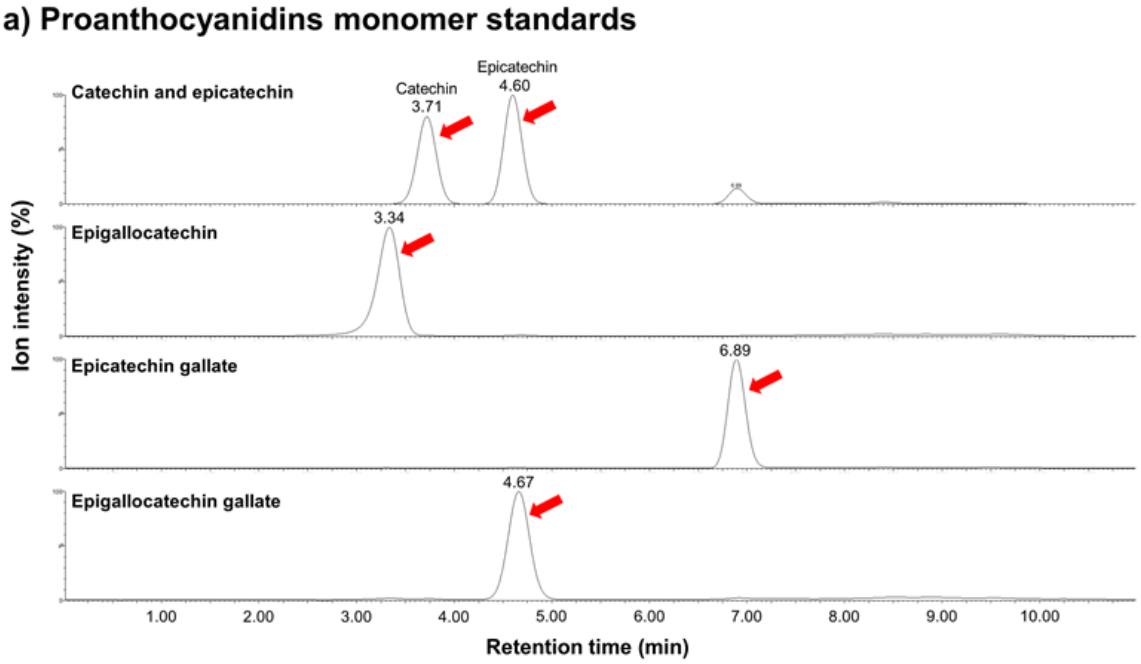

Supplementary figure S3.1-1. Mass spectrometry chromatograms to determine the retention times of the pure proanthocyanidin standards, catechin, epicatechin, epigallocatechin, epicatechin gallate, and epigallocatechin gallate.

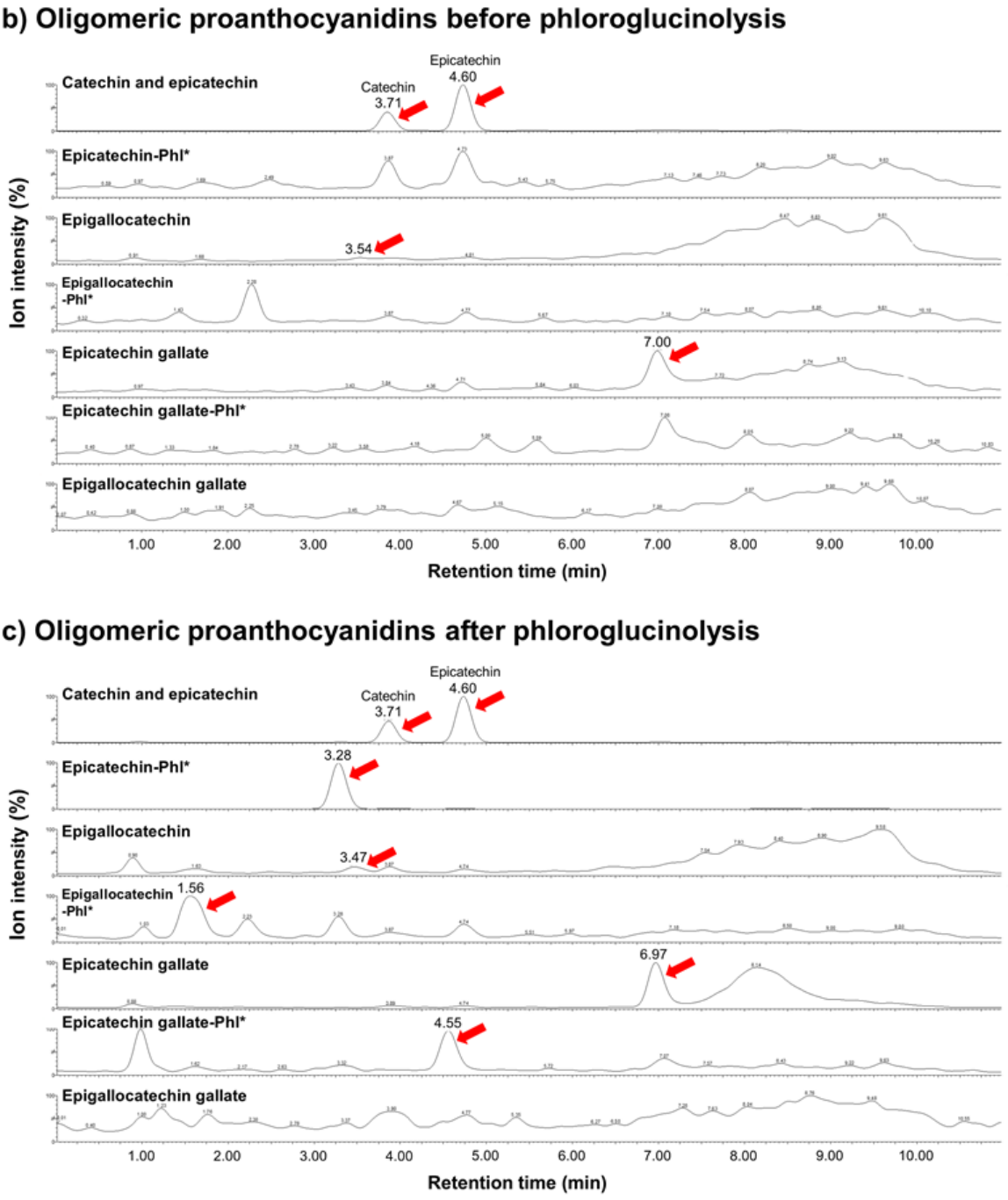

Supplementary figure S3.1-2. Mass spectrometry chromatograms of oligomeric proanthocyanidins extract before and after the phloroglucinolysis reaction to detect and quantify proanthocyanidin monomers, catechin, epicatechin, epigallocatechin, epicatechin gallate, epigallocatechin gallate, and their phloroglucinol adducts. Phl*, phloroglucinol adduct.

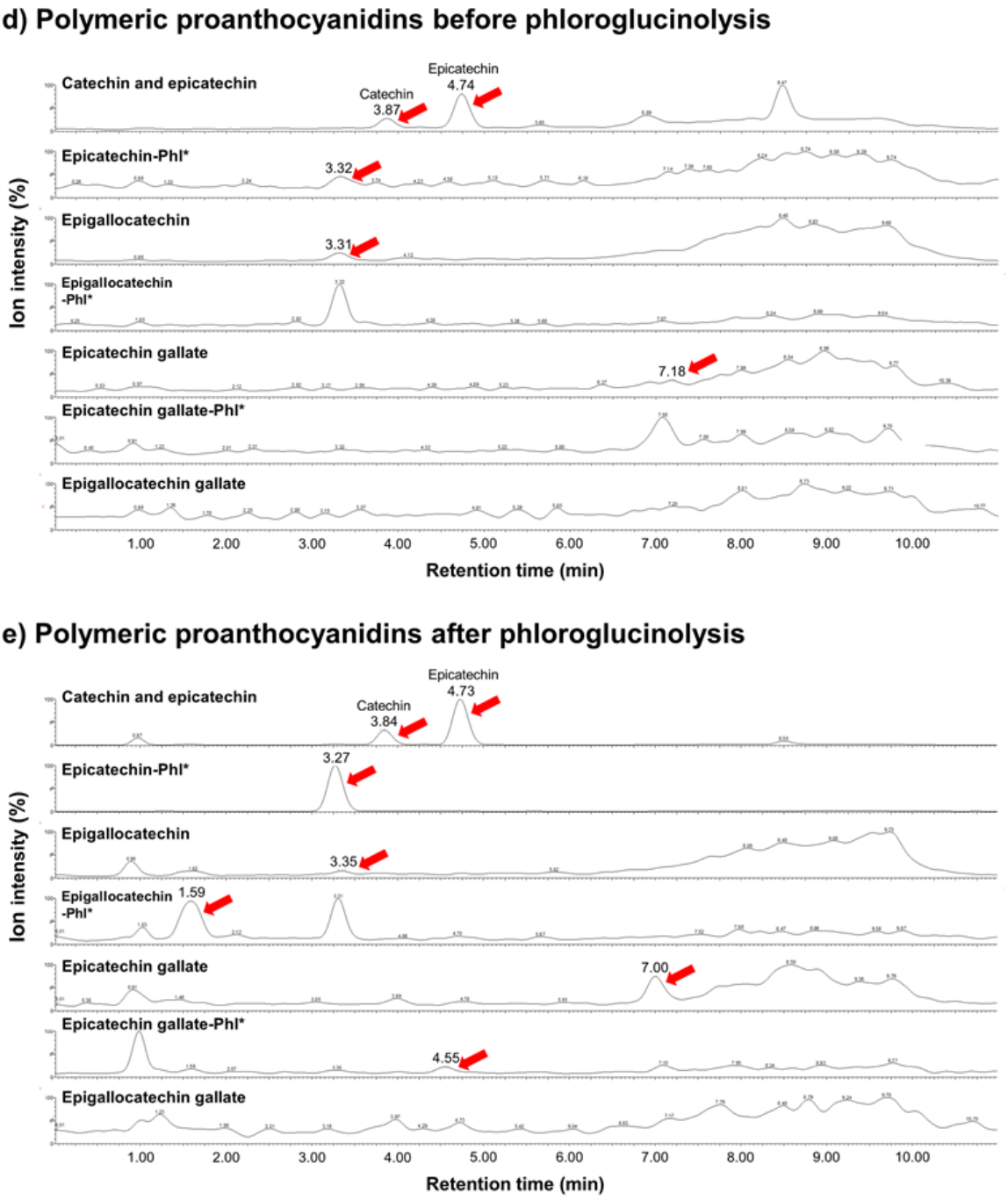

Supplementary figure S3.1-3. Mass spectrometry chromatograms of polymeric proanthocyanidins extract before and after the phloroglucinolysis reaction to detect and quantify proanthocyanidin monomers, catechin, epicatechin, epigallocatechin, epicatechin gallate, epigallocatechin gallate, and their phloroglucinol adducts. Phl*, phloroglucinol adduct.

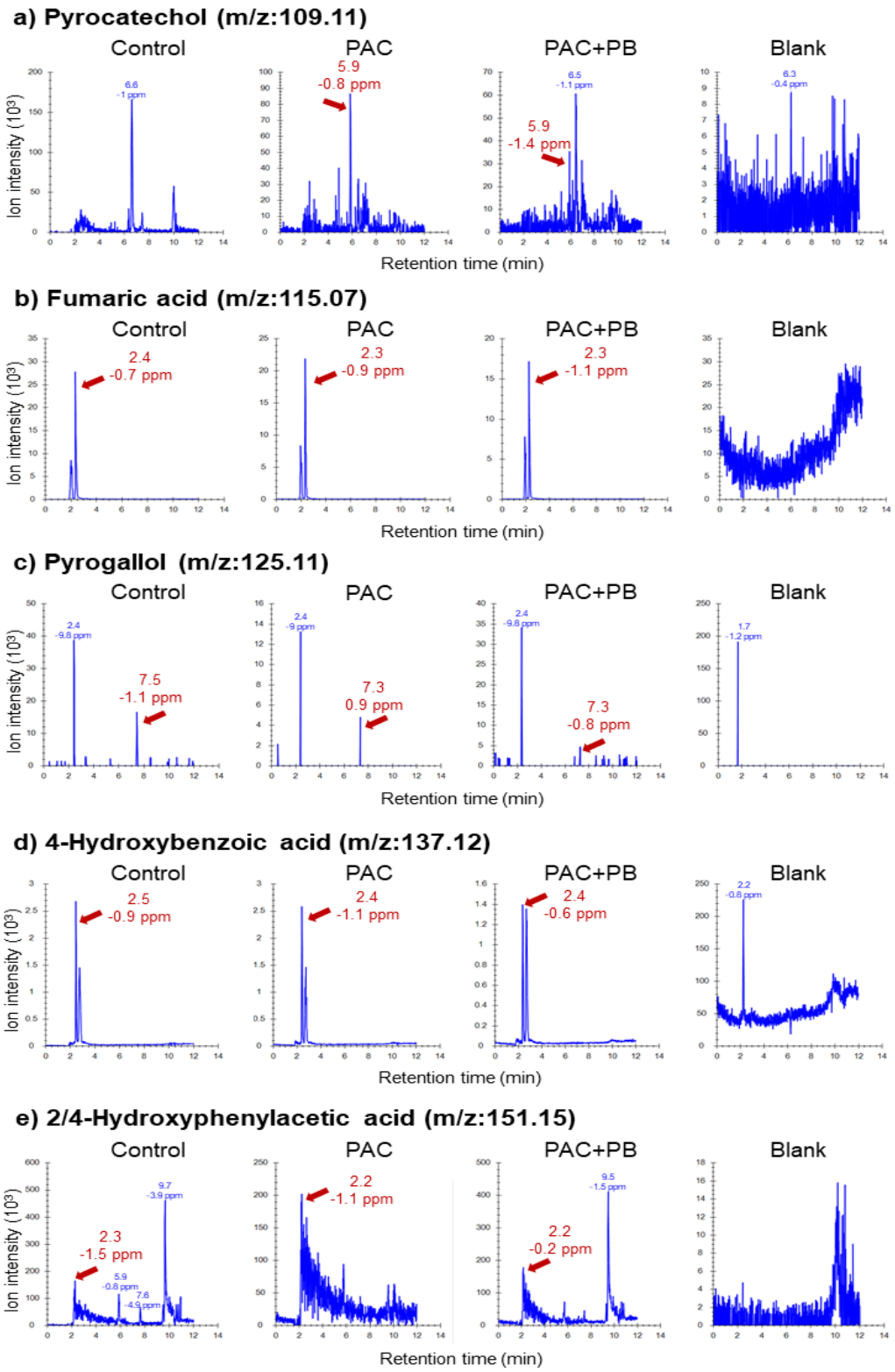

Supplementary figure S3.2-1. High-resolution mass spectrometry chromatograms suggesting the presence of pyrocatechol, fumaric acid, pyrogallol, 4-hydroxybenzoic acid, and 2 or 4-hydroxyphenylacetic acid in the mice liver tissues.

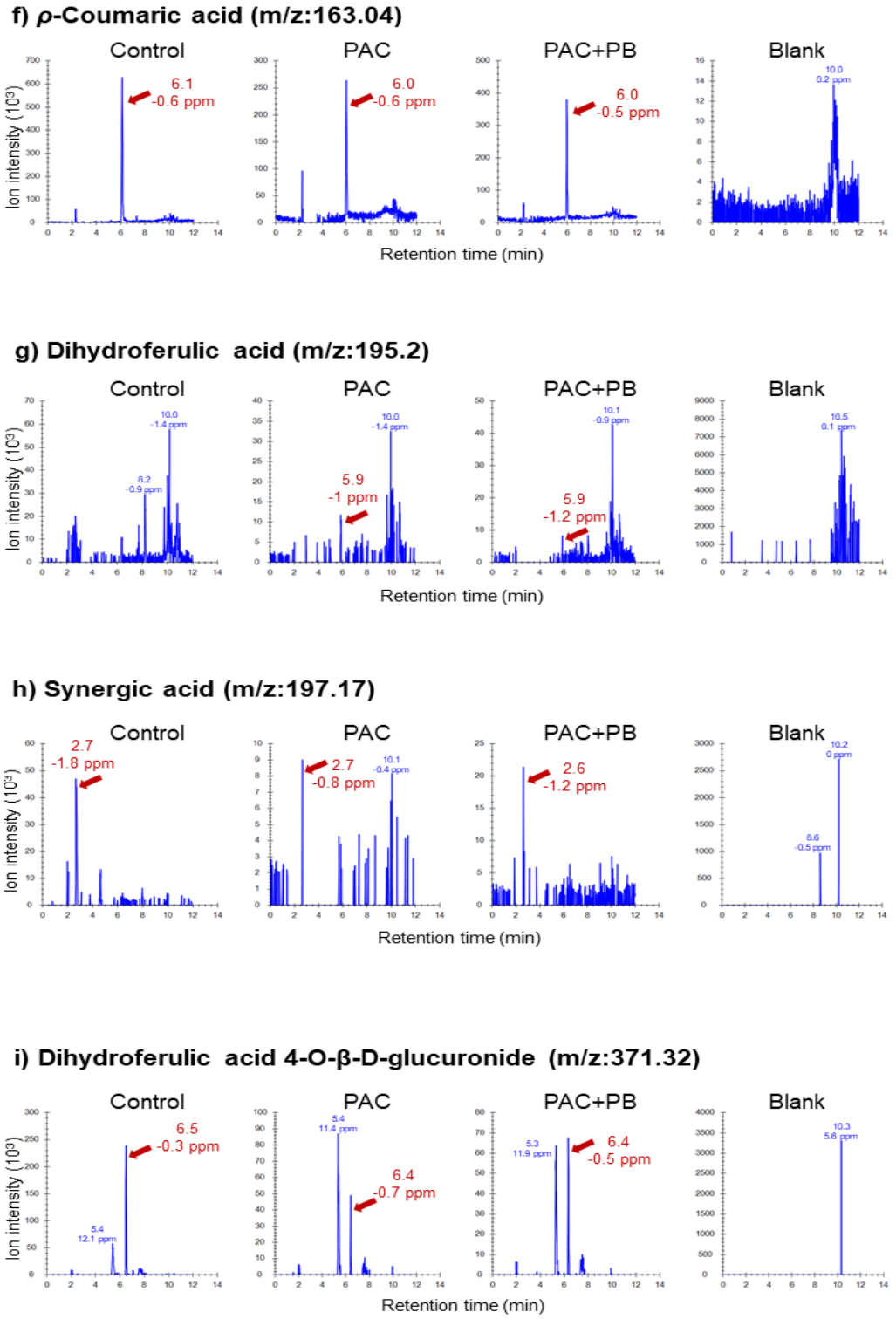

Supplementary figure S3.2-2. High-resolution mass spectrometry chromatograms suggesting the presence of *ρ*-coumaric acid, dihydroferulic acid, synergic acid, and dihydroferulic acid 4-*O*-*β*-D-glucuronide in the mice liver tissues.

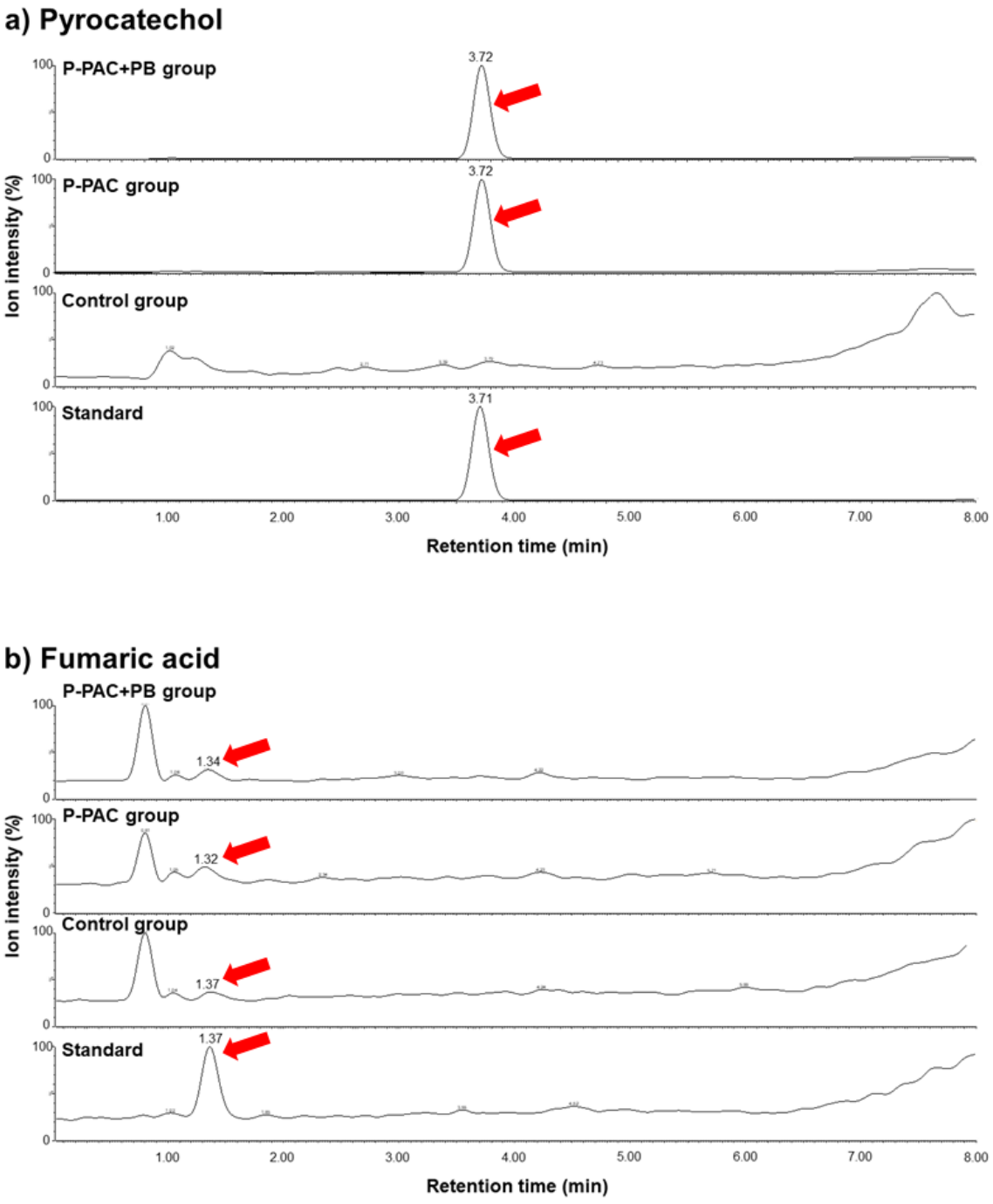

Supplementary figure S3.3-1. Mass spectrometry chromatograms to confirm the presence of pyrocatechol and fumaric acid in concentrated mice liver extracts by comparing retention times with standards. These chromatograms were also used to quantify pyrocatechol and fumaric acid concentrations in concentrated mice liver extracts. P-PAC+PB group, mice supplemented with both polymeric proanthocyanidins and probiotic bacteria; P-PAC group, mice supplemented only with polymeric proanthocyanidins; control group, mice supplemented with control chow diet.

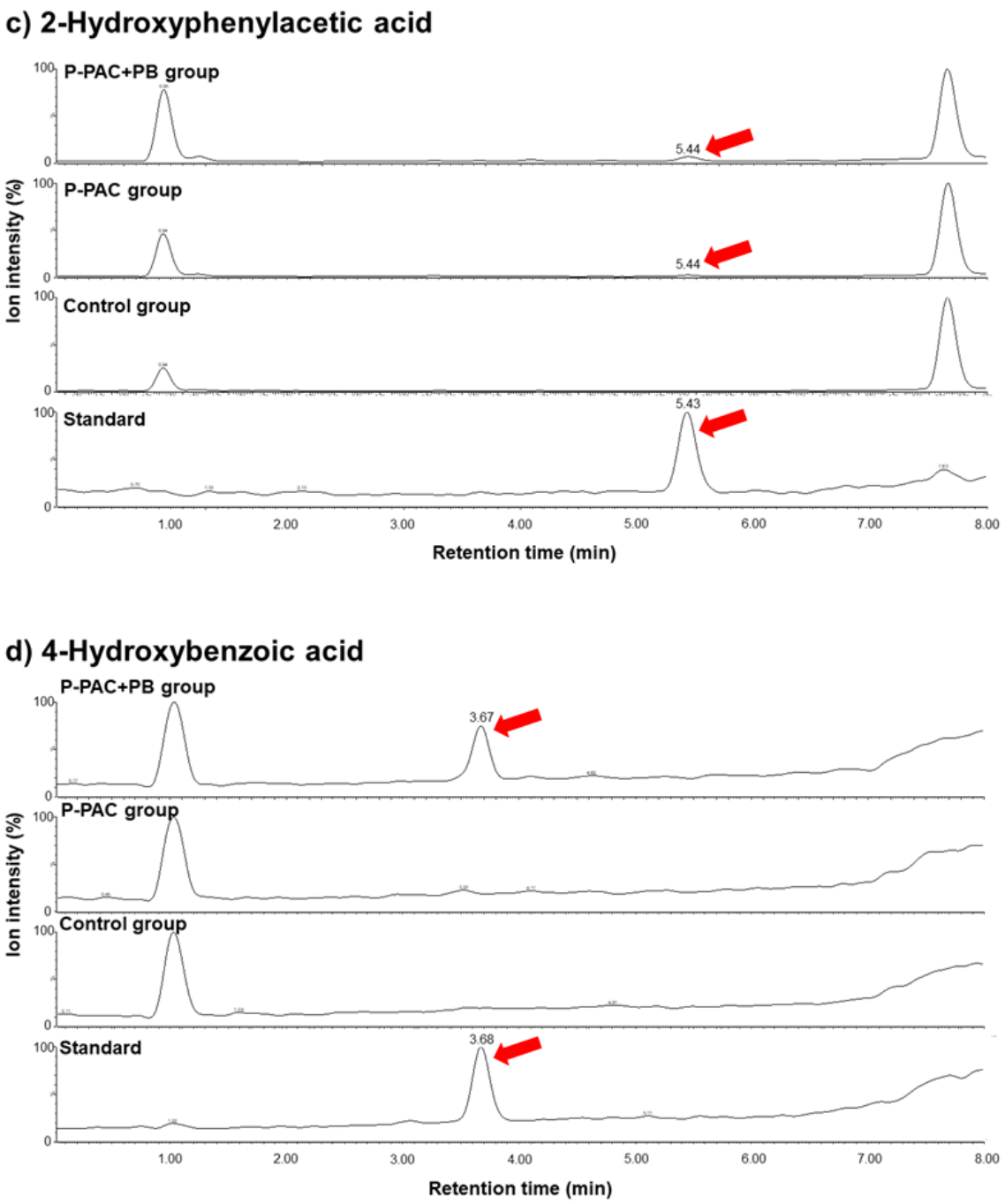

Supplementary figure S3.3-2. Mass spectrometry chromatograms to confirm the presence of 2-hydroxyphenylacetic acid and 4-hydroxybenzoic acid in concentrated mice liver extracts by comparing retention times with standards. These chromatograms were also used to quantify 2-hydroxyphenylacetic acid and 4-hydroxybenzoic acid concentrations in concentrated mice liver extracts. P-PAC+PB group, mice supplemented with both polymeric proanthocyanidins and probiotic bacteria; P-PAC group, mice supplemented only with polymeric proanthocyanidins; control group, mice supplemented with control chow diet.

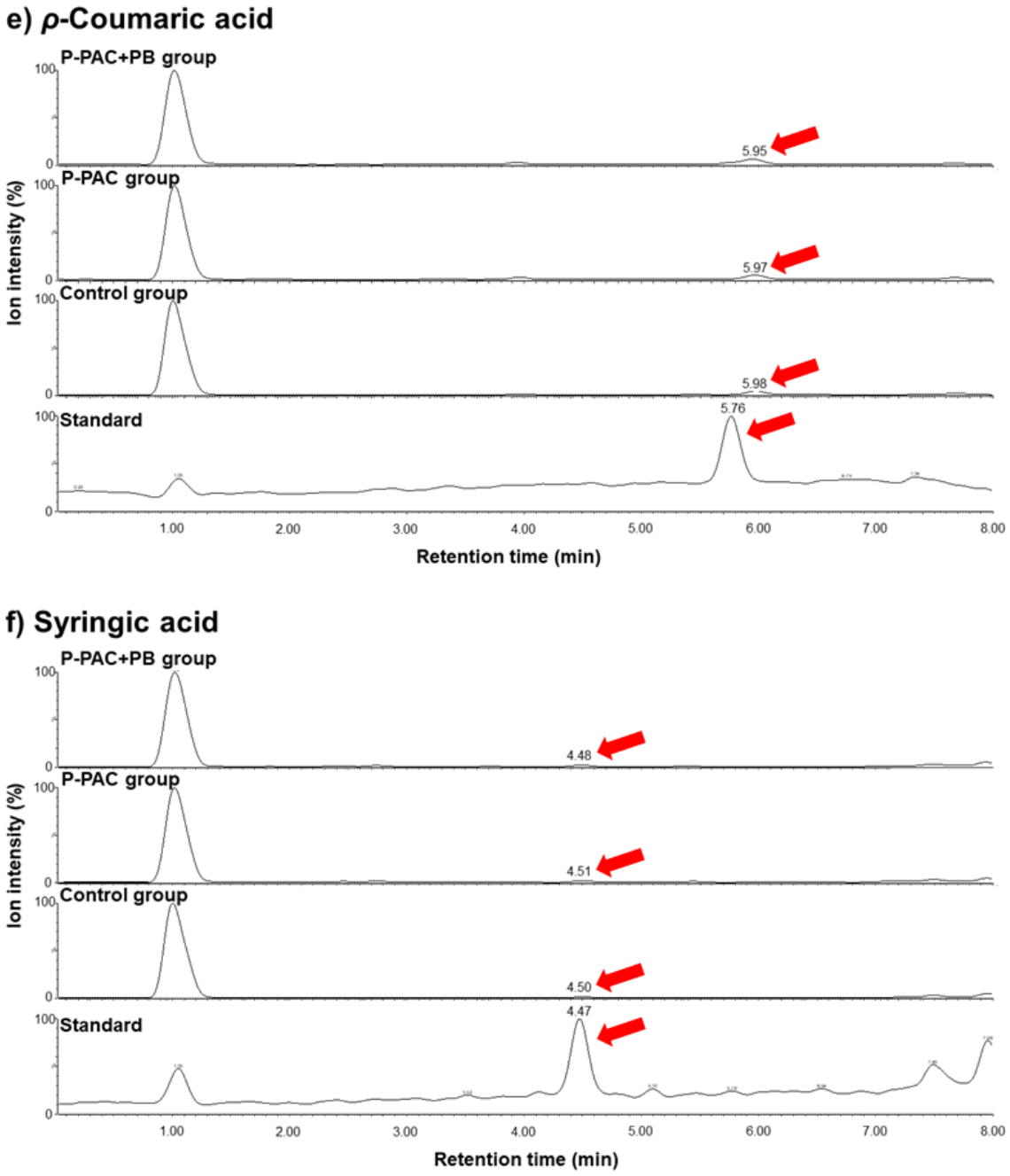

Supplementary figure S3.3-3. Mass spectrometry chromatograms to confirm the presence of *ρ*-coumaric acid and syringic acid in concentrated mice liver extracts by comparing retention times with standards. These chromatograms were also used to quantify *ρ*-coumaric acid and syringic acid concentrations in concentrated mice liver extracts. P-PAC+PB group, mice supplemented with both polymeric proanthocyanidins and probiotic bacteria; P-PAC group, mice supplemented only with polymeric proanthocyanidins; control group, mice supplemented with control chow diet.

3.10. REFERENCES

Arapitsas, P., Perenzoni, D., Guella, G., Mattivi, F., 2021. Improving the phloroglucinolysis protocol and characterization of sagrantino wines proanthocyanidins. Molecules 26, 1087. https://doi.org/10.3390/molecules26041087

Caporaso, J.G., Kuczynski, J., Stombaugh, J., Bittinger, K., Bushman, F.D., Costello, E.K., Fierer, N., Peña, A.G., Goodrich, J.K., Gordon, J.I., Huttley, G.A., Kelley, S.T., Knights, D., Koenig, J.E., Ley, R.E., Lozupone, C.A., McDonald, D., Muegge, B.D., Pirrung, M., Reeder, J., Sevinsky, J.R., Turnbaugh, P.J., Walters, W.A., Widmann, J., Yatsunenko, T., Zaneveld, J., Knight, R., 2010. QIIME allows analysis of high-throughput community sequencing data. Nat. Methods 7, 335–336. https://doi.org/10.1038/nmeth.f.303

Casanova-Martí, À., Serrano, J., J. Portune, K., Sanz, Y., Teresa Blay, M., Terra, X., Ardévol, A., Pinent, M., 2018. Grape seed proanthocyanidins influence gut microbiota and enteroendocrine secretions in female rats. Food Funct. 9, 1672–1682. https://doi.org/10.1039/C7FO02028G

Chelakkot, C., Ghim, J., Ryu, S.H., 2018. Mechanisms regulating intestinal barrier integrity and its pathological implications. Exp. Mol. Med. 50, 1–9. https://doi.org/10.1038/s12276-018-0126-x

Chen, Z., Tian, R., She, Z., Cai, J., Li, H., 2020. Role of oxidative stress in the pathogenesis of nonalcoholic fatty liver disease. Free Radic. Biol. Med. 152, 116–141. https://doi.org/10.1016/j.freeradbiomed.2020.02.025

Choy, Y.Y., Quifer-Rada, P., Holstege, D.M., Frese, S.A., Calvert, C.C., Mills, D.A., Lamuela-Raventos, R.M., Waterhouse, A.L., 2014. Phenolic metabolites and substantial microbiome changes in pig feces by ingesting grape seed proanthocyanidins. Food Funct. 5, 2298–2308. https://doi.org/10.1039/C4FO00325J

Cires, M.J., Wong, X., Carrasco-Pozo, C., Gotteland, M., 2017. The gastrointestinal tract as a key target organ for the health-promoting effects of dietary proanthocyanidins. Front. Nutr. 3, 57. https://doi.org/10.3389/fnut.2016.00057

Comeau, A.M., Douglas, G.M., Langille, M.G.I., 2017. Microbiome helper: a custom and streamlined workflow for microbiome research. mSystems 2. https://doi.org/10.1128/mSystems.00127-16

De, A., Duseja, A., 2020. Natural history of simple steatosis or nonalcoholic fatty liver. J. Clin. Exp. Hepatol. 10, 255–262. https://doi.org/10.1016/j.jceh.2019.09.005

Duan, Y., Pan, X., Luo, J., Xiao, X., Li, J., Bestman, P.L., Luo, M., 2022. Association of inflammatory cytokines with non-alcoholic fatty liver disease. Front. Immunol. 13, 880298. https://doi.org/10.3389/fimmu.2022.880298

Fernando, W., Goralski, K.B., Hoskin, D.W., Rupasinghe, H.P.V., 2020. Metabolism and pharmacokinetics of a novel polyphenol fatty acid ester phloridzin docosahexaenoate in Balb/c female mice. Sci. Rep. 10, 21391. https://doi.org/10.1038/s41598-020-78369-0

Ferro, D., Baratta, F., Pastori, D., Cocomello, N., Colantoni, A., Angelico, F., Del Ben, M., 2020. New insights into the pathogenesis of non-alcoholic fatty liver disease: gut-derived lipopolysaccharides and oxidative stress. Nutrients 12, 2762. https://doi.org/10.3390/nu12092762

Gil-Cardoso, K., Comitato, R., Ginés, I., Ardévol, A., Pinent, M., Virgili, F., Terra, X., Blay, M., 2019. Protective effect of proanthocyanidins in a rat model of mild intestinal inflammation and impaired intestinal permeability induced by LPS. Mol. Nutr. Food Res. 63, 1800720. https://doi.org/10.1002/mnfr.201800720

Gu, L., Kelm, M.A., Hammerstone, J.F., Beecher, G., Holden, J., Haytowitz, D., Gebhardt, S., Prior, R.L., 2004. Concentrations of proanthocyanidins in common foods and estimations of normal consumption. J. Nutr. 134, 613–617. https://doi.org/10.1093/jn/134.3.613

Hamesch, K., Borkham-Kamphorst, E., Strnad, P., Weiskirchen, R., 2015. Lipopolysaccharide-induced inflammatory liver injury in mice. Lab. Anim. 49, 37–46. https://doi.org/10.1177/0023677215570087

Hervás, G., Pérez, V., Giráldez, F.J., Mantecón, A.R., Almar, M.M., Frutos, P., 2003. Intoxication of sheep with quebracho tannin extract. J. Comp. Pathol. 129, 44–54. https://doi.org/10.1016/S0021-9975(02)00168-8

Hoebinger, C., Rajcic, D., Hendrikx, T., 2022. Oxidized lipids: common immunogenic drivers of non-alcoholic fatty liver disease and atherosclerosis. Front. Cardiovasc. Med. 8, 824481. https://doi.org/10.3389/fcvm.2021.824481

Hollander, D., Kaunitz, J.D., 2020. The “leaky gut”: tight junctions but loose associations? Dig. Dis. Sci. 65, 1277–1287. https://doi.org/10.1007/s10620-019-05777-2

Huang, C., Yang, Y., Li, W.-X., Wu, X.-Q., Li, X.-F., Ma, T.-T., Zhang, L., Meng, X.-M., Li, J., 2015. Hyperin attenuates inflammation by activating PPAR-γ in mice with acute liver injury (ALI) and LPS-induced RAW264.7 cells. Int. Immunopharmacol. 29, 440–447. https://doi.org/10.1016/j.intimp.2015.10.017

Huber, G. M., Rupasinghe, H. P. V., 2009. Phenolic profiles and antioxidant properties of apple skin extracts. J. Food Sci. 74, C693–C700. https://doi.org/10.1111/j.1750-3841.2009.01356.x

Huby, T., Gautier, E.L., 2022. Immune cell-mediated features of non-alcoholic steatohepatitis. Nat Rev Immunol 22, 429–443. https://doi.org/10.1038/s41577-021-00639-3

Kennedy, J.A., Jones, G.P., 2001. Analysis of proanthocyanidin cleavage products following acid-catalysis in the presence of excess phloroglucinol. J. Agric. Food Chem. 49, 1740–1746. https://doi.org/10.1021/jf001030o

Kessoku, T., Kobayashi, T., Imajo, K., Tanaka, K., Yamamoto, A., Takahashi, K., Kasai, Y., Ozaki, A., Iwaki, M., Nogami, A., Honda, Y., Ogawa, Y., Kato, S., Higurashi, T., Hosono, K., Yoneda, M., Okamoto, T., Usuda, H., Wada, K., Kobayashi, N., Saito, S., Nakajima, A., 2021. Endotoxins and non-alcoholic fatty liver disease. Front. Endocrinol. 12, 770986. https://doi.org/10.3389/fendo.2021.770986

Khan, H.U., Aamir, K., Jusuf, P.R., Sethi, G., Sisinthy, S.P., Ghildyal, R., Arya, A., 2021. Lauric acid ameliorates lipopolysaccharide (LPS)-induced liver inflammation by mediating TLR4/MyD88 pathway in Sprague Dawley (SD) rats. Life Sci. 265, 118750. https://doi.org/10.1016/j.lfs.2020.118750

Khoshbaten, M., Aliasgarzadeh, A., Masnadi, K., Farhang, S., Tarzamani, M.K., Babaei, H., Kiani, J., Zaare, M., Najafipoor, F., 2010. Grape seed extract to improve liver function in patients with nonalcoholic fatty liver change. Saudi J. Gastroenterol. Off. J. Saudi Gastroenterol. Assoc. 16, 194–197. https://doi.org/10.4103/1319-3767.65197

Krawczyk, B., Wityk, P., Gałęcka, M., Michalik, M., 2021. The many faces of Enterococcus spp.-commensal, probiotic and opportunistic pathogen. Microorganisms 9, 1900. https://doi.org/10.3390/microorganisms9091900

Li, M., Feng, L., Jiang, W.-D., Wu, P., Liu, Y., Jiang, J., Kuang, S.-Y., Tang, L., Zhou, X.-Q., 2020. Condensed tannins decreased the growth performance and impaired intestinal immune function in on-growing grass carp (Ctenopharyngodon idella). Br. J. Nutr. 123, 737–755. https://doi.org/10.1017/S0007114519003295

Li, Y., Hansen, S.L., Borst, L.B., Spears, J.W., Moeser, A.J., 2016. Dietary iron deficiency and oversupplementation increase intestinal permeability, ion transport, and inflammation in pigs. J. Nutr. 146, 1499–1505. https://doi.org/10.3945/jn.116.231621

Liu, W., Zhao, S., Wang, J., Shi, J., Sun, Y., Wang, W., Ning, G., Hong, J., Liu, R., 2017. Grape seed proanthocyanidin extract ameliorates inflammation and adiposity by modulating gut microbiota in high-fat diet mice. Mol. Nutr. Food Res. 61, 1601082. https://doi.org/10.1002/mnfr.201601082

Mbatha, K.R., Downs, C.T., Nsahlai, I.V., 2002. The effects of graded levels of dietary tannin on the epithelial tissue of the gastro-intestinal tract and liver and kidney masses of Boer goats. Anim. Sci. 74, 579–586. https://doi.org/10.1017/S1357729800052735

McPherson, S., Anstee, Q.M., Henderson, E., Day, C.P., Burt, A.D., 2013. Are simple noninvasive scoring systems for fibrosis reliable in patients with NAFLD and normal ALT levels? Eur. J. Gastroenterol. Hepatol. 25, 652–658. https://doi.org/10.1097/MEG.0b013e32835d72cf

Mercurio, M.D., Dambergs, R.G., Herderich, M.J., Smith, P.A., 2007. High throughput analysis of red wine and grape phenolicsadaptation and validation of methyl cellulose precipitable tannin assay and modified somers color assay to a rapid 96 well plate format. J. Agric. Food Chem. 55, 4651–4657. https://doi.org/10.1021/jf063674n

Nakashima, M., Hisada, M., Goda, N., Tenno, T., Kotake, A., Inotsume, Y., Kameoka, I., Hiroaki, H., 2020. Opposing effect of naringenin and quercetin on the junctional compartment of MDCK II cells to modulate the tight junction. Nutrients 12, 3285. https://doi.org/10.3390/nu12113285

Nallathambi, R., Poulev, A., Zuk, J.B., Raskin, I., 2020. Proanthocyanidin-rich grape seed extract reduces inflammation and oxidative stress and restores tight junction barrier function in Caco-2 colon cells. Nutrients 12, 1623. https://doi.org/10.3390/nu12061623

Ohhira, M., Motomura, W., Fukuda, M., Yoshizaki, T., Takahashi, N., Tanno, S., Wakamiya, N., Kohgo, Y., Kumei, S., Okumura, T., 2007. Lipopolysaccharide induces adipose differentiation-related protein expression and lipid accumulation in the liver through inhibition of fatty acid oxidation in mice. J. Gastroenterol. 42, 969–978. https://doi.org/10.1007/s00535-007-2119-8

Ou, K., Gu, L., 2014. Absorption and metabolism of proanthocyanidins. J. Funct. Foods 7, 43–53. https://doi.org/10.1016/j.jff.2013.08.004

Pais de Barros, J.-P., Gautier, T., Sali, W., Adrie, C., Choubley, H., Charron, E., Lalande, C., Le Guern, N., Deckert, V., Monchi, M., Quenot, J.-P., Lagrost, L., 2015. Quantitative lipopolysaccharide analysis using HPLC/MS/MS and its combination with the limulus amebocyte lysate assay[S]. J. Lipid Res. 56, 1363–1369. https://doi.org/10.1194/jlr.D059725

Pradhan, D., Mallappa, R.H., Grover, S., 2020. Comprehensive approaches for assessing the safety of probiotic bacteria. Food Control 108, 106872. https://doi.org/10.1016/j.foodcont.2019.106872

Rauf, A., Imran, M., Abu-Izneid, T., Iahtisham-Ul-Haq, Patel, S., Pan, X., Naz, S., Sanches Silva, A., Saeed, F., Rasul Suleria, H.A., 2019. Proanthocyanidins: A comprehensive review. Biomed. Pharmacother. 116, 108999. https://doi.org/10.1016/j.biopha.2019.108999

Rossi, F., Amadoro, C., Colavita, G., 2019. Members of the Lactobacillus genus complex (LGC) as opportunistic pathogens: A review. Microorganisms 7, 126. https://doi.org/10.3390/microorganisms7050126

Rupasinghe, H.P.V., Parmar, I., Neir, S.V., 2019. Biotransformation of cranberry proanthocyanidins to probiotic metabolites by Lactobacillus rhamnosus enhances their anticancer activity in HepG2 cells in vitro. Oxid. Med. Cell. Longev. 2019, 4750795. https://doi.org/10.1155/2019/4750795

Roy, D., Mandal, S., Sen, G., Mukhopadhyay, S., Biswas, T., 2010. 14-Deoxyandrographolide desensitizes hepatocytes to tumour necrosis factor-alpha-induced apoptosis through calcium-dependent tumour necrosis factor receptor superfamily member 1A release via the NO/cGMP pathway. Br. J. Pharmacol. 160, 1823–1843. https://doi.org/10.1111/j.1476-5381.2010.00836.x

Roy, D.N., Mandal, S., Sen, G., Biswas, T., 2009. Superoxide anion mediated mitochondrial dysfunction leads to hepatocyte apoptosis preferentially in the periportal region during copper toxicity in rats. Chem. Biol. Interact. 182, 136–147. https://doi.org/10.1016/j.cbi.2009.08.014

Roy, D.N., Sen, G., Chowdhury, K.D., Biswas, T., 2011. Combination therapy with andrographolide and d-penicillamine enhanced therapeutic advantage over monotherapy with d-penicillamine in attenuating fibrogenic response and cell death in the periportal zone of liver in rats during copper toxicosis. Toxicol. Appl. Pharmacol. 250, 54–68. https://doi.org/10.1016/j.taap.2010.09.027

Sallam, I.E., Abdelwareth, A., Attia, H., Aziz, R.K., Homsi, M.N., von Bergen, M., Farag, M.A., 2021. Effect of gut microbiota biotransformation on dietary tannins and human health implications. Microorganisms 9, 965. https://doi.org/10.3390/microorganisms9050965

Sano, A., 2017. Safety assessment of 4-week oral intake of proanthocyanidin-rich grape seed extract in healthy subjects. Food Chem. Toxicol., Second international symposium on phytochemicals in medicine and food (2-ISPMF) 108, 519–523. https://doi.org/10.1016/j.fct.2016.11.021

Sheng, K., Zhang, G., Sun, M., He, S., Kong, X., Wang, J., Zhu, F., Zha, X., Wang, Y., 2020. Grape seed proanthocyanidin extract ameliorates dextran sulfate sodium-induced colitis through intestinal barrier improvement, oxidative stress reduction, and inflammatory cytokines and gut microbiota modulation. Food Funct. 11, 7817–7829. https://doi.org/10.1039/D0FO01418D

Su, Y.-R., Tsai, Y.-C., Hsu, C.-H., Chao, A.-C., Lin, C.-W., Tsai, M.-L., Mi, F.-L., 2015. Effect of grape seed proanthocyanidin–gelatin colloidal complexes on stability and in vitro digestion of fish oil emulsions. J. Agric. Food Chem. 63, 10200–10208. https://doi.org/10.1021/acs.jafc.5b04814

Sumida, Y., Niki, E., Naito, Y., Yoshikawa, T., 2013. Involvement of free radicals and oxidative stress in NAFLD/NASH. Free Radic. Res. 47, 869–880. https://doi.org/10.3109/10715762.2013.837577

Tao, W., Zhang, Y., Shen, X., Cao, Y., Shi, J., Ye, X., Chen, S., 2019. Rethinking the mechanism of the health benefits of proanthocyanidins: absorption, metabolism, and interaction with gut microbiota. Compr. Rev. Food Sci. Food Saf. 18, 971–985. https://doi.org/10.1111/1541-4337.12444

Thilakarathna, W.P.D.W., Rupasinghe, H.P.V., 2022. Optimization of the extraction of proanthocyanidins from grape seeds using ultrasonication-assisted aqueous ethanol and evaluation of anti-steatosis activity in vitro. Molecules 27, 1363. https://doi.org/10.3390/molecules27041363

Thilakarathna, W.P.D.W., Rupasinghe, H.P.V., 2019. Microbial metabolites of proanthocyanidins reduce chemical carcinogen-induced DNA damage in human lung epithelial and fetal hepatic cells in vitro. Food Chem. Toxicol. 125, 479–493. https://doi.org/10.1016/j.fct.2019.02.010

Thilakarathna, W.P.D.W., Langille, M.G.I, Rupasinghe, H.P.V., 2018. Polyphenol-based prebiotics and synbiotics: potential for cancer chemoprevention. Curr. Opin. Food Sci. 20, 51–57. https://doi.org/10.1016/j.cofs.2018.02.011

Trivedi, P.P., Jena, G.B., 2013. Ulcerative colitis-induced hepatic damage in mice: studies on inflammation, fibrosis, oxidative DNA damage and GST-P expression. Chem Biol Interact 201, 19–30. https://doi.org/10.1016/j.cbi.2012.12.004

Unusan, N., 2020. Proanthocyanidins in grape seeds: An updated review of their health benefits and potential uses in the food industry. J. Funct. Foods 67, 103861. https://doi.org/10.1016/j.jff.2020.103861

Wen, L., Duffy, A., 2017. Factors influencing the gut microbiota, inflammation, and type 2 diabetes. J. Nutr. 147, 1468S-1475S. https://doi.org/10.3945/jn.116.240754

Wong, V.W.-S., Wong, G.L.-H., Tsang, S.W.-C., Hui, A.Y., Chan, A.W.-H., Choi, P.C.-L., Chim, A.M.-L., Chu, S., Chan, F.K.-L., Sung, J.J.-Y., Chan, H.L.-Y., 2009. Metabolic and histological features of non-alcoholic fatty liver disease patients with different serum alanine aminotransferase levels. Aliment. Pharmacol. Ther. 29, 387–396. https://doi.org/10.1111/j.1365-2036.2008.03896.x

Yang, G., Xue, Y., Zhang, H., Du, M., Zhu, M.-J., 2015. Favourable effects of grape seed extract on intestinal epithelial differentiation and barrier function in IL10-deficient mice. Br. J. Nutr. 114, 15–23. https://doi.org/10.1017/S0007114515001415

Yogalakshmi, B., Sreeja, S., Geetha, R., Radika, M.K., Anuradha, C.V., 2013. Grape seed proanthocyanidin rescues rats from steatosis: A comparative and combination study with metformin. J. Lipids. https://doi.org/10.1155/2013/153897

Yun, S., Zhang, T., Li, M., Chen, B., Zhao, G., 2011. Proanthocyanidins inhibit iron absorption from soybean (glycine max) seed ferritin in rats with iron deficiency anemia. Plant Foods Hum. Nutr. 66, 212–217. https://doi.org/10.1007/s11130-011-0240-6

Zeng, X., Zhu, M., Liu, X., Chen, X., Yuan, Y., Li, L., Liu, J., Lu, Y., Cheng, J., Chen, Y., 2020. Oleic acid ameliorates palmitic acid induced hepatocellular lipotoxicity by inhibition of ER stress and pyroptosis. Nutr. Metab. 17, 11. https://doi.org/10.1186/s12986-020-0434-8

Zhang, L., Carmody, R.N., Kalariya, H.M., Duran, R.M., Moskal, K., Poulev, A., Kuhn, P., Tveter, K.M., Turnbaugh, P.J., Raskin, I., Roopchand, D.E., 2018. Grape proanthocyanidin-induced intestinal bloom of Akkermansia muciniphila is dependent on its baseline abundance and precedes activation of host genes related to metabolic health. J. Nutr. Biochem. 56, 142–151. https://doi.org/10.1016/j.jnutbio.2018.02.009

CHAPTER 4. PROANTHOCYANIDINS BIOTRANSFORMED BY *SACCHAROMYCES CEREVISIAE* PREVENT THE PATHOGENESIS OF STEATOSIS AND PROGRESSION TO STEATOHEPATITIS *IN VITRO*

The data presented in this chapter will be published in a peer-reviewed scientific journal.

Thilakarathna, W.P.D.W. and Rupasinghe H.P.V.

Author contributions: W.P.D.W. Thilakarathna performed all the experiments, analyzed the data, and drafted the manuscript. H.P. Vasantha Rupasinghe, the principal investigator, acquired the funds and resources, supervised the project, and reviewed the manuscript. Both authors have made intellectual contributions to the manuscript. Both authors have read and approved the final manuscript.

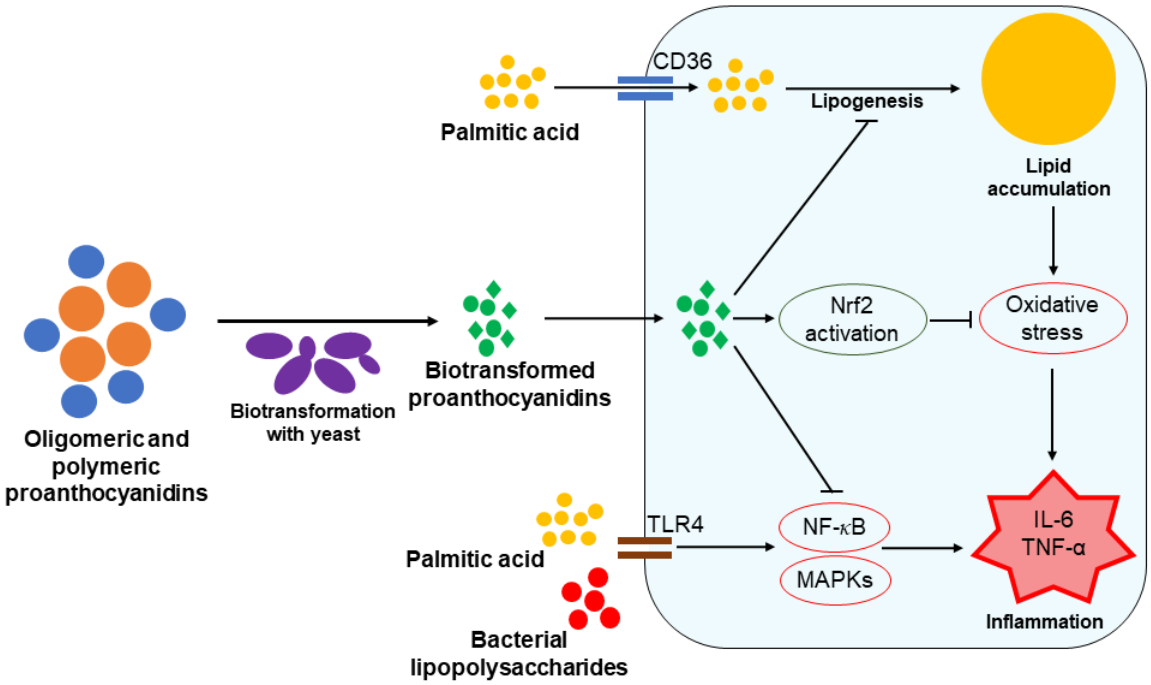

Chapter 4. Graphical abstract

4.1. ABSTRACT

Oligomeric and polymeric proanthocyanidins (PAC) were biotransformed with *Saccharomyces cerevisiae* (baker's yeast) to improve bioavailability and bioactivity. Biotransformation with yeast significantly increased the bioavailability of PAC *in vitro*. Bioactivity of biotransformed (BT)-PAC and non-BT-PAC was compared in palmitic acid (PA)-induced steatosis/nonalcoholic fatty liver disease (NAFLD) and PA together with bacterial lipopolysaccharides (LPS)-induced nonalcoholic steatohepatitis (NASH) models of AML12 hepatocytes. BT-PAC reduced the PA-induced cellular oxidative stress and lipid accumulation. BT-PAC may modulate key regulators of cellular lipid metabolism to mitigate PA-induced lipid accumulation. Activation of nuclear factor erythroid 2-related factor 2 (Nrf2) signalling by BT-PAC may aid mitigation of NAFLD. BT-PAC may prevent the progression of steatosis to NASH *in vitro* by suppressing cellular inflammation. Non-BT-PAC is less potent in the activation of Nrf2 signalling and reduction of cellular lipotoxicity and inflammation, compared to the BT-PAC. Yeast-mediated biotransformation significantly enhances the bioavailability of PAC and the bioactivity against steatosis and NASH.

Keywords: biotransformation, nonalcoholic fatty liver disease, nonalcoholic steatohepatitis, nuclear factor erythroid 2-related factor 2, proanthocyanidins, yeast

4.2. INTRODUCTION

Proanthocyanidins (PAC), also known as condensed tannins, are the oligomers or polymers of monomeric flavan-3-ol molecules such as catechin and epicatechin. PAC are abundantly found in plants and plant-derived food and agri-food wastes. The therapeutic effects of PAC are well elucidated against multiple diseases (Rauf et al., 2019). PAC are categorized as oligomeric PAC (OPAC) and polymeric PAC (PPAC) based on the degree of polymerization. PAC molecules with a degree of polymerization between 2 to 10 are the OPAC, and ones with a degree of polymerization over 10 are the PPAC (Vazquez-Flores et al., 2018). The majority of the dietary PAC in commonly consumed foods is polymeric (Gu et al., 2004). Thus, the bioavailability of dietary PAC is low, as PAC larger than tetramers are not absorbable (Ou and Gu, 2014). The unabsorbable PAC are catabolized into simple metabolites by the colonic microbiota. The therapeutic effects of these metabolites are previously established (Thilakarathna and Rupasinghe, 2019).

The potential of yeast strains to degrade OPAC and PPAC is demonstrated by several studies (Nogueira et al., 2008; Pedan et al., 2017). Also, PAC can alter metabolites produced by yeast cells through the regulation of metabolism (Li et al., 2020). However, the current knowledge of PAC metabolites and their therapeutic effects is limited. Probiotic yeast strains such as *Saccharomyces* (*S.*) *boulardii* are potent in ameliorating liver diseases (Cui et al., 2022). Nonalcoholic fatty liver disease (NAFLD) is the most common chronic liver disease in the world. About 30% of the global population is affected by NAFLD with the number of new cases predicted to increase rapidly (Younossi et al., 2023). The simple steatosis characterized by excessive hepatic lipid accumulation remains non-progressive in many NAFLD patients, nonetheless, the disease can progress into nonalcoholic

steatohepatitis (NASH), liver fibrosis, and hepatocellular carcinoma in some patients. NASH differs from steatosis by the manifestation of inflammation and progressive fibrosis in addition to excessive lipid accumulation (Takaki et al., 2013). Currently, no approved drugs are available for NASH (Cui et al., 2022), emphasizing the need for prevention and mitigation strategies. Probiotic *S. boulardii* can reduce the risk of liver diseases by inhibiting pathogens, protecting gut barrier function, preventing gut microbiota dysbiosis, and immunomodulation (Cui et al., 2022). Similarly, PAC have been demonstrated to ameliorate NAFLD through multiple mechanisms (Su et al., 2018). However, inefficient colonic catabolism of PAC (Niwano et al., 2022) together with low bioavailability may diminish the therapeutic effects of dietary PAC against steatosis and NASH. Thus, we attempted to biotransform OPAC and PPAC into bioavailable and biologically active metabolites by incubating them with *S. cerevisiae*. The bioactivity of biotransformed (BT)-PAC and non-BT-PAC was compared using steatosis and NASH models of AML12 cells *in vitro*. Biotransformation with *S. cerevisiae* may enhance the potential of PAC to mitigate steatosis/NASH, thus, enhancing hepatoprotective activity. The findings of this study are useful to develop PAC-based dietary supplements and functional foods to reduce the pathogenesis and progression of steatosis and NASH.

4.3. MATERIALS AND METHODS

4.3.1. PAC extraction, purification, and fractionation

PAC required for this study were extracted from grape seed powder (GSP) by using an acetone-based extraction method (Rupasinghe et al., 2019). The GSP was provided by Royal Grapeseed, Milton, NY, USA. The GSP originated from a mixture of seeds belonging to commercial grape varieties; *Vitis (V.) vinifera*, *V. labrusca*, and hybrids of

native American species with *V. vinifera*. Initially, the lipid in GSP was removed by ultrasonication with hexane. Crude PAC was extracted by using an acetone-based extraction solvent (70% acetone, 29.9% deionized (DI) water, and 0.1% formic acid *v:v:v*) with ultrasonication. The crude PAC was purified and fractionated by eluting through a flash chromatography column packed with brominated styrenic adsorbent beads. Sugars and simple phenolics in the crude PAC were removed by eluting the flash chromatography column with DI water. OPAC and PPAC were eluted from the flash chromatography column by using 80% aqueous ethanol and 70% aqueous acetone, respectively. The PAC concentrations in the OPAC and PPAC extracts were 54.4 ± 4.81 and 14.4 ± 2.35 mg catechin equivalence (CE)/g dry sample, respectively, as measured by a methylcellulose precipitable tannins assay (Thilakarathna et al., 2023). The mean degree of polymerization of the OPAC and PPAC were 3.41 ± 0.29 and 15.1 ± 0.15, respectively, as measured by a phloroglucinolysis-based PAC degradation method (Thilakarathna et al., 2023).

4.3.2. *S. cerevisiae* cultures

The yeast growth medium (YGM) was formulated by mixing yeast extract (3 g), malt extract (3 g), dextrose (10 g), and peptone (5 g) in DI water (1 L) and adjusting the final acidity to pH 6.2 level. A commercial yeast sample, *S. cerevisiae* (ex-bayanus, Lalvin EC-1118^{TM}) was purchased from Lallemand Inc., Montreal, QC, Canada. The commercial *S. cerevisiae* sample (5 g) was rehydrated by mixing with 50 mL of DI water at 35 °C for 20 min. After rehydration, 1 mL of the rehydrated *S. cerevisiae* sample was inoculated into 100 mL of the YGM and incubated at 30 °C. *S. cerevisiae* cultures were maintained by periodically inoculating fresh YGM with *S. cerevisiae* cultures and incubating them at 30 °C.

4.3.3. Toxicity of PAC in *S. cerevisiae* cultures

Toxicity of OPAC and PPAC in *S. cerevisiae* cultures was determined to find non-toxic concentrations for the PAC biotransformation experiments (Supplementary Fig. S4.1). YGM with different concentrations of OPAC and PPAC (10 – 1000 µg/mL) were prepared and filtered through 0.22 µm syringe filters. YGM-PAC aliquots of 950 µL were inoculated with 50 µL of fresh *S. cerevisiae* culture (5% inoculation) of 1.0 optical density at 600 nm (OD_{600}). Inoculated samples were incubated at 30 °C for 24 h and pipetted into a 96-well plate (200 µL/well) in triplicates after mixing thoroughly. OD_{600} value of each well was measured, and results were expressed as % growth of *S. cerevisiae* compared to the negative control.

4.3.4. Biotransformation of PAC by *S. cerevisiae*

The potential of *S. cerevisiae* to biotransform OPAC and PPAC into simple metabolites was studied. YGM aliquots (5 mL) with OPAC or PPAC (250 µg/mL) was inoculated with a fresh *S. cerevisiae* culture (5% inoculation with a *S. cerevisiae* culture of 1.0 OD_{600}) and incubated for 0 – 8 days at 30 °C while continuously shaking. Biotransformation of OPAC and PPAC was conducted in YGM with three different concentrations of dextrose (25, 50, and 100% of the recommended dextrose quantity) to understand the effect of YGM sugar concentration on the PAC biotransformation process. PAC metabolites generated during the biotransformation were extracted by ethyl acetate-based liquid-liquid separation. Initially, *S. cerevisiae* cells were lysed by ultrasonication for 10 min. *S. cerevisiae* cells and cell debris were separated from the culture medium by centrifugation at 3,000 × *g* for 10 min. The culture medium devoid of *S. cerevisiae* cells was mixed with 2.5 mL of ethyl acetate and vortexed for 5 min. The aqueous YGM and

ethyl acetate layers were allowed to separate for 1 h and the ethyl acetate layer was collected without disturbing the YGM layer. The collected ethyl acetate layer was completely evaporated under nitrogen gas. Extracted PAC metabolites were redissolved in 1 mL of 80% aqueous ethanol. The potential of *S. cerevisiae* to biotransform PAC was evaluated by measuring variations of total PAC content (TPAC) and total phenolic content (TPC). The TPAC variation was measured by 4-dimethylaminocinnamaldehyde (DMAC) assay and results were expressed as µg CE/mL YGM (Bhullar and Rupasinghe, 2015). The TPC variation was measured by Folin-Ciocalteu (FC) assay and results were expressed as µg gallic acid equivalence (GAE)/mL YGM (Thilakarathna et al., 2021). Also, variations of PAC monomers, catechin and epicatechin, concentrations during the PAC biotransformation in YGM with 50% dextrose (50% YGM) were studied by ultra-high performance liquid chromatography (UHPLC)-electrospray ionization (ESI)-mass spectrometry (MS) (Rupasinghe et al., 2019).

4.3.5. Detection and quantification of metabolites generated by PAC biotransformation

The metabolites generated by the *S. cerevisiae*-mediated biotransformation of OPAC and PPAC were initially detected by high-resolution mass spectrometry (HRMS). The biotransformation process was scaled-up to 40 mL and conducted for four and eight days. PAC biotransformation and metabolites extraction was conducted as described in the section 4.3.4. After the nitrogen evaporation of the ethyl acetate layer, the extracted PAC metabolites were redissolved in 500 µL of 80% aqueous ethanol to prepare a PAC metabolite concentrate for HRMS analysis. The HRMS analysis was conducted using a UHPLC ESI Xevo G2-XS QT high-resolution mass spectrometer (Waters, Beverley, MA,

USA). Identification of PAC metabolites was performed in the data-dependant acquisition (DDA) mode and DDA data were analyzed by the Compound Discoverer software version 3.3 (Thermo Fisher Scientific, Waltham, MA, USA). The Compound Discoverer workflow was (Supplementary Fig. S4.2) consisted of multiple databases, mzCloud, Arita Lab 6549 Flavonoid Structure Database, Natural Products Atlas (van Santen et al., 2022), FooDB, and Phenol-Explorer (Rothwell et al., 2013) to identify PAC metabolites generated by the *S. cerevisiae*-mediated PAC biotransformation. The software was able to identify many possible PAC metabolites at both ms1 and ms2 levels. PAC metabolites that are most likely to be produced by the biotransformation process and detected at the ms2 level were further analyzed by UHPLC-ESI-MS to confirm their presence and quantified by using reference analytical standards (Rupasinghe et al., 2019).

4.3.6. Cell lines and culture conditions

Cell uptake and biological activity of BT-PAC *vs.* non-BT-PAC were compared by using Caco-2 and AML12 cells, respectively. Caco-2 (HBT-37™) colorectal adenocarcinoma epithelial cells and AML12 (CRL-2254™) normal mouse hepatocytes were purchased from the ATCC®, Manassas, VA, USA. Caco-2 cells were cultured in minimum essential medium (MEM) supplemented with 20% fetal bovine serum (FBS), L-glutamine (4 mM), and penicillin (100 U/mL)-streptomycin (100 µg/mL). AML12 cells were cultured in DMEM:F12 medium supplemented with 10% FBS, 5 mL of 100× insulin-transferrin-selenium (ITS) solution, dexamethasone (40 ng/mL), and penicillin (100 U/mL)-streptomycin (100 µg/mL). Caco-2 and AML12 cells were cultured at 37 °C in a humidified incubator with 5% CO_2 atmosphere. Cells were sub-cultured at the 80% confluency level.

4.3.7. *In vitro* bioavailability of BT-PAC *vs*. non-BT-PAC

The *in vitro* bioavailability of BT-PAC and non-BT-PAC was compared by measuring the uptake into Caco-2 cells and permeability through Caco-2 cell monolayers. Non-cytotoxic concentrations of BT-PAC and non-BT-PAC in Caco-2 cells were determined by MTS cell viability assay (Supplementary Fig. S4.3-1) (Thilakarathna and Rupasinghe, 2022). Initially, non-cytotoxic concentrations of BT-PAC and non-BT-PAC with similar CE (µg CE/mL) values were determined by the DMAC assay to make rational comparisons. The CE values of BT-OPAC and BT-PPAC at 500 µg/mL level were similar to non-BT-OPAC at 54 µg/mL and to non-BT-PPAC at 37 µg/mL levels, respectively.

4.3.7.1. Cellular uptake of BT-PAC and non-BT-PAC

Caco-2 cells were seeded in 6-well plates at a density of 0.5×10^6 cells/well and incubated at 37 °C for four days to reach confluency. Cells were treated with BT-OPAC (500 µg/mL), BT-PPAC (500 µg/mL), non-BT-OPAC (56 µg/mL), and non-BT-PPAC (38 µg/mL) for 4 h. Cells were gently washed (×3) with phosphate-buffered saline (PBS) and harvested by using trypsin-EDTA solution. Cells were separated from the cell culture medium and trypsin-EDTA solution by centrifuging at 2,000 × *g* for 5 min. The cell pellet was washed in PBS and centrifuged again at 2,000 × *g* for 5 min. The resulting cell pellet was mixed with 200 µL of 80% aqueous ethanol and ultrasonicated for 5 min. The aqueous ethanol-cell suspension was centrifuged at 3,000 × *g* for 15 min to remove cell debris and collect PAC dissolved in the aqueous ethanol. PAC concentrations in aqueous ethanol extracts were determined by the DMAC assay (Bhullar and Rupasinghe, 2015).

4.3.7.2. Permeation of BT-PAC and non-BT-PAC through Caco-2 cell monolayers

Caco-2 cells were seeded in 6-well transwell membrane plates at a density of 2.5 × 10^5 cells/well and incubated at 37 °C for eight days to obtain Caco-2 cell monolayers (Thilakarathna et al., 2023). The basolateral chambers (bottom) of the wells were pipetted with 500 µL of PBS solution. The apical chambers (top) of the wells were pipetted with 1 mL of culture medium containing BT-OPAC (500 µg/mL), BT-PPAC (500 µg/mL), non-BT-OPAC (56 µg/mL), or non-BT-PPAC (38 µg/mL). After 6 h, PBS solution in the basolateral chambers was collected and analyzed for PAC concentrations by the DMAC assay (Bhullar and Rupasinghe, 2015).

4.3.8. Potential of BT-PAC *vs.* non-BT-PAC to ameliorate steatosis

The biological activity of BT-PAC and non-BT-PAC was compared in a steatosis model of AML12 cells *in vitro*. The potential of BT-PAC and non-BT-PAC to ameliorate steatosis was evaluated by measuring the reductions in palmitic acid (PA)-induced cellular oxidative stress and cellular lipid accumulation. Initially, non-cytotoxic concentrations of BT-PAC and non-BT-PAC in AML12 cells were established by the MTS cell viability assay (Supplementary Fig. S4.3-2) (Thilakarathna and Rupasinghe, 2022). To measure the cellular oxidative stress reduction, cells were pre-treated with non-BT-PAC at 25 µg/mL level and with PAC biotransformed for 1, 2, 4, and 8 days at 25 and 250 µg/mL levels for 24 h. After the pre-treatment with PAC, cells were exposed to PA (200 µM) in a complete DMEM:F12 culture medium for 24 h to induce cellular oxidative stress. PA-induced cellular oxidative stress reduction was studied by measuring cellular reactive oxygen species (ROS) concentrations by the 2′,7′-dichlorofluorescein diacetate (DCFDA) assay (Thilakarathna and Rupasinghe, 2022).

To measure the cellular lipid accumulation reduction, cells were pre-treated with non-BT-PAC (25 μg/mL) and the PAC biotransformed for 4 and 8 days (25 and 250 μg/mL) for 24 h. Then, cells were exposed to PA (200 μM) in DMEM:F12 complete culture medium for 24 h. Reduction of the PA-induced cellular lipid accumulation was visualized and quantified by the oil red O (ORO) staining of the cellular lipids (Thilakarathna and Rupasinghe, 2022).

4.3.9. BT-PAC-mediated mechanisms to ameliorate cellular lipid accumulation

AML12 cells were serum-starved for 12 h by using FBS-free DMEM:F12 culture medium. Cells were pre-treated with non-BT-OPAC, non-BT-PPAC, OPAC biotransformed for four days (BT-$OPAC_4$), and PPAC biotransformed for four days (BT-$PPAC_4$) for 24 h. Cells were pretreated with non-BT-PAC at 25 μg/mL level and with BT-PAC at 25 and 250 μg/mL levels. Then, cells were exposed to PA (200 μM) in complete DMEM:F12 culture medium for 24 h. Cellular protein levels of key regulators of lipid metabolism were measured by the western blot technique (Thilakarathna and Rupasinghe, 2019). Primary antibodies, peroxisome proliferator-activated receptor (PPAR)-α (sc-398394) and sterol regulatory element-binding protein 1 (SREBP1, sc-13551) were purchased from Santa Cruz Biotechnology, Dallas, Texas, USA. The cluster of differentiation 36 (CD36, 74002S), acetyl-CoA carboxylase (ACC, 3676S), phospho (*p*)-ACC (*p*-ACC, 11818S), fatty acid synthase (FAS, 3180S), PPAR-γ (2443S), and β-actin (12620S) were purchased from Cell Signaling Technology, Inc., Danvers, MA, USA. Anti-mouse (7076P2) and anti-rabbit (7074S) secondary antibodies were purchased from the same company. β-Actin was used as the housekeeping protein to normalize the levels of targeted proteins and results were expressed relative to the negative control.

4.3.10. Activation of nuclear factor erythroid 2-related factor 2 (Nrf2) pathway by BT-PAC

AML12 cells were serum-starved for 12 h by using FBS-free DMEM:F12 culture medium. Cells were pre-treated with non-BT-OPAC, non-BT-PPAC, BT-$OPAC_4$, and BT-$PPAC_4$ for 3 h and exposed to PA (200 μM) in complete DMEM:F12 culture medium for 3 h. Cells were pretreated with non-BT-PAC at 25 μg/mL level and with BT-PAC at 25 and 250 μg/mL levels. The potential of BT-PAC to activate the Nrf2 pathway was evaluated by the visualization of Nrf2 nuclear translocation (Pilar Valdecantos et al., 2015) and by measuring the integrated fluorescence intensity/cell by the CellProfiler software (version 4.2.1) as previously described (Bray et al., 2015).

Phosphorylation of Nrf2 (*p*-Nrf2/ Nrf2 ratio) and the levels of kelch-like ECH-associated protein 1 (KEAP1) protein and catalase, glutathione peroxidase (GPx), and superoxide dismutase (SOD) antioxidant enzymes were also measured by the western blotting (Thilakarathna and Rupasinghe, 2019). *β*-Actin was used as the housekeeping protein to normalize the expressions of targeted proteins and results were expressed relative to the negative control. Nrf2 (ab62352) and *p*-Nrf2 (ab76026) primary antibodies were purchased from Abcam, Cambridge, MA, USA. KEAP1 (4678S), catalase (14097S), GPx (3206S), and SOD (4266S) primary antibodies were purchased from Cell Signaling Technology, Inc., Danvers, MA, USA.

4.3.11. Potential of BT-PAC to prevent progression of steatosis to NASH

AML12 cells were serum-starved for 12 h and pre-treated with non-BT-OPAC, non-BT-PPAC, BT-$OPAC_4$, and BT-$PPAC_4$ in complete DMEM:F12 culture medium for 24 h. Cells were pretreated with non-BT-PAC at 25 μg/mL level and with BT-PAC at 25

and 250 µg/mL levels. Cells were first exposed to PA (200 µM) in complete DMEM:F12 culture medium for 24 h to induce cellular lipid accumulation. Then, the cells were exposed to bacteria lipopolysaccharides (LPS, 100 ng/mL) from *Escherichia coli* O55:B5 (MilliporeSigma, Oakville, ON, Canada) for 6 h to induce inflammation in the presence of PA (200 µM). Expression of inflammatory cytokines, Interleukin (IL)-1β, IL-6, and tumour necrosis factor (TNF)-α were evaluated by measuring the mRNA expression levels by reverse transcription-quantitative polymerase chain reaction (RT-qPCR) assay. mRNA expression levels of toll-like receptor 4 (TLR4), extracellular signal-regulated protein kinase 1 (ERK1), ERK2, c-Jun N-terminal Kinase (JNK), nuclear factor-kappa-light-chain-enhancer of activated B cells (NF-κB), c-Fos, and c-Jun were measured to study the mechanisms of PAC-mediated cellular inflammation reduction. To conduct the RT-qPCR assay, cells were extracted, and RNA was isolated and purified by Aurum™ Total RNA Mini Kit (7326820) and cDNA was synthesized from the extracted RNA by using iScript™ cDNA Synthesis Kit (1708891) according to the instructions given by the manufacturer. PCR amplification was achieved by using a thermal cycle of; 95 °C for 1 min, 40 repeated cycles of 95 °C for 15 s, and 66 °C for 30 s with SsoAdvanced™ Universal SYBR® Green Supermix (172-5274). Data were collected and analyzed by the Bio-Rad CFX Maestro 2.3 software (Bio-Rad, Hercules, CA, USA). β-Actin and GAPDH were used as the reference genes to normalize the expression of targeted genes. Results were expressed as normalized $2-^{\Delta\Delta Ct}$ relative to the negative control. PCR primers for the targeted mRNA (Supplementary table S4.1) and all the kits were purchased from Bio-Rad Laboratories (Canada) Ltd. (Mississauga, ON, Canada).

Expressions of the genes measured by the RT-qPCR were also measured at the protein level by the western blot technique (Thilakarathna and Rupasinghe, 2019). TLR4 (14358S), *p*-ERK1/2, ERK1/2 (4695S), *p*-JNK (9251S), JNK (9252S), *p*-NF-κB (3033S), NF-κB (4764S), *p*-c-Jun (2361S), c-Jun (9165S), *p*-c-Fos (5348S), c-Fos (4384S), IL-1*β* (31202), IL-6 (12912S), and TNF-*α* (3707S) primary antibodies were purchased from Cell Signaling Technology, Inc., Danvers, MA, USA. *β*-Actin was used as the housekeeping protein to normalize the expression of targeted proteins and results were expressed relative to the negative control.

4.3.12. Statistical analysis

The experimental data were analyzed by the Minitab® statistical software (version 19.2020.1). Results were expressed as mean ± standard deviation of three individual experiments. Means were compared by the one-way analysis of variance (ANOVA) with Tukey's multiple mean comparisons at 95% confidence level.

4.4. RESULTS

4.4.1. Potential of *S. cerevisiae* cultures to biotransform PAC

The TPAC and TPC gradually increased during the biotransformation of OPAC and PPAC up to four days and plateaued thereafter (Fig. 4.1a and b). This TPAC and TPC increment was observed in all three YGM with different concentrations of dextrose. However, the increment of TPAC and TPC was significantly higher when OPAC and PPAC biotransformation were conducted in 50% YGM. A slight reduction in the TPAC was observed within the first six hours (0.25 days) of the OPAC and PPAC biotransformation. A drastic increment in the TPAC and TPC was not observed in the *S. cerevisiae* controls incubated without PAC in the YGM. In 50% YGM, the catechin and

epicatechin concentrations gradually increased for up to four days and plateaued thereafter (Fig. 4.1c). Catechin and epicatechin were not detected in the *S. cerevisiae* controls incubated without PAC in YGM.

4.4.2. Metabolites generated by PAC biotransformation

HRMS analysis suggested the presence of many unique metabolites in *S. cerevisiae* cultures incubated with OPAC and PPAC compared to the controls. Several metabolites are most likely to be the result of the PAC biotransformation process since they are present exclusively in the *S. cerevisiae* cultures incubated with OPAC and PPAC (Table 4.1). Interestingly, concentrations of some of these metabolites significantly vary between the PAC biotransformed for four and eight days. *S. cerevisiae* cultures may biotransform OPAC and PPAC into unique simple metabolites and the length of the biotransformation process can significantly affect the concentrations of these metabolites.

4.4.3. Bioavailability of BT-PAC *vs.* non-BT-PAC

Caco-2 cells could uptake significantly higher amounts of BT-OPAC$_{4-8}$ and BT-PPAC$_{4-8}$ compared to the non-BT-OPAC and non-BT-PPAC, respectively (Fig. 4.2a.i). Also, the permeability of BT-OPAC$_{4-8}$ and BT-PPAC$_{4-8}$ was significantly higher compared to their non-biotransformed counterparts (Fig. 4.2a.ii). Biotransformation of OPAC and PPAC with *S. cerevisiae* cultures can significantly enhance their bioavailability *in vitro*.

4.4.4. Potential of BT-PAC *vs.* non-BT-PAC to ameliorate PA-induced lipotoxicity

The reductions in PA-induced lipotoxicity were compared by measuring the cellular ROS generation and cellular lipid accumulation. Both non-BT-PAC and BT-PAC significantly reduced the cellular ROS levels elevated by the PA (Fig. 4.2b). The effect of

non-BT-PAC and PAC biotransformed for one and two days was similar in cellular ROS reduction. The highest potential for ROS reduction was observed for BT-OPAC$_{4-8}$ and BT-PPAC$_{4-8}$. Interestingly, ROS reduction by BT-OPAC$_{4-8}$, and BT-PPAC$_{4-8}$ was not concentration dependant. Similar to the cellular ROS reduction, both non-BT-PAC and BT-PAC significantly reduced the PA-induced cellular lipid accumulation (Fig. 4.2c). However, the reduction of the cellular lipid accumulation was more prominent for BT-OPAC$_4$ and BT-PPAC$_4$ compared to their non-biotransformed counterparts. Also, higher concentrations (25 *vs*. 250 μg/mL) of BT-OPAC$_4$ and BT-PPAC$_4$ were more effective in reducing cellular lipid accumulation. Biotransformation of OPAC and PPAC with *S. cerevisiae* cultures significantly enhanced their ability to ameliorate PA-induced lipotoxicity *in vitro*.

4.4.5. Mechanisms of BT-PAC in the reduction of PA-induced cellular lipid accumulation

The expressions of key regulators of cellular lipid metabolism were measured at the protein level. PA substantially increased the protein levels of CD36, SREBP1, ACC, FAS, and PPARγ_{1-2}, while reducing PPAR-α to promote cellular lipid accumulation. BT-OPAC$_4$ and BT-PPAC$_4$ could significantly reduce the cellular protein levels of CD36, SREBP1, ACC, FAS, and PPAR-γ_{1-2} while increasing the level of PPAR-α to mitigate lipid accumulation in AML12 cells (Fig. 4.3). The non-BT-PAC depicted similar effect on the expressions of targeted lipid metabolism regulators. However, these effects were not statistically significant. BT-PAC can regulate cellular lipid metabolism to ameliorate PA-induced lipid accumulation.

4.4.6. Activation of the Nrf2 pathway by BT-PAC

The potential of BT-$OPAC_4$ and BT-$PPAC_4$ to activate the Nrf2 pathway under PA-induced lipotoxicity was studied. Exposure of the cells to PA did not significantly influence the nuclear translocation of Nrf2 (Fig. 4.4a). Both non-BT-PAC and BT-PAC increased the nuclear translocation of Nrf2 compared to the vehicle control. The promotion of Nrf2 nuclear translocation by BT-$OPAC_4$ and non-BT-PAC was similar at 25 μg/mL level. However, BT-$PPAC_4$ at 25 μg/mL level could significantly increase the Nrf2 nuclear translocation compared to the non-BT-PAC. Moreover, the ability of BT-$OPAC_4$ and BT-$PPAC_4$ to promote Nrf2 nuclear translocation was concentration-dependent with higher concentrations depicting a better ability to translocate Nrf2 into the nucleus (Fig. 4.4a). Activation of the Nrf2 pathway by BT-PAC was further studied by measuring the cellular protein levels of key Nrf2 regulators and Nrf2 pathway downstream antioxidant enzymes (Fig. 4.4b). PA did not significantly influence the cellular level of KEAP1 protein and activation (phosphorylation) of Nrf2. However, PA diminished the levels of antioxidant enzymes, GPx, and SOD. Both BT-$OPAC_4$ and BT-$PPAC_4$ could significantly reduce the level of KEAP1 protein and increase the phosphorylation of Nrf2, suggesting the potential of BT-PAC to activate the Nrf2 pathway. Furthermore, BT-$OPAC_4$ and BT-$PPAC_4$ increased the cellular levels of the antioxidant enzyme catalase and restored the GPx and SOD antioxidant enzyme levels diminished by the PA. Non-BT-PAC did not influence the levels of KEAP1 protein and phosphorylation of Nrf2. Also, non-BT-PAC could not increase the catalase enzyme level and restore the GPx and SOD enzyme levels reduced by the PA. The potential of OPAC and PPAC to activate the Nrf2 pathway under PA-induced lipotoxicity can be enhanced by biotransformation with *S. cerevisiae*.

4.4.7. Potential of BT-PAC to reduce PA and LPS-induced cellular inflammation

Exposure of cells to PA and LPS significantly increased the cellular mRNA levels of the proinflammatory cytokines IL-6 and TNF-α (Fig. 4.5g and h). The mRNA levels of the proinflammatory cytokine regulators, TLR4, ERK1, ERK2, JNK, and c-Fos were also significantly increased by PA and LPS (Fig. 4.5g – f). However, the mRNA level of NF-κB, a major regulator of proinflammatory cytokines, was not affected by PA and LPS. Both non-BT-PAC and BT-PAC reduced the TNF-α mRNA levels upregulated by PA and LPS (Fig. 4.5h). The reduction of elevated TNF-α mRNA levels by BT-OPAC$_4$ and non-BT-OPAC was similar at 25 µg/mL concentration. However, BT-OPAC$_4$ at higher concentrations (250 µg/mL) and BT-PPAC$_4$ at both 25 and 250 µg/mL concentrations could significantly reduce TNF-α mRNA levels compared to non-BT-PAC. Non-BT-PAC and BT-OPAC$_4$ at 25 µg/mL concentration did not reduce the elevated IL-6 mRNA levels. BT-OPAC$_4$ at 250 µg/mL concentration and BT-PPAC$_4$ at both 25 and 250 µg/mL concentrations significantly reduced the elevated IL-6 mRNA levels (Fig. 4.5g). BT-OPAC$_4$ and BT-PPAC$_4$ were effective in the reduction of cellular TLR4, ERK1, ERK2, JNK, and c-Fos mRNA levels. Even though, not effective as BT-PAC, non-BT-OPAC and non-BT-PPAC significantly reduced the mRNA levels of ERK1 and JNK, respectively. The RT-qPCR analysis was unable to detect any expression for the IL-1β, p38, and c-Jun.

We further studied the effects of BT-PAC on the expression of proinflammatory cytokines and their regulators at the cellular protein level (Fig. 4.6). Exposure of cells to PA and LPS significantly increased the protein levels of IL-6, TNF-α, and TLR4 together with the activation (phosphorylation) of ERKs, JNK, and c-FOS. However, contradicting RT-qPCR results, exposure to PA and LPS significantly promoted the phosphorylation of

NF-κB and c-Jun in the cells. Both non-BT-PAC and BT-PAC were effective in the reduction of elevated TNF-α protein levels in the cells (Fig. 4.6i). However, BT-PAC was more effective in the reduction of TNF-α protein levels. Only BT-PAC could significantly reduce the elevated IL-6 protein levels (Fig. 4.6h). Similarly, BT-PAC was effective in the reduction of NF-κB, c-FOS, and c-Jun phosphorylation and cellular levels of TLR4. Both BT-PAC and non-BT-PAC reduced the activation of ERKs and JNK. However, BT-PAC was more effective in the suppression of ERKs phosphorylation compared to the non-BT-PAC. Biotransformation of the OPAC and PPAC can boost their potential to ameliorate cellular inflammation induced by the PA and LPS.

4.5. DISCUSSION

The potential of *S. cerevisiae* cultures to biotransform OPAC and PPAC was studied. The ability of *S. cerevisiae* and other bacteria to degrade or metabolize PAC is reported in previous studies (Pedan et al., 2017). Considerable increments in the monomeric and dimeric PAC concentrations were observed during cocoa beans fermentation. Interestingly, an increase of monomeric and dimeric PAC had occurred amidst declining concentrations of PAC with a degree of polymerization of three and higher (Pedan et al., 2017), suggesting the depolymerization of large PAC molecules. During the PAC biotransformation process, the TPAC significantly increased. PAC degradation may have increased the number of terminal units for the DMAC to react with (Wallace and Giusti, 2010) and depict higher PAC concentrations by the DMAC assay. A slight reduction in the TPAC during the first six hours (0.25 days) of OPAC and PPAC biotransformation was observed. A similar reduction of total water-soluble PAC occurred during the fermentation of sorghum meal (Bvochora et al., 1999). The initial reduction of

PAC may have been caused by the high affinity and adsorption of PAC molecules to the *S. cerevisiae* cell wall. The PAC affinity and adsorption to the *S. cerevisiae* cell wall are proven to grow weaker with fermentation (winemaking) (Mekoue Nguela et al., 2015), leading to increased concentrations of free PAC in YGM after the initial PAC reduction. The TPC in YGM also increased during the PAC biotransformation. A similar TPC increment was observed when green coffee beans were fermented with a mixture of *Saccharomyces* strains (Haile and Kang, 2019). In contrast, some studies have reported minimal effects or reduction of TPC during *S. cerevisiae*-mediated fermentation (Vernhet et al., 2020; Zou et al., 2017). It is important to note that these studies were designed to ferment plant material as a whole rather than biotransforming PAC alone. During the PAC biotransformation, TPAC and TPC were significantly influenced by the dextrose concentration in YGM. Limiting the dextrose (sugar) in YGM may have prompted *S. cerevisiae* cultures to utilize PAC as an alternative carbon source. Yeast strains isolated from rotten wood are capable of assimilating tannic acid (polyphenol) and other simple phenolics when cultured in a sugar-free growth medium (Middelhoven, 2006). Further studies are required to investigate the influence of growth medium sugar levels on the degradation of PAC by *S. cerevisiae*.

In this study, *S. cerevisiae* cultures were able to biotransform OPAC and PPAC into many simple metabolites. Several metabolites identified only in the BT-PAC, including pyrogallol, hydroxyphenyl acetates, hydroxycinnamates, and benzoates are commonly known metabolites derived by microbial degradation of PAC (Thilakarathna and Rupasinghe, 2019). Gallic acid and 4-hydroxyphenylacetamide were also detected exclusively in the BT-PAC. Increasing levels of gallic acid had been previously observed

during the alcoholic fermentation of persimmons (*Diospyros kaki*) by the *S. cerevisiae* (Zou et al., 2017). Hydroxylated phenylacetamide derivatives had been detected in the urine of individuals consuming whole-grain sourdough rye bread (Beckmann et al., 2013). Sourdough bread fermentation is governed by natural yeast and lactic acid bacteria (Pétel et al., 2017). However, these hydroxylated phenylacetamide derivatives were assumed to derive from the degradation of benzoxazinoids in the rye (Beckmann et al., 2013). Benzaldehydes and methyl-benzaldehydes had been detected during the fermentation of coffee beans (Ruta and Farcasanu, 2021) and bee pollens (Zhang et al., 2022) with different yeast strains. Also, 3-aminosalicylic acid had been detected exclusively in the bee pollens fermented with *S. cerevisiae* (Zhang et al., 2022). Both coffee beans (Mehari et al., 2021) and bee pollens (Al-Salem et al., 2020) are sources of flavonoids and other phenolic compounds. 2-Aminoacetophenone had been identified as a metabolite generated during the fermentation of grape must (Álvarez-Fernández et al., 2020), suggesting the potential of yeasts to generate acetophenone derivatives. It is also important to consider the potential of PAC to alter metabolism in *S. cerevisiae* cells to generate unique metabolites. PAC can influence the expression of genes in *S. cerevisiae* important for vitamin, amino acids, carbohydrate, and lipid metabolism (Li et al., 2020). Phenyllactic acid is a product of yeasts by the catabolism of aromatic amino acids (Álvarez-Fernández et al., 2020). In the current study, PAC may have altered the *S. cerevisiae* metabolism to generate higher concentrations of 3-phenyllactic acid. Studies indicating the ability of *S. cerevisiae* to produce aminophenol and derivatives are limited.

Biotransformation with *S. cerevisiae* significantly increased the bioavailability of OPAC and PPAC *in vitro*. The bioavailability of the PAC depends on the degree of

polymerization with absorbability drastically declining with increasing degree of polymerization (Ou and Gu, 2014). In the current study, catechin and epicatechin levels significantly increased during the biotransformation process indicating the degradation of larger PAC molecules into smaller ones (Pedan et al., 2017). Thus, improvement in OPAC and PPAC bioavailability should have resulted from the degradation into molecules with a lesser degree of polymerization.

Initially, the bioactivities of non-BT-PAC and BT-PAC were compared in AML12 cells induced for lipotoxicity by PA. Subsequently, this cell model was further expanded into a NASH model by inducing inflammation using LPS, based on the two-hit theory of NASH pathogenesis. The first-hit signifies cellular lipid accumulation/steatosis and the second-hit induces cellular inflammation by LPS (Takaki et al., 2013). As demonstrated by the current study, PA can induce cellular lipid accumulation/steatosis, oxidative stress, and dysregulate lipid metabolism (Nissar et al., 2015; Trepiana et al., 2020). Both BT-PAC and non-BT-PAC effectively reduced the PA-induced ROS generation and lipid accumulation in the AML12 cells. PAC can ameliorate PA-induced lipotoxicity through multiple mechanisms. Procyanidin B2 can ameliorate oxidative stress induced by oleate and PA in human hepatocytes by scavenging the ROS, neutralizing superoxide anion radicals, and preserving the mitochondrial membrane potential (Su et al., 2018). The same study demonstrated the potential of procyanidin B2 to suppress cellular lipid accumulation through upregulating lipid degradation by increased lysosomal biogenesis (Su et al., 2018). Moreover, the potential of procyanidin B2 to ameliorate chemically-induced oxidative stress and DNA damage (Suraweera et al., 2023) can be beneficial to protect the liver against environmental toxins.

The potential of PA to induce cellular lipotoxicity through upregulation of *de novo* lipogenesis genes, CD36, SREBP1, PPAR-γ (Nissar et al., 2015), ACC, and FAS (Trepiana et al., 2020), is previously reported in multiple hepatic cell lines. PA also inhibits the expression of PPAR-α, an important regulator of cellular lipid homeostasis (Popeijus et al., 2014). In the current study, BT-PAC restored the cellular protein levels of these metabolic regulators disturbed by the PA overload. CD36 is a fatty acid transporter and overexpression of CD36 is known to associate with cellular lipid accumulation. PAC can ameliorate the overexpression of CD36 in rats administered with lard oil (Quesada et al., 2012). SREBP1 is a major regulator of cellular lipid metabolism (Li et al., 2017). The hypolipidemic effects of PAC are mediated by the suppression of SREBP1 through the upregulation of orphan nuclear receptor small heterodimer partner (SHP) (Del Bas et al., 2008) and inhibition of the mammalian target of rapamycin complex 1 (mTORC1) (Li et al., 2017). PPARs regulate multiple functions of hepatic lipid metabolism, including, fatty acid uptake, fatty acid storage, and β-oxidation. In NAFLD patients, hepatic expression of PPAR-γ is increased while PPAR-α is repressed (Liss and Finck, 2017). Procyanidin B2 can suppress the expression of PPAR-γ by regulating miR-483-5p in 3T3-L1 preadipocyte cells to inhibit adipogenesis (Zhang et al., 2017). PPAR-α facilitates the catabolism of cellular lipids. The ability of PAC to upregulate PPAR-α to mitigate hyperlipidemia had been demonstrated in rats (Yogalakshmi et al., 2013). PAC can also preserve cellular lipid homeostasis by suppressing the expression of ACC and FAS in type-2 diabetic mice (Tie et al., 2020). Regulation of ACC and FAS can occur through adenosine 5-monophosphate activated protein kinase (AMPK)/ACC/carnitine palmitoyl transferase 1A (CPT1A) signalling (Tie et al., 2020). The same study demonstrated that B-type procyanidins are

more effective in reducing cellular lipid accumulation compared to catechin and epicatechin. Among the B-type procyanidins, B1 and B3 procyanidins are more potent in reducing cellular lipid accumulation (Tie et al., 2020), suggesting that the hypolipidemic activity of PAC is structure dependent. In the current study, non-BT-PAC was not effective in restoring cellular protein levels of the tested lipid metabolic regulators disturbed by the PA. Biotransformation with *S. cerevisiae* may convert OPAC and PPAC into molecules more potent in reducing cellular lipid accumulation and BT-PAC may mitigate lipid accumulation through multiple mechanisms (Fig. 4.7a).

PAC can increase the activity of cellular antioxidant enzymes, GPx, SOD, and catalase to mitigate fatty acids-induced oxidative stress (Su et al., 2018). Nrf2 is a major regulator of the cellular antioxidant defense system, especially under oxidative stress. Upregulation of the cellular antioxidant enzymes is a key mechanism of Nrf2-mediated oxidative stress mitigation (Suraweera et al., 2020). Hepatic oxidative stress is a major contributor to NAFLD pathogenesis and steatosis progression into NASH. Therefore, Nrf2 activation is considered a novel therapeutic target for the mitigation of steatosis and NASH (Xu et al., 2019). PAC can upregulate hepatic activation of Nrf2 through multiple mechanisms (Liu et al., 2018; Truong et al., 2014). PAC drastically increases the Nrf2 activation in HepG2 cells through ERK and phosphoinositide 3-kinase (PI3K)/protein kinase B (AKT) signalling (Truong et al., 2014). In lead acetate-induced hepatotoxicity, PAC can ameliorate hepatic injury through activation of the Nrf2 pathway by AKT/glycogen synthase kinase 3 beta (GSK-3β)/Fyn signalling and downregulation of miRNA153 (Liu et al., 2018). In the current study, both non-BT-PAC and BT-PAC significantly increased the nuclear translocation of Nrf2. Activation of Nrf2 was more

prominent with BT-PAC as shown by the phosphorylation of Nrf2 and cellular levels of Nrf2 pathway downstream antioxidant enzymes. Activation of the Nrf2 by PAC is structure-dependent (Chen et al., 2022). Biotransformation of OPAC and PPAC by *S. cerevisiae* may increase the concentration of PAC metabolites that are more potent in Nrf2 activation.

PA and LPS can induce hepatic inflammation through TLR4 signalling by activating the NF-κB and mitogen-activated protein kinase (MAPK) inflammatory signalling cascades (Lee et al., 2017; Yang et al., 2022). Both BT-PAC and non-BT-PAC were effective in reducing the PA and LPS-induced inflammation as shown by the reduced TNF-α expression. However, BT-PAC demonstrated better inflammatory activity by significantly reducing the IL-6 expression in addition to the TNF-α. A similar reduction in the expressions of IL-6 and TNF-α by grape seed PAC administration had been observed in a mice model of chemically-induced steatohepatitis (Huang et al., 2020). In LX-2 human hepatic stellate cells induced for inflammation by LPS, grape seed PAC downregulated the expressions of proinflammatory cytokines IL-1β, IL-6, and IL-8 by suppressing TLR4/NF-κB signalling. Suppression of NF-κB may have been mediated by the downregulated expression of MAPK, JNK, ERK, and p38 (Lee et al., 2017). Similarly, PAC can inhibit the production of IL-6 and TNF-α in Raw 264.7 macrophages by suppressing the expressions of NF-κB and AP-1 transcription factor of c-Jun. Reduction of the inflammation in macrophages may have been mediated by the suppression of MAPK, ERK, JNK, and p38 (Limtrakul et al., 2016). Also, CD36 and PPARs (γ and α) regulate the cellular inflammatory response through NF-κB and AP-1 signalling (Cao et al., 2016; Korbecki et al., 2019). The ability of the CD36 to activate NF-κB and AP-1 in primary goat

mammary epithelial cells when stimulated by LPS is previously reported (Cao et al., 2016). Activation of PPARs during inflammatory responses can inhibit the activity of NF-κB (Korbecki et al., 2019). The BT-PAC was able to restore cellular protein levels of CD36 and PPARs altered by the PA. Therefore, CD36 and PPARs regulation by BT-PAC may have contributed to ameliorating PA and LPS-induced inflammation in the AML12 cells. Thus, BT-PAC may ameliorate cellular inflammation through multiple mechanisms (Fig. 4.7b).

The improved bioactivities of BT-PAC compared to non-BT-PAC can be due to the PAC metabolites generated during the biotransformation process. Pyrogallol had been recognized as an Nrf2 pathway activator *in vitro* (Liu et al., 2022). Both pyrogallol and gallic acid depict anti-inflammatory activity in macrophages stimulated by LPS. To mitigate LPS-induced inflammation, pyrogallol suppressed the NF-κB activation and promoted the MAPK/heme oxygenase-1 signalling (Chantarasakha et al., 2022). Phloroglucinol, another potential metabolite by the *S. cerevisiae*-mediated biotransformation of PAC, can ameliorate PA-induced NAFLD conditions in HepG2 cells (Drygalski et al., 2021). Phloroglucinol significantly reduces cellular oxidative stress, steatosis, and NF-κB expression while promoting the activity of cellular antioxidant enzymes (Drygalski et al., 2021). Multiple studies have demonstrated the benefits of gallic acid as a potential therapeutic agent for NAFLD (Fanaei et al., 2021; Zhang et al., 2023). The ability of gallic acid to reduce NAFLD risk through inhibiting *de novo* lipogenesis by the activation of AMPK signalling (Zhang et al., 2023) aligns with the findings of the current study. Activation of AMPK can upregulate PPAR-α, a major promoter of cellular lipid β-oxidation (Zhang et al., 2023). Moreover, gallic acid reduces inflammation in rats

with NAFLD by suppressing NF-κB expression and alleviating oxidative stress by promoting the activity of the Nrf2 pathway (Fanaei et al., 2021). Hydroxyphenylacetic acids are potent in reducing acetaminophen-induced hepatotoxicity by activation of the Nrf2 pathway (Zhao et al., 2018). Hydroxyphenylacetic acids can also inhibit the production of inflammatory cytokines in lung tissues and macrophages (Liu et al., 2014). Thus, 2-hydroxyphenylacetic acid generated by the PAC biotransformation may have contributed to Nrf2 activation and inflammation reduction in the current study. Colonic microbiota can convert hydroxyphenylacetic acids into benzoic acid derivatives (Manach et al., 2004). 3,5-Dihydroxybenzoic acid (protocatechuic acid) mitigates the risk of NAFLD by reducing oxidative stress and inflammation, regulating glucose and lipid metabolism, and increasing energy expenditure by brown adipose tissues (Gao et al., 2022). Derivatives of hydroxycinnamic acids are potent in ameliorating NAFLD pathogenesis through similar mechanisms (Alam et al., 2016). 2,4,6-Trihydroxyacetophenone, also known as phloracetophenone, protects the liver against carbon tetrachloride-induced damage by counteracting oxidative stress by increasing the activity of cellular antioxidant enzymes (Ferreira et al., 2010). Further studies are required to investigate the potential of 3-aminophenol, 4-hydroxyphenylacetamide, 3-aminosalicylic acid, and 3-phenyllactic acid to inhibit NAFLD pathogenesis. Biotransformation of the OPAC and PPAC by *S. cerevisiae* can significantly increase the bioactivity against cellular lipid accumulation and inflammation. Biotransformation of OPAC and PPAC by *S. cerevisiae* improved the bioavailability while generating PAC molecules of low degree of polymerization and bioactive metabolites potent in the reduction of risk of steatosis and NASH.

4.6 CONCLUSIONS

S. cerevisiae can biotransform OPAC and PPAC into simple metabolites and the ability of *S. cerevisiae* to biotransform PAC is affected by the dextrose (sugar) concentration in YGM. The bioavailability of PAC can be significantly increased by the biotransformation with *S. cerevisiae*. Both BT-PAC and non-BT-PAC ameliorate the PA-induced ROS production and lipid accumulation *in vitro*. However, BT-PAC is more effective in the reduction of ROS and cellular lipid accumulation. BT-PAC may reduce cellular lipid accumulation by modulating the expression of key regulators of *de novo* lipogenesis. BT-PAC is significantly more potent in the activation of the Nrf2 pathway and upregulation of cellular antioxidant enzyme levels compared to the non-BT-PAC. BT-PAC hinders the progression of steatosis to NASH *in vitro* by repressing the PA and LPS-induced inflammation through suppression of TLR4/NF-κB and TLR4/MAPK signalling cascades. Non-BT-PAC is less potent in the reduction of PA and LPS-induced inflammation compared to BT-PAC. The findings of this study are useful to develop PAC-based strategies to mitigate the pathogenesis of NAFLD and the progression of simple steatosis into NASH, by improving the bioavailability and bioactivity of PAC.

4.7. ACKNOWLEDGEMENT

This research received funds from the Discovery grant of the Natural Sciences and Engineering Research Council (NSERC) of Canada (RGPIN2016 05369) to H.P.V. Rupasinghe. The authors are grateful for the David A. Crowe Graduate Fellowship to W.P.D.W. Thilakarathna and Killam Chair funds of H.P.V. Rupasinghe.

Table 4.1. Concentrations of the proanthocyanidin metabolites exclusively detected in the yeast growth medium during the biotransformation of proanthocyanidins.

Metabolite	m/z (ESI^-)	Rt (min)	Concentrations in growth medium (µg/mL)			
			$OPAC_4$	$OPAC_8$	$PPAC_4$	$PPAC_8$
3-Aminophenol	108	1.54	0.16^b	0	0.30 ± 0.01^a	0
Pyrogallol and phloroglucinol (pyrogallol equivalence)	125	0.90	0.46 ± 0.07^a	0.43 ± 0.03^a	0.38 ± 0.03^a	0.35 ± 0.04^a
4-Hydroxyphenylacetamide	150	0.92	0.07 ± 0.01^b	0.06^b	0.14 ± 0.01^a	0.15 ± 0.01^a
2-HPA and 2,4-D-6-MB (2-HPA equivalence)	151	0.95	1.07 ± 0.08^b	1.10 ± 0.04^b	0.26^c	1.73 ± 0.07^a
3-Aminosalicylic	152	0.93	0.04^b	0.04^b	0.01^c	0.06^a
2,3-DHB and 3,5-DHB (2,3-DHB equivalence)	153	0.95	0.52 ± 0.04b	0.45 ± 0.01c	0.72 ± 0.02a	0.40 ± 0.02c
2-Hydroxycinnamic acid	163	0.91	0.15^c	0.17 ± 0.01^b	0.14^d	0.19^a
3-Phenyllactic acid	165	0.93	0.09 ± 0.01^d	0.18 ± 0.01^c	0.26 ± 0.01^b	0.33 ± 0.01^a
2,4,6-Trihydroxyacetophenone	167	0.92	0.21 ± 0.01^a	0.13 ± 0.01^b	0.08^c	0
Gallic acid	169	0.88	0.39 ± 0.09^a	0.41 ± 0.01^a	0.37 ± 0.02^a	0.34 ± 0.06^a

Concentrations of the potential proanthocyanidin (PAC) metabolites are given in means ± standard deviations of three individual experiments. Means that do not share a similar letter across a row are significantly different at 95% confidence level. 2,3-DHB, 2,3-Dihydroxybenzoic acid; 2,4-D-6-MB, 2,4-Dihydroxy-6-methylbenzaldehyde; 2-HPA, 2-hydroxyphenylacetic acid; 3,5-DHB, 3,5-dihydroxybenzoic acid; m/z (ESI^-), mass-to-charge ratio in electrospray ionization negative mode; $OPAC_4$: oligomeric PAC biotransformed for four days; $OPAC_8$: oligomeric PAC biotransformed for eight days; $PPAC_4$: polymeric PAC biotransformed for four days; $PPAC_8$: polymeric PAC biotransformed for eight days; Rt, retention time.

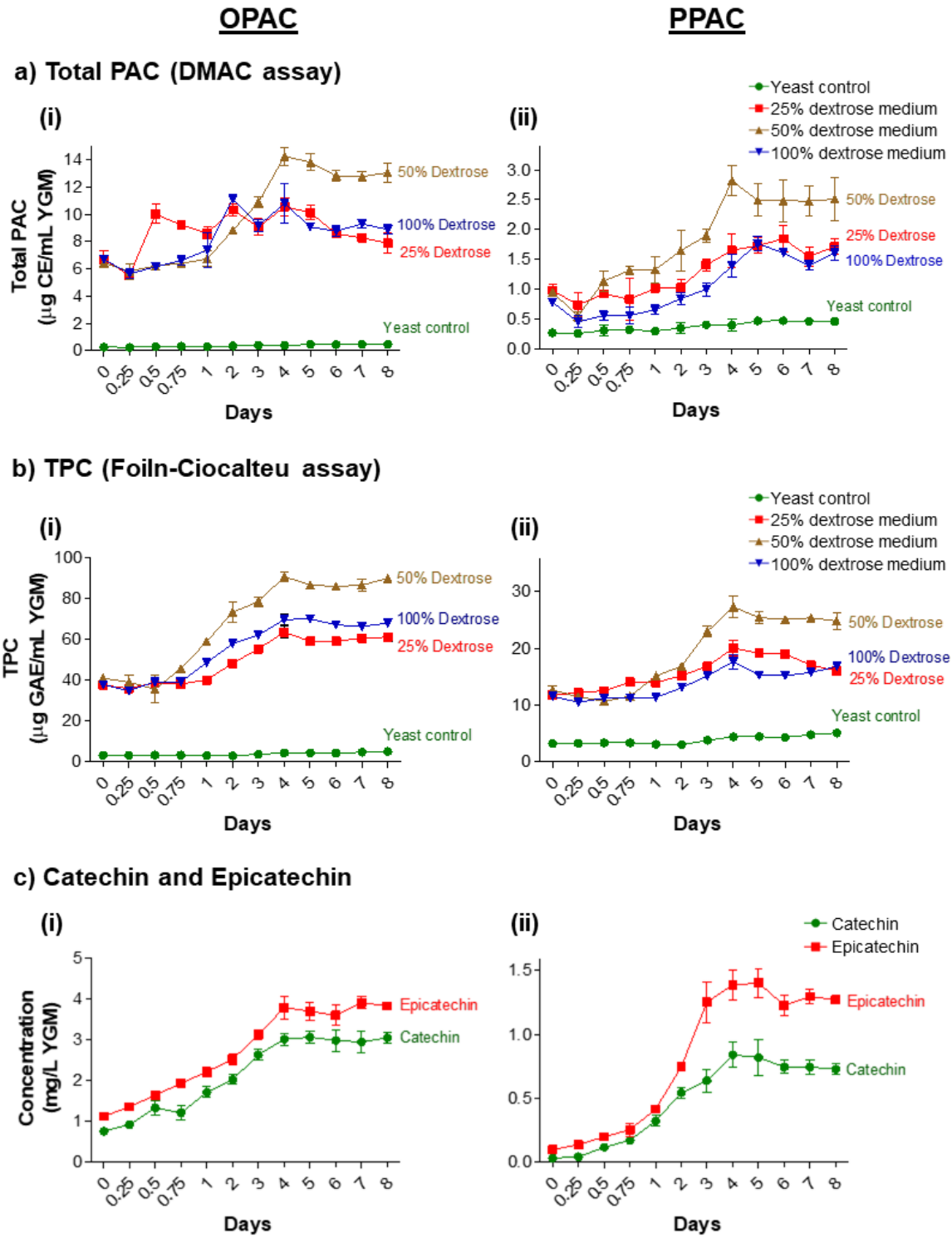
OPAC
PPAC
a) Total PAC (DMAC assay)
(i)
Total PAC (µg CE/mL YGM)
50% Dextrose
100% Dextrose
25% Dextrose
Yeast control
Days
(ii)
Yeast control
25% dextrose medium
50% dextrose medium
100% dextrose medium
50% Dextrose
25% Dextrose
100% Dextrose
Yeast control
Days
b) TPC (Foiln-Ciocalteu assay)
(i)
TPC (µg GAE/mL YGM)
50% Dextrose
100% Dextrose
25% Dextrose
Yeast control
Days
(ii)
Yeast control
25% dextrose medium
50% dextrose medium
100% dextrose medium
50% Dextrose
100% Dextrose
25% Dextrose
Yeast control
Days
c) Catechin and Epicatechin
(i)
Concentration (mg/L YGM)
Epicatechin
Catechin
Days
(ii)
Catechin
Epicatechin
Epicatechin
Catechin
Days

Figure 4.1. Variations of total proanthocyanidins content (TPAC) (a), total phenolic content (TPC) (b), and proanthocyanidin (PAC) monomers, catechin and epicatechin (c) in yeast growth medium (YGM) during the biotransformation of PAC. Oligomeric PAC (OPAC) and polymeric PAC (PPAC) were incubated with S. cerevisiae cultures for eight days to biotransform into simple metabolites. YGMs with three different dextrose levels (25, 50, and 100% of the original recipe) were experimented with for the PAC biotransformation. DMAC, 4-dimethylaminocinnamaldehyde; CE, catechin equivalence; GAE, gallic acid equivalence.

a) Bioavailability of non-BT-PAC and BT-PAC

i) Cellular uptake by Caco-2 cells

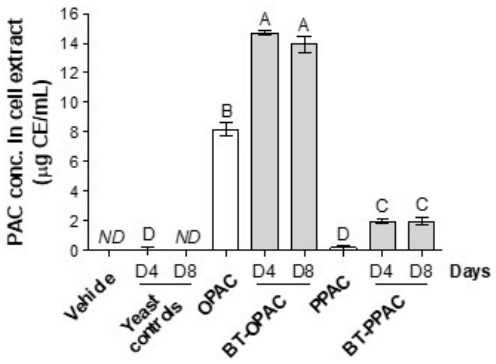

ii) Permeability through Caco-2 cell monolayer

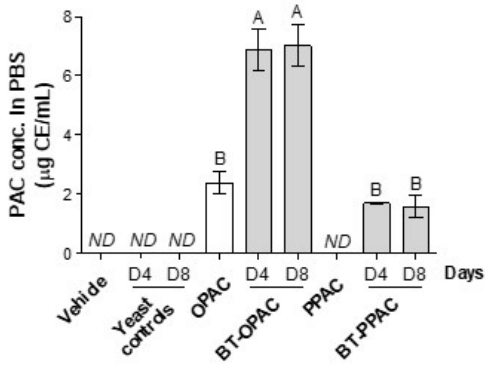

b) Potential of non-BT-PAC and BT-PAC to reduce PA-induced ROS production

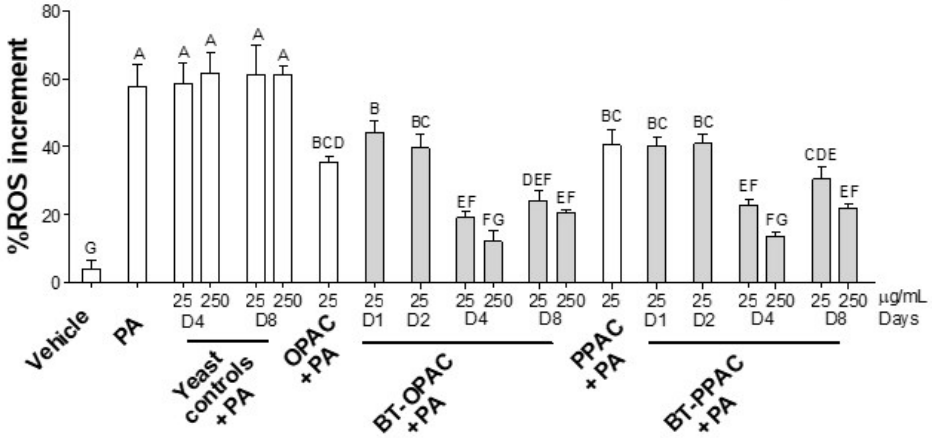

c) Reduction of PA-induced cellular lipid accumulation by non-BT-PAC and BT-PAC

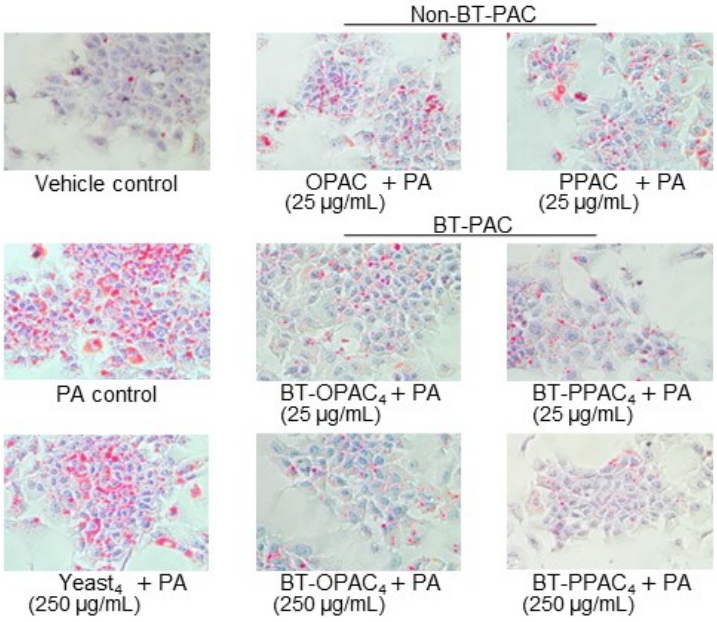

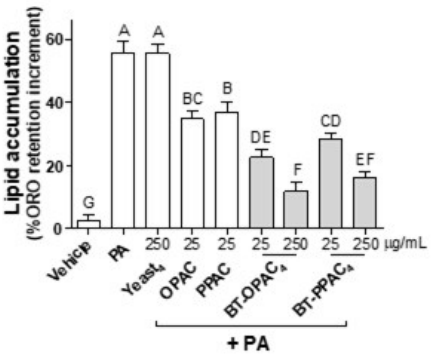

Figure 4.2. Comparison of the bioavailability of biotransformed (BT) and non-BT proanthocyanidins (PAC) (a), and the potential to ameliorate palmitic acid (PA)-induced cellular reactive oxygen species production (ROS) (b) and cellular lipid accumulation (c). Means that do not share a similar letter are significantly different. BT-$OPAC_4$, oligomeric PAC biotransformed for four days; BT-PPAC, BT-$PPAC_4$, polymeric PAC biotransformed for four days; D1 – D8, biotransformed for 1 – 8 days; ND, not detected; OPAC, oligomeric PAC; PPAC, polymeric PAC; $Yeast_4$, S. cerevisiae incubated for four days.

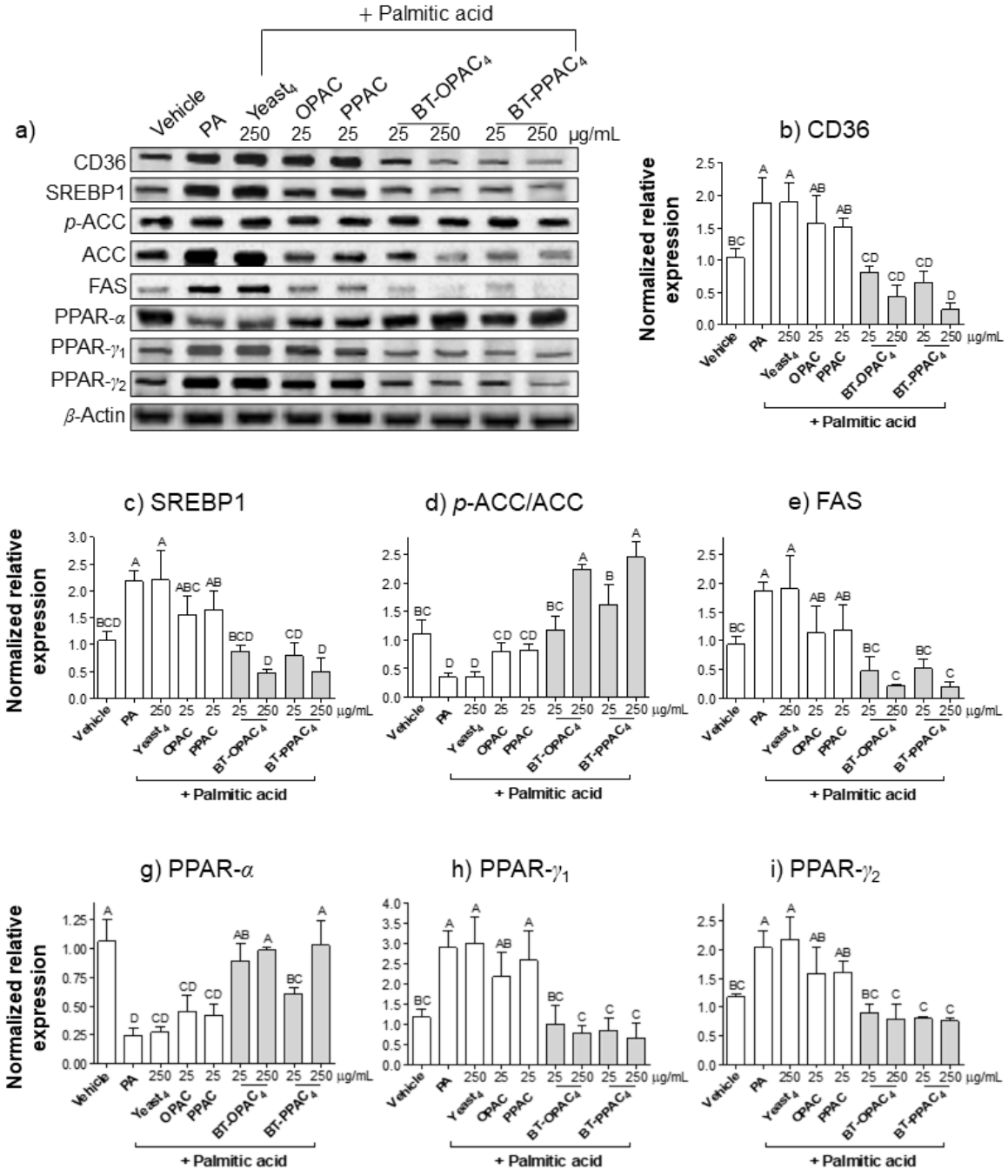
a)
+ Palmitic acid
Vehicle
PA
Yeast4
OPAC
PPAC
BT-OPAC4
BT-PPAC4
250 25 25 25 250 25 250 μg/mL
CD36
SREBP1
p-ACC
ACC
FAS
PPAR-α
PPAR-γ1
PPAR-γ2
β-Actin
b) CD36
c) SREBP1
d) p-ACC/ACC
e) FAS
g) PPAR-α
h) PPAR-γ1
i) PPAR-γ2
Normalized relative expression
+ Palmitic acid

Figure 4.3. Mechanisms of biotransformed (BT) and non-BT proanthocyanidin (PAC) in the reduction of palmitic acid (PA)-induced cellular lipid accumulation. Means that do not share a similar letter are significantly different. ACC, acetyl-CoA carboxylase; BT-$OPAC_4$, oligomeric PAC biotransformed for four days; BT-$PPAC_4$, polymeric PAC biotransformed for four days; CD36, cluster of differentiation 36; FAS, fatty acid synthase; OPAC, oligomeric PAC; *p*-ACC, phospho-acetyl-CoA carboxylase; PPAC, polymeric PAC; PPAR, peroxisome proliferator-activated receptor; SREBP1, sterol regulatory element-binding protein 1; $Yest_4$, *S. cerevisiae* incubated for four days.

a) Nuclear translocation of Nrf2

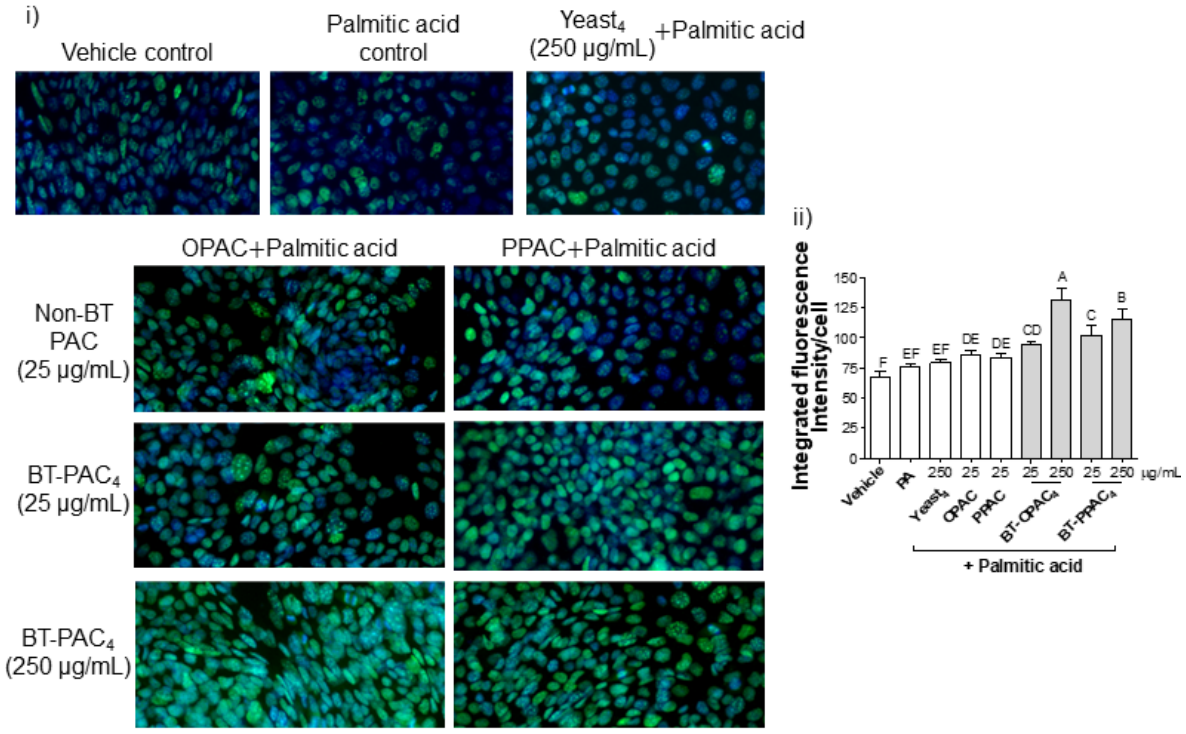

b) Nrf2 phosphorylation and expression of antioxidant enzymes

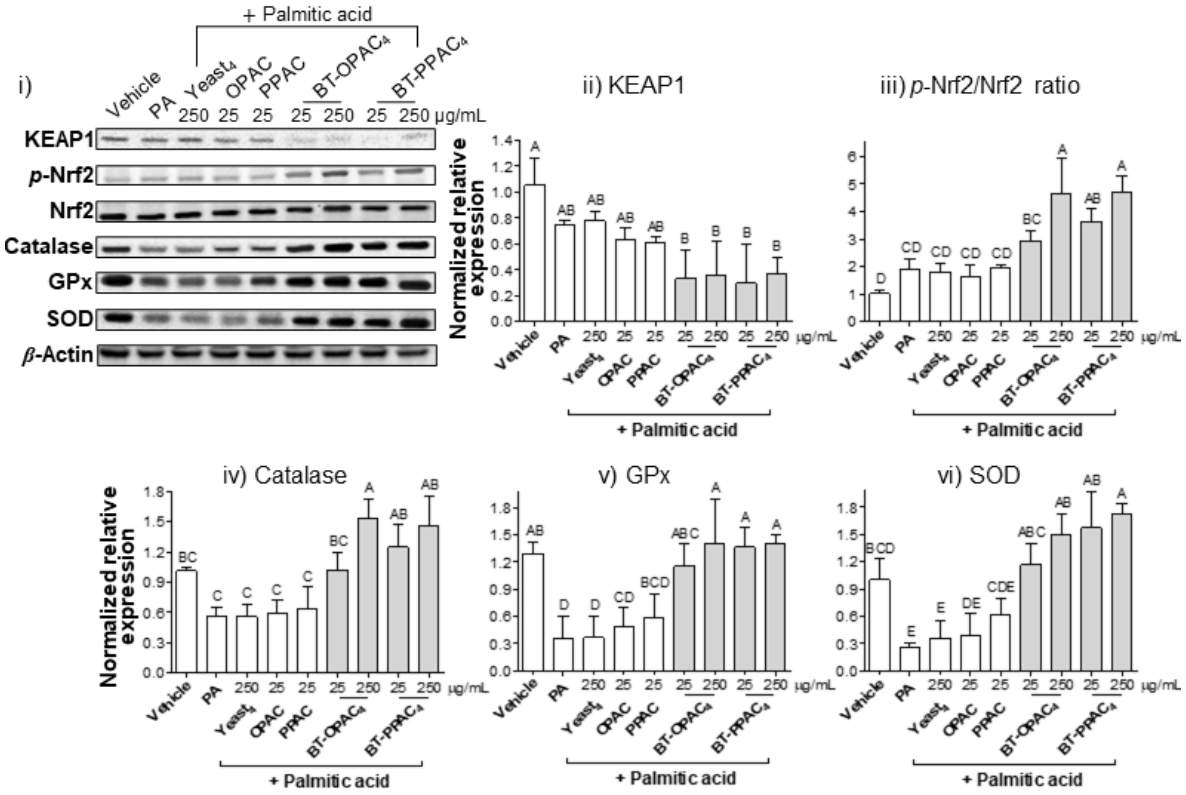

Figure 4.4. Activation of the nuclear factor erythroid 2–related factor 2 (Nrf2) pathway by biotransformed (BT) and non-BT proanthocyanidins (PAC). Nrf2 nuclear translocation in the AML12 cells pretreated with PAC and exposed to palmitic acid (PA) was visualized and measured (a). Cellular protein levels of the Nrf2 complex components and Nrf2 pathway downstream antioxidant enzymes were also measured (b). Means that do not share a similar letter are significantly different. BT-$OPAC_4$, oligomeric PAC biotransformed for four days; BT-$PPAC_4$, polymeric PAC biotransformed for four days; GPx, glutathione peroxidase; KEAP1, kelch-like ECH-associated protein 1; OPAC, oligomeric PAC; *p*-Nrf2, phospho-Nrf2; PPAC, polymeric PAC; SOD, superoxide dismutase; $Yeast_4$, *S. cerevisiae* incubated for four days.

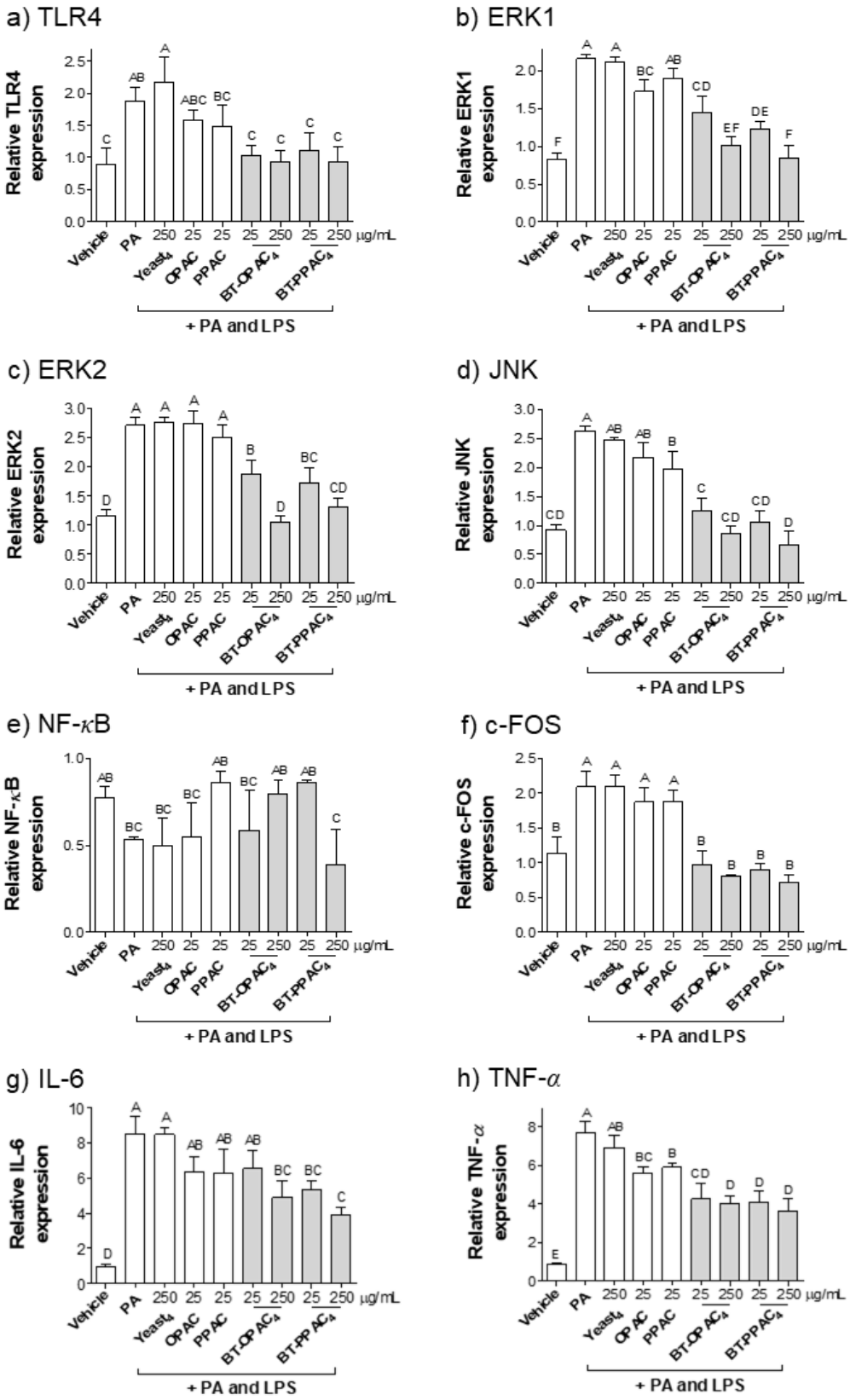
a) TLR4
Relative TLR4 expression
b) ERK1
Relative ERK1 expression
c) ERK2
Relative ERK2 expression
d) JNK
Relative JNK expression
e) NF-κB
Relative NF-κB expression
f) c-FOS
Relative c-FOS expression
g) IL-6
Relative IL-6 expression
h) TNF-α
Relative TNF-α expression
Vehicle
PA
250
Yeast4
OPAC
PPAC
BT-OPAC4
BT-PPAC4
μg/mL
+ PA and LPS

Figure 4.5. Reduction of palmitic acid (PA) and lipopolysaccharide (LPS)-induced cellular inflammation by biotransformed (BT) and non-BT proanthocyanidins (PAC) as measured by reverse transcription quantitative real-time polymerase chain reaction (RT-qPCR) analysis. Means that do not share a similar letter are significantly different. BT-$OPAC_4$, oligomeric PAC biotransformed for four days; BT-$PPAC_4$, polymeric PAC biotransformed for four days; ERK, extracellular signal-regulated protein kinase; IL-6, interleukin-6; JNK, c-Jun N-terminal Kinase; NF-κB, nuclear factor-kappa-light-chain-enhancer of activated B cells; OPAC, oligomeric proanthocyanidins; PPAC, polymeric proanthocyanidins; TLR4, toll-like receptor 4; TNF-α, tumor necrosis factor-alpha; $Yeast_4$, *S. cerevisiae* incubated for four days.

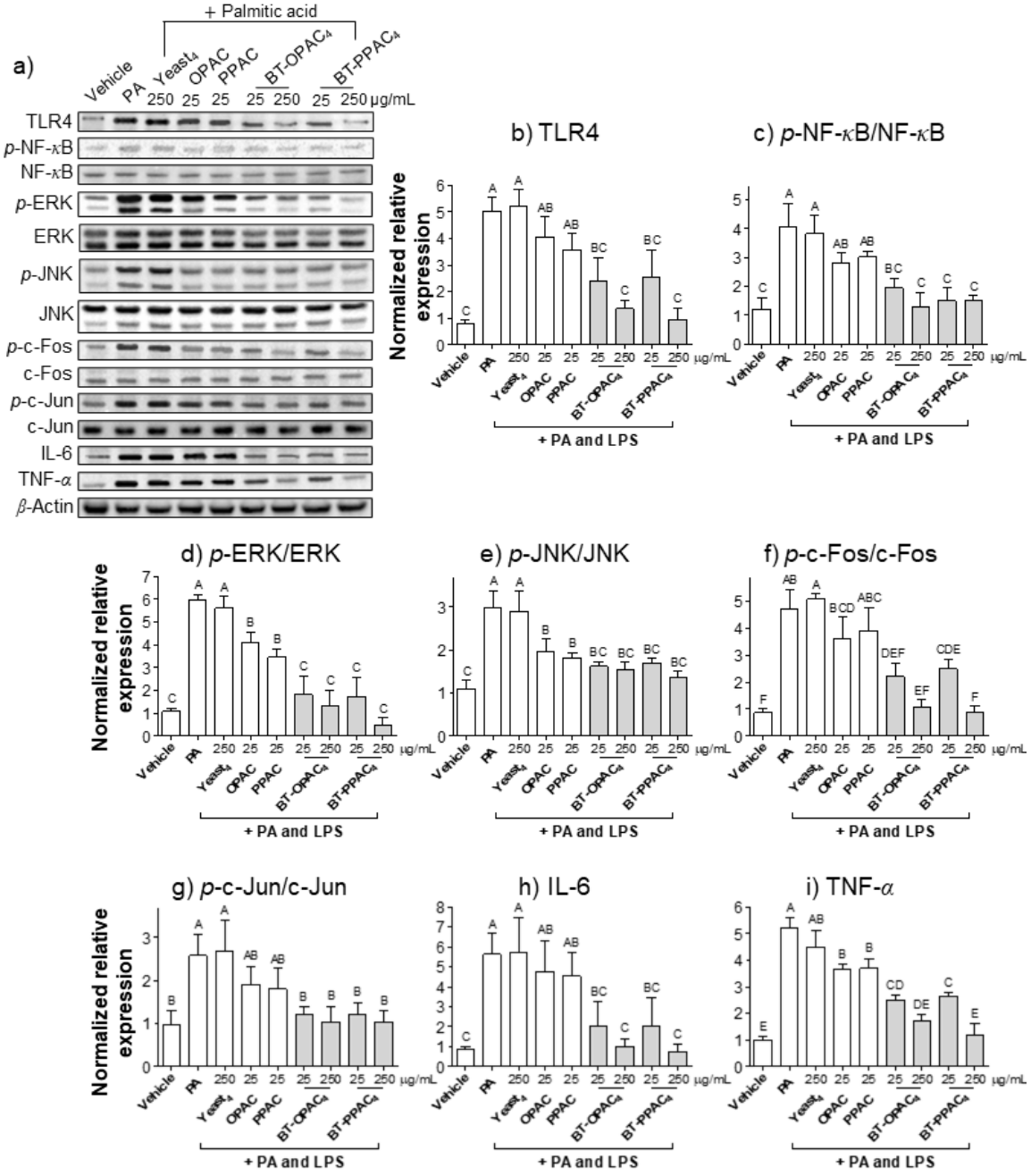
a)
+ Palmitic acid
Vehicle
PA
Yeast4
OPAC
PPAC
BT-OPAC4
BT-PPAC4
250 25 25 25 250 25 250 μg/mL
TLR4
p-NF-κB
NF-κB
p-ERK
ERK
p-JNK
JNK
p-c-Fos
c-Fos
p-c-Jun
c-Jun
IL-6
TNF-α
β-Actin
b) TLR4
c) p-NF-κB/NF-κB
d) p-ERK/ERK
e) p-JNK/JNK
f) p-c-Fos/c-Fos
g) p-c-Jun/c-Jun
h) IL-6
i) TNF-α
Normalized relative expression
+ PA and LPS

Figure 4.6. Reduction of palmitic acid (PA) and lipopolysaccharide (LPS)-induced cellular inflammation by biotransformed (BT) and non-BT proanthocyanidins (PAC) as measured by western blot analysis. Means that do not share a similar letter are significantly different. BT-OPAC$_4$, oligomeric PAC biotransformed for four days; BT-PPAC$_4$, polymeric PAC biotransformed for four days; ERK, extracellular signal-regulated protein kinase; IL-6, interleukin-6; JNK, c-Jun N-terminal kinase; NF-κB, nuclear factor-kappa-light-chain-enhancer of activated B cells; OPAC, oligomeric PAC; *p*-, phosphorylated protein; PPAC, polymeric PAC; TLR4, toll-like receptor 4; TNF-α, tumor necrosis factor-alpha; Yeast$_4$, *S. cerevisiae* incubated for four days.

a) Cellular lipid accumulation reduction by biotransformed proanthocyanidins

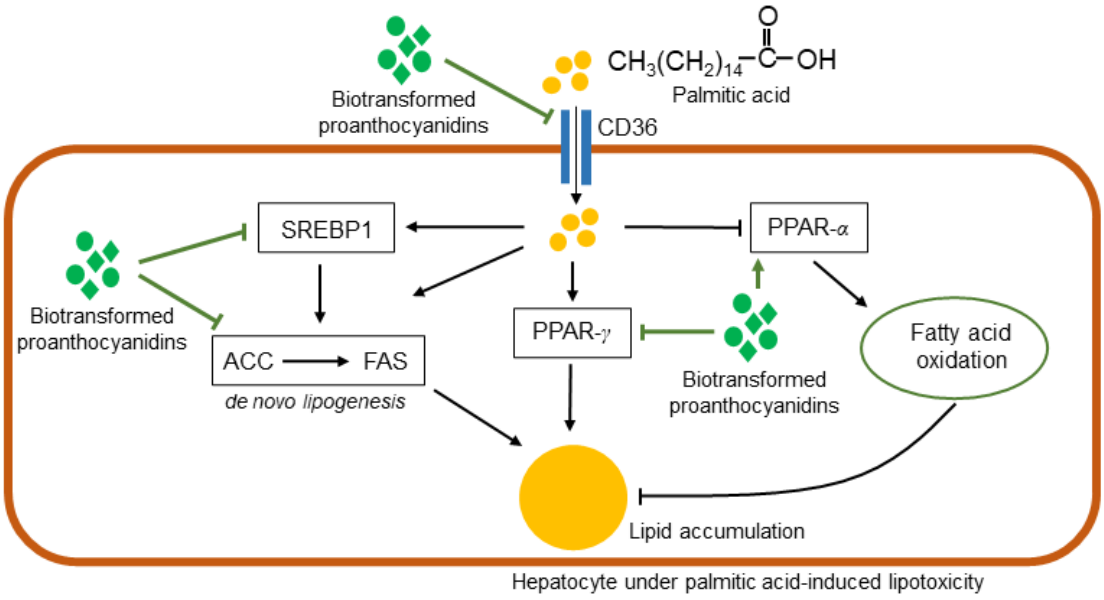

b) Cellular inflammation reduction by biotransformed proanthocyanidins

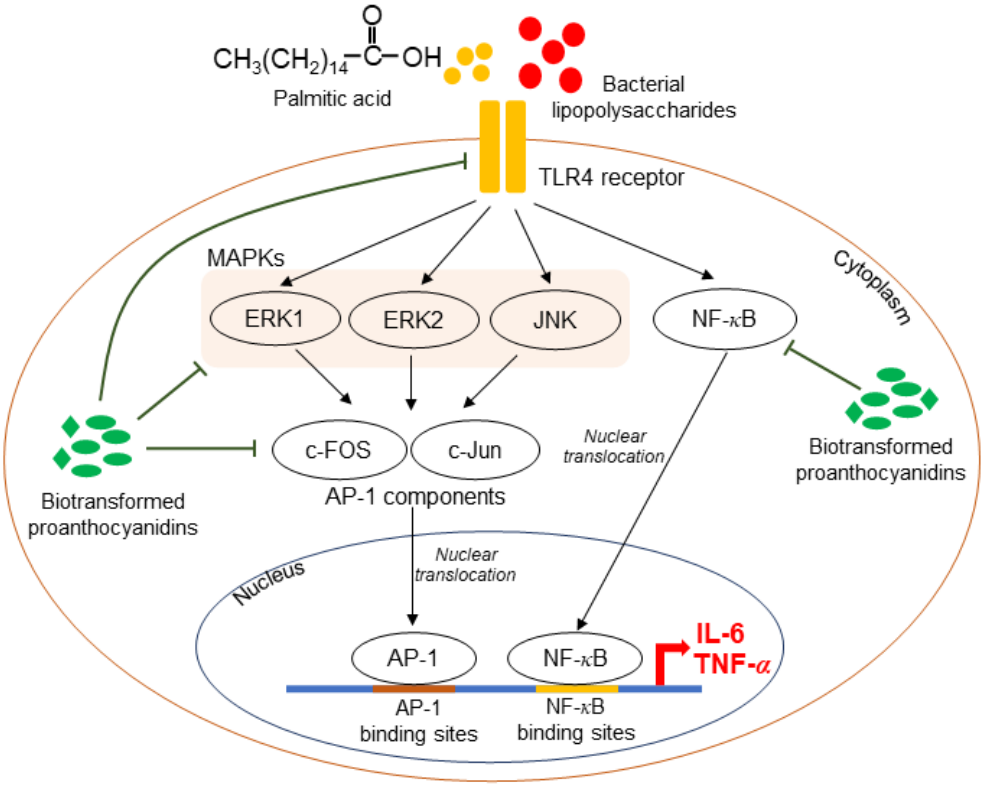

Figure 4.7. Mechanisms of biotransformed proanthocyanidins (BT-PAC) in the reduction of palmitic acid (PA)-induced cellular lipid accumulation (a) and PA and lipopolysaccharide (LPS)-induced cellular inflammation (b). CD36 facilitates the cellular uptake of palmitic acid. Palmitic acid in cells can dysregulate lipid metabolism and increase cellular lipid accumulation by promoting the expressions of SREBP1, PPAR-γ, and de novo lipogenesis enzymes, ACC and FAS. PA can also promote cellular lipid accumulation by restricting fatty acid oxidation through the downregulation of PPAR-α. Biotransformed PAC can ameliorate PA-induced cellular lipid accumulation by the downregulation of CD36, PPAR-γ, SREBP1, ACC, and FAS, and the upregulation of PPAR-α. In cellular inflammation (b), palmitic acid and LPS can bind with TLR4 receptors and activate MAPK and NF-κB-mediated inflammatory responses. MAPK such as ERK1, ERK2, and JNK can upregulate AP-1 components, c-FOS and c-Jun. AP-1 and NF-κB can translocate into the cell nucleus and attach with binding sites to produce proinflammatory cytokines IL-6 and TNF-α. BT-PAC can reduce PA and LPS-induced cellular inflammation by the downregulation of TLR4, MAPK (ERK1, ERK2, and JNK), AP-1 components (c-FOS and c-Jun), and NF-κB. ACC, acetyl-CoA carboxylase; AP-1, activator protein 1; CD36, cluster of differentiation 36; ERK, extracellular signal-regulated protein kinase; FAS, fatty acid synthase; IL-6, interleukin-6; JNK, c-Jun N-terminal Kinase; MAPK, mitogen-activated protein kinases; NF-κB, nuclear factor-kappa-light-chain-enhancer of activated B cells; PPAR, peroxisome proliferator-activated receptor; SREBP1, sterol regulatory element-binding protein 1; TLR4, toll-like receptor 4; TNF-α, tumor necrosis factor-alpha.

4.8. SUPPLEMENTARY TABLE

Supplementary table S4.1. Forward and reverse primer sequences used in the RT-qPCR analysis.

Gene	Forward	Reverse	Accession No.
1) GAPDH	GGGAAGCCCATCACCATCTT	GCCTTCTCCATGGTGGTGAA	NM_008084.3
2) β-Actin	CTCTGGCTCCTAGCACCATGAAGA	GTAAAACGCAGCTCAGTAACAGTCCG	NM_007393.5
3) IL-1β	GAAATGCCACCTTTTGACAGTG	TGGATGCTCTCATCAGGACAG	NM_008361
4) IL-6	CTGCAAGAGACTTCCATCCAG	AGTGGTATAGACAGGTCTGTTGG	NM_031168
5) TNF-α	CAGGCGGTGCCTATGTCTC	CGATCACCCCGAAGTTCAGTAG	NM_013693
6) TLR4	ACTCAGCAAAGTCCCTGATGACA	AGGTGGTGTAAGCCATGCCA	NM_021297.3
7) NF-κB	AAGAACAGAGACCGCTGGTG	CAGGTTCTGCATCCCCTCTG	XM_006509023.5
8) p38 (MAPK14)	GCCGCTTAGTCACATACCACT	GTCCCCGTCAGACGCATTAT	NM_001357724.1
9) JNK1 (MAPK8)	CTTCAGAAGCAGAAGCCCCA	TGTGCTAAAGGAGACGGCTG	NM_016700.4
10) ERK1 (MAPK3)	ACACTGGCTTTCTGACGGAG	TGATGCGCTTGTTTGGGTTG	NM_011952.2
11) ERK2 (MAPK1)	TTGCTTTCTCTCCCGCACAA	AGCCCTTGTCCTGACCAATTT	NM_011949.3
12) Jun (AP-1)	AAGAAGCTCACAAGTCCGGG	GAGGGCATCGTCGTAGAAGG	NM_010591.2
13) FOS (AP-1)	TGTTCCTGGCAATAGCGTGT	TCAGACCACCTCGACAATGC	NM_010234.3

4.9. SUPPLEMENTARY FIGURES

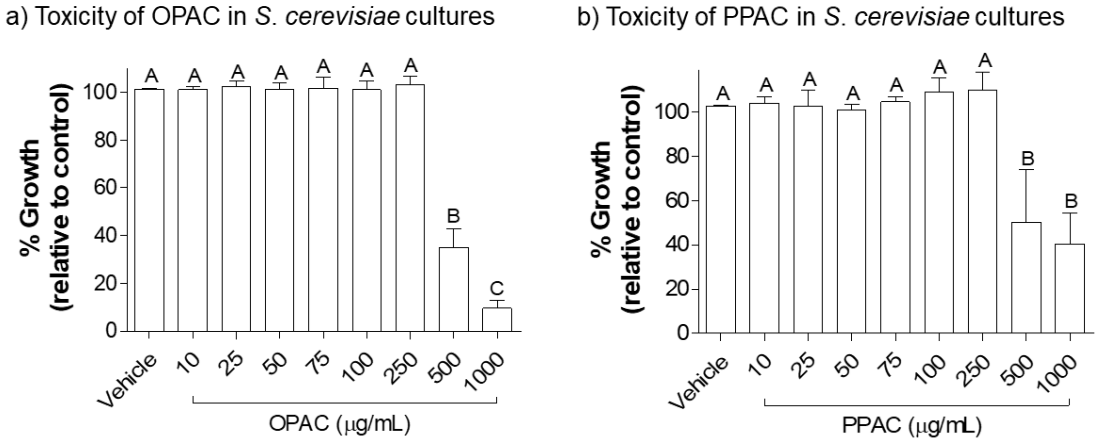

Supplementary Figure S4.1. Toxicity of oligomeric proanthocyanidins (OPAC) (a) and polymeric proanthocyanidins (PPAC) (b) in *Saccharomyces cerevisiae* cultures. *S. cerevisiae* cultures were incubated with different concentrations (10 – 1000 μg/mL) of OPAC and PPAC for 24 hours and absorbance of the yeast growth medium was measured at 600 nm wavelength (OD_{600}). Growth of the *S. cerevisiae* cultures in different concentrations of proanthocyanidins were measured by comparing the OD_{600} values to the negative control. Results were expressed as mean % growth of *S. cerevisiae* cultures of three independent experiments. Means that do not share a similar letter are significantly different at 95% confidence level.

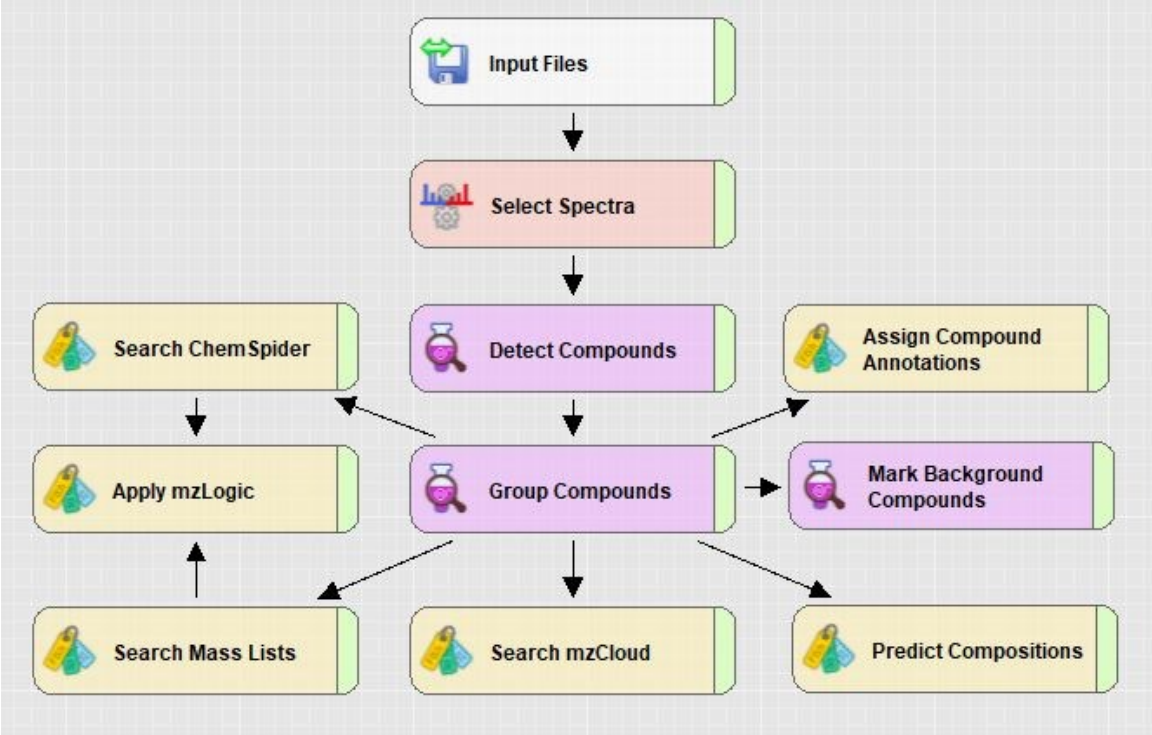

Supplementary Figure S4.2. Workflow tree used to analyze high-resolution mass spectrometry data by the Compound Discoverer software.

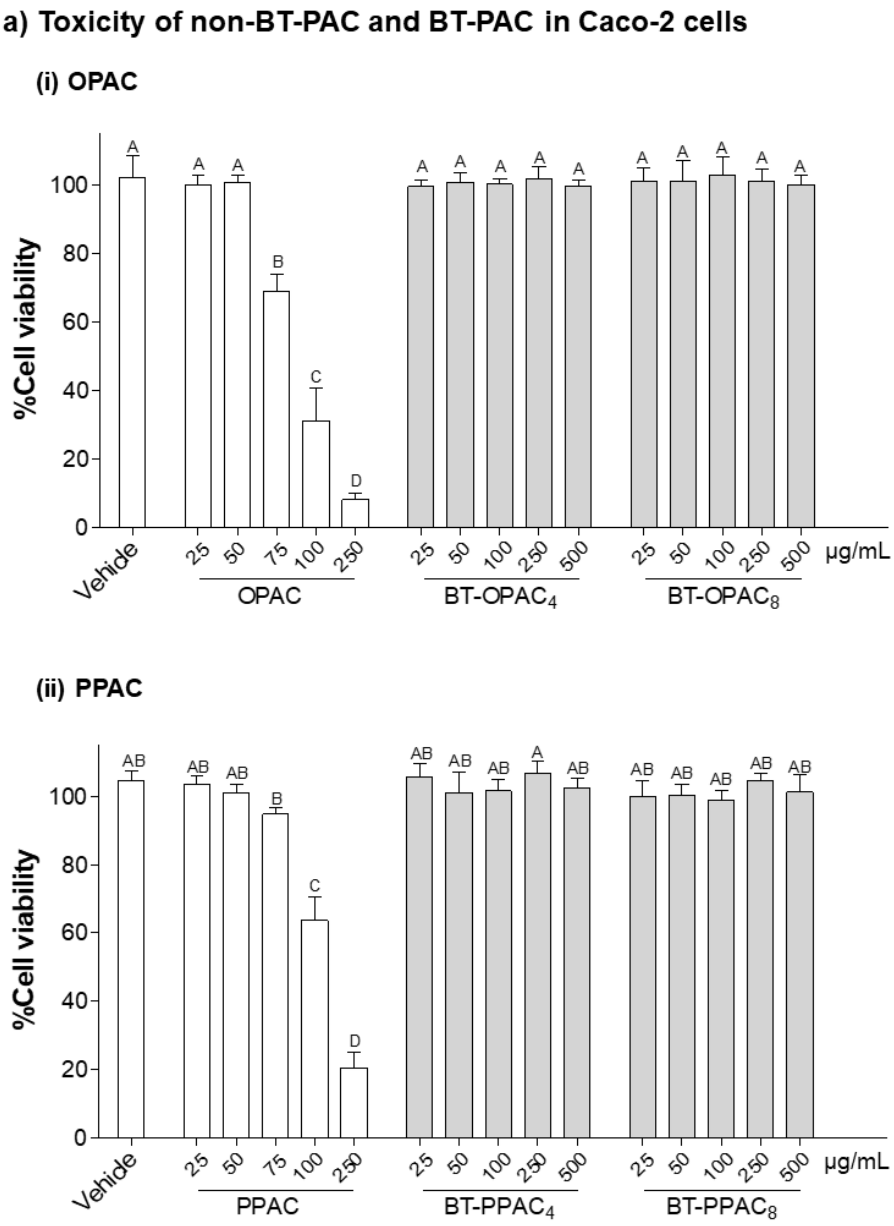

Supplementary Figure S4.3-1. Toxicity of biotransformed (BT)-proanthocyanidins (PAC) and non-BT-PAC in Caco-2 cells. Cells were treated with different concentrations of PAC (25 – 500 µg/mL) for 24 hours. Cells were incubated with MTS/phenazine methosulphate (PMS) in phosphate-buffered saline solution (MTS, 333 µg/mL; PMS, 25 µM of final concentration) for 2.5 hours at 37 °C and absorbance was measured at 490 nm wavelength. Cell viabilities at different PAC concentrations were measured by comparing the absorbances to the negative control. Results were expresses as mean % cell viability of three independent experiments. Means that do not share a similar letter are significantly different at 95% confidence level. BT-OPAC$_4$ and BT-OPAC$_8$, oligomeric PAC biotransformed for four and eight days; BT-PPAC$_4$ and BT-PPAC$_8$, polymeric PAC biotransformed for four and eight days; OPAC, oligomeric PAC; PPAC, polymeric PAC.

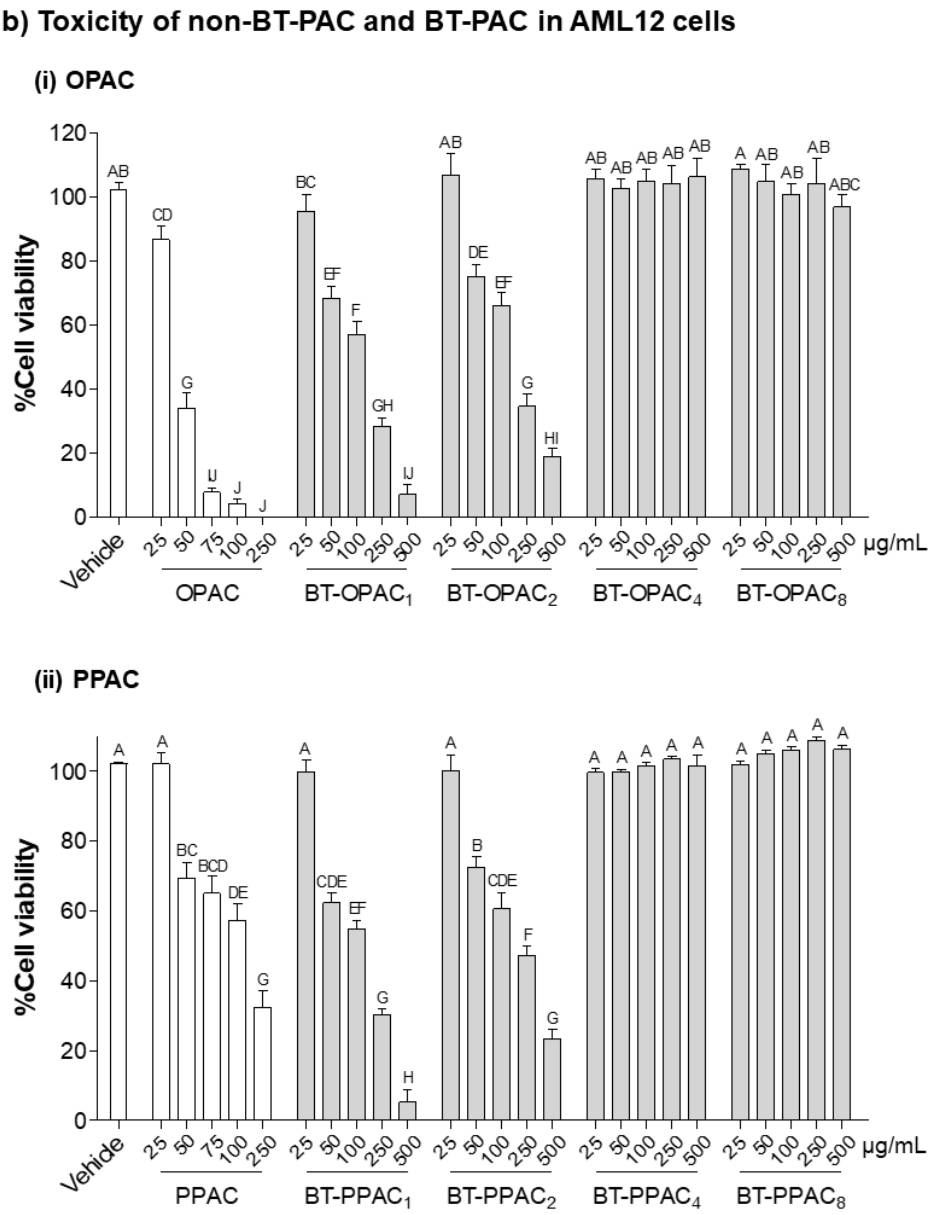

Supplementary figure S4.3-2. Toxicity of biotransformed (BT)-proanthocyanidins (PAC) and non-BT-PAC in AML12 cells. Cells were treated with different concentrations of PAC (25 – 500 µg/mL) for 24 hours. Cells were incubated with MTS/phenazine methosulphate (PMS) in phosphate-buffered saline solution (MTS, 333 µg/mL; PMS, 25 µM of final concentration) for 2.5 hours at 37 °C and absorbance was measured at 490 nm wavelength. Cell viabilities at different PAC concentrations were measured by comparing the absorbances to the negative control. Results were expresses as mean % cell viability of three independent experiments. Means that do not share a similar letter are significantly different at 95% confidence level. BT-$OPAC_2$ – BT-$OPAC_8$, oligomeric PAC biotransformed for two to eight days; BT-$PPAC_2$ – BT-$PPAC_8$, polymeric PAC biotransformed for two to eight days; OPAC, oligomeric PAC; PPAC, polymeric PAC.

4.10. REFERENCES

Alam, M.A., Subhan, N., Hossain, H., Hossain, M., Reza, H.M., Rahman, M.M., Ullah, M.O., 2016. Hydroxycinnamic acid derivatives: a potential class of natural compounds for the management of lipid metabolism and obesity. Nutrition & metabolism 13, 27. https://doi.org/10.1186/s12986-016-0080-3

Al-Salem, H.S., Al-Yousef, H.M., Ashour, A.E., Ahmed, A.F., Amina, M., Issa, I.S., Bhat, R.S., 2020. Antioxidant and hepatorenal protective effects of bee pollen fractions against propionic acid-induced autistic feature in rats. Food Science & Nutrition 8, 5114–5127. https://doi.org/10.1002/fsn3.1813

Álvarez-Fernández, M.A., Carafa, I., Vrhovsek, U., Arapitsas, P., 2020. Modulating wine aromatic amino acid catabolites by using *Torulaspora delbrueckii* in sequentially inoculated fermentations or *Saccharomyces cerevisiae* alone. Microorganisms 8, 1349. https://doi.org/10.3390/microorganisms8091349

Beckmann, M., Lloyd, A.J., Haldar, S., Seal, C., Brandt, K., Draper, J., 2013. Hydroxylated phenylacetamides derived from bioactive benzoxazinoids are bioavailable in humans after habitual consumption of whole grain sourdough rye bread. Molecular Nutrition & Food Research 57, 1859–1873. https://doi.org/10.1002/mnfr.201200777

Bhullar, K.S., Rupasinghe, H.P.V., 2015. Antioxidant and cytoprotective properties of partridgeberry polyphenols. Food Chemistry 168, 595–605. https://doi.org/10.1016/j.foodchem.2014.07.103

Bray, M., Vokes, M.S., Carpenter, A.E., 2015. Using CellProfiler for automatic identification and measurement of biological objects in images. Current Protocols in Molecular Biology 109. https://doi.org/10.1002/0471142727.mb1417s109

Bvochora, J.M., Reed, J.D., Read, J.S., Zvauya, R., 1999. Effect of fermentation processes on proanthocyanidins in sorghum during preparation of Mahewu, a non-alcoholic beverage. Process Biochemistry 35, 21–25. https://doi.org/10.1016/S0032-9592(99)00027-8

Cao, D., Luo, J., Chen, D., Xu, H., Shi, H., Jing, X., Zang, W., 2016. CD36 regulates lipopolysaccharide-induced signaling pathways and mediates the internalization of *Escherichia coli* in cooperation with TLR4 in goat mammary gland epithelial cells. Scientific Reports 6, 23132. https://doi.org/10.1038/srep23132

Chantarasakha, K., Asawapanumas, T., Suntivich, R., Panya, A., Phonsatta, N., Thiennimitr, P., Laoteng, K., Tepaamorndech, S., 2022. Hatakabb, a herbal extract, contains pyrogallol as the novel mediator inhibiting LPS-induced TNF-α production by NF-κB inactivation and HMOX-1 upregulation. Journal of Functional Foods 90, 104992. https://doi.org/10.1016/j.jff.2022.104992

Chen, J., Chen, Y., Zheng, Y., Zhao, J., Yu, H., Zhu, J., 2022. Relationship between neuroprotective effects and structure of procyanidins. Molecules 27, 2308. https://doi.org/10.3390/molecules27072308

Cui, B., Lin, L., Wang, B., Liu, W., Sun, C., 2022. Therapeutic potential of *Saccharomyces boulardii* in liver diseases: from passive bystander to protective performer? Pharmacological Research 175, 106022. https://doi.org/10.1016/j.phrs.2021.106022

Del Bas, J.M., Ricketts, M.L., Baiges, I., Quesada, H., Ardevol, A., Salvadó, M.J., Pujadas, G., Blay, M., Arola, L., Bladé, C., Moore, D.D., Fernandez-Larrea, J., 2008. Dietary procyanidins lower triglyceride levels signaling through the nuclear receptor small heterodimer partner. Molecular Nutrition & Food Research 52, 1172–1181. https://doi.org/10.1002/mnfr.200800054

Drygalski, K., Siewko, K., Chomentowski, A., Odrzygóźdź, C., Zalewska, A., Krętowski, A., Maciejczyk, M., 2021. Phloroglucinol strengthens the antioxidant barrier and reduces oxidative/nitrosative stress in nonalcoholic fatty liver disease (NAFLD). Oxidative Medicine & Cellular Longevity 2021, e8872702. https://doi.org/10.1155/2021/8872702

Fanaei, H., Mard, S.A., Sarkaki, A., Goudarzi, G., Khorsandi, L., 2021. Gallic acid treats dust-induced NAFLD in rats by improving the liver's anti-oxidant capacity and inhibiting ROS/NFκβ/TNFα inflammatory pathway. Iranian Journal of Basic Medical Sciences 24, 240–247. https://doi.org/10.22038/IJBMS.2021.51036.11603

Ferreira, E.A., Gris, E.F., Felipe, K.B., Correia, J.F.G., Cargnin-Ferreira, E., Wilhelm Filho, D., Pedrosa, R.C., 2010. Potent hepatoprotective effect in CCl4-induced hepatic injury in mice of phloroacetophenone from Myrcia multiflora. Libyan Journal of Medicine 5, 10.3402/ljm.v5i0.4891. https://doi.org/10.3402/ljm.v5i0.4891

Gao, Y., Tian, R., Liu, H., Xue, H., Zhang, R., Han, S., Ji, L., Huang, W., Zhan, J., You, Y., 2022. Research progress on intervention effect and mechanism of protocatechuic acid on nonalcoholic fatty liver disease. Critical Reviews in Food Science & Nutrition 62, 9053–9075. https://doi.org/10.1080/10408398.2021.1939265

Gu, L., Kelm, M.A., Hammerstone, J.F., Beecher, G., Holden, J., Haytowitz, D., Gebhardt, S., Prior, R.L., 2004. Concentrations of proanthocyanidins in common foods and estimations of normal consumption. The Journal of Nutrition 134, 613–617. https://doi.org/10.1093/jn/134.3.613

Haile, M., Kang, W.H., 2019. Antioxidant activity, total polyphenol, flavonoid and tannin contents of fermented green coffee beans with selected yeasts. Fermentation 5, 29. https://doi.org/10.3390/fermentation5010029

Huang, T., Zhang, Y., Zhang, W., Lin, T., Chen, L., Yang, B., Wu, L., Yang, J., Zhang, D., 2020. Attenuation of perfluorooctane sulfonate-induced steatohepatitis by grape seed proanthocyanidin extract in mice. BioMed Research International 2020, 8818160. https://doi.org/10.1155/2020/8818160

Korbecki, J., Bobiński, R., Dutka, M., 2019. Self-regulation of the inflammatory response by peroxisome proliferator-activated receptors. Inflammation Research 68, 443–458. https://doi.org/10.1007/s00011-019-01231-1

Lee, J.-W., Kim, Y.I., Kim, Y., Choi, M., Min, S., Joo, Y.H., Yim, S.-V., Chung, N., 2017. Grape seed proanthocyanidin inhibits inflammatory responses in hepatic stellate cells by modulating the MAPK, Akt and NF-κB signaling pathways. International Journal of Molecular Medicine 40, 226–234. https://doi.org/10.3892/ijmm.2017.2997

Li, J., Zhu, K., Zhao, H., 2020. Transcriptome analysis reveals the protection mechanism of proanthocyanidins for *Saccharomyces cerevisiae* during wine fermentation. Scientific Reports 10, 6676. https://doi.org/10.1038/s41598-020-63631-2

Li, X., Sui, Y., Wu, Q., Xie, B., Sun, Z., 2017. Attenuated mTOR Signaling and enhanced glucose homeostasis by dietary supplementation with lotus seedpod oligomeric procyanidins in streptozotocin (STZ)-induced diabetic mice. Journal of Agriculture & Food Chemistry 65, 3801–3810. https://doi.org/10.1021/acs.jafc.7b00233

Limtrakul, P., Yodkeeree, S., Pitchakarn, P., Punfa, W., 2016. Anti-inflammatory effects of proanthocyanidin-rich red rice extract via suppression of MAPK, AP-1 and NF-κB pathways in Raw 264.7 macrophages. Nutrition Research & Practice 10, 251–258. https://doi.org/10.4162/nrp.2016.10.3.251

Liss, K.H.H., Finck, B.N., 2017. PPARs and nonalcoholic fatty liver disease. Biochimie 136, 65–74. https://doi.org/10.1016/j.biochi.2016.11.009

Liu, B., Jiang, H., Lu, J., Baiyun, R., Li, S., Lv, Y., Li, D., Wu, H., Zhang, Z., 2018. Grape seed procyanidin extract ameliorates lead-induced liver injury via miRNA153 and AKT/GSK-3β/Fyn-mediated Nrf2 activation. The Journal of Nutritional Biochemistry 52, 115–123. https://doi.org/10.1016/j.jnutbio.2017.09.025

Liu, C., Boeren, S., Miro Estruch, I., Rietjens, I.M.C.M., 2022. The gut microbial metabolite pyrogallol is a more potent inducer of Nrf2-associated gene expression than its parent compound green tea (-)-epigallocatechin gallate. Nutrients 14, 3392. https://doi.org/10.3390/nu14163392

Liu, Z., Xi, R., Zhang, Z., Li, W., Liu, Y., Jin, F., Wang, X., 2014. 4-Hydroxyphenylacetic acid attenuated inflammation and edema via suppressing HIF-1α in seawater aspiration-induced lung injury in rats. International Journal of Molecular Sciences 15, 12861–12884. https://doi.org/10.3390/ijms150712861

Manach, C., Scalbert, A., Morand, C., Rémésy, C., Jiménez, L., 2004. Polyphenols: food sources and bioavailability. The American Journal of Clinical Nutrition 79, 727–747. https://doi.org/10.1093/ajcn/79.5.727

Mehari, B., Chandravanshi, B.S., Redi-Abshiro, M., Combrinck, S., McCrindle, R., Atlabachew, M., 2021. Polyphenol contents of green coffee beans from different regions of Ethiopia. International Journal of Food Properties 24, 17–27. https://doi.org/10.1080/10942912.2020.1858866

Mekoue Nguela, J., Sieczkowski, N., Roi, S., Vernhet, A., 2015. Sorption of grape proanthocyanidins and wine polyphenols by yeasts, inactivated yeasts, and yeast cell walls. Journal of Agriculture & Food Chemistry 63, 660–670. https://doi.org/10.1021/jf504494m

Middelhoven, W.J., 2006. Polysaccharides and phenolic compounds as substrate for yeasts isolated from rotten wood and description of *Cryptococcus fagi* sp.nov. Antonie Van Leeuwenhoek 90, 57–67. https://doi.org/10.1007/s10482-006-9060-3

Nissar, A.U., Sharma, L., Tasduq, S.A., 2015. Palmitic acid induced lipotoxicity is associated with altered lipid metabolism, enhanced CYP450 2E1 and intracellular calcium mediated ER stress in human hepatoma cells. Toxicology Research 4, 1344–1358. https://doi.org/10.1039/C5TX00101C

Niwano, Y., Kohzaki, H., Shirato, M., Shishido, S., Nakamura, K., 2022. Metabolic fate of orally ingested proanthocyanidins through the digestive tract. Antioxidants 12, 17. https://doi.org/10.3390/antiox12010017

Nogueira, A., Guyot, S., Marnet, N., Lequéré, J.M., Drilleau, J.-F., Wosiacki, G., 2008. Effect of alcoholic fermentation in the content of phenolic compounds in cider processing. Brazilian Archives of Biology & Technology 51, 1025–1032. https://doi.org/10.1590/S1516-89132008000500020

Ou, K., Gu, L., 2014. Absorption and metabolism of proanthocyanidins. Journal of Functional Foods 7, 43–53. https://doi.org/10.1016/j.jff.2013.08.004

Pedan, V., Fischer, N., Bernath, K., Hühn, T., Rohn, S., 2017. Determination of oligomeric proanthocyanidins and their antioxidant capacity from different chocolate manufacturing stages using the NP-HPLC-online-DPPH methodology. Food Chemistry 214, 523–532. https://doi.org/10.1016/j.foodchem.2016.07.094

Pétel, C., Onno, B., Prost, C., 2017. Sourdough volatile compounds and their contribution to bread: A review. Trends in Food Science & Technology 59, 105–123. https://doi.org/10.1016/j.tifs.2016.10.015

Pilar Valdecantos, M., Prieto-Hontoria, P.L., Pardo, V., Módol, T., Santamaría, B., Weber, M., Herrero, L., Serra, D., Muntané, J., Cuadrado, A., Moreno-Aliaga, M.J., Alfredo Martínez, J., Valverde, Á.M., 2015. Essential role of Nrf2 in the protective effect of lipoic acid against lipoapoptosis in hepatocytes. Free Radical Biology & Medicine 84, 263–278. https://doi.org/10.1016/j.freeradbiomed.2015.03.019

Popeijus, H.E., van Otterdijk, S.D., van der Krieken, S.E., Konings, M., Serbonij, K., Plat, J., Mensink, R.P., 2014. Fatty acid chain length and saturation influences PPARα transcriptional activation and repression in HepG2 cells. Molecular Nutrition & Food Research 58, 2342–2349. https://doi.org/10.1002/mnfr.201400314

Quesada, H., Díaz, S., Pajuelo, D., Fernández-Iglesias, A., Garcia-Vallvé, S., Pujadas, G., Salvadó, M.J., Arola, L., Bladé, C., 2012. The lipid-lowering effect of dietary proanthocyanidins in rats involves both chylomicron-rich and VLDL-rich fractions. British Journal of Nutrition 108, 208–217. https://doi.org/10.1017/S0007114511005472

Rauf, A., Imran, M., Abu-Izneid, T., Iahtisham-Ul-Haq, Patel, S., Pan, X., Naz, S., Sanches Silva, A., Saeed, F., Rasul Suleria, H.A., 2019. Proanthocyanidins: a comprehensive review. Biomedicine & Pharmacotherapy 116, 108999. https://doi.org/10.1016/j.biopha.2019.108999

Rothwell, J.A., Perez-Jimenez, J., Neveu, V., Medina-Remón, A., M'Hiri, N., García-Lobato, P., Manach, C., Knox, C., Eisner, R., Wishart, D.S., Scalbert, A., 2013. Phenol-explorer 3.0: a major update of the phenol-explorer database to incorporate data on the effects of food processing on polyphenol content. Database (Oxford) 2013, bat070. https://doi.org/10.1093/database/bat070

Rupasinghe, H.P.V., Parmar, I., Neir, S.V., 2019. Biotransformation of cranberry proanthocyanidins to probiotic metabolites by lactobacillus rhamnosus enhances their anticancer activity in HepG2 cells *in vitro*. Oxidative Medicine & Cellular Longevity 2019. https://doi.org/10.1155/2019/4750795

Ruta, L.L., Farcasanu, I.C., 2021. Coffee and yeasts: from flavor to biotechnology. Fermentation 7, 9. https://doi.org/10.3390/fermentation7010009

Su, H., Li, Y., Hu, D., Xie, L., Ke, H., Zheng, X., Chen, W., 2018. Procyanidin B2 ameliorates free fatty acids-induced hepatic steatosis through regulating TFEB-mediated lysosomal pathway and redox state. Free Radical Biology & Medicine 126, 269–286. https://doi.org/10.1016/j.freeradbiomed.2018.08.024

Suraweera, T.L., Merlin, J.P., Dellaire, D., Xu, Z., Rupasinghe, H.P.V., 2023. Genistein and procyanidin B2 reduce carcinogen-induced reactive oxygen species and DNA damage through the activation of Nrf2/ARE cell signaling in bronchial epithelial cells in vitro. Internation Journal of Molecular Sciences 24 (4), 3676. https://doi.org/10.3390/ijms24043676

Suraweera, T.L., Rupasinghe, H.P.V., Dellaire, G., Xu, Z., 2020. Regulation of Nrf2/ARE pathway by dietary flavonoids: a friend or foe for cancer management? Antioxidants 9, 973. https://doi.org/10.3390/antiox9100973

Takaki, A., Kawai, D., Yamamoto, K., 2013. Multiple hits, including oxidative stress, as pathogenesis and treatment target in non-alcoholic steatohepatitis (NASH). International Journal of Molecular Sciences 14, 20704–20728. https://doi.org/10.3390/ijms141020704

Thilakarathna, W.P.D.W., Langille, M.G.I., Rupasinghe, H.P.V., 2023. hepatotoxicity of polymeric proanthocyanidins is caused by translocation of bacterial lipoplysaccharides through impaired gut epithelium. Toxicology Letters 379, 35–47. https://doi.org/10.1016/j.toxlet.2023.03.005

Thilakarathna, W.P.D.W., Rupasinghe, H.P.V., 2022. Optimization of the extraction of proanthocyanidins from grape seeds using ultrasonication-assisted aqueous ethanol and evaluation of anti-steatosis activity *in vitro*. Molecules 27, 1363. https://doi.org/10.3390/molecules27041363

Thilakarathna, W.P.D.W., Rupasinghe, H.P.V., 2019. Microbial metabolites of proanthocyanidins reduce chemical carcinogen-induced DNA damage in human lung epithelial and fetal hepatic cells in vitro. Food and Chemical Toxicology 125, 479–493. https://doi.org/10.1016/j.fct.2019.02.010

Thilakarathna, W.P.D.W., Yu, C.H.J., Rupasinghe, H.P.V., 2021. Variations in nutritional and microbial composition of napa cabbage kimchi during refrigerated storage. Journal of Food Processing and Preservation 45, e16065. https://doi.org/10.1111/jfpp.16065

Tie, F., Wang, J., Liang, Y., Zhu, S., Wang, Z., Li, G., Wang, H., 2020. Proanthocyanidins ameliorated deficits of lipid metabolism in type 2 diabetes mellitus via inhibiting adipogenesis and improving mitochondrial function. International Journal of Molecular Sciences 21, 2029. https://doi.org/10.3390/ijms21062029

Trepiana, J., Krisa, S., Renouf, E., Portillo, M.P., 2020. Resveratrol metabolites are able to reduce steatosis in cultured hepatocytes. Pharmaceuticals (Basel) 13, 285. https://doi.org/10.3390/ph13100285

Truong, V.-L., Bak, M.-J., Jun, M., Kong, A.-N.T., Ho, C.-T., Jeong, W.-S., 2014. Antioxidant defense and hepatoprotection by procyanidins from almond (*Prunus amygdalus*) skins. Journal of Agriculture & Food Chemistry 62, 8668–8678. https://doi.org/10.1021/jf5027247

van Santen, J.A., Poynton, E.F., Iskakova, D., McMann, E., Alsup, T.A., Clark, T.N., Fergusson, C.H., Fewer, D.P., Hughes, A.H., McCadden, C.A., Parra, J., Soldatou, S., Rudolf, J.D., Janssen, E.M.-L., Duncan, K.R., Linington, R.G., 2022. The natural products atlas 2.0: a database of microbially-derived natural products. Nucleic Acids Research 50, D1317–D1323. https://doi.org/10.1093/nar/gkab941

Vazquez-Flores, A.A., Martinez-Gonzalez, A.I., Alvarez-Parrilla, E., Díaz-Sánchez, Á.G., de la Rosa, L.A., González-Aguilar, G.A., Aguilar, C.N., 2018. Proanthocyanidins with a Low degree of polymerization are good inhibitors of digestive enzymes because of their ability to form specific interactions: a hypothesis. Journal of Food Science 83, 2895–2902. https://doi.org/10.1111/1750-3841.14386

Vernhet, A., Carrillo, S., Rattier, A., Verbaere, A., Cheynier, V., Nguela, J.M., 2020. Fate of anthocyanins and proanthocyanidins during the alcoholic fermentation of thermovinified red musts by different *Saccharomyces cerevisiae* strains. Journal of Agriculture and Food Chemistry 68, 3615–3625. https://doi.org/10.1021/acs.jafc.0c00413

Wallace, T.C., Giusti, M.M., 2010. Evaluation of parameters that affect the 4-dimethylaminocinnamaldehyde assay for flavanols and proanthocyanidins. Journal of Food Science 75, C619–C625. https://doi.org/10.1111/j.1750-3841.2010.01734.x

Xu, D., Xu, M., Jeong, S., Qian, Y., Wu, H., Xia, Q., Kong, X., 2019. The role of Nrf2 in liver disease: novel molecular mechanisms and therapeutic approaches. Frontiers in Pharmacology 9, 1428. https://doi.org/10.3389/fphar.2018.01428

Yang, W., Zhu, L., Lai, S., Ding, Q., Xu, T., Guo, R., Dou, X., Chai, H., Yu, Z., Li, S., 2022. Cimifugin ameliorates lipotoxicity-induced hepatocyte damage and steatosis through TLR4/p38 MAPK- and SIRT1-involved pathways. Oxidative Medicine & Cellular Longevity 2022, 4557532. https://doi.org/10.1155/2022/4557532

Yogalakshmi, B., Sreeja, S., Geetha, R., Radika, M.K., Anuradha, C.V., 2013. Grape Seed Proanthocyanidin Rescues Rats from Steatosis: A comparative and combination study with metformin. Journal of Lipids 2013, 1–11. https://doi.org/10.1155/2013/153897

Younossi, Z.M., Golabi, P., Paik, J.M., Henry, A., Van Dongen, C., Henry, L., 2023. The global epidemiology of nonalcoholic fatty liver disease (NAFLD) and nonalcoholic steatohepatitis (NASH): a systematic review. Hepatology 10.1097/HEP.0000000000000004. https://doi.org/10.1097/HEP.0000000000000004

Zhang, H., Lu, Q., Liu, R., 2022. Widely targeted metabolomics analysis reveals the effect of fermentation on the chemical composition of bee pollen. Food Chemistry 375, 131908. https://doi.org/10.1016/j.foodchem.2021.131908

Zhang, J., Huang, Y., Shao, H., Bi, Q., Chen, J., Ye, Z., 2017. Grape seed procyanidin B2 inhibits adipogenesis of 3T3-L1 cells by targeting peroxisome proliferator-activated receptor γ with miR-483-5p involved mechanism. Biomedicine & Pharmacotherapy 86, 292–296. https://doi.org/10.1016/j.biopha.2016.12.019

Zhang, J., Zhang, W., Yang, L., Zhao, W., Liu, Z., Wang, E., Wang, J., 2023. Phytochemical gallic acid alleviates nonalcoholic fatty liver disease via AMPK-ACC-PPARa axis through dual regulation of lipid metabolism and mitochondrial function. Phytomedicine 109, 154589. https://doi.org/10.1016/j.phymed.2022.154589

Zhao, H., Jiang, Z., Chang, X., Xue, H., Yahefu, W., Zhang, X., 2018. 4-Hydroxyphenylacetic Acid prevents acute apap-induced liver injury by increasing phase II and antioxidant enzymes in mice. Frontiers in Pharmacology 9, 653. https://doi.org/10.3389/fphar.2018.00653

Zou, B., Wu, J., Yu, Y., Xiao, G., Xu, Y., 2017. Evolution of the antioxidant capacity and phenolic contents of persimmon during fermentation. Food Science & Biotechnology 26, 563–571. https://doi.org/10.1007/s10068-017-0099-x

CHAPTER 5. GENERAL CONCLUSIONS

5.1. Overview of the thesis and major findings of the research

Nonalcoholic fatty liver disease (NAFLD) is the most prominent chronic liver disease worldwide. The prevalence of NAFLD is predicted to increase and impact more than half of the global adult population by 2040 (Le et al., 2022). However, a medical drug approved by the United States Food and Drug Administration (FDA) is currently unavailable to treat NAFLD. Thus, effective strategies are necessary to control this rising epidemic. Dietary interventions, especially the administration of probiotics and bioactive phytochemicals such as polyphenols, have shown the potential to reduce the risk of NAFLD. Oligomeric and polymeric proanthocyanidins (PAC) are the most abundant dietary polyphenols. Dietary PAC are capable of reducing the risk of NAFLD through multiple mechanisms. However, the bioactivities of PAC against NAFLD are limited by their low bioavailability. Therefore, I established the proof of concept for developing PAC-based synbiotics through biotransforming PAC into bioavailable and bioactive metabolites. In future, the development of PAC-based synbiotics may improve the beneficial effects of both PAC and probiotics, synergistically. Initially, I developed and optimized an ultrasonication-assisted aqueous ethanol-based PAC extraction method to obtain food-grade PAC from grape seeds. The majority of currently available PAC extraction methods utilize toxic extraction solvents such as acetone, ethyl acetate, and methanol that can leave harmful solvent residues in the extracted PAC. The new ethanol-based extraction method generated the highest PAC yield when extraction was conducted under the optimum conditions of 47% aqueous ethanol, 60 °C temperature, 10.14:1 solvent to solid ratio, and 53 min sonication time. The ethanol-based extraction method could recover more PAC

from the grape seeds compared to the conventional acetone-based extraction method. In ethanol-based PAC extraction, the extraction efficiencies are similar for the grape seeds and grape seed powder. Therefore, the ethanol-based extraction method for grape seeds is advantageous for industrial-scale PAC extraction, since grinding grape seeds into a powder is not required. The developed PAC extraction method could obtain a mixture of PAC monomers, dimers, oligomers, and polymers from the grape seeds. According to a phloroglucinolysis-based characterization conducted later, the PAC extracted by the ethanol-based method had a low mean degree of polymerization (MDP) compared to the acetone-based method (4.82 ± 0.12 *vs*. 9.26 ± 0.22). PAC with a low MDP is more desirable for food and nutraceutical applications as such PAC are considerably more bioavailable (Iannuzzo et al., 2022). The bioactivity of the PAC extracted by the ethanol-based method was evaluated in a palmitic acid-induced steatosis model of AML12 mouse hepatocytes. The extracted PAC could significantly reduce the palmitic acid-induced oxidative stress and lipid accumulation in the AML12 cells. Moreover, the retention of PAC in grape mash after fermentation in wine production was evaluated by the new ethanol-based extraction method. PAC content in the grape mash significantly declined during the fermentation, yet retained a considerable quantity of PAC to be recognized as a source for PAC extraction. The developed ethanol-based extraction method can recover PAC from grape seeds and grape by-products of the winemaking. Thus, PAC required to formulate PAC-based synbiotics can be extracted from the by-products of wine production by using the developed ethanol-based extraction method.

The current knowledge on the potential of probiotic bacteria to biotransform oligomeric PAC (OPAC) and polymeric PAC (PPAC) is limited. Therefore, I evaluated

the ability of a mixture of *Lactobacillus* and *Bifidobacterium* probiotic bacteria together with novel probiotic bacteria *Akkermansia muciniphila* (AM) to biotransform PPAC into bioavailable metabolites in C57BL/6 mice. Probiotic bacteria may biotransform PPAC into unique bioavailable metabolites such as 4-hydroxybenzoic acid that are not produced by the natural gut microbiota-mediated PAC degradation. Probiotic bacteria may also increase the efficiency of PPAC biotransformation in the mice's colon. I further evaluated the effects of PPAC and probiotic bacteria supplementation on the gut microbiota of mice to identify any shift beneficial for NAFLD mitigation. However, this supplementation approach did not alter the gut microbiota composition as demonstrated by the α-diversity indices, Firmicutes/Bacteroidetes ratio, and relative frequency (%) of the AM. During the dissection of mice, I observed liver abnormalities in the mice administered with the PPAC alone or combined with the probiotics. Histological evaluation of the liver tissues suggested the presence of nonalcoholic steatohepatitis (NASH) in mice administered with the PPAC. Further experimentation revealed that PPAC impair the gut epithelial barrier function by reducing the expressions of tight-junction (TJ) proteins. Bacterial lipopolysaccharides (LPS) may have translocated into the livers of mice through the impaired gut epithelium and subsequently induced NASH. In contrast, the OPAC upregulated the expression of TJ protein, claudin-3 *in vitro*, suggesting possible opposing effects of OPAC and PPAC on the expressions of gut epithelial TJ proteins. The probiotic bacteria are capable of biotransforming the PPAC into bioavailable metabolites in mice. PAC are generally recognized as safe for human consumption and reports on the toxic effects of PAC are extremely limited. This study reported for the first time that PPAC may indirectly induce liver injury.

Considering the possible liver toxicity that can be caused by PPAC, I attempted to conduct the PAC biotransformation *in vitro*, so that PPAC can be converted into non-toxic metabolites. Also, biotransformation was performed by using *Saccharomyces cerevisiae* instead of the probiotic bacteria with the expectation of generating more unique bioactive metabolites. Both OPAC and PPAC were biotransformed by incubating with *S. cerevisiae*. The PAC biotransformation efficiency significantly varied depending on the sugar concentration of the *S. cerevisiae* growth medium. A partial restriction of the sugars in the growth medium may promote PAC biotransformation. *S. cerevisiae* biotransformed both OPAC and PPAC into many bioactive metabolites. The bioavailability of biotransformed (BT)-OPAC and BT-PPAC were significantly higher than non-BT-OPAC and non-BT-PPAC, respectively, as measured by uptake into Caco-2 cells and permeability through Caco-2 cell monolayers *in vitro*. The BT-OPAC and BT-PPAC were first evaluated in a palmitic acid-induced steatosis model of AML12 cells. BT-PAC could significantly reduce the palmitic acid-induced lipid accumulation in AML12 cells. BT-PAC reduced cellular lipid accumulation by suppressing the *de novo* lipogenesis and promoting the fatty acid *β*-oxidation. Moreover, BT-PAC ameliorated the palmitic acid-induced oxidative stress in the AML12 cells. BT-PAC activated the nuclear factor erythroid 2–related factor 2 (Nrf2) antioxidant pathway and upregulated the expression of cellular antioxidant enzymes. Activation of the Nrf2 pathway is considered a novel therapeutic target for NAFLD risk mitigation by resolving oxidative stress-mediated hepatic injury. As expected, the bioactivities of BT-OPAC and BT-PPAC were significantly more prominent compared to their non-BT counterparts. I also studied the potential of BT-PAC to reduce the progression of steatosis to NASH by using a palmitic acid and LPS-induced two-hit NASH model of

AML12 cells. Progression of the simple hepatic steatosis to NASH is signified by the induction of hepatic inflammation. BT-OPAC and BT-PPAC may reduce the progression of hepatic steatosis to NASH by suppressing the toll-like receptor 4 (TLR4)-mediated activation of nuclear factor-kappa-light-chain-enhancer of activated B cells (NF-κB) and mitogen-activated protein kinases (MAPK) inflammatory signalling pathways. The potential of BT-OPAC and BT-PPAC to mitigate the palmitic acid and LPS-induced inflammation in the AML12 cells was significantly more prominent compared to their non-biotransformed counterparts. *S. cerevisiae* biotransformed OPAC and PPAC into metabolites that can significantly reduce the pathogenesis of NAFLD and progression into NASH *in vitro*. Taken together, my doctoral thesis research presents a potentially novel approach to mitigate the risk of NAFLD by the development of PAC-based synbiotics. However, such synbiotics must be critically evaluated for their negative health effects.

5.2. Limitations of the research and future directions

Development of an ethanol-based PAC extraction method

The developed PAC extraction method is assisted by ultrasonication to improve extraction efficiency. During the PAC extraction, ultrasonication was conducted at the fixed 1000 W power level. In future studies, the effect of different ultrasonication power levels on the extraction efficiency of PAC can be investigated. Also, the two different modes of ultrasonication, the continuous and pulse modes, can be further studied to select the most efficient mode of operation for PAC extraction. Optimization of the ultrasonication power level and selection of the appropriate operation mode is important to save energy while ensuring the maximum PAC extraction efficiency (Kobus et al., 2021).

Characterization of the PAC

In the current study, characterization of the PAC extracted from grape seeds was performed by a method based on PAC depolymerization through phloroglucinolysis. The phloroglucinolysis reaction can depolymerize the PAC by cleaving the interflavan bonds, releasing the terminal subunit as a PAC monomer, and stabilizing the extension subunits as phloroglucinol adducts. Ideally, for the quantification of phloroglucinol adducts in the reaction mixture, standard concentration curves from each phloroglucinol adduct are required. This requires the chemical synthesis of phloroglucinol adducts by reacting the PAC monomers with phloroglucinol (Arapitsas et al., 2021; Kennedy and Jones, 2001). In the current study, phloroglucinol adducts were quantified based on the standard concentration curves created for the corresponding PAC monomers rather than the phloroglucinol adducts. Therefore, the MDP values calculated for PAC may have deviated from the true MDP values.

The potential of probiotic bacteria to biotransform PPAC

The potential of probiotic bacteria to biotransform PPAC was investigated in a C57BL/6 mouse model. The PPAC and probiotic bacteria were administered by mixing into the feed pellets which enabled the mice to consume PPAC and probiotic bacteria throughout the day. I anticipated this supplementation approach will provide sufficient time for beneficial changes in the gut microbiota and probiotic bacteria to biotransform PPAC. However, many of the studies attempting to detect PAC metabolites had administered PAC through oral gavage (Pereira-Caro et al., 2020; Prasain and Barnes, 2020). Also, the PAC metabolites can be excreted with urine and feces during supplementation over an extended period, thus, reducing the measurable concentrations of PAC metabolites in blood plasma

and organ tissues. Therefore, in future studies, oral gavage mouse models may provide more knowledge on the PAC metabolites produced by the probiotic bacteria. For instance, C57BL/6 mice can be supplemented with PPAC and probiotic bacteria through oral gavage and mice blood plasma and tissues can be analyzed for the PAC metabolites after 1, 2, 4, 6, 12, and 24 h of the gavage. Moreover, the urine and feces of the mice can also be analyzed to identify the PAC metabolites (Pereira-Caro et al., 2020). In the current study, PPAC supplementation was unable to increase the abundance of AM bacteria or improve the composition of mice's gut microbiota as suggested by previous studies (Redondo-Castillejo et al., 2023; Zhang et al., 2018). Also, the administration of PPAC compromised the gut epithelial barrier function in mice. However, several other studies had demonstrated the potential of PAC to protect the gut epithelial barrier function (Ferreira et al., 2023; Redondo-Castillejo et al., 2023). Such discrepancies may have occurred due to the opposing effects of OPAC and PPAC. In the mouse gut and Caco-2 cell monolayers, PPAC could reduce the expressions of TJ proteins while OPAC increased the expression of TJ protein, claudin-3, in the Caco-2 cell monolayers. Therefore, further experiments can be recommended to compare the effects of OPAC and PPAC on the gut microbiota and gut epithelial barrier function.

The potential of S. cerevisiae to biotransform PAC

S. cerevisiae is capable of biotransforming the OPAC and PPAC into simple metabolites. In the current study, PAC biotransformation was achieved by the incubation of PAC with *S. cerevisiae* cultures under aerobic conditions. In future research, it is interesting to investigate the potential of *S. cerevisiae* to biotransform PAC under anaerobic conditions and evaluate the bioactivities of resulting metabolites. Metabolic products of *S.*

cerevisiae can considerably vary when the biotransformation process is conducted under anaerobic conditions (Tronchoni et al., 2022).

The ability of *S. cerevisiae* to biotransform PPAC into simple metabolites may reduce the liver toxicity that could cause by PPAC. Also, the BT-OPAC and BT-PPAC were potent in reducing cellular lipid accumulation and inflammation *in vitro*, suggesting their beneficial effects in NAFLD and NASH. However, the low liver toxicity and bioactivities of the BT-PAC must be further investigated and established by using appropriate *in vivo* models. Moreover, in future studies, different strains of yeast can be tested to identify the most suitable strains for PAC biotransformation. Currently, yeast supplements containing baker's *S. cerevisiae* are commercially available. These supplements are considered to be good sources of protein, vitamins, and trace minerals (Jach et al., 2022). The addition of PAC into supplements containing live yeast may improve the bioactivities of these supplements. Moreover, such supplements can be used as ingredients in functional foods. These supplements may act as PAC-based synbiotics by biotransforming the PAC into bioavailable and bioactive metabolites. Therefore, the current study presents novel approaches to develop functional food ingredients that have the potential to be used in the prevention or treatment of NAFLD and other diseases.

5.3. Significance of the research and concluding remarks

NAFLD is the most common chronic liver disease in the world. Despite the prevalence of NAFLD is predicted to increase, an FDA-approved drug is not available to treat the disease. Therefore, I investigated the potential to develop PAC-based synbiotics capable of mitigating the risk of NAFLD. Initially, I developed an ethanol-based extraction method to obtain the food-grade PAC required to formulate PAC-based synbiotics. Most

of the current PAC extraction methods use toxic organic solvents that can leave harmful chemical residues in the extracted PAC. Also, grape by-products of wine fermentation were identified as a source for PAC extraction. Grape by-products are an abundant and economical source for the extraction of PAC required to manufacture PAC-based synbiotics on a large scale. Limited knowledge of the potential of probiotic bacteria to biotransform PAC, especially PPAC, is a major hurdle to developing PAC-based synbiotics. I established the potential of probiotic bacteria to biotransform PPAC into unique metabolites and improve PPAC biotransformation efficiency in the C57BL/6 mice. Moreover, the bioavailability of these metabolites was confirmed by their presence in the liver tissues of mice. Administration of the PPAC caused NASH in mice. Further experimentation revealed that PPAC can indirectly induce NASH in mice by impairing gut epithelial barrier function. LPS can translocate into the livers of mice through the impaired gut epithelium and induce NASH. Liver toxicity due to PPAC is not reported before. As per my knowledge, this is the first study that shows the potential of PPAC to induce hepatic injury through an indirect mechanism. Moreover, the current research suggested the converse effects of OPAC and PPAC on the expressions of TJ proteins. This emphasizes the need to explore the bioactivities of different fractions of PAC separately and characterize the PAC in supplements to ensure optimum health benefits and safety. Taken together, these results indicate the potential to develop PAC-based synbiotics and the critical need to evaluate such synbiotics for harmful health effects. Similar to the probiotic bacteria, *S. cerevisiae* was able to biotransform OPAC and PPAC into simple metabolites *in vitro*. Biotransformation of the PPAC *in vitro*, before administration/consumption, may be a viable strategy to mitigate the liver toxicity of PPAC while harnessing the beneficial

health effects. Moreover, the current study demonstrates the ability to utilize non-conventional probiotics for the formulation of PAC-based and other synbiotics. Evaluation of the bioactivities of BT-OPAC and BT-PPAC in steatosis and NASH cell models *in vitro* revealed that biotransformation can significantly improve the beneficial effects of PAC against NAFLD. Both BT-OPAC and BT-PPAC were able to mitigate palmitic acid-induced lipid accumulation (steatosis) in AML12 cells by suppressing the *de novo* lipogenesis and promoting fatty acids *β*-oxidation. Also, the BT-PAC could significantly ameliorate the palmitic acid and LPS-induced inflammation in the AML12 cells by suppressing the TLR4-mediated activation of NF-*κ*B and MAPK inflammatory signalling cascades. Therefore, the current study demonstrates the importance of PAC biotransformation to improve the bioactivities against NAFLD. Also, this research provides insight into BT-PAC-mediated mechanisms to reduce the risk of NAFLD by mitigating cellular lipid accumulation and inflammation. The ability of BT-PAC to activate the Nrf2 antioxidant pathway may present a novel approach to mitigate hepatic injury in NAFLD by resolving the hepatic oxidative stress.

To summarize, my doctoral thesis research provides the fundamental knowledge required to develop PAC-based synbiotics for reducing the risk of NAFLD and NASH. This study presents a new ethanol-based PAC extraction process and a sustainable source for the extraction of food-grade PAC, required to manufacture PAC-based synbiotics. I have established the potential of probiotic bacteria and *S. cerevisiae* to biotransform PAC into bioactive metabolites. These metabolites can reduce the risk of NAFLD and NASH by mitigating cellular lipid accumulation and inflammation *in vitro*. Future research needs to be aimed at the development of PAC-based synbiotic food products and the assessment of

these food products to reduce the risk of NAFLD and NASH using pre-clinical experimental models and human studies. I believe the findings of this research will lay the foundation for developing many novel synbiotic food products targeting the prevention of human chronic diseases.

BIBLIOGRAPHY

Actis-Goretta, L., Lévèques, A., Giuffrida, F., Romanov-Michailidis, F., Viton, F., Barron, D., Duenas-Paton, M., Gonzalez-Manzano, S., Santos-Buelga, C., Williamson, G., Dionisi, F., 2012. Elucidation of (−)-epicatechin metabolites after ingestion of chocolate by healthy humans. Free Radical Biology and Medicine 53, 787–795. https://doi.org/10.1016/j.freeradbiomed.2012.05.023

Actis-Goretta, L., Lévèques, A., Rein, M., Teml, A., Schäfer, C., Hofmann, U., Li, H., Schwab, M., Eichelbaum, M., Williamson, G., 2013. Intestinal absorption, metabolism, and excretion of (–)-epicatechin in healthy humans assessed by using an intestinal perfusion technique. The American Journal of Clinical Nutrition 98, 924–933. https://doi.org/10.3945/ajcn.113.065789

Adinolfi, L.E., Rinaldi, L., Guerrera, B., Restivo, L., Marrone, A., Giordano, M., Zampino, R., 2016. NAFLD and NASH in HCV Infection: prevalence and significance in hepatic and extrahepatic manifestations. International Journal of Molecular Sciences 17, 803. https://doi.org/10.3390/ijms17060803

Ahn, S.B., Jun, D.W., Kang, B.-K., Lim, J.H., Lim, S., Chung, M.-J., 2019. Randomized, double-blind, placebo-controlled study of a multispecies probiotic mixture in nonalcoholic fatty liver disease. Scientific Reports 9, 5688. https://doi.org/10.1038/s41598-019-42059-3

Al-Eryani, L., Wahlang, B., Falkner, K.C., Guardiola, J.J., Clair, H.B., Prough, R.A., Cave, M., 2015. Identification of environmental chemicals associated with the development of toxicant-associated fatty liver disease in rodents. Toxicologic Pathology 43, 482–497. https://doi.org/10.1177/0192623314549960

Alkhouri, N., Gornicka, A., Berk, M.P., Thapaliya, S., Dixon, L.J., Kashyap, S., Schauer, P.R., Feldstein, A.E., 2010. Adipocyte apoptosis, a link between obesity, insulin resistance, and hepatic steatosis. Journal of Biological Chemistry 285, 3428–3438. https://doi.org/10.1074/jbc.M109.074252

Amer, M.A., Othman, A.I., EL-Missiry, M.A., Farag, A.A., Amer, M.E., 2022. Proanthocyanidins attenuated liver damage and suppressed fibrosis in CCl4-treated rats. Environmental Science & Pollution Research 29, 91127–91138. https://doi.org/10.1007/s11356-022-22051-7

Aoki, R., Onuki, M., Hattori, K., Ito, M., Yamada, T., Kamikado, K., Kim, Y.-G., Nakamoto, N., Kimura, I., Clarke, J.M., Kanai, T., Hase, K., 2021. Commensal microbe-derived acetate suppresses NAFLD/NASH development via hepatic FFAR2 signalling in mice. Microbiome 9, 188. https://doi.org/10.1186/s40168-021-01125-7

Appeldoorn, M.M., Vincken, J.-P., Aura, A.-M., Hollman, P.C.H., Gruppen, H., 2009a. Procyanidin dimers are metabolized by human microbiota with 2-(3,4-dihydroxyphenyl)acetic acid and 5-(3,4-dihydroxyphenyl)-γ-valerolactone as the major metabolites. Journal of Agricultural & Food Chemistry. 57, 1084–1092. https://doi.org/10.1021/jf803059z

Appeldoorn, M.M., Vincken, J.-P., Gruppen, H., Hollman, P.C.H., 2009b. Procyanidin dimers A1, A2, and B2 are absorbed without conjugation or methylation from the small intestine of rats. The Journal of Nutrition 139, 1469–1473. https://doi.org/10.3945/jn.109.106765

Arai, N., Miura, K., Aizawa, K., Sekiya, M., Nagayama, M., Sakamoto, H., Maeda, H., Morimoto, N., Iwamoto, S., Yamamoto, H., 2022. Probiotics suppress nonalcoholic steatohepatitis and carcinogenesis progression in hepatocyte-specific PTEN knockout mice. Scientific Reports 12, 16206. https://doi.org/10.1038/s41598-022-20296-3

Arapitsas, P., Perenzoni, D., Guella, G., Mattivi, F., 2021. Improving the phloroglucinolysis protocol and characterization of Sagrantino wines proanthocyanidins. Molecules 26, 1087. https://doi.org/10.3390/molecules26041087

Atan, N.A.D., Koushki, M., Motedayen, M., Dousti, M., Sayehmiri, F., Vafaee, R., Norouzinia, M., Gholami, R., 2017. Type 2 diabetes mellitus and non-alcoholic fatty liver disease: a systematic review and meta-analysis. Gastroenterology & Hepatology from Bed to Bench 10, S1–S7.

Axling, U., Olsson, C., Xu, J., Fernandez, C., Larsson, S., Ström, K., Ahrné, S., Holm, C., Molin, G., Berger, K., 2012. Green tea powder and *Lactobacillus plantarum* affect gut microbiota, lipid metabolism and inflammation in high-fat fed C57BL/6J mice. Nutrition & Metabolism 9, 105. https://doi.org/10.1186/1743-7075-9-105

Bakhshimoghaddam, F., Shateri, K., Sina, M., Hashemian, M., Alizadeh, M., 2018. Daily consumption of synbiotic yogurt decreases liver steatosis in patients with nonalcoholic fatty liver disease: A randomized controlled clinical trial. The Journal of Nutrition 148, 1276–1284. https://doi.org/10.1093/jn/nxy088

Balakrishnan, M., Patel, P., Dunn-Valadez, S., Dao, C., Khan, V., Ali, H., El-Serag, L., Hernaez, R., Sisson, A., Thrift, A.P., Liu, Y., El-Serag, H.B., Kanwal, F., 2021. Women have a lower risk of nonalcoholic fatty liver disease but a higher risk of progression *vs* men: A systematic review and meta-analysis. Clinical Gastroenterology & Hepatology 19, 61-71.e15. https://doi.org/10.1016/j.cgh.2020.04.067

Barros, F., Awika, J.M., Rooney, L.W., 2012. Interaction of tannins and other sorghum phenolic compounds with starch and effects on *in vitro* starch digestibility. Journal of Agricultural & Food Chemistry. 60, 11609–11617. https://doi.org/10.1021/jf3034539

Bataller, R., Brenner, D.A., 2005. Liver fibrosis. Journal of Clinical Investigation 115, 209–218. https://doi.org/10.1172/JCI200524282

Beaumont, M., Neyrinck, A.M., Olivares, M., Rodriguez, J., de Rocca Serra, A., Roumain, M., Bindels, L.B., Cani, P.D., Evenepoel, P., Muccioli, G.G., Demoulin, J.-B., Delzenne, N.M., 2018. The gut microbiota metabolite indole alleviates liver inflammation in mice. FASEB Jornal 32, 6681–6693. https://doi.org/10.1096/fj.201800544

Bechmann, L.P., Gieseler, R.K., Sowa, J.-P., Kahraman, A., Erhard, J., Wedemeyer, I., Emons, B., Jochum, C., Feldkamp, T., Gerken, G., Canbay, A., 2010. Apoptosis is associated with CD36/fatty acid translocase upregulation in non-alcoholic steatohepatitis. Liver International 30, 850–859. https://doi.org/10.1111/j.1478-3231.2010.02248.x

Bedossa, P., 2017. Pathology of non-alcoholic fatty liver disease. Liver International 37, 85–89. https://doi.org/10.1111/liv.13301

Berriot-Varoqueaux, N., Aggerbeck, L.P., Samson-Bouma, M., Wetterau, J.R., 2000. The role of the microsomal triglygeride transfer protein in abetalipoproteinemia. Annual Review of Nutrition 20, 663–697. https://doi.org/10.1146/annurev.nutr.20.1.663

Blondin, D.P., Tingelstad, H.C., Noll, C., Frisch, F., Phoenix, S., Guérin, B., Turcotte, É.E., Richard, D., Haman, F., Carpentier, A.C., 2017. Dietary fatty acid metabolism of brown adipose tissue in cold-acclimated men. Nature Communications 8, 14146. https://doi.org/10.1038/ncomms14146

Bougarne, N., Weyers, B., Desmet, S.J., Deckers, J., Ray, D.W., Staels, B., De Bosscher, K., 2018. Molecular actions of PPARα in lipid metabolism and inflammation. Endocrine Reviews 39, 760–802. https://doi.org/10.1210/er.2018-00064

Boutari, C., Perakakis, N., Mantzoros, C.S., 2018. Association of adipokines with development and progression of nonalcoholic fatty liver disease. Endocrinology Metabolism 33, 33–43. https://doi.org/10.3803/EnM.2018.33.1.33

Brouwers, B., Hesselink, M.K.C., Schrauwen, P., Schrauwen-Hinderling, V.B., 2016. Effects of exercise training on intrahepatic lipid content in humans. Diabetologia 59, 2068–2079. https://doi.org/10.1007/s00125-016-4037-x

Bugianesi, E., Moscatiello, S., Ciaravella, M.F., Marchesini, G., 2010. Insulin resistance in nonalcoholic fatty liver disease. Current Pharmaceutical Design 16, 1941–1951. https://doi.org/10.2174/138161210791208875

Buzzetti, E., Pinzani, M., Tsochatzis, E.A., 2016. The multiple-hit pathogenesis of non-alcoholic fatty liver disease (NAFLD). Metabolism 65, 1038–1048. https://doi.org/10.1016/j.metabol.2015.12.012

Cádiz-Gurrea, M.D.L.L., Borrás-Linares, I., Lozano-Sánchez, J., Joven, J., Fernández-Arroyo, S., Segura-Carretero, A., 2017. Cocoa and grape seed byproducts as a source of antioxidant and anti-inflammatory proanthocyanidins. International Journal of Molecular Sciences 18, 376. https://doi.org/10.3390/ijms18020376

Cai, G., Su, H., Zhang, J., 2020. Protective effect of probiotics in patients with non-alcoholic fatty liver disease. Medicine (Baltimore) 99, e21464. https://doi.org/10.1097/MD.0000000000021464

Cai, J., Zhang, X., Chen, P., Li, Y., Liu, S., Liu, Q., Zhang, H., Wu, Z., Song, K., Liu, J., Shan, B., Liu, Y., 2022. The ER stress sensor inositol-requiring enzyme 1α in Kupffer cells promotes hepatic ischemia-reperfusion injury. Journal of Biological Chemistry 298, 101532. https://doi.org/10.1016/j.jbc.2021.101532

Caldwell, S., Lackner, C., 2017. Perspectives on NASH histology: Cellular ballooning. Annals of Hepatology 16, 182–184. https://doi.org/10.5604/16652681.1231562

Carpino, G., Del Ben, M., Pastori, D., Carnevale, R., Baratta, F., Overi, D., Francis, H., Cardinale, V., Onori, P., Safarikia, S., Cammisotto, V., Alvaro, D., Svegliati-Baroni, G., Angelico, F., Gaudio, E., Violi, F., 2020. Increased liver localization of lipopolysaccharides in human and experimental NAFLD. Hepatology 72, 470–485. https://doi.org/10.1002/hep.31056

Cha, J.-Y., Kim, D.-H., Chun, K.-H., 2018. The role of hepatic macrophages in nonalcoholic fatty liver disease and nonalcoholic steatohepatitis. Laboratory Animal Research 34, 133–139. https://doi.org/10.5625/lar.2018.34.4.133

Chen, B., Sun, L., Zeng, G., Shen, Z., Wang, K., Yin, L., Xu, F., Wang, P., Ding, Y., Nie, Q., Wu, Q., Zhang, Z., Xia, J., Lin, J., Luo, Y., Cai, J., Krausz, K.W., Zheng, R., Xue, Y., Zheng, M.-H., Li, Y., Yu, C., Gonzalez, F.J., Jiang, C., 2022. Gut bacteria alleviate smoking-related NASH by degrading gut nicotine. Nature 610, 562–568. https://doi.org/10.1038/s41586-022-05299-4

Chen, J., Thomsen, M., Vitetta, L., 2019. Interaction of gut microbiota with dysregulation of bile acids in the pathogenesis of nonalcoholic fatty liver disease and potential therapeutic implications of probiotics. Journal of Cellular Biochemistry 120, 2713–2720. https://doi.org/10.1002/jcb.27635

Chen, J., Vitetta, L., 2020. Gut microbiota metabolites in NAFLD pathogenesis and therapeutic implications. International Journal of Molecular Sciences 21. https://doi.org/10.3390/ijms21155214

Chen, M., Liu, J., Yang, W., Ling, W., 2017. Lipopolysaccharide mediates hepatic stellate cell activation by regulating autophagy and retinoic acid signaling. Autophagy 13, 1813–1827. https://doi.org/10.1080/15548627.2017.1356550

Chen, X., Zhang, Z., Li, H., Zhao, J., Wei, X., Lin, W., Zhao, X., Jiang, A., Yuan, J., 2020. Endogenous ethanol produced by intestinal bacteria induces mitochondrial dysfunction in non-alcoholic fatty liver disease. Journal of Gastroenterology and Hepatology 35, 2009–2019. https://doi.org/10.1111/jgh.15027

Chen, Y., Zhang, J., Cui, W., Silverstein, R.L., 2022. CD36, a signaling receptor and fatty acid transporter that regulates immune cell metabolism and fate. Journal of Experimental Medicine 219, e20211314. https://doi.org/10.1084/jem.20211314

Chen, Z., Tian, R., She, Z., Cai, J., Li, H., 2020. Role of oxidative stress in the pathogenesis of nonalcoholic fatty liver disease. Free Radical Biology and Medicine 152, 116–141. https://doi.org/10.1016/j.freeradbiomed.2020.02.025

Chiang, J.Y.L., Ferrell, J.M., 2020. Bile acid receptors FXR and TGR5 signaling in fatty liver diseases and therapy. American Journal of Physiology-Gastrointestinal & Liver Physiology 318, G554–G573. https://doi.org/10.1152/ajpgi.00223.2019

Cho, Y.-E., Kim, D.-K., Seo, W., Gao, B., Yoo, S.-H., Song, B.-J., 2021. Fructose promotes leaky gut, endotoxemia and liver fibrosis through CYP2E1-mediated oxidative and nitrative stress. Hepatology 73, 2180–2195. https://doi.org/10.1002/hep.30652

Cho, Y.-J., Lee, H.G., Seo, K.-H., Yokoyama, W., Kim, H., 2018. Antiobesity effect of prebiotic polyphenol-rich grape seed flour supplemented with probiotic kefir-derived lactic acid bacteria. Journal of Agricultural & Food Chemistry. 66, 12498–12511. https://doi.org/10.1021/acs.jafc.8b03720

Cichoż-Lach, H., Michalak, A., 2014. Oxidative stress as a crucial factor in liver diseases. World Journal of Gastroenterology 20, 8082–8091. https://doi.org/10.3748/wjg.v20.i25.8082

Clifford, B.L., Sedgeman, L.R., Williams, K.J., Morand, P., Cheng, A., Jarrett, K.E., Chan, A.P., Brearley-Sholto, M.C., Wahlström, A., Ashby, J.W., Barshop, W., Wohlschlegel, J., Calkin, A.C., Liu, Y., Thorell, A., Meikle, P.J., Drew, B.G., Mack, J.J., Marschall, H.-U., Tarling, E.J., Edwards, P.A., de Aguiar Vallim, T.Q., 2021. FXR activation protects against NAFLD via bile-acid-dependent reductions in lipid absorption. Cell Metabolism 33, 1671-1684.e4. https://doi.org/10.1016/j.cmet.2021.06.012

D'Aquila, T., Hung, Y.-H., Carreiro, A., Buhman, K.K., 2016. Recent discoveries on absorption of dietary fat: Presence, synthesis, and metabolism of cytoplasmic lipid droplets within enterocytes. Biochimica et Biophysica Acta (BBA) - Molecular & Cell Biology of Lipids 1861, 730–747. https://doi.org/10.1016/j.bbalip.2016.04.012

de Camargo, A.C., Regitano-d'Arce, M.A.B., Rasera, G.B., Canniatti-Brazaca, S.G., do Prado-Silva, L., Alvarenga, V.O., Sant'Ana, A.S., Shahidi, F., 2017. Phenolic acids and flavonoids of peanut by-products: Antioxidant capacity and antimicrobial effects. Food Chemistry 237, 538–544. https://doi.org/10.1016/j.foodchem.2017.05.046

Demaria, T.M., Crepaldi, L.D., Costa-Bartuli, E., Branco, J.R., Zancan, P., Sola-Penna, M., 2023. Once a week consumption of Western diet over twelve weeks promotes sustained insulin resistance and non-alcoholic fat liver disease in C57BL/6 J mice. Scientific Reports 13, 3058. https://doi.org/10.1038/s41598-023-30254-2

Deprez, S., Mila, I., Huneau, J.-F., Tome, D., Scalbert, A., 2001. Transport of proanthocyanidin dimer, trimer, and polymer across monolayers of human intestinal epithelial Caco-2 cells. Antioxidants & Redox Signaling 3, 957–967. https://doi.org/10.1089/152308601317203503

DeZwaan-McCabe, D., Sheldon, R.D., Gorecki, M.C., Guo, D.-F., Gansemer, E.R., Kaufman, R.J., Rahmouni, K., Gillum, M.P., Taylor, E.B., Teesch, L.M., Rutkowski, D.T., 2017. ER stress inhibits liver fatty acid oxidation while unmitigated stress leads to anorexia-induced lipolysis and both liver and kidney steatosis. Cell Reports 19, 1794–1806. https://doi.org/10.1016/j.celrep.2017.05.020

Dong, N.-Q., Lin, H.-X., 2021. Contribution of phenylpropanoid metabolism to plant development and plant–environment interactions. Journal of Integrative Plant Biology 63, 180–209. https://doi.org/10.1111/jipb.13054

Donnelly, K.L., Smith, C.I., Schwarzenberg, S.J., Jessurun, J., Boldt, M.D., Parks, E.J., 2005. Sources of fatty acids stored in liver and secreted via lipoproteins in patients with nonalcoholic fatty liver disease. Journal of Clinical Investigation 115, 1343–1351. https://doi.org/10.1172/JCI23621

Donovan, J.L., Crespy, V., Manach, C., Morand, C., Besson, C., Scalbert, A., Rémésy, C., 2001. Catechin is metabolized by both the small intestine and liver of rats. The Journal of Nutrition 131, 1753–1757. https://doi.org/10.1093/jn/131.6.1753

Donovan, J.L., Lee, A., Manach, C., Rios, L., Morand, C., Scalbert, A., Rémésy, C., 2002. Procyanidins are not bioavailable in rats fed a single meal containing a grapeseed extract or the procyanidin dimer B3. British Journal of Nutrition 87, 299–306. https://doi.org/10.1079/BJN2001517

Eslamparast, T., Poustchi, H., Zamani, F., Sharafkhah, M., Malekzadeh, R., Hekmatdoost, A., 2014. Synbiotic supplementation in nonalcoholic fatty liver disease: a randomized, double-blind, placebo-controlled pilot study1,2,3. The American Journal of Clinical Nutrition 99, 535–542. https://doi.org/10.3945/ajcn.113.068890

Falkevall, A., Mehlem, A., Folestad, E., Ning, F.C., Osorio-Conles, Ó., Radmann, R., de Hollanda, A., Wright, S.D., Scotney, P., Nash, A., Eriksson, U., 2023. Inhibition of VEGF-B signaling prevents non-alcoholic fatty liver disease development by targeting lipolysis in the white adipose tissue. Journal of Hepatology. https://doi.org/10.1016/j.jhep.2023.01.014

Fei, N., Bruneau, A., Zhang, X., Wang, R., Wang, J., Rabot, S., Gérard, P., Zhao, L., 2020. Endotoxin producers overgrowing in human gut microbiota as the causative agents for nonalcoholic fatty liver disease. mBio 11, e03263-19. https://doi.org/10.1128/mBio.03263-19

Feldman, F., Koudoufio, M., El-Jalbout, R., Sauvé, M.F., Ahmarani, L., Sané, A.T., Ould-Chikh, N.-E.-H., N'Timbane, T., Patey, N., Desjardins, Y., Stintzi, A., Spahis, S., Levy, E., 2023. Cranberry proanthocyanidins as a therapeutic strategy to curb metabolic syndrome and fatty liver-associated disorders. Antioxidants 12, 90. https://doi.org/10.3390/antiox12010090

Fernando, D.H., Forbes, J.M., Angus, P.W., Herath, C.B., 2019. Development and progression of non-alcoholic fatty liver disease: The role of advanced glycation end products. International Journal of Molecular Sciences 20, 5037. https://doi.org/10.3390/ijms20205037

Ferreira, Y.A.M., Jamar, G., Estadella, D., Pisani, L.P., 2023. Proanthocyanidins in grape seeds and their role in gut microbiota-white adipose tissue axis. Food Chemistry 404, 134405. https://doi.org/10.1016/j.foodchem.2022.134405

Fiorucci, S., Zampella, A., Ricci, P., Distrutti, E., Biagioli, M., 2022. Immunomodulatory functions of FXR. Molecular & Cellular Endocrinology 551, 111650. https://doi.org/10.1016/j.mce.2022.111650

Fisher, J.E., Mckenzie, T.J., Lillegard, J.B., Yu, Y., Juskewitch, J.E., Nedredal, G.I., Brunn, G.J., Yi, E.S., Smyrk, T.C., Nyberg, S.L., 2013. Role of Kupffer cells and toll-like receptor 4 in acetaminophen-induced acute liver failure. Journal of Surgical Research 180, 147–155. https://doi.org/10.1016/j.jss.2012.11.051

Francque, S., Verrijken, A., Caron, S., Prawitt, J., Paumelle, R., Derudas, B., Lefebvre, P., Taskinen, M.-R., Van Hul, W., Mertens, I., Hubens, G., Van Marck, E., Michielsen, P., Van Gaal, L., Staels, B., 2015. PPARα gene expression correlates with severity and histological treatment response in patients with non-alcoholic steatohepatitis. Journal of Hepatology 63, 164–173. https://doi.org/10.1016/j.jhep.2015.02.019

Friedman, S.L., Neuschwander-Tetri, B.A., Rinella, M., Sanyal, A.J., 2018. Mechanisms of NAFLD development and therapeutic strategies. Nature Medicine 24, 908–922. https://doi.org/10.1038/s41591-018-0104-9

Fuchs, A., Samovski, D., Smith, G.I., Cifarelli, V., Farabi, S.S., Yoshino, J., Pietka, T., Chang, S.-W., Ghosh, S., Myckatyn, T.M., Klein, S., 2021. Associations among adipose tissue immunology, inflammation, exosomes and insulin sensitivity in people with obesity and nonalcoholic fatty liver disease. Gastroenterology 161, 968-981.e12. https://doi.org/10.1053/j.gastro.2021.05.008

Fujita, K., Nozaki, Y., Wada, K., Yoneda, M., Fujimoto, Y., Fujitake, M., Endo, H., Takahashi, H., Inamori, M., Kobayashi, N., Kirikoshi, H., Kubota, K., Saito, S., Nakajima, A., 2009. Dysfunctional very-low-density lipoprotein synthesis and release is a key factor in nonalcoholic steatohepatitis pathogenesis. Hepatology 50, 772–780. https://doi.org/10.1002/hep.23094

Fukunishi, S., Sujishi, T., Takeshita, A., Ohama, H., Tsuchimoto, Y., Asai, A., Tsuda, Y., Higuchi, K., 2014. Lipopolysaccharides accelerate hepatic steatosis in the development of nonalcoholic fatty liver disease in Zucker rats. Journal of Clinical Biochemistry & Nutrition 54, 39–44. https://doi.org/10.3164/jcbn.13-49

Gandhi, C.R., 2020. Pro- and anti-fibrogenic functions of gram-negative bacterial lipopolysaccharide in the liver. Frontiers in Medicine (Lausanne) 7, 130. https://doi.org/10.3389/fmed.2020.00130

Gandhi, C.R., 2012. Oxidative stress and hepatic stellate cells: A paradoxical relationship. Trends in Cell & Molecular Biology 7, 1–10.

Giorgio, V., Prono, F., Graziano, F., Nobili, V., 2013. Pediatric non alcoholic fatty liver disease: old and new concepts on development, progression, metabolic insight and potential treatment targets. BMC Pediatrics 13, 40. https://doi.org/10.1186/1471-2431-13-40

Gomaraschi, M., Fracanzani, A.L., Dongiovanni, P., Pavanello, C., Giorgio, E., Da Dalt, L., Norata, G.D., Calabresi, L., Consonni, D., Lombardi, R., Branchi, A., Fargion, S., 2019. Lipid accumulation impairs lysosomal acid lipase activity in hepatocytes: Evidence in NAFLD patients and cell cultures. Biochimica et Biophysica Acta (BBA) - Molecular and Cell Biology of Lipids 1864, 158523. https://doi.org/10.1016/j.bbalip.2019.158523

Goyal, A., Arora, H., Arora, S., 2020. Prevalence of fatty liver in metabolic syndrome. Journal of Family Medicine & Primary Care 9, 3246. https://doi.org/10.4103/jfmpc.jfmpc_1108_19

Gu, L., House, S.E., Rooney, L., Prior, R.L., 2007. Sorghum bran in the diet dose dependently increased the excretion of catechins and microbial-derived phenolic acids in female rats. Journal of Agricultural & Food Chemistry 55, 5326–5334. https://doi.org/10.1021/jf070100p

Gu, L., Kelm, M.A., Hammerstone, J.F., Beecher, G., Holden, J., Haytowitz, D., Gebhardt, S., Prior, R.L., 2004. Concentrations of proanthocyanidins in common foods and estimations of normal consumption. Journal of Nutrition 134, 613–617. https://doi.org/10.1093/jn/134.3.613

Gu, Y., Li, X., Chen, H., Sun, Y., Yang, L., Ma, Y., Yong Chan, E.C., 2022. Antidiabetic effects of multi-species probiotic and its fermented milk in mice via restoring gut microbiota and intestinal barrier. Food Bioscience 47, 101619. https://doi.org/10.1016/j.fbio.2022.101619

Gunaratne, A., Wu, K., Li, D., Bentota, A., Corke, H., Cai, Y.-Z., 2013. Antioxidant activity and nutritional quality of traditional red-grained rice varieties containing proanthocyanidins. Food Chemistry 138, 1153–1161. https://doi.org/10.1016/j.foodchem.2012.11.129

Guo, C., Chen, W.-D., Wang, Y.-D., 2016. TGR5, not only a metabolic regulator. Frontiers in Physiology 7, 646. https://doi.org/10.3389/fphys.2016.00646

Hamesch, K., Borkham-Kamphorst, E., Strnad, P., Weiskirchen, R., 2015. Lipopolysaccharide-induced inflammatory liver injury in mice. Lab Animal 49, 37–46. https://doi.org/10.1177/0023677215570087

Hanlin, R.L., Kelm, M.A., Wilkinson, K.L., Downey, M.O., 2011. Detailed characterization of proanthocyanidins in skin, seeds, and wine of shiraz and cabernet sauvignon wine grapes (Vitis vinifera). Journal of Agricultural & Food Chemistry 12.

Hashemnia, S.M.R., Meshkani, R., Zamani-Garmsiri, F., Shabani, M., Tajabadi-Ebrahimi, M., Ragerdi Kashani, I., Siadat, S.D., Mohassel Azadi, S., Emamgholipour, S., 2023. Amelioration of obesity-induced white adipose tissue inflammation by Bacillus coagulans T4 in a high-fat diet-induced obese murine model. Life Sciences 314, 121286. https://doi.org/10.1016/j.lfs.2022.121286

He, F., Pan, Q.-H., Shi, Y., Duan, C.-Q., 2008. Biosynthesis and genetic regulation of proanthocyanidins in plants. Molecules 13, 2674–2703. https://doi.org/10.3390/molecules13102674

Heeren, J., Scheja, L., 2021. Metabolic-associated fatty liver disease and lipoprotein metabolism. Molecular Metabolism 50, 101238. https://doi.org/10.1016/j.molmet.2021.101238

Horie, Y., Suzuki, A., Kataoka, E., Sasaki, T., Hamada, K., Sasaki, J., Mizuno, K., Hasegawa, G., Kishimoto, H., Iizuka, M., Naito, M., Enomoto, K., Watanabe, S., Mak, T.W., Nakano, T., 2004. Hepatocyte-specific Pten deficiency results in steatohepatitis and hepatocellular carcinomas. Journal of Clinical Investigation 113, 1774–1783. https://doi.org/10.1172/JCI200420513

Hu, H., Tian, M., Ding, C., Yu, S., 2019. The C/EBP homologous protein (CHOP) transcription factor functions in endoplasmic reticulum stress-induced apoptosis and microbial infection. Frontiers in Immunology 9, 3083. ttps://doi.org/10.3389/fimmu.2018.03083

Iannuzzo, F., Piccolo, V., Novellino, E., Schiano, E., Salviati, E., Summa, V., Campiglia, P., Tenore, G.C., Maisto, M., 2022. A food-grade method for enhancing the levels of low molecular weight proanthocyanidins with potentially high intestinal bioavailability. International Journal of Molecular Sciences 23, 13557. https://doi.org/10.3390/ijms232113557

Igarashi, Y., Tanaka, M., Okada, H., Hashimoto, Y., Kumagai, M., Yamaoka, M., Nishimura, H., Fukui, M., 2022. Visceral adipose tissue quality was associated with nonalcoholic fatty liver disease, independent of its quantity. Nutrition, Metabolism & Cardiovascular Diseases 32, 973–980. https://doi.org/10.1016/j.numecd.2022.01.009

Illesca, P., Valenzuela, R., Espinosa, A., Echeverría, F., Soto-Alarcon, S., Ortiz, M., Videla, L.A., 2019. Hydroxytyrosol supplementation ameliorates the metabolic disturbances in white adipose tissue from mice fed a high-fat diet through recovery of transcription factors Nrf2, SREBP-1c, PPAR-γ and NF-κB. Biomedicine & Pharmacotherapy 109, 2472–2481. https://doi.org/10.1016/j.biopha.2018.11.120

Jach, M.E., Serefko, A., Ziaja, M., Kieliszek, M., 2022. Yeast protein as an easily accessible food source. Metabolites 12, 63. https://doi.org/10.3390/metabo12010063

Jasirwan, C.O.M., Lesmana, C.R.A., Hasan, I., Sulaiman, A.S., Gani, R.A., 2019. The role of gut microbiota in non-alcoholic fatty liver disease: pathways of mechanisms. Bioscience of Microbiota, Food and Health 38, 81. https://doi.org/10.12938/bmfh.18-032

Jasirwan, C.O.M., Muradi, A., Hasan, I., Simadibrata, M., Rinaldi, I., 2021. Correlation of gut Firmicutes/Bacteroidetes ratio with fibrosis and steatosis stratified by body mass index in patients with non-alcoholic fatty liver disease. Bioscience of Microbiota, Food & Health 40, 50–58. https://doi.org/10.12938/bmfh.2020-046

Ji, Y., Gao, Y., Chen, H., Yin, Y., Zhang, W., 2019. Indole-3-acetic acid alleviates nonalcoholic fatty liver disease in mice via attenuation of hepatic lipogenesis, and oxidative and inflammatory stress. Nutrients 11, 2062. https://doi.org/10.3390/nu11092062

Jiang, M., Wu, Y.-L., Li, X., Zhang, Y., Xia, K.-L., Cui, B.-W., Lian, L.-H., Nan, J.-X., 2017. Oligomeric proanthocyanidin derived from grape seeds inhibited NF-κB signaling in activated HSC: Involvement of JNK/ERK MAPK and PI3K/Akt pathways. Biomedicine & Pharmacotherapy 93, 674–680. https://doi.org/10.1016/j.biopha.2017.06.105

Juárez-Fernández, M., Porras, D., Petrov, P., Román-Sagüillo, S., García-Mediavilla, M.V., Soluyanova, P., Martínez-Flórez, S., González-Gallego, J., Nistal, E., Jover, R., Sánchez-Campos, S., 2021. The synbiotic combination of *Akkermansia muciniphila* and quercetin ameliorates early obesity and NAFLD through gut microbiota reshaping and bile acid metabolism modulation. Antioxidants 10, 2001. https://doi.org/10.3390/antiox10122001

Kang, Y., Kang, X., Yang, H., Liu, H., Yang, X., Liu, Q., Tian, H., Xue, Y., Ren, P., Kuang, X., Cai, Y., Tong, M., Li, L., Fan, W., 2022. *Lactobacillus acidophilus* ameliorates obesity in mice through modulation of gut microbiota dysbiosis and intestinal permeability. Pharmacological Research 175, 106020. https://doi.org/10.1016/j.phrs.2021.106020

Kawano, Y., Cohen, D.E., 2013. Mechanisms of hepatic triglyceride accumulation in non-alcoholic fatty liver disease. Journal of Gastroenterology 48, 434–441. https://doi.org/10.1007/s00535-013-0758-5

Kennedy, J.A., Jones, G.P., 2001. Analysis of proanthocyanidin cleavage products following acid-catalysis in the presence of excess phloroglucinol. Journal of Agricultural & Food Chemistry. 49, 1740–1746. https://doi.org/10.1021/jf001030o

Khan, A., Ding, Z., Ishaq, M., Bacha, A.S., Khan, I., Hanif, A., Li, W., Guo, X., 2021. Understanding the effects of gut microbiota dysbiosis on nonalcoholic fatty liver disease and the possible probiotics role: Recent updates. International Journal of Biological Sciences 17, 818–833. https://doi.org/10.7150/ijbs.56214

Kim, S.H., Kwon, D., Kwak, J.-H., Lee, S., Lee, Y.-H., Yun, J., Son, T.G., Jung, Y.-S., 2018. Tunicamycin-induced ER stress is accompanied with oxidative stress via abrogation of sulfur amino acids metabolism in the liver. International Journal of Molecular Sciences 19, 4114. https://doi.org/10.3390/ijms19124114

Knaze, V., Zamora-Ros, R., Luján-Barroso, L., Romieu, I., Scalbert, A., Slimani, N., Riboli, E., Rossum, C.T.M. van, Bueno-de-Mesquita, H.B., Trichopoulou, A., Dilis, V., Tsiotas, K., Skeie, G., Engeset, D., Quirós, J.R., Molina, E., Huerta, J.M., Crowe, F., Wirfäl, E., Ericson, U., Peeters, P.H.M., Kaaks, R., Teucher, B., Johansson, G., Johansson, I., Tumino, R., Boeing, H., Drogan, D., Amiano, P., Mattiello, A., Khaw, K.-T., Luben, R., Krogh, V., Ardanáz, E., Sacerdote, C., Salvini, S., Overvad, K., Tjønneland, A., Olsen, A., Boutron-Ruault, M.-C., Fagherazzi, G., Perquier, F., González, C.A., 2012. Intake estimation of total and individual flavan-3-ols, proanthocyanidins and theaflavins, their food sources and determinants in the European prospective investigation into cancer and nutrition (EPIC) study. British Journal of Nutrition 108, 1095–1108. https://doi.org/10.1017/S0007114511006386

Kneeman, J.M., Misdraji, J., Corey, K.E., 2012. Secondary causes of nonalcoholic fatty liver disease. Therapeutic Advances in Gastroenterology 5, 199–207. https://doi.org/10.1177/1756283X11430859

Kobus, Z., Krzywicka, M., Pecyna, A., Buczaj, A., 2021. Process efficiency and energy consumption during the ultrasound-assisted extraction of bioactive substances from hawthorn berries. Energies 14, 7638. https://doi.org/10.3390/en14227638

Kolaric, T.O., Nincevic, V., Kuna, L., Duspara, K., Bojanic, K., Vukadin, S., Raguz-Lucic, N., Wu, G.Y., Smolic, M., 2021. Drug-induced fatty liver disease: Pathogenesis and treatment. Journal of Clinical & Translational Hepatology 9, 731–737. https://doi.org/10.14218/JCTH.2020.00091

Koliaki, C., Szendroedi, J., Kaul, K., Jelenik, T., Nowotny, P., Jankowiak, F., Herder, C., Carstensen, M., Krausch, M., Knoefel, W.T., Schlensak, M., Roden, M., 2015. Adaptation of hepatic mitochondrial function in humans with non-alcoholic fatty liver is lost in steatohepatitis. Cell Metabolism 21, 739–746. https://doi.org/10.1016/j.cmet.2015.04.004

Kong, C., Gao, R., Yan, X., Huang, L., Qin, H., 2019. Probiotics improve gut microbiota dysbiosis in obese mice fed a high-fat or high-sucrose diet. Nutrition 60, 175–184. https://doi.org/10.1016/j.nut.2018.10.002

Kosmalski, M., Ziółkowska, S., Czarny, P., Szemraj, J., Pietras, T., 2022. The coexistence of nonalcoholic fatty liver disease and type 2 diabetes mellitus. Journal of Clinical Medicine 11, 1375. https://doi.org/10.3390/jcm11051375

Krawczyk, B., Wityk, P., Gałęcka, M., Michalik, M., 2021. The many faces of Enterococcus spp.-commensal, probiotic and opportunistic pathogen. Microorganisms 9, 1900. https://doi.org/10.3390/microorganisms9091900

Kuchay, M.S., Martínez-Montoro, J.I., Choudhary, N.S., Fernández-García, J.C., Ramos-Molina, B., 2021. Non-alcoholic fatty liver disease in lean and non-obese individuals: Current and future challenges. Biomedicines 9, 1346. https://doi.org/10.3390/biomedicines9101346

Kumar, V., Sharma, A., Kohli, S.K., Bali, S., Sharma, M., Kumar, R., Bhardwaj, R., Thukral, A.K., 2019. Differential distribution of polyphenols in plants using multivariate techniques. Biotechnology Research & Innovation 3, 1–21. https://doi.org/10.1016/j.biori.2019.03.001

Kwon, J.-H., Lee, H.G., Seo, K.-H., Kim, H., 2019. Combination of whole grapeseed flour and newly isolated kefir lactic acid bacteria reduces high-fat-induced hepatic steatosis. Molecular Nutrition & Food Research 63, 1801040. https://doi.org/10.1002/mnfr.201801040

Ky, I., Le Floch, A., Zeng, L., Pechamat, L., Jourdes, M., Teissedre, P.-L., 2016. Tannins, in: Caballero, B., Finglas, P.M., Toldrá, F. (Eds.), Encyclopedia of Food and Health. Academic Press, Oxford, pp. 247–255. https://doi.org/10.1016/B978-0-12-384947-2.00683-8

Le, M.H., Yeo, Y.H., Zou, B., Barnet, S., Henry, L., Cheung, R., Nguyen, M.H., 2022. Forecasted 2040 global prevalence of nonalcoholic fatty liver disease using hierarchical bayesian approach. Clinical & Molecular Hepatology 28, 841–850. https://doi.org/10.3350/cmh.2022.0239

Lebeaupin, C., Vallée, D., Hazari, Y., Hetz, C., Chevet, E., Bailly-Maitre, B., 2018. Endoplasmic reticulum stress signalling and the pathogenesis of non-alcoholic fatty liver disease. Journal of Hepatology 69, 927–947. https://doi.org/10.1016/j.jhep.2018.06.008

Lee, N.Y., Shin, M.J., Youn, G.S., Yoon, S.J., Choi, Y.R., Kim, H.S., Gupta, H., Han, S.H., Kim, B.K., Lee, D.Y., Park, T.S., Sung, H., Kim, B.Y., Suk, K.T., 2021. *Lactobacillus* attenuates progression of nonalcoholic fatty liver disease by lowering cholesterol and steatosis. Clinical & Molecular Hepatology 27, 110–124. https://doi.org/10.3350/cmh.2020.0125

Leguisamo, N.M., Lehnen, A.M., Machado, U.F., Okamoto, M.M., Markoski, M.M., Pinto, G.H., Schaan, B.D., 2012. GLUT4 content decreases along with insulin resistance and high levels of inflammatory markers in rats with metabolic syndrome. Cardiovascular Diabetology 11, 100. https://doi.org/10.1186/1475-2840-11-100

Li, H., Herrmann, T., Seeßle, J., Liebisch, G., Merle, U., Stremmel, W., Chamulitrat, W., 2022. Role of fatty acid transport protein 4 in metabolic tissues: Insights into obesity and fatty liver disease. Bioscience Reports 42, BSR20211854. https://doi.org/10.1042/BSR20211854

Li, M., Feng, L., Jiang, W.-D., Wu, P., Liu, Y., Jiang, J., Kuang, S.-Y., Tang, L., Zhou, X.-Q., 2020. Condensed tannins decreased the growth performance and impaired intestinal immune function in on-growing grass carp (*Ctenopharyngodon idella*). British Journal of Nutrition 123, 737–755. https://doi.org/10.1017/S0007114519003295

Li, S., Hong, M., Tan, H.-Y., Wang, N., Feng, Y., 2016. Insights into the role and interdependence of oxidative stress and inflammation in liver diseases. Oxidative Medicine and Cellular Longevity 2016, e4234061. https://doi.org/10.1155/2016/4234061

Li, X., Zhang, B., Hu, Y., Zhao, Y., 2021. New Insights into gut-bacteria-derived indole and its derivatives in intestinal and liver diseases. Frontiers in Pharmacology 12, 769501. https://doi.org/10.3389/fphar.2021.769501

Lim, I., Ha, J., 2021. Biosynthetic pathway of proanthocyanidins in major cash crops. Plants (Basel) 10, 1792. https://doi.org/10.3390/plants10091792

Lin, Y., Feng, X., Cao, X., Miao, R., Sun, Y., Li, R., Ye, J., Zhong, B., 2022. Age patterns of nonalcoholic fatty liver disease incidence: Heterogeneous associations with metabolic changes. Diabetology & Metabolic Syndrome 14, 181. https://doi.org/10.1186/s13098-022-00930-w

Lund, M.N., 2021. Reactions of plant polyphenols in foods: Impact of molecular structure. Trends in Food Science & Technology 112, 241–251. https://doi.org/10.1016/j.tifs.2021.03.056

Luo, M., Yan, J., Wu, L., Wu, J., Chen, Zheng, Jiang, J., Chen, Zhiyun, He, B., 2021. Probiotics alleviated nonalcoholic fatty liver disease in high-fat diet-fed rats via gut microbiota/FXR/FGF15 signaling pathway. Journal of Immunology Research 2021, 2264737. https://doi.org/10.1155/2021/2264737

Lytle, K.A., Bush, N.C., Triay, J.M., Kellogg, T.A., Kendrick, M.L., Swain, J.M., Gathaiya, N.W., Hames, K.C., Jensen, M.D., 2019. Hepatic fatty acid balance and hepatic fat content in humans with severe obesity. The Journal of Clinical Endocrinology & Metabolism 104, 6171–6181. https://doi.org/10.1210/jc.2019-00875

Maeda, H., Ishima, Y., Saruwatari, J., Mizuta, Y., Minayoshi, Y., Ichimizu, S., Yanagisawa, H., Nagasaki, T., Yasuda, K., Oshiro, S., Taura, M., McConnell, M.J., Oniki, K., Sonoda, K., Wakayama, T., Kinoshita, M., Shuto, T., Kai, H., Tanaka, M., Sasaki, Y., Iwakiri, Y., Otagiri, M., Watanabe, H., Maruyama, T., 2022. Nitric oxide facilitates the targeting Kupffer cells of a nano-antioxidant for the treatment of NASH. Journal of Controlled Release 341, 457–474. https://doi.org/10.1016/j.jconrel.2021.11.039

Mahmoud, O.M., Mahmoud, G.A.E., Atta, H., Abbas, W.A., Ahmed, H.M., Abozaid, M.A.A., 2023. Visceral and subcutaneous fat, muscle mass, and liver volume as noninvasive predictors of the progress of non-alcoholic fatty liver disease. Egyptian Journal of Radiology and Nuclear Medicine 54, 5. https://doi.org/10.1186/s43055-022-00949-z

Malhi, H., Guicciardi, M.E., Gores, G.J., 2010. Hepatocyte death: A clear and present danger. Physiology Reviews 90, 1165–1194. https://doi.org/10.1152/physrev.00061.2009

Mannino, G., Chinigò, G., Serio, G., Genova, T., Gentile, C., Munaron, L., Bertea, C.M., 2021. Proanthocyanidins and where to find them: A meta-analytic approach to investigate their chemistry, biosynthesis, distribution, and effect on human health. Antioxidants (Basel) 10, 1229. https://doi.org/10.3390/antiox10081229

Marjot, T., Moolla, A., Cobbold, J.F., Hodson, L., Tomlinson, J.W., 2020. Nonalcoholic fatty liver disease in adults: Current Concepts in etiology, outcomes, and management. Endocrine Reviews 41, 66–117. https://doi.org/10.1210/endrev/bnz009

Martin, K., Hatab, A., Athwal, V.S., Jokl, E., Hanley, K.P., 2021. Genetic contribution to non-alcoholic fatty liver disease and prognostic implications. Current Diabetes Reports 21. https://doi.org/10.1007/s11892-021-01377-5

Mbatha, K.R., Downs, C.T., Nsahlai, I.V., 2002. The effects of graded levels of dietary tannin on the epithelial tissue of the gastro-intestinal tract and liver and kidney masses of Boer goats. Animal Science 74, 579–586. https://doi.org/10.1017/S1357729800052735

Mendoza-Wilson, A.M., Castro-Arredondo, S.I., Espinosa-Plascencia, A., Robles-Burgueño, M. del R., Balandrán-Quintana, R.R., Bermúdez-Almada, M. del C., 2016. Chemical composition and antioxidant-prooxidant potential of a polyphenolic extract and a proanthocyanidin-rich fraction of apple skin. Heliyon 2, e00073. https://doi.org/10.1016/j.heliyon.2016.e00073

Meshulam, T., Simard, J.R., Wharton, J., Hamilton, J.A., Pilch, P.F., 2006. Role of caveolin-1 and cholesterol in transmembrane fatty acid movement. Biochemistry 45, 2882–2893. https://doi.org/10.1021/bi051999b

Miller, K.B., Stuart, D.A., Smith, N.L., Lee, C.Y., McHale, N.L., Flanagan, J.A., Ou, B., Hurst, W.J., 2006. Antioxidant Activity and polyphenol and procyanidin contents of selected commercially available cocoa-containing and chocolate products in the United States. Journal of Agricultural & Food Chemistry 54, 4062–4068. https://doi.org/10.1021/jf060290o

Milner, E., Stevens, B., An, M., Lam, V., Ainsworth, M., Dihle, P., Stearns, J., Dombrowski, A., Rego, D., Segars, K., 2021. Utilizing probiotics for the prevention and treatment of gastrointestinal diseases. Frontiers in Microbiology 12, 689958. https://doi.org/ 10.3389/fmicb.2021.689958

Miquilena-Colina, M.E., Lima-Cabello, E., Sánchez-Campos, S., García-Mediavilla, M.V., Fernández-Bermejo, M., Lozano-Rodríguez, T., Vargas-Castrillón, J., Buqué, X., Ochoa, B., Aspichueta, P., González-Gallego, J., García-Monzón, C., 2011. Hepatic fatty acid translocase CD36 upregulation is associated with insulin resistance, hyperinsulinaemia and increased steatosis in non-alcoholic steatohepatitis and chronic hepatitis C. Gut 60, 1394–1402. https://doi.org/10.1136/gut.2010.222844

Mofidi, F., Poustchi, H., Yari, Z., Nourinayyer, B., Merat, S., Sharafkhah, M., Malekzadeh, R., Hekmatdoost, A., 2017. Synbiotic supplementation in lean patients with non-alcoholic fatty liver disease: a pilot, randomised, double-blind, placebo-controlled, clinical trial. British Journal of Nutrition 117, 662–668. https://doi.org/10.1017/S0007114517000204

Mojiri-Forushani, H., Hemmati, A., Khanzadeh, A., Zahedi, A., 2022. Effectiveness of grape seed extract in patients with nonalcoholic fatty liver: A randomized double-blind clinical study. Hepatitis Monthly 22. https://doi.org/10.5812/hepatmon-132309

Morán-Salvador, E., López-Parra, M., García-Alonso, V., Titos, E., Martínez-Clemente, M., González-Périz, A., López-Vicario, C., Barak, Y., Arroyo, V., Clària, J., 2011. Role for PPARγ in obesity-induced hepatic steatosis as determined by hepatocyte- and macrophage-specific conditional knockouts. FASEB Journal 25, 2538–2550. https://doi.org/10.1096/fj.10-173716

Mu, T., Peng, L., Xie, X., He, H., Shao, Q., Wang, X., Zhang, Y., 2022. Single nucleotide polymorphism of genes associated with metabolic fatty liver disease. Journal of Oncology 2022, 9282557. https://doi.org/10.1155/2022/9282557

Mundi, M.S., Velapati, S., Patel, J., Kellogg, T.A., Abu Dayyeh, B.K., Hurt, R.T., 2020. Evolution of NAFLD and its management. Nutrition in Clinical Practice 35, 72–84. https://doi.org/10.1002/ncp.10449

Naguib, G., Morris, N., Yang, S., Fryzek, N., Haynes-Williams, V., Huang, W.C.A., Norman-Wheeler, J., Rotman, Y., 2020. Dietary fatty acid oxidation is decreased in non-alcoholic fatty liver disease: A palmitate breath test study. Liver International 40, 590–597. https://doi.org/10.1111/liv.14309

Nan, B., Yang, C., Li, L., Ye, H., Yan, H., Wang, M., Yuan, Y., 2021. Allicin alleviated acrylamide-induced NLRP3 inflammasome activation via oxidative stress and endoplasmic reticulum stress in Kupffer cells and SD rats liver. Food & Chemical Toxicology 148, 111937. https://doi.org/10.1016/j.fct.2020.111937

Nassir, F., Rector, R.S., Hammoud, G.M., Ibdah, J.A., 2015. Pathogenesis and prevention of hepatic steatosis. Gastroenterology & Hepatology 11, 167–175.

Nie, Y., Stürzenbaum, S.R., 2019. Proanthocyanidins of natural origin: Molecular mechanisms and implications for lipid disorder and aging-associated diseases. Advances in Nutrition 10, 464–478. https://doi.org/10.1093/advances/nmy118

Nissar, A.U., Sharma, L., Tasduq, S.A., 2015. Palmitic acid induced lipotoxicity is associated with altered lipid metabolism, enhanced CYP450 2E1 and intracellular calcium mediated ER stress in human hepatoma cells. Toxicology Research 4, 1344–1358. https://doi.org/10.1039/C5TX00101C

Okamoto, M., Miyake, T., Kitai, K., Furukawa, S., Yamamoto, S., Senba, H., Kanzaki, S., Deguchi, A., Koizumi, M., Ishihara, T., Miyaoka, H., Yoshida, O., Hirooka, M., Kumagi, T., Abe, M., Matsuura, B., Hiasa, Y., 2018. Cigarette smoking is a risk factor for the onset of fatty liver disease in nondrinkers: A longitudinal cohort study. PLoS One 13, e0195147. https://doi.org/10.1371/journal.pone.0195147

Orita, A., Musou-Yahada, A., Shoji, T., Oki, T., Ohta, H., 2019. Comparison of anthocyanins, proanthocyanidin oligomers and antioxidant capacity between cowpea and grain legumes with colored seed coat. Food Science & Technology Research 25, 287–294. https://doi.org/10.3136/fstr.25.287

Ottaviani, J.I., Kwik-Uribe, C., Keen, C.L., Schroeter, H., 2012. Intake of dietary procyanidins does not contribute to the pool of circulating flavanols in humans. The American Journal of Clinical Nutrition 95, 851–858. https://doi.org/10.3945/ajcn.111.028340

Ou, K., Gu, L., 2014. Absorption and metabolism of proanthocyanidins. Journal of Functional Foods 7, 43–53. https://doi.org/10.1016/j.jff.2013.08.004

Ou, K., Sarnoski, P., Schneider, K.R., Song, K., Khoo, C., Gu, L., 2014. Microbial catabolism of procyanidins by human gut microbiota. Molecular Nutrition & Food Research 58, 2196–2205. https://doi.org/10.1002/mnfr.201400243

Özcan, E., Rozycki, M.R., Sela, D.A., 2021. Cranberry proanthocyanidins and dietary oligosaccharides synergistically modulate lactobacillus plantarum physiology. Microorganisms 9, 656. https://doi.org/10.3390/microorganisms9030656

Panahi, G., Pasalar, P., Zare, M., Rizzuto, R., Meshkani, R., 2018. High glucose induces inflammatory responses in HepG2 cells via the oxidative stress-mediated activation of NF-κB, and MAPK pathways in HepG2 cells. Archives of Physiology & Biochemistry 124, 468–474. https://doi.org/10.1080/13813455.2018.1427764

Pandey, K.B., Rizvi, S.I., 2009. Plant polyphenols as dietary antioxidants in human health and disease. Oxidative Medicine & Cellular Longevity 2, 270–278. https://doi.org/10.4161/oxim.2.5.9498

Pang, Q., Zhang, J.-Y., Song, S.-D., Qu, K., Xu, X.-S., Liu, S.-S., Liu, C., 2015. Central obesity and nonalcoholic fatty liver disease risk after adjusting for body mass index. World Journal of Gastroenterology 21, 1650–1662. https://doi.org/10.3748/wjg.v21.i5.1650

Park, J.-W., Kim, S.-E., Lee, N.Y., Kim, J.-H., Jung, J.-H., Jang, M.-K., Park, S.-H., Lee, M.-S., Kim, D.-J., Kim, H.-S., Suk, K.T., 2022. Role of microbiota-derived metabolites in alcoholic and non-alcoholic fatty liver diseases. International Journal of Molecular Sciences 23, 426. https://doi.org/10.3390/ijms23010426

Parker, R., 2018. The role of adipose tissue in fatty liver diseases. Liver Research 2, 35–42. https://doi.org/10.1016/j.livres.2018.02.002

Pawlak, M., Lefebvre, P., Staels, B., 2015. Molecular mechanism of PPARα action and its impact on lipid metabolism, inflammation and fibrosis in non-alcoholic fatty liver disease. Journal of Hepatology 62, 720–733. https://doi.org/10.1016/j.jhep.2014.10.039

Pereira-Caro, G., Gaillet, S., Luis Ordóñez, J., Mena, P., Bresciani, L., A. Bindon, K., Rio, D.D., Rouanet, J.-M., Manuel Moreno-Rojas, J., Crozier, A., 2020. Bioavailability of red wine and grape seed proanthocyanidins in rats. Food & Function 11, 3986–4001. https://doi.org/10.1039/D0FO00350F

Petrescu, A.D., Grant, S., Williams, E., An, S.Y., Seth, N., Shell, M., Amundsen, T., Tan, C., Nadeem, Y., Tjahja, M., Weld, L., Chu, C.S., Venter, J., Frampton, G., McMillin, M., DeMorrow, S., 2022. Leptin enhances hepatic fibrosis and inflammation in a mouse model of cholestasis. The American Journal of Pathology 192, 484–502. https://doi.org/10.1016/j.ajpath.2021.11.008

Pettinelli, P., Videla, L.A., 2011. Up-regulation of PPAR-γ mRNA expression in the liver of obese patients: An Additional reinforcing lipogenic mechanism to SREBP-1c induction. The Journal of Clinical Endocrinology & Metabolism 96, 1424–1430. https://doi.org/10.1210/jc.2010-2129

Podszun, M.C., Alawad, A.S., Lingala, S., Morris, N., Huang, W.-C.A., Yang, S., Schoenfeld, M., Rolt, A., Ouwerkerk, R., Valdez, K., Umarova, R., Ma, Y., Fatima, S.Z., Lin, D.D., Mahajan, L.S., Samala, N., Violet, P.-C., Levine, M., Shamburek, R., Gharib, A.M., Kleiner, D.E., Garraffo, H.M., Cai, H., Walter, P.J., Rotman, Y., 2020. Vitamin E treatment in NAFLD patients demonstrates that oxidative stress drives steatosis through upregulation of de-novo lipogenesis. Redox Biology 37, 101710. https://doi.org/10.1016/j.redox.2020.101710

Polyzos, S.A., Kountouras, J., Zavos, C., 2009. The multi-hit process and the antagonistic roles of tumor necrosis factor-alpha and adiponectin in non alcoholic fatty liver disease. Hippokratia 13, 127.

Polyzos, S.A., Toulis, K.A., Goulis, D.G., Zavos, C., Kountouras, J., 2011. Serum total adiponectin in nonalcoholic fatty liver disease: a systematic review and meta-analysis. Metabolism 60, 313–326. https://doi.org/10.1016/j.metabol.2010.09.003

Prasain, J.K., Barnes, S., 2020. Cranberry polyphenols-gut microbiota interactions and potential health benefits: An updated review. Food Frontiers 1, 459–464. https://doi.org/10.1002/fft2.56

Qiu, Y., Liu, S., Chen, H.-T., Yu, C.-H., Teng, X.-D., Yao, H.-T., Xu, G.-Q., 2013. Upregulation of caveolin-1 and SR-B1 in mice with non-alcoholic fatty liver disease. Hepatobiliary & Pancreatic Diseases International 12, 630–636. https://doi.org/10.1016/S1499-3872(13)60099-5

Ran, L.-S., Wu, Y.-Z., Gan, Y.-W., Wang, H.-L., Wu, L.-J., Zheng, C.-M., Ming, Y., Xiong, R., Li, Y.-L., Lei, S.-H., Wang, X., Lao, X.-Q., Zhang, H.-M., Wang, L., Chen, C., Zhao, C.-Y., 2023. Andrographolide ameliorates hepatic steatosis by suppressing FATP2-mediated fatty acid uptake in mice with nonalcoholic fatty liver disease. Journal of Natural Medicines 77, 73–86. https://doi.org/10.1007/s11418-022-01647-w

Rau, M., Rehman, A., Dittrich, M., Groen, A.K., Hermanns, H.M., Seyfried, F., Beyersdorf, N., Dandekar, T., Rosenstiel, P., Geier, A., 2018. Fecal SCFAs and SCFA-producing bacteria in gut microbiome of human NAFLD as a putative link to systemic T-cell activation and advanced disease. United European Gastroenterol Journal 6, 1496–1507. https://doi.org/10.1177/2050640618804444

Rauf, A., Imran, M., Abu-Izneid, T., Iahtisham-Ul-Haq, Patel, S., Pan, X., Naz, S., Sanches Silva, A., Saeed, F., Rasul Suleria, H.A., 2019. Proanthocyanidins: A comprehensive review. Biomedicine & Pharmacotherapy 116, 108999. https://doi.org/10.1016/j.biopha.2019.108999

Redondo-Castillejo, R., Garcimartín, A., Hernández-Martín, M., López-Oliva, M.E., Bocanegra, A., Macho-González, A., Bastida, S., Benedí, J., Sánchez-Muniz, F.J., 2023. Proanthocyanidins: impact on gut microbiota and intestinal action mechanisms in the prevention and treatment of metabolic syndrome. International Journal of Molecular Sciences 24, 5369. https://doi.org/10.3390/ijms24065369

Rennert, C., Heil, T., Schicht, G., Stilkerich, A., Seidemann, L., Kegel-Hübner, V., Seehofer, D., Damm, G., 2020. Prolonged lipid accumulation in cultured primary human hepatocytes rather leads to ER Stress than oxidative stress. International Journal of Molecular Sciences 21, 7097. https://doi.org/10.3390/ijms21197097

Reynoso-Camacho, R., Sotelo-González, A.M., Patiño-Ortiz, P., Rocha-Guzmán, N.E., Pérez-Ramírez, I.F., 2021. Berry by-products obtained from a decoction process are a rich source of low- and high-molecular weight extractable and non-extractable polyphenols. Food & Bioproducts Processing 127, 371–387. https://doi.org/10.1016/j.fbp.2021.03.014

Rezayat, A.A., Moghadam, M.D., Nour, M.G., Shirazinia, M., Ghodsi, H., Rouhbakhsh Zahmatkesh, M.R., Tavakolizadeh Noghabi, M., Hoseini, B., Akhavan Rezayat, K., 2018. Association between smoking and non-alcoholic fatty liver disease: A systematic review and meta-analysis. SAGE Open Med 6, 2050312117745223. https://doi.org/10.1177/2050312117745223

Riazi, K., Swain, M.G., Congly, S.E., Kaplan, G.G., Shaheen, A.-A., 2022. Race and ethnicity in non-alcoholic fatty liver disease (NAFLD): A narrative review. Nutrients 14, 4556. https://doi.org/10.3390/nu14214556

Rich, N.E., Oji, S., Mufti, A.R., Browning, J.D., Parikh, N.D., Odewole, M., Mayo, H., Singal, A.G., 2018. Racial and ethnic disparities in nonalcoholic fatty liver disease prevalence, severity, and outcomes in the United States: A systematic review and meta-analysis. Clinical Gastroenterology & Hepatology 16, 198-210.e2. https://doi.org/10.1016/j.cgh.2017.09.041

Ring, A., Le Lay, S., Pohl, J., Verkade, P., Stremmel, W., 2006. Caveolin-1 is required for fatty acid translocase (FAT/CD36) localization and function at the plasma membrane of mouse embryonic fibroblasts. Biochimica et Biophysica Acta 1761, 416–423. https://doi.org/10.1016/j.bbalip.2006.03.016

Rios, L.Y., Bennett, R.N., Lazarus, S.A., Rémésy, C., Scalbert, A., Williamson, G., 2002. Cocoa procyanidins are stable during gastric transit in humans. The American Journal of Clinical Nutrition 76, 1106–1110. https://doi.org/10.1093/ajcn/76.5.1106

Rockey, D.C., Du, Q., Shi, Z., 2019. Smooth muscle α-actin deficiency leads to decreased liver fibrosis via impaired cytoskeletal signaling in hepatic stellate cells. The American Journal of Pathology 189, 2209–2220. https://doi.org/10.1016/j.ajpath.2019.07.019

Rossi, F., Amadoro, C., Colavita, G., 2019. Members of the *Lactobacillus* Genus Complex (LGC) as opportunistic pathogens: A review. Microorganisms 7, 126. https://doi.org/10.3390/microorganisms7050126

Rotundo, L., Persaud, A., Feurdean, M., Ahlawat, S., Kim, H.-S., 2018. The association of leptin with severity of non-alcoholic fatty liver disease: A population-based study. Clinical & Molecular Hepatology 24, 392–401. https://doi.org/10.3350/cmh.2018.0011

Rupasinghe, H.P.V., Kean, C., 2008. Polyphenol concentrations in apple processing by-products determined using electrospray ionization mass spectrometry. Canadian Journal of Plant Science 88, 759–762. https://doi.org/10.4141/CJPS07146

Rupasinghe, H.P.V., Parmar, I., Neir, S.V., 2019. Biotransformation of cranberry proanthocyanidins to probiotic metabolites by *Lactobacillus rhamnosus* enhances their anticancer activity in HepG2 cells *in vitro*. Oxidative Medicine & Cellular Longevity 2019. https://doi.org/10.1155/2019/4750795

Sabotta, C.M., Kwan, S.-Y., Petty, L.E., Below, J.E., Joon, A., Wei, P., Fisher-Hoch, S.P., McCormick, J.B., Beretta, L., 2022. Genetic variants associated with circulating liver injury markers in Mexican Americans, a population at risk for non-alcoholic fatty liver disease. Frontiers in Genetics 13, 995488. https://doi.org/10.3389/fgene.2022.995488

Samtiya, M., Aluko, R.E., Dhewa, T., Moreno-Rojas, J.M., 2021. Potential health benefits of plant food-derived bioactive components: An overview. Foods 10, 839. https://doi.org/10.3390/foods10040839

Sánchez-Moreno, C., Cao, G., Ou, B., Prior, R.L., 2003. Anthocyanin and proanthocyanidin content in selected white and red wines. Oxygen radical absorbance capacity comparison with nontraditional wines obtained from highbush blueberry. Journal of Agricultural & Food Chemistry 51, 4889–4896. https://doi.org/10.1021/jf030081t

Sánchez-Patán, F., Cueva, C., Monagas, M., Walton, G.E., Gibson, G.R., Martín-Álvarez, P.J., Victoria Moreno-Arribas, M., Bartolomé, B., 2012. Gut microbial catabolism of grape seed flavan-3-ols by human faecal microbiota. Targetted analysis of precursor compounds, intermediate metabolites and end-products. Food Chemistry 131, 337–347. https://doi.org/10.1016/j.foodchem.2011.08.011

Sankararaman, S., Noriega, K., Velayuthan, S., Sferra, T., Martindale, R., 2023. Gut microbiome and its impact on obesity and obesity-related disorders. Current Gastroenterology Reports 25, 31–44. https://doi.org/10.1007/s11894-022-00859-0

Sano, A., 2017. Safety assessment of 4-week oral intake of proanthocyanidin-rich grape seed extract in healthy subjects. Food & Chemical Toxicology 108, 519–523. https://doi.org/10.1016/j.fct.2016.11.021

Savic, D., Hodson, L., Neubauer, S., Pavlides, M., 2020. The importance of the fatty acid transporter L-carnitine in non-alcoholic fatty liver disease (NAFLD). Nutrients 12, 2178. https://doi.org/10.3390/nu12082178

Schmitt, J., Kong, B., Stieger, B., Tschopp, O., Schultze, S.M., Rau, M., Weber, A., Müllhaupt, B., Guo, G.L., Geier, A., 2015. Protective effects of farnesoid X receptor (FXR) on hepatic lipid accumulation are mediated by hepatic FXR and independent of intestinal FGF15 signal. Liver International 35, 1133–1144. https://doi.org/10.1111/liv.12456

Seo, K.-H., Kim, D.-H., Yokoyama, W.H., Kim, H., 2020. Synbiotic effect of whole grape seed flour and newly isolated kefir lactic acid bacteria on intestinal microbiota of diet-induced obese mice. Journal of Agricultural & Food Chemistry 68, 13131–13137. https://doi.org/10.1021/acs.jafc.0c01240

Sharma, R., Kumari, M., Kumari, A., Sharma, A., Gulati, A., Gupta, M., Padwad, Y., 2019. Diet supplemented with phytochemical epigallocatechin gallate and probiotic Lactobacillus fermentum confers second generation synbiotic effects by modulating cellular immune responses and antioxidant capacity in aging mice. European Journal of Nutrition 58, 2943–2957. https://doi.org/10.1007/s00394-018-01890-6

Shelness, G.S., Sellers, J.A., 2001. Very-low-density lipoprotein assembly and secretion. Current Opinion in Lipidology 12, 151–157.

Shen, F., Zheng, R.-D., Sun, X.-Q., Ding, W.-J., Wang, X.-Y., Fan, J.-G., 2017. Gut microbiota dysbiosis in patients with non-alcoholic fatty liver disease. Hepatobiliary & Pancreatic Diseases International 16, 375–381. https://doi.org/10.1016/S1499-3872(17)60019-5

Shinjo, S., Jiang, S., Nameta, M., Suzuki, T., Kanai, M., Nomura, Y., Goda, N., 2017. Disruption of the mitochondria-associated ER membrane (MAM) plays a central role in palmitic acid–induced insulin resistance. Experimental Cell Research 359, 86–93. https://doi.org/10.1016/j.yexcr.2017.08.006

Singh, S., Allen, A.M., Wang, Z., Prokop, L.J., Murad, M.H., Loomba, R., 2015. Fibrosis progression in nonalcoholic fatty liver *vs* nonalcoholic steatohepatitis: A systematic review and meta-analysis of paired-biopsy studies. Clinical Gastroenterology & Hepatology 13, 643-654.e9. https://doi.org/10.1016/j.cgh.2014.04.014

Skat-Rørdam, J., Højland Ipsen, D., Lykkesfeldt, J., Tveden-Nyborg, P., 2019. A role of peroxisome proliferator-activated receptor γ in non-alcoholic fatty liver disease. Basic & Clinical Pharmacology & Toxicology 124, 528–537. https://doi.org/10.1111/bcpt.13190

Smith, G.I., Shankaran, M., Yoshino, M., Schweitzer, G.G., Chondronikola, M., Beals, J.W., Okunade, A.L., Patterson, B.W., Nyangau, E., Field, T., Sirlin, C.B., Talukdar, S., Hellerstein, M.K., Klein, S., 2020. Insulin resistance drives hepatic de novo lipogenesis in nonalcoholic fatty liver disease. Journal of Clinical Investigation 130, 1453–1460. https://doi.org/10.1172/JCI134165

Smuda, S.S., Mohsen, S.M., Olsen, K., Aly, M.H., 2018. Bioactive compounds and antioxidant activities of some cereal milling by-products. Journal of Food Science & Technology 55, 1134–1142. https://doi.org/10.1007/s13197-017-3029-2

Song, M.J., Malhi, H., 2019. The unfolded protein response and hepatic lipid metabolism in non-alcoholic fatty liver disease. Pharmacology & Therapeutics 203, 107401. https://doi.org/10.1016/j.pharmthera.2019.107401

Spencer, J.P.E., Chaudry, F., Pannala, A.S., Srai, S.K., Debnam, E., Rice-Evans, C., 2000. Decomposition of cocoa procyanidins in the gastric milieu. Biochemical & Biophysical Research Communications 272, 236–241. https://doi.org/10.1006/bbrc.2000.2749

Spencer, J.P.E., Schroeter, H., Shenoy, B., S. Srai, S.K., Debnam, E.S., Rice-Evans, C., 2001. Epicatechin is the primary bioavailable form of the procyanidin dimers B2 and B5 after transfer across the small intestine. Biochemical & Biophysical Research Communications 285, 588–593. https://doi.org/10.1006/bbrc.2001.5211

Stalmach, A., Mullen, W., Steiling, H., Williamson, G., Lean, M.E.J., Crozier, A., 2010. Absorption, metabolism, and excretion of green tea flavan-3-ols in humans with an ileostomy. Molecular Nutrition & Food Research 54, 323–334. https://doi.org/10.1002/mnfr.200900194

Stoupi, S., Williamson, G., Drynan, J.W., Barron, D., Clifford, M.N., 2010. A comparison of the in vitro biotransformation of (–)-epicatechin and procyanidin B2 by human faecal microbiota. Molecular Nutrition & Food Research 54, 747–759. https://doi.org/10.1002/mnfr.200900123

Su, H., Li, Y., Hu, D., Xie, L., Ke, H., Zheng, X., Chen, W., 2018. Procyanidin B2 ameliorates free fatty acids-induced hepatic steatosis through regulating TFEB-mediated lysosomal pathway and redox state. Free Radical Biology & Medicine 126, 269–286. https://doi.org/10.1016/j.freeradbiomed.2018.08.024

Sun, H.Y., Gu, A.X., Huang, B.Y., Zhang, T., Li, J.P., Shan, A.S., 2022. Dietary grape seed proanthocyanidin alleviates the liver injury induced by long-term high-fat diets in Sprague Dawley rats. Frontiers in Veterinary Science 9, 959906. https://doi.org/10.3389/fvets.2022.959906

Suresh, D., Srinivas, A.N., Kumar, D.P., 2020. Etiology of hepatocellular carcinoma: Special focus on fatty liver disease. Frontiers in Oncology 10, 601710. https://doi.org/10.3389/fonc.2020.601710

Swanson, K.S., Gibson, G.R., Hutkins, R., Reimer, R.A., Reid, G., Verbeke, K., Scott, K.P., Holscher, H.D., Azad, M.B., Delzenne, N.M., Sanders, M.E., 2020. The international scientific association for probiotics and prebiotics (ISAPP) consensus statement on the definition and scope of synbiotics. Nature Reviews Gastroenterology & Hepatology 17, 687–701. https://doi.org/10.1038/s41575-020-0344-2

Takeda, M., Sakaguchi, T., Hiraide, T., Shibasaki, Y., Morita, Y., Kikuchi, H., Ikegami, K., Setou, M., Konno, H., Takeuchi, H., 2018. Role of caveolin-1 in hepatocellular carcinoma arising from non-alcoholic fatty liver disease. Cancer Science 109, 2401–2411. https://doi.org/10.1111/cas.13659

Tang, C., Meng, F., Pang, X., Chen, M., Zhou, L., Lu, Z., Lu, Y., 2020. Protective effects of *Lactobacillus acidophilus* NX2-6 against oleic acid-induced steatosis, mitochondrial dysfunction, endoplasmic reticulum stress and inflammatory responses. Journal of Functional Foods 74, 104206. https://doi.org/10.1016/j.jff.2020.104206

Tang, C., Tan, B., Sun, X., 2021. Elucidation of interaction between whey proteins and proanthocyanidins and its protective effects on proanthocyanidins during *in-vitro* digestion and storage. Molecules 26, 5468. https://doi.org/10.3390/molecules26185468

Tang, C., Zhou, W., Shan, M., Lu, Z., Lu, Y., 2022. Yogurt-derived Lactobacillus plantarum Q16 alleviated high-fat diet-induced non-alcoholic fatty liver disease in mice. Food Science and Human Wellness 11, 1428–1439. https://doi.org/10.1016/j.fshw.2022.04.034

Tanoli, T., Yue, P., Yablonskiy, D., Schonfeld, G., 2004. Fatty liver in familial hypobetalipoproteinemia: roles of the APOB defects, intra-abdominal adipose tissue, and insulin sensitivity. Journal of Lipid Research 45, 941–947. https://doi.org/10.1194/jlr.M300508-JLR200

Tao, W., Wei, C., Shen, S., Wang, M., Chen, S., Ye, X., Cao, Y., 2020. Mainly dimers and trimers of chinese bayberry leaves proanthocyanidins (BLPs) are utilized by gut microbiota: *In vitro* digestion and fermentation coupled with Caco-2 transportation. Molecules 25, 184. https://doi.org/10.3390/molecules25010184

Tao, W., Zhang, Y., Shen, X., Cao, Y., Shi, J., Ye, X., Chen, S., 2019. Rethinking the mechanism of the health benefits of proanthocyanidins: Absorption, metabolism, and interaction with gut microbiota. Comprehensive Reviews in Food Science & Food Safety 18, 971–985. https://doi.org/10.1111/1541-4337.12444

Tariq, R., Axley, P., Singal, A.K., 2020. Extra-hepatic manifestations of nonalcoholic fatty liver disease: A review. Journal of Clinical & Experimental Hepatology 10, 81–87. https://doi.org/10.1016/j.jceh.2019.07.008

Teixeira, A., Baenas, N., Dominguez-Perles, R., Barros, A., Rosa, E., Moreno, D.A., Garcia-Viguera, C., 2014. Natural bioactive compounds from winery by-products as health promoters: A review. International Journal of Molecular Sciences 15, 15638–15678. https://doi.org/10.3390/ijms150915638

Thiele, N.D., Wirth, J.W., Steins, D., Koop, A.C., Ittrich, H., Lohse, A.W., Kluwe, J., 2017. TIMP-1 is upregulated, but not essential in hepatic fibrogenesis and carcinogenesis in mice. Scientific Reports 7, 714. https://doi.org/10.1038/s41598-017-00671-1

Thilakarathna, W.P.D.W., Rupasinghe, H.P.V., 2022. Optimization of the extraction of proanthocyanidins from grape seeds using ultrasonication-assisted aqueous ethanol and evaluation of anti-steatosis activity *in vitro*. Molecules 27, 1363. https://doi.org/10.3390/molecules27041363

Thomas, C., Gioiello, A., Noriega, L., Strehle, A., Oury, J., Rizzo, G., Macchiarulo, A., Yamamoto, H., Mataki, C., Pruzanski, M., Pellicciari, R., Auwerx, J., Schoonjans, K., 2009. TGR5-mediated bile acid sensing controls glucose homeostasis. Cell Metabolism 10, 167–177. https://doi.org/10.1016/j.cmet.2009.08.001

Tilg, H., Adolph, T.E., Moschen, A.R., 2021. Multiple parallel hits hypothesis in nonalcoholic fatty liver disease: Revisited after a decade. Hepatology 73, 833–842. https://doi.org/10.1002/hep.31518

Tokoro, M., Gotoh, K., Kudo, Y., Hirashita, Y., Iwao, M., Arakawa, M., Endo, M., Oribe, J., Masaki, T., Honda, K., Kakuma, T., Seike, M., Murakami, K., Shibata, H., 2020. α-Tocopherol suppresses hepatic steatosis by increasing CPT-1 expression in a mouse model of diet-induced nonalcoholic fatty liver disease. Obesity Science & Practice 7, 91–99. https://doi.org/10.1002/osp4.460

Tong, W., Chen, X., Song, X., Chen, Y., Jia, R., Zou, Y., Li, L., Yin, L., He, C., Liang, X., Ye, G., Lv, C., Lin, J., Yin, Z., 2020. Resveratrol inhibits LPS-induced inflammation through suppressing the signaling cascades of TLR4-NF-κB/MAPKs/IRF3. Experimental & Therapeutic Medicine 19, 1824–1834. https://doi.org/10.3892/etm.2019.8396

Torra, I.P., Claudel, T., Duval, C., Kosykh, V., Fruchart, J.-C., Staels, B., 2003. Bile acids induce the expression of the human peroxisome proliferator-activated receptor α gene via activation of the farnesoid X receptor. Molecular Endocrinology 17, 259–272. https://doi.org/10.1210/me.2002-0120

Torre, S.D., 2020. Non-alcoholic fatty liver disease as a canonical example of metabolic inflammatory-based liver disease showing a sex-specific prevalence: Relevance of estrogen signaling. Frontiers in Endocrinology 11, 572490. https://doi.org/10.3389/fendo.2020.572490

Tronchoni, J., Gonzalez, R., Guindal, A.M., Calleja, E., Morales, P., 2022. Exploring the suitability of Saccharomyces cerevisiae strains for winemaking under aerobic conditions. Food Microbiology 101, 103893. https://doi.org/10.1016/j.fm.2021.103893

Tuladhar, P., Sasidharan, S., Saudagar, P., 2021. 17 - Role of phenols and polyphenols in plant defense response to biotic and abiotic stresses, in: Jogaiah, S. (Ed.), Biocontrol Agents and Secondary Metabolites. Woodhead Publishing, pp. 419–441. https://doi.org/10.1016/B978-0-12-822919-4.00017-X

van der Windt, D.J., Sud, V., Zhang, H., Tsung, A., Huang, H., 2018. The effects of physical exercise on fatty liver disease. Gene Expression 18, 89–101. https://doi.org/10.3727/105221617X15124844266408

Vasques-Monteiro, I.M.L., Silva-Veiga, F.M., Miranda, C.S., de Andrade Gonçalves, É.C.B., Daleprane, J.B., Souza-Mello, V., 2021. A rise in Proteobacteria is an indicator of gut-liver axis-mediated nonalcoholic fatty liver disease in high-fructose-fed adult mice. Nutrition Research 91, 26–35. https://doi.org/10.1016/j.nutres.2021.04.008

Vazquez-Flores, A.A., Martinez-Gonzalez, A.I., Alvarez-Parrilla, E., Díaz-Sánchez, Á.G., de la Rosa, L.A., González-Aguilar, G.A., Aguilar, C.N., 2018. Proanthocyanidins with a low degree of polymerization are good inhibitors of digestive enzymes because of their ability to form specific interactions: A hypothesis. Journal of Food Science 83, 2895–2902. https://doi.org/10.1111/1750-3841.14386

Verardo, V., Cevoli, C., Pasini, F., Gómez-Caravaca, A.M., Marconi, E., Fabbri, A., Caboni, M.F., 2015. Analysis of oligomer proanthocyanidins in different barley genotypes using high-performance liquid chromatography–fluorescence detection–mass spectrometry and near-infrared methodologies. Journal of Agricultural & Food Chemistry 63, 4130–4137. https://doi.org/10.1021/acs.jafc.5b01425

Villanueva, C.J., Monetti, M., Shih, M., Zhou, P., Watkins, S.M., Bhanot, S., Farese, R.V., 2009. A specific role for dgat1 in hepatic steatosis due to exogenous fatty acids. Hepatology 50, 434–442. https://doi.org/10.1002/hep.22980

Vogiatzoglou, A., Mulligan, A.A., Lentjes, M.A.H., Luben, R.N., Spencer, J.P.E., Schroeter, H., Khaw, K.-T., Kuhnle, G.G.C., 2015. Flavonoid Intake in European Adults (18 to 64 Years). PLOS ONE 10, e0128132. https://doi.org/10.1371/journal.pone.0128132

Vrhovsek, U., Rigo, A., Tonon, D., Mattivi, F., 2004. Quantitation of polyphenols in different apple varieties. Journal of Agricultural & Food Chemistry 52, 6532–6538. https://doi.org/10.1021/jf049317z

Wang, B., Jiang, X., Cao, M., Ge, J., Bao, Q., Tang, L., Chen, Y., Li, L., 2016. Altered fecal microbiota correlates with liver biochemistry in nonobese patients with non-alcoholic fatty liver disease. Scientific Reports 6, 32002. https://doi.org/10.1038/srep32002

Wang, D., Wei, Y., Pagliassotti, M.J., 2006. Saturated fatty acids promote endoplasmic reticulum stress and liver injury in rats with hepatic steatosis. Endocrinology 147, 943–951. https://doi.org/10.1210/en.2005-0570

Wang, J., He, W., Tsai, P.-J., Chen, P.-H., Ye, M., Guo, J., Su, Z., 2020. Mutual interaction between endoplasmic reticulum and mitochondria in nonalcoholic fatty liver disease. Lipids in Health and Disease 19, 72. https://doi.org/10.1186/s12944-020-01210-0

Wang, L., Yi, J., Guo, J., Ren, X., 2023. Weigh change across adulthood is related to the presence of NAFLD: results from NHANES III. Journal of Translational Medicine 21, 142. https://doi.org/10.1186/s12967-023-04007-8

Wang, M., Mao, H., Chen, J., Li, Q., Ma, W., Zhu, N., Qi, L., Wang, J., 2022. Chinese bayberry (*Myrica rubra* Sieb. et Zucc.) leaves proanthocyanidins alleviate insulin-resistance via activating PI3K/AKT pathway in HepG2 cells. Journal of Functional Foods 99, 105297. https://doi.org/10.1016/j.jff.2022.105297

Wang, M., Zhang, B., Hu, J., Nie, S., Xiong, T., Xie, M., 2020. Intervention of five strains of *Lactobacillus* on obesity in mice induced by high-fat diet. Journal of Functional Foods 72, 104078. https://doi.org/10.1016/j.jff.2020.104078

Wang, P., Liu, Y., Zhang, L., Wang, W., Hou, H., Zhao, Y., Jiang, X., Yu, J., Tan, H., Wang, Y., Xie, D.-Y., Gao, L., Xia, T., 2020. Functional demonstration of plant flavonoid carbocations proposed to be involved in the biosynthesis of proanthocyanidins. The Plant Journal 101, 18–36. https://doi.org/10.1111/tpj.14515

Wang, X., Rao, H., Liu, F., Wei, L., Li, H., Wu, C., 2021. Recent advances in adipose tissue dysfunction and its role in the pathogenesis of non-alcoholic fatty liver disease. Cells 10, 3300. https://doi.org/10.3390/cells10123300

Wang, Y., Chung, S.-J., Song, W.O., Chun, O.K., 2011. Estimation of daily proanthocyanidin intake and major food sources in the U.S. diet. The Journal of Nutrition 141, 447–452. https://doi.org/10.3945/jn.110.133900

Wang, Y.-D., Chen, W.-D., Yu, D., Forman, B.M., Huang, W., 2011. The G-protein-coupled bile acid receptor, Gpbar1 (TGR5), negatively regulates hepatic inflammatory response through antagonizing nuclear factor kappa light-chain enhancer of activated B cells (NF-κB) in mice. Hepatology 54, 1421–1432. https://doi.org/10.1002/hep.24525

Watanabe, M., Houten, S.M., Wang, L., Moschetta, A., Mangelsdorf, D.J., Heyman, R.A., Moore, D.D., Auwerx, J., 2004. Bile acids lower triglyceride levels via a pathway involving FXR, SHP, and SREBP-1c. Journal of Clinical Investigation 113, 1408–1418. https://doi.org/10.1172/JCI21025

Wu, Y., Mo, R., Zhang, M., Zhou, W., Li, D., 2022. Grape seed proanthocyanidin alleviates intestinal inflammation through gut microbiota-bile acid crosstalk in mice. Frontiers in Nutrition 8, 786682. https://doi.org/10.3389/fnut.2021.786682

Xia, Y., Li, Q., Zhong, W., Dong, J., Wang, Z., Wang, C., 2011. L-carnitine ameliorated fatty liver in high-calorie diet/STZ-induced type 2 diabetic mice by improving mitochondrial function. Diabetology & Metabolic Syndrome 3, 31. https://doi.org/10.1186/1758-5996-3-31

Xiao, Y., Yang, C., Xu, H., Wu, Q., Zhou, Y., Zhou, X., Miao, J., 2020. Procyanidin B2 prevents dyslipidemia via modulation of gut microbiome and related metabolites in high-fat diet fed mice. Journal of Functional Foods 75, 104285. https://doi.org/10.1016/j.jff.2020.104285

Xie, G., Jiang, R., Wang, X., Liu, P., Zhao, A., Wu, Y., Huang, F., Liu, Z., Rajani, C., Zheng, X., Qiu, J., Zhang, X., Zhao, S., Bian, H., Gao, X., Sun, B., Jia, W., 2021. Conjugated secondary 12α-hydroxylated bile acids promote liver fibrogenesis. EBioMedicine 66, 103290. https://doi.org/10.1016/j.ebiom.2021.103290

Xiong, J., Chen, X., Zhao, Z., Liao, Y., Zhou, T., Xiang, Q., 2022. A potential link between plasma short-chain fatty acids, TNF-α level and disease progression in non-alcoholic fatty liver disease: A retrospective study. Experimental & Therapeutic Medicine 24, 598. https://doi.org/10.3892/etm.2022.11536

Xue, W., Wang, J., Jiang, W., Shi, C., Wang, X., Huang, Y., Hu, C., 2020. Caveolin-1 alleviates lipid accumulation in NAFLD associated with promoting autophagy by inhibiting the Akt/mTOR pathway. European Journal of Pharmacology 871, 172910. https://doi.org/10.1016/j.ejphar.2020.172910

Yang, M., Qi, X., Li, N., Kaifi, J.T., Chen, S., Wheeler, A.A., Kimchi, E.T., Ericsson, A.C., Scott Rector, R., Staveley-O'Carroll, K.F., Li, G., 2023. Western diet contributes to the pathogenesis of non-alcoholic steatohepatitis in male mice via remodeling gut microbiota and increasing production of 2-oleoylglycerol. Nature Communications 14, 228. https://doi.org/10.1038/s41467-023-35861-1

Yang, S., Zhang, Y., Li, W., You, B., Yu, J., Huang, X., Yang, R., 2021. Gut microbiota composition affects procyanidin A2-attenuated atherosclerosis in ApoE–/– mice by modulating the bioavailability of its microbial metabolites. Journal of Agricultural & Food Chemistry 69, 6989–6999. https://doi.org/10.1021/acs.jafc.1c00430

Yogalakshmi, B., Sreeja, S., Geetha, R., Radika, M.K., Anuradha, C.V., 2013. grape seed proanthocyanidin rescues rats from steatosis: A comparative and combination study with metformin. Journal of Lipids 2013, 1–11. https://doi.org/10.1155/2013/153897

Yokota, K., Kimura, H., Ogawa, S., Akihiro, T., 2013. analysis of A-type and B-type highly polymeric proanthocyanidins and their biological activities as nutraceuticals. Journal of Chemistry 2013, e352042. https://doi.org/10.1155/2013/352042

Yoon, S.J., Yu, J.S., Min, B.H., Gupta, H., Won, S.-M., Park, H.J., Han, S.H., Kim, B.-Y., Kim, K.H., Kim, B.K., Joung, H.C., Park, T.-S., Ham, Y.L., Lee, D.Y., Suk, K.T., 2023. Bifidobacterium-derived short-chain fatty acids and indole compounds attenuate nonalcoholic fatty liver disease by modulating gut-liver axis. Frontiers in Microbiology 14, 1129904. https://doi.org/10.3389/fmicb.2023.1129904

Younossi, Z.M., Golabi, P., Paik, J.M., Henry, A., Van Dongen, C., Henry, L., 2023. The global epidemiology of nonalcoholic fatty liver disease (NAFLD) and nonalcoholic steatohepatitis (NASH): A systematic review. Hepatology 77, 1335–1347. https://doi.org/10.1097/HEP.0000000000000004

Yu, D., Huang, T., Tian, B., Zhan, J., 2020. Advances in biosynthesis and biological functions of proanthocyanidins in horticultural plants. Foods 9, 1774. https://doi.org/10.3390/foods9121774

Yu, K., Song, Y., Lin, J., Dixon, R.A., 2022. The complexities of proanthocyanidin biosynthesis and its regulation in plants. Plant Communications 4, 100498. https://doi.org/10.1016/j.xplc.2022.100498

Zeng, H., Qin, H., Liao, M., Zheng, E., Luo, X., Xiao, A., Li, Y., Chen, L., Wei, L., Zhao, L., Ruan, X.Z., Yang, P., Chen, Y., 2022. CD36 promotes de novo lipogenesis in hepatocytes through INSIG2-dependent SREBP1 processing. Molecular Metabolism 57, 101428. https://doi.org/10.1016/j.molmet.2021.101428

Zeng, S., Wu, F., Chen, M., Li, Y., You, M., Zhang, Y., Yang, P., Wei, L., Ruan, X.Z., Zhao, L., Chen, Y., 2022. Inhibition of fatty acid translocase (FAT/CD36) palmitoylation enhances hepatic fatty acid *β*-oxidation by increasing its localization to mitochondria and interaction with long-chain acyl-CoA synthetase 1. Antioxidants & Redox Signaling 36, 1081–1100. https://doi.org/10.1089/ars.2021.0157

Zhang, J., Yang, Y., Huang, H., Xie, H., Huang, M., Jiang, W., Ding, B., Zhu, Q., 2022. TNF-α/TNFR1 regulates the polarization of Kupffer cells to mediate trichloroethylene-induced liver injury. Ecotoxicology & Environmental Safety 230, 113141. https://doi.org/10.1016/j.ecoenv.2021.113141

Zhang, L., Carmody, R.N., Kalariya, H.M., Duran, R.M., Moskal, K., Poulev, A., Kuhn, P., Tveter, K.M., Turnbaugh, P.J., Raskin, I., Roopchand, D.E., 2018. Grape proanthocyanidin-induced intestinal bloom of *Akkermansia muciniphila* is dependent on its baseline abundance and precedes activation of host genes related to metabolic health. The Journal of Nutritional Biochemistry 56, 142–151. https://doi.org/10.1016/j.jnutbio.2018.02.009

Zhang, Y., Chen, S., Wei, C., Chen, J., Ye, X., 2017. Proanthocyanidins from Chinese bayberry (*Myrica rubra* Sieb. et Zucc.) leaves regulate lipid metabolism and glucose consumption by activating AMPK pathway in HepG2 cells. Journal of Functional Foods 29, 217–225. https://doi.org/10.1016/j.jff.2016.12.030

Zhang, Y., Pan, H., Ye, X., Chen, S., 2022. Proanthocyanidins from Chinese bayberry leaves reduce obesity and associated metabolic disorders in high-fat diet-induced obese mice through a combination of AMPK activation and an alteration in gut microbiota. Food & Function 13, 2295–2305. https://doi.org/10.1039/D1FO04147A

Zhao, L., Zhang, C., Luo, X., Wang, P., Zhou, W., Zhong, S., Xie, Y., Jiang, Y., Yang, P., Tang, R., Pan, Q., Hall, A.R., Luong, T.V., Fan, J., Varghese, Z., Moorhead, J.F., Pinzani, M., Chen, Y., Ruan, X.Z., 2018. CD36 palmitoylation disrupts free fatty acid metabolism and promotes tissue inflammation in non-alcoholic steatohepatitis. Journal of Hepatology 69, 705–717. https://doi.org/10.1016/j.jhep.2018.04.006

Zhong, H., Xue, Y., Lu, X., Shao, Q., Cao, Y., Wu, Z., Chen, G., 2018. The effects of different degrees of procyanidin polymerization on the nutrient absorption and digestive enzyme activity in mice. Molecules 23, 2916. https://doi.org/10.3390/molecules23112916

Zhou, J., Zheng, Q., Chen, Z., 2022. The Nrf2 pathway in liver diseases. Frontiers in Cell and Developmental Biology 10, 826204. https://doi.org/10.3389/fcell.2022.826204

Zhu, L., Baker, S.S., Gill, C., Liu, W., Alkhouri, R., Baker, R.D., Gill, S.R., 2013. Characterization of gut microbiomes in nonalcoholic steatohepatitis (NASH) patients: A connection between endogenous alcohol and NASH. Hepatology 57, 601–609. https://doi.org/10.1002/hep.26093

Zommiti, M., Feuilloley, M.G.J., Connil, N., 2020. Update of probiotics in human world: A nonstop source of benefactions till the end of time. Microorganisms 8, 1907. https://doi.org/10.3390/microorganisms8121907

APPENDIX A. COPYRIGHT PERMISSION

Chapter 2. Optimization of the extraction of proanthocyanidins from grape seeds using ultrasonication-assisted aqueous ethanol and evaluation of anti-steatosis activity *in vitro*

Permission to include a published article in doctoral thesis

Wasitha Praveen de Wass Thilakarathna <ws714884@dal.ca>
Fri 2023-06-02 9:46 AM
To:molecules@mdpi.com <molecules@mdpi.com>

1 attachments (23 KB)
Copyright_MDPI.docx;

Dear Molecules Editor(s),

I am a Ph.D. Candidate in the Faculty of Agriculture, Dalhousie University, Canada. I published an article in your prestigious journal under the title "Optimization of the extraction of proanthocyanidins from grape seeds using ultrasonication-assisted aqueous ethanol and evaluation of anti-steatosis activity *in vitro*".
(Thilakarathna, W.P.D.W., Rupasinghe H.P.V., 2022. Optimization of the extraction of proanthocyanidins from grape seeds using ultrasonication-assisted aqueous ethanol and evaluation of anti-steatosis activity *in vitro*. Molecules 27 (4), 1363. https://doi.org/ 10.3390/molecules27041363)

I would like to get your permission to include this article in my doctoral thesis as a full chapter. Can you kindly return me the attached letter with the required information and signature. This letter must be included in my thesis for it to be accepted by the thesis clerk.

Thank you and best regards.

Wasitha P.D.W. Thilakarathna
Ph.D. candidate
Department of Plant, Food, and Environmental Sciences
Faculty of Agriculture
Dalhousie University, Truro, NS, Canada
+1 902 4013768
wasitha@dal.ca

Re: Permission to include a published article in doctoral thesis

Molecules <molecules@mdpi.com>
Tue 2023-06-06 3:43 AM
To:Wasitha Praveen de Wass Thilakarathna <ws714884@dal.ca>

Dear Dr. Thilakarathna,

It is fine.

Kind regards,
Larry Li
Managing Editor of Molecules
Email: larry.li@mdpi.com

Impact Factor for /Molecules/ (2021): 4.927
CiteScore for /Molecules/ (2021): 5.9 - Q1 (Chemistry (miscellaneous))

Molecules is recruiting Guest Editors/Reviewers for the following sections:
https://www.mdpi.com/journal/molecules/sections/natural_products_chemistry. If you or you know someone who might be interested in these positions, please feel free to contact us. We would be glad to provide more information.

We invite you to follow us on Twitter @Molecules_MDPI

https://www.mdpi.com/journal/molecules

MDPI Wuhan Office
No. 88, Youkeyuan Road, Fenghuo Technology Building, 2nd Floor, Hubei Province, Wuhan 430070, China

Chapter 3. Biotransformation of polymeric proanthocyanidins by using probiotic bacteria in C57BL/6 mice.

From: Wasitha Thilakarathna
Date: Friday, June 02, 2023 12:59 PM GMT

I am a Ph.D. Candidate in the Faculty of Agriculture, Dalhousie University, Canada. I published an article in your prestigious journal Toxicology Letters under the title "Hepatotoxicity of polymeric proanthocyanidins is caused by translocation of bacterial lipopolysaccharides through impaired gut epithelium".
(Thilakarathna, W.P.D.W., Langille, M.G.I., Rupasinghe H.P.V., 2023. Hepatotoxicity of polymeric proanthocyanidins is caused by translocation of bacterial lipopolysaccharides through impaired gut epithelium. Toxicology Letters 379 (2023), 35 – 47. https://doi.org/10.1016/ j.toxlet.2023.03.005)
I would like to get your permission to include this article in my doctoral thesis as a full chapter. Can you kindly return me the attached letter with the required information and signature. This letter must be included in my thesis for it to be accepted by the thesis clerk.
Thank you and best regards.

Re: Permission to include a published article in doctoral thesis [230602-018134]

Permissions Helpdesk <permissionshelpdesk@elsevier.com>
Mon 2023-06-05 3:30 AM
To:Wasitha Praveen de Wass Thilakarathna <wasitha@dal.ca>

Dear Wasitha Thilakarathna,

Thank you so much for contacting us.

Please note that, as one of the authors of this article, you retain the right to reuse it in your thesis/dissertation. You do not require formal permission to do so. You are permitted to post this Elsevier article online if it is embedded within your thesis subject to proper acknowledgment;

Our preferred acknowledgement wording will be :

Example: "This article/chapter was published in Publication title, Vol number, Author(s), Title of article, Page Nos, Copyright Elsevier (or appropriate Society name) (Year)."

All the best for your thesis submission!

Kind regards,

Kaveri Thakuria

Senior Copyrights Coordinator

ELSEVIER | HCM - Health Content Management

Visit Elsevier Permissions